TRANSITION IN BOUNDARY LAYER FLOWS

by

IAIN D GARDINER, BSc (Hons)

Department of Mechanical and
Industrial Engineering

Thesis submitted to the C.N.A.A. for
the Degree of Doctor of Philosophy

March 1987

Dundee College of Technology

Boundary Layer Wind Tunnel Facility

DECLARATION

I hereby declare that the following work has been composed by myself and that this dissertation has not been presented for any previous award of the C.N.A.A. or any other University.

[redacted]

Iain D Gardiner

Transition in Boundary Layer Flows

by

Iain D Gardiner

Abstract

An experimental investigation of transition in boundary layer flows under the influence of various freestream conditions is described.

Velocity profiles are obtained automatically by means of a stepper-motor driven traverse mechanism which carries a hot wire probe connected to a constant temperature anemometer and associated instrumentation. This was achieved by use of a data acquisition and control facility centred around a microcomputer with a Eurocard rack mounted extension. The automatic boundary layer traverse is software controlled and the data obtained is stored in a disc file for subsequent analysis and graphical display. As an integral part of this facility a successful method of obtaining reliable intermittency values from a hot wire signal was developed.

The influence of freestream turbulence and pressure gradient upon transition within a boundary layer developing on a flat plate is elucidated by a series of controlled experiments.

From the data accumulated, the concept of statistical similarity in transition regions is extended to include moderate non-zero pressure gradients, with the streamwise mean intermittency distribution described by the normal distribution function.

An original correlation which accounts for the influence of freestream turbulence in zero pressure gradient flows, and the combined influence of freestream turbulence and pressure gradient in adverse pressure gradient flows, on the transition length Reynolds number R_σ, is presented. (The limited amount of favourable pressure gradient data precluded the extension of the correlation to include favourable pressure gradient flows).

A further original contribution was the derivation of an intermittency weighted function which describes the development of the boundary layer energy thickness through the transition region.

A general boundary layer integral prediction scheme based on existing established integral techniques for the laminar and turbulent boundary layers with an intermittency modelled transition region, has been developed and applied successfully to a range of test data.

COURSES & CONFERENCES ATTENDED

DATE	TITLE & LOCATION	CONTENT
11-13 April 1984	"Hot Wire Anemometry" Cranfield Institute of Technology	A series of lectures and 'hands on' experiments giving valuable experience on both practical and theoretical aspects of hot wire anemometry techniques.
2-30 May 1984	"New Technology Applications in Manufacturing Industry" Dundee College of Technology	A series of evening lectures and demonstrations relating to principles of digital control.
11-13 Sept 1985	Conference on "Developments in measurements and instrumentation in Engineering" Hatfield Polytechnic	The paper "A low cost data acquisition system based on a BBC microcomputer" by Milne, J S, Fraser, C J and Gardiner, I D was presented by J S Milne.
7-10 April 1986	Second International Conference on "Micro-computers in Engineering: Development and Application of Software" University College of Swansea	The paper "Application of a microcomputer for control, data acquisition and modelling in transitional boundary layer studies" by Fraser C J, Milne J S and Gardiner, I D was presented by C J Fraser.

ACKNOWLEDGEMENTS

I wish to thank my supervisors, Mr J S Milne and Dr C J Fraser, who at all times throughout the duration of this project have willingly proferred their advice upon every aspect of the work described herein.

My gratitude extends to the technical and secretarial staff of the Department of Mechanical Engineering for their valuable friendship over the past three years and also to Liz for her efforts in the typing of this thesis.

Finally, the financial support of the Scottish Education Department during the period 1983-86 is acknowledged.

NOMENCLATURE

Symbol	Function	Connotation	Units
a	-	Tani's profile parameter	-
C	-	constant in the law of the wall	-
Cf	-	local skin friction coefficient	-
Cp	-	Pressure coefficient	-
H_{12} or H	δ^*/θ	Shape factor	-
H_{32}	δ^{**}/θ	Shape factor	-
k	-	Von Karman constant in law of the wall = 0.41	-
Rx	$\frac{x\,U_\infty}{\nu}$	Length Reynolds Number	-
R_σ	$\frac{\sigma\,U_\infty}{\nu}$	Transition length Reynolds Number	-
R_λ	$\frac{\lambda\,U_\infty}{\nu}$	Transition length Reynolds Number	-
R_θ	$\frac{\theta\,U_\infty}{\nu}$	Momentum thickness Reynolds Number	-
R_{δ^*}	$\frac{\delta^*\,U_\infty}{\nu}$	displacement thickness Reynolds Number	
Tu	$\sqrt{\overline{u^2}}/U_\infty \times 100$	freestream turbulence intensity	%
$\overline{u}$		local mean velocity	m/s
U_∞		freestream velocity	m/s
U_0		freestream velocity at leading edge	m/s
u_τ	$\sqrt{\tau_0/\rho}$	Wall friction velocity	m/s
u^+	$\overline{u}/U_\tau$	dimensionless velocity	-

Symbol	Function	Connotation	Units
u', v', w'		fluctuating Velocity components in x, y, z directions respectively	m/s
$\overline{x}$		location of the 50% intermittency point	mm
x		streamwise co-ordinate	mm
y		transverse co-ordinate	mm
z		spanwise co-ordinate	mm
y^+		dimensionless y co-ordinate	-
γ		local intermittency	-
$\overline{\gamma}$		mean 'near wall' intermittency	-
δ		boundary layer thickness at $\overline{u} = 0.995\ U_\infty$	mm
δ^*	$\int_0^\infty \left(1 - \overline{u}/U_\infty\right) dy$	displacement thickness	mm
θ	$\int_0^\infty u/U_\infty \left(1 - \overline{u}/U_\infty\right) dy$	momentum thickness	mm
δ^{**}	$\int_0^\infty \overline{u}/U_\infty \left\{1 - \left(u/U_\infty\right)^2\right\} dy$	Energy thickness	mm
λ		transition normalising length	
λ_p	$\frac{\delta^2}{\nu} \frac{dU_\infty}{dx}$	Pohlhausen pressure parameter	-
λ_θ	$\frac{\theta^2}{\nu} \frac{dU_\infty}{dx}$	modified Pohlhausen/Thwaites parameter	-
μ		fluid dynamic viscosity	kg/ms
ν		fluid kinematic viscosity	m^2/s
ρ		air density	kg/m^3
π		Coles "wake" profile parameter	-
σ		Standard deviation of mean intermittency distribution	mm

Symbol	Function	Connotation	Units
τ_o		Wall shear stress	
ζ	$\frac{x-x_s}{\lambda}$	transition normalising co-ordinate	-
ζ	$\frac{x-\bar{x}}{\sigma}$	transition normalising co-ordinate	-
η	$\frac{x-x_s}{x_e-x_s}$	transition normalising co-ordinate	-
$\ell_1(\lambda_\theta)$	-	Thwaites relationships between ℓ_1 and λ_θ	

Subscripts

e - related to the end of transition

i - denoting initial conditions

l - relating to transition length

L - related to the laminar region

o - denoting conditions at the leading edge

s - related to the start of transition

t - related to the transition region

T - related to the turbulent region

Other symbols, not noted here, are defined within the text.

CONTENTS

APPENDICES

STATEMENT OF OBJECTIVES

1) To review the literature on the current conceptional understanding of the transition process.

2) To improve the flow in the existing boundary layer wind tunnel test facility.

3) To investigate the suitability of a microcomputer based system with analogue-to-digital conversion facilities for the acquisition of data, from a hot wire signal, in laminar, turbulent and transitional boundary layers.

4) To develop suitable microcomputer software for the control of an automatic boundary layer traverse; for the logging of velocity profile data and for the subsequent analysis and reduction.

5) To set up flows with different combinations of pressure gradient and freestream turbulence level and to measure the boundary layer development under the influence of these effects.

6) To obtain transition onset and length data in both zero and non zero pressure gradients at a range of freestream turbulence levels.

7) To investigate the concept of statistical similarity of transition regions in non-zero pressure gradients and to consider methods of representing this similarity, if it exists.

8) To review the current methods of predicting the onset and length of transition.

9) To investigate the effect of freestream turbulence level and freestream pressure distribution on the transition length and to correlate these effects.

10) To develop a general boundary layer integral prediction model, based on an intermittency weighted transition region, for the development of the transitional boundary layer growth and to develop microcomputer codes for this model.

CHAPTER 1

Introduction

1.1 Early experiments

Until Prandtl's epoch making lecture at the beginning of this century the science of fluid dynamics had been developing along two different branches; one being the dynamics of frictionless fluids called *hydrodynamics*, which was regarded as an academic subject incapable of practical application, and the other being the empirical science of *hydraulics* based on correlations of large amounts of experimental data. This diversificacion arose from the inability of the hydrodynamicists to predict real solutions to practical engineering problems. Prandtl, with his paper on "Fluid Motion with Very Small Friction" read before the Mathematical Congress in Heidelberg in 1904, took the first steps to unifying these two branches by showing that it was possible to analyse viscous flows precisely in cases which had great practical importance. Prandtl described, with the aid of simple experiments, how the flow around a body could be divided into two regions: A thin layer in contact with the surface in which viscous forces were significant and the remaining region outside this layer where viscous forces can be neglected. Although acceptance of Prandtl's paper was initially very slow, it is now considered to mark the birth of modern boundary layer theory.

Even before Prandtl had presented his 1904 paper and established the boundary layer equations, Osborne Reynolds (1883) had applied himself to the problem of transition. Reynolds postulated that the breakdown of a laminar flow to turbulence was a consequence of instability in the laminar flow. This hypothesis which was further developed by Rayleigh is now known as the Reynolds-Rayleigh hypothesis and to this day is still highly regarded.

In 1914 Prandtl carried out his famous experiments on spheres and observed that the flow in a boundary layer could also be either laminar or turbulent and furthermore, that the position at which transition occurred significantly affected the flow around a body and hence the calculation of the drag on the body.

1.2 Stability of laminar flow

Stability theory for viscous fluid flows was developed independently by both Orr (1907) and Sommerfeld (1909) and resulted in what is now known as the Orr-Sommerfeld equation. This equation was derived from a finite disturbance analysis of the Navier-Stokes and continuity equations and is the starting point for all stability calculations. No practical solution to this equation was obtained until the late 1920's when, not surprisingly, the breakthrough came from one of Prandtl's students, Tollmein (1929) who computed theoretically the critical Reynolds number at which the laminar flow becomes unstable to a travelling wave type of disturbance. Schlichting (1933) later extended Tollmein's calculations to amplified two dimensional disturbances which are now recognised as Tollmein-Schlichting waves.

Despite the notable achievement of both Tollmein and Schlichting their work was disregarded for almost a decade until two of Dryden's co-workers, Schubauer and Skramstad (1943) conducted experiments on a flat plate in a wind tunnel with very low residual turbulence. In these experiments Schubauer and Skramstad forced the boundary layer to oscillate by vibrating a thin magnetic ribbon immersed in the layer. At certain Reynolds numbers they observed that the oscillations were amplified and that transition to turbulence was preceeded by these amplified oscillations. These experiments were regarded as confirmation of the previously purely theoretical concept of Tollmein-Schlichting waves and critical Reynolds number. The reason these observations had not been made in earlier experiments was considered to be due to the high levels of freestream turbulence,typical of earlier experiments, masking the existence of amplified waves.

1.3 Transition to turbulence

In 1936 Dryden observed that near the beginning of transition turbulent *bursts* occurred randomly and at infrequent intervals and that further downstream the bursts occurred more frequently and were of longer duration until finally the flow was continuously turbulent. The intermittent appearance of the turbulence in this region was interpreted by Dryden as a wandering irregular line of abrupt transition about a mean position. However, it is now certain that this interpretation was incorrect and that the so-called transition region is composed of Emmons (1951) type *turbulent spots* which grow in size as they are transported downstream.

Emmons advanced the concept of turbulent spots on the basis of experiments conducted on equipment built to demonstrate a simple water table analogy to supersonic flow. In addition to the anticipated supersonic phenomenon, Emmons noticed the appearance of strange *turbulent bursts* and had the foresight to recognise this as the breakdown of the laminar flow. He observed that the transition region was filled with a random collection of these turbulent bursts or *spots* which appeared to grow at a constant rate and independently of each other. From these observations Emmons deduced a source density function which described the production of turbulent spots, and showed how this could be related to the probability of the flow being turbulent at a given point, namely, the intermittency factor $\bar{\gamma}$.

Following Emmons paper in 1951, the existence of turbulent spots in a boundary layer was confirmed experimentally by Mitchner (1954) and Schubauer & Klebanoff (1956). Mitchner's technique of artificially generating turbulent spots by means of an electric spark was used by Schubauer & Klebanoff to make detailed measurements of the spot growth and geometry. The shape of Schubauer & Klebanoff's artificially generated turbulent spots is shown in fig. [1.3.1] below.

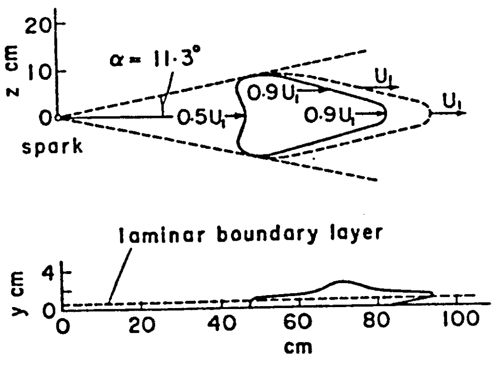

Fig. 1.3.1

More recently conditional sampling techniques have been used by Wygnanski et al (1976) and Arnal (1977) to measure the mean velocity profiles in and out of turbulent spots, in a transition region, and have shown that the flow within a turbulent spot is characteristic of a turbulent boundary layer. Gad-el-Hak et al (1981) used a rather novel flow visualisation technique to obtain an excellent series of colour photographs showing the growth of a turbulent spot on a flat plate towed through a tank of water. These photographs show that the characteristic shape of the turbulent spot remains unchanged as the spot grows and is swept downstream with the mean flow.

So far the mechanism of the process leading to turbulent flow has been elucidated on the basis of controlled experiments such as those by Klebanoff, Tidstorm & Sargent (1962) and although no theory exists for the prediction of transition, the breakdown process is qualitatively well defined.

The breakdown process begins with the amplification of Tollmein-Schlichting waves which become associated at some stage with a concentration of vorticity along discrete lines. These subsequently distort into vortex loops which themselves go through a process of distortion and extension until they finally break into localised bursts of turbulence ie turbulent spots. The turbulent spots then grow, laterally as well as axially, until they eventually coalesce to form a completely turbulent flow field.

This process can be simplified into three stages.

(i) Amplification of small disturbances.

(ii) Generation of localised areas, or spots, of turbulence.

(iii) Growth and spread of turbulent spots.

While theories of the Tollmein-Schlichting type have achieved a fair amount of success in predicting the influence of various effects on the limit of laminar stability (stage (i)) they give no indication of the point at which transition occurs (stage (ii)).

1.4 Practical significance of transition

Transition from laminar to turbulent flow is not only an important problem of fundamental research in fluid mechanics but possesses many important ramifications. For example, the drag of a body placed in a stream as well as the rate at which heat is transferred from a solid wall to a fluid moving past it, depend very strongly on whether the flow in the boundary layer is laminar or turbulent. The occurrence of transition can sometimes be beneficial, for example in delaying separation or in promoting more rapid diffusion of heat and sometimes it can be detrimental in increasing skin friction and promoting undesirable high rates of heat transfer. Whether beneficial or detrimental the accurate prediction of its position on a body is obviously of paramount importance to the computation of the boundary layer development over a body, and hence the calculation of the aerodynamic and thermodynamic performance of the body.

One rather crude method of calculating the boundary layer development on a surface is to assume that transition from the laminar to turbulent flow state occurs instantaneously at the transition point, and to overlap the laminar and turbulent boundary layer parameters at this point. This method may be substantiated in some cases when the length over which the boundary layer degenerates from the laminar to turbulent flow state, ie the transition length, is small in comparison to the length of the body itself. However, in situations where the transition region occupies a significant proportion of the body surface then the length over which the transition metamorphosis takes place will be of great significance to the development of the boundary layer.

One practical example of a situation where the transition region occupies a high proportion of a body surface is a modern gas turbine blade. Turner (1971) observed that the boundary layer over a turbine blade can be transitional for up to 70% of its chord. In such a case the quality of the boundary layer prediction through the transition region can influence the blade aerodynamic efficiency and, through its impact on cooling design, the cycle efficiency and hardware durability of the turbine. Therefore accurate prediction of the boundary layer development through transition which is dependent on accurate prediction of the onset and length of transition, is of prime importance.

1.5 Prediction of transition onset

The transition point, which lies some distance downstream of the point of laminar instability, can be defined as the point at which the mean laminar boundary layer parameters begin to deviate from their typical laminar values and is normally considered to be the point where the laminar flow breaks down to random turbulence, ie the appearance of first turbulent spots. In general transition is known to be influenced by a number of factors such as: surface roughness, freestream turbulence, pressure gradient, Mach number, surface curvature, Reynolds number etc. Because of the complex manner in which the various factors influence the position of the transition point and the extent of the transition region, theorists have been unable to solve the transition problem analytically. For this reason the design engineer has had to rely on empirical and semi-empirical models, based on experimental data, to obtain solutions to practical engineering problems. Obviously the accuracy of any solution will depend on the quality of the experimental data, the degree of correlation and the number of influencing factors that are accounted for in the model. Two of the most dominant factors which influence transition are the pressure gradient and freestream turbulence intensity, consequently any empirical model should, at least, account for their effects.

Various methods for predicting the position of the transition point are available, all operating on an empirical or semi-empirical basis but with varying transition criteria and basic assumptions. These methods have been reviewed by a number of researchers eg Tani (1969), Hall & Gibbings (1972), Reshotko (1976) and more recently in an excellently complete review by Arnal (1984). It is not intended therefore, to repeat this work here but merely to briefly describe the empirical and semi-empirical approach to the prediction of transition point.

Semi-empirical approach: This approach includes the "so-called" e^n methods formed on the basis of the linear stability theory and correlations from low turbulence wind tunnel experiments. The first of these methods was developed by Smith & Gamberoni (1956) and independently by Van Ingen (1956). They observed that the maximum amplification ratio of the initial disturbances, as computed by the stability theory, at the observed position of transition was roughly equal for all cases investigated. According to Smith & Gamberoni, this critical value of amplification ratio is approximately e^9.

Since this method was first introduced various modifications to the original calculation method have been made, for example by Jaffe, Okamura & Smith (1970) and others. However the method remains essentially as originally developed, the key to success of the method lying in the judicious choice of the exponent factor, ranging anywhere from about 8 to 11.

e^n methods are only applicable for flows with low freestream turbulence levels (say <0.2%). At higher freestream turbulence levels the Tollmein-Schlichting mode to transition is thought to be *by-passed*, transition then being due to pressure fluctuations in the freestream, Taylor (1936).

Another method which can be classed as having a semi-empirical approach, as it includes some theoretical elements, is that of Van Driest & Blumer (1963). This was developed on Liepmann's (1936) idea that transition occurred when the ratio of local turbulent to viscous shear stress reached some critical value. By using Taylors' (1936) hypothesis for freestream turbulence effects and the Pohlhausen (1921) forth-degree velocity profile an expression involving two adjustable constants has been derived for transition Reynolds number in terms of pressure gradient parameter, λ_p, and freestream turbulence. The constants in this expression being adjusted to fit experimental data.

Wholly empirical approach These methods are based on the assumption that the local transition Reynolds number can be determined, through correlation of controlled experimental results, as a function of the factors which influence transition. Whether the prediction based on local Reynolds number is accurate or not depends on whether all the important parameters are taken into account.

The method of Michel (1951) which comprises only one relationship between the momentum thickness Reynolds number and the axial length Reynolds number at transition, is probably the simplest of those methods. Michel's curve can be fitted by the expression.

$$R_{\theta_s} = 1.535\ R_{x_s}^{\ 0.44} \qquad \text{............ 1.1}$$

When the corresponding flow Reynolds numbers coincide with Michel's curve ie equation 1.1 then transition is "predicted". Other early methods worthy of note are those of Granville (1953) and Crabtree (1957) both using a single curve of R_{θ_s} against a pressure gradient parameter λ_θ as a transition criteria. However, Granville's method differs from Crabtree's in that he attempted to make an allowance for the upstream flow history by assuming that only the boundary layer growth after the point of stability was of any consequence. Granville therefore plotted (R_{θ_s} - $R_{\theta_{cr}}$), where $R_{\theta_{cr}}$ is the value of R_θ at the stability limit, against the mean value of λ_θ over the unstable part of the boundary layer. As was the case for the e^n methods these early methods are realy only applicable to low freestream turbulence flows.

The more recent methods of Dunham (1972), Seyb (1972) and Abu-Ghannam & Shaw (1980) directly correlate the momentum thickness Reynolds number at transition against the local pressure gradient parameter λ_{θ_s} and the freestream turbulence level. The most recent of these ie Abu-Ghannam and Shaw's is probably the most reliable as it is based on a vast amount of experimental data obtained from a variety of sources.

1.6 Boundary layer development through transitions (present investigations)

Assuming the transition point is known the problem then is to compute the boundary layer development through the transition region itself, the extent of which may be longer than the laminar layer which precedes it. An important parameter characterising the transitional boundary layer is the mean "near wall" intermittency factor $\bar{\gamma}$ which represents the fraction of time that the flow is turbulent. The model presented in this thesis is based on the 'so-called' "intermittency method", in which the laminar and turbulent boundary layer quantities are weighted by $\bar{\gamma}$. Thus the first task is to describe the streamwise evolution of the intermittency factor $\bar{\gamma}$ through the transition region.

There are other methods, such as that of McDonald & Fish (1973) which do not require the knowledge of $\bar{\gamma}$. Such methods involve finite difference solution of the mean flow and some form of eddy viscosity. However these methods require the use of refined finite difference grids with perhaps more than 100 grid points across the boundary layer. This makes such approaches uncomfortably slow in engineering design applications, See Forrest (1977). Such methods have not been considered further in this investigation.

Schubauer & Klebanoff (1956) measured the streamwise distribution of $\bar{\gamma}$ for a number of zero pressure gradient flows where conditions leading to transition were varied and, although in each case the transition lengths were different, the distribution followed the general shape of the Gaussian integral curve. The standard deviation σ was calculated for each experiment, and all the data collapsed on to a single curve when $\bar{\gamma}$ was plotted as a function of the normal stream co-ordinate $\zeta = {}^{x-\bar{x}}/_{\sigma}$ where $\bar{x} = x(\gamma{=}0.5)$. (The value of σ is a measure of the spread of the data about the 50% intermittency point and, if the transition region is defined in the limits $0.01 < \gamma < 0.99$ then σ can be related directly to the transition length).

Schubauer and Klebanoff, from these observations, postulated that transition regions in all zero pressure gradient flows, long or short, were statistically similar. This concept was corroborated by Dhawan & Narasimha (1958) although in contrast to Schubauer & Klebanoff they proposed a different distribution function of intermittency:

$$\bar{\gamma} = 1 - \exp^{-0.412\xi} \qquad \text{............ 1.2}$$

where $\xi = (x - x_S)/\lambda$ is the normalised stream co-ordinate with λ as a measure of the intermittency spread given by

$$\lambda = (x \text{ at } \bar{\gamma} = 0.75) - (x \text{ at } \bar{\gamma} = 0.25)$$

(By defining the transition region in the same limits as before λ can also be related directly to the transition length).

A similar method with yet a different intermittency distribution function has also been proposed by Abu-Ghannam & Shaw (1980).

All three of the methods for defining the intermittency distribution have been considered in this investigation and the concept of statistical similarity for non-zero pressure gradient cases has been examined.

Unless the length of the transition region (which can be related directly to σ or λ) is known, none of the methods constitute a means of calculating the streamwise intermittency distribution $\overline{\gamma}$. For this reason Dhawan & Narasimha proposed the existence of a relationship between the transition Reynolds number (R_{x_s}) and a transition length Reynolds number based on λ ie ($R\lambda$):

$$R\lambda = R_{x_s}^{\ 0.8} \qquad \text{............ 1.2}$$

This relationship, although known to be in error by more than 100% in some cases and agreed to be very approximate by Dhawan & Narasimha in their original paper, is used as the basis of many prediction methods which require the transition length to be known eg. Abu-Ghannam & Shaw (1980), Brown & Burton (1978), Fraser (1979), Martin et al (1978).

The validity of this relationship is reviewed and a new correlation, based on data gathered during this investigation and on the limited amount of existing data available, is proposed for defining the transition length. The new correlation accounts directly for the effect of freestream turbulence and pressure gradient on the transition length and is in the form:

$$R_\sigma = f(Tu,\ \lambda_\theta) \qquad \text{............ 1.4}$$

The development of this relationship is discussed in detail in Chapter 6.

Dhawan & Narasimha also proposed that the transition region could adequately be described as a region of alternate laminar and turbulent flow. With the intermittency distribution known they assumed that the transitional mean velocity profiles could be expressed as an intermittency weighted average of the laminar and turbulent velocity profiles ie:

$$\left(u/U_\infty\right)_t = (1 - \gamma)\left(u/U_\infty\right)_L + \gamma\left(u/U_\infty\right)_T \qquad \ldots\ldots\ldots\ldots\ 1.5$$

Qualitative measurements made in the transition region in the present investigation substantiate this model, as do the detailed conditionally sampled measurements of Arnal (1977) and Wygnanski (1976).

These observations of Dhawan & Narasimha along with the intermittency distribution of Schubauer & Klebanoff and the present correlation for transition length are formulated into a computational model for predicting the boundary layer development through transition. The laminar and turbulent boundary layer components are obtained from the established integral techniques of Tani (1954) for the laminar boundary layer and Alber (1968) for the turbulent boundary layer.

The development of the model is discussed in detail in Chapter 7 and a comparison of predictions obtained from the model against a sample of past and present data is made.

1.7 Microcomputer involvement

During the last decade the most significant improvements in instrumentation and measurement have been centred on the development of microelectronics, with particular reference to microprocessors which have added a new dimension of intelligence and control in measurement systems. The operational flexibility of the microcomputer allows the same machine a functional role in the data taking process, the analysis and reduction of the primary data and the mathematical modelling of the observed phenomenon.

A large proportion of the present study was devoted to the development and commissioning of a microcomputer data acquisition and control system based on a BBC microcomputer with a Double Disc drive unit for the storage of software and data files. This system contributed significantly to the speed at which reliable accurate data could be obtained and processed. The computational model described in the previous section was also programmed to run on the same BBC micro thus exploiting the full potential of the system.

The development of this system has resulted in the publication of two papers ie Milne, Fraser & Gardiner (1985) and Fraser, Milne & Gardiner (1986). A further paper by Fraser, Gardiner & Milne (1987) is to be presented at the 5th International Conference on "Numerical Methods in Laminar and Turbulent Flow" to be held in Montreal, CANADA in July 6th - July 10th 1987.

CHAPTER TWO

EXPERIMENTAL FACILITIES

2.1 Wind tunnel test facility

All experiments during this investigation were conducted in a purpose built, open return, boundary layer wind tunnel. Details of the design of this tunnel are given by Fraser (1979). The tunnel was originally designed for the study of two dimensional, incompressible flat plate boundary layer flow and has an adjustable roof which enables the boundary layer to be subjected to adverse, zero and favourable pressure gradients. Moderately low freestream turbulence levels (around 0.35%) can be obtained in this facility and it has recently been modified to allow higher turbulence levels to be generated within the test section through the use of various turbulence generating grids. A schematic diagram of the tunnel is shown in fig. 2.1.1.

The tunnel consists of a series of damping screens, an inlet contraction, a rectangular working section, a square to round section diffuser and a variable speed 2 hp D.C. motor which drives a six blade propeller fan.

The damping screens, situated upstream of the inlet contraction, are designed for the double purpose of reducing the spanwise nonuniformity in the flow, as suggested by East (1972), and reducing the freestream turbulence level by removing large scale eddies and inducing lower scale eddies which rapidily decay downstream of the grids, Dryden & Schubauer (1947). The inlet contraction which is of rectangular section, has an aspect ratio of 2/1 and an area reduction ratio of 9/1. The contraction is designed to further reduce the freestream turbulence and accelerate the flow into the working section. Downstream of the inlet contraction is the working section. This is of rectangular cross section 227 mm x 450 mm x 2.5 m with an adjustable height roof to enable variable pressure gradient flows to be set up in the test section.

Situated within the tunnel working section is the instrument carriage which was designed to give three-dimensional flexibility for the hot wire sensor positioning. The carriage runs on two horizontal rails fixed to the tunnel side walls, which allows streamwise flexibility in the probe positioning, and a cross slide, to which all the necessary measuring equipment and vertical traversing gear can be attached, allows for spanwise positioning. Positioning in the spanwise and streamwise direction is done manually from inside the working section with the vertical traversing being carried out remotely using the DISA Sweep drive unit (type 52B01) in conjunction with a stepper motor (type 52C01) which drives through reduction gearing, a rack and pinnion. The rack being ultimately attached to the probe sensing head. A photograph of the probe traversing mechanism is shown in fig. [2.1.2].

A pitotstatic tube, coupled to an inclined manometer, is in permanent place at the entrance to the working section above the plate leading edge. This enables the reference approach velocity at the leading edge of the plate to be continuously monitored. Access to the working section is via four hinged doors on the front wall.

A flexible coupling joins the exit of the working section to the diffuser. The purpose of this flexible coupling was twofold, firstly, to prevent vibrations from the fan and motor being transmitted to the working section and secondly to provide a pliable seal between the variable height roof and the diffuser.

The diffuser merges from a square to a round section over its 1.5 m length. The section at the upstream end is 450 mm x 450 mm and the diameter at the downstream end is 800 mm.

The six blade fan propeller is housed in a 700 mm long cylindrical casing and is driven by a 2 hp variable speed motor. The motor has a maximum speed of 1440 rpm giving a maximum reference velocity at the entrance to the working section of nominally 20 m/s.

2.2 The boundary layer Plate

The boundary layer plate is a 6 mm thick aluminium sheet 2.4 m long and completely spans the working section. The plate is fixed to two rails which are bolted through the tunnel floor onto the main supporting framework. Along the centre line of the plate are a series of pressure tappings set at 50 mm pitch and these tappings are connected to a multitube inclined manometer. Originally the plate was positioned 50 mm above the working section floor at zero incidence to the approach flow and the leading edge was symmetrically sharpened and bent downwards to ensure that the stagnation point would occur on the upper surface of the plate leading edge. Previous results from earlier work, Fraser (1979), showed that natural transition on the plate occurred at values of Rx well below those obtained by other researchers such as Van Driest & Blumer (1963), Hall & Gibbings (1972) and Abu-Ghannam & Shaw (1980). This early transition was initially thought to be caused by the leading edge geometry so, the front of the plate was removed and a new straight symmetrically shaped leading edge was machined on the plate and hand worked to merge tangentially to the plate horizontal surface. To ensure the stagnation point would occur on the top surface of the leading edge the whole plate was then inclined at -½° to the oncoming flow. Fig. [2.2.1] shows the new leading edge geometry. To obtain this -½° of incidence the plate leading edge was lowered to 23 mm from the tunnel floor rather than the trailing edge being raised. However, as can be seen from the tunnel approach velocity profiles fig. [2.2.2] the leading edge of the plate is still well clear of the boundary layer developing on the tunnel floor.

2.3 Preliminary Tests & Tunnel Modifications

An initial study to determine the flow regimes over the modified flat plate, in a zero pressure gradient, was carried out by positioning the probe approximately 1 mm from the plate surface and observing the trace from the constant temperature anemometer (DISA 55M10), on an oscilloscope, at numerous spanwise and streamwise positions. This study gave an indication of the regions of laminar, transitional and turbulent flow over the plate. As can be seen from fig. [2.3.1], there appears to be large disturbances which emanate from the tunnel side walls and grow downstream, progressively encroaching into the flat plate test flow. This phenomenon, although not often reported, is thought to be a common occurrence in boundary layer wind tunnels. It was observed by Coles & Savas (1979) who stated, *"The useful region of the plate sruface was severely limited by transverse contamination from the sidewalls"*, and more recently by Blair (1982). For this reason all test measurements were restricted to the tunnel centreline.

Even with this restriction imposed, values of Rx_s still fell far short of those expected therefore, it was decided to make further improvements to the tunnel to, at least, delay the start of the transition to obtain values of R_{x_s} approaching those of Abu-Ghannam & Shaw (1980).

Initial improvements were

(i) A suction port was added to the underside of the tunnel 500 mm from the leading edge in an attempt to improve the flow over the leading edge of the plate.

Oil and smoke flow visualisation techniques showed that this suction made no difference to the flow over the leading edge and in fact the flow in this region was fairly good with no signs of separation occurring on the topside near the leading edge.

(ii) The tunnel roof side wall seals were replaced as smoke tests revealed an inflow to the tunnel working section from the atmosphere, through inadequate sealing at the joint between the adjustable roof and the tunnel side walls.

(iii) The seals around the working section access doors were replaced as the original "draftproofing" had perished.

None of these improvements delayed the start of transition on the plate, in fact it was discovered after all these "improvements" had been made that transition was actually occurring earlier than ever on the test surface.

This was very disappointing, but after much deliberation on this problem the reason for the early transition was eventually traced to the fact that the three turbulence damping screens at the intake to the tunnel had been cleaned, removing a fair quantity of dust which had accumulated on them and appeared to be increasing their effectiveness. The addition of two further screens, one of a manmade micromesh fabric (used for wind breaks) was placed at the front of the bank of screens and the other, a 40 mesh stainless-steel wire mesh grid, placed at the rear of the bank of screens. Details of the screens are given in fig. [2.3.2]. The addition of these extra screens did not significantly decrease the level of natural freestream turbulence in the tunnel but did greatly improve the flow over the plate and established values of Rx_S, on the centre line of the plate, of the same order of those obtained by Abu-Ghannam & Shaw (1980), fig. [2.3.3].

2.4 Turbulence Generating Grids

The various freestream turbulence levels required throughout this investigation were produced by placing turbulence generating grids close to the contraction entrance, about 400 mm downstream of the contraction front edge, see fig. [2.1.1]. This arrangement differs from that used in many of the early investigations of this subject in that the grids are located in the inlet contraction and not downstream of it at the entrance to the test section. The benefits derived from this, as reported by Blair (1983), are that the turbulence generated in the test section is more homogeneous and has a much lower decay rate along the test section. This is illustrated in fig. [2.4.1].

(The advantage of locating the grids in this position require that coarser grids be used to achieve given test section turbulence levels).

The grids designed gave turbulence intensities of approximately 0.45%, 0.75% and 1.45% in the test section of the tunnel. These grids will now be referred to as grid 1, grid 2 and grid 3 respectively.

Grid 1: is a wire grid of mesh size 25 mm and rod diameter 2.5 mm.

Grid 2: is a wooden grid of mesh size 25 mm and rod diameter 5.5 mm.

Grid 3: is a wooden grid of mesh size 38 mm and is made from 6 x 12 mm rectangular section strips.

Further details of the grids are given in fig. [2.4.2].

2.5 Freestream Pressure Gradients

The range of pressure gradients required for this investigation were introduced by adjusting the variable height roof to give the required velocity distribution within the test section. This proved to be a difficult and very time consuming task as slight alterations in the roof height could affect the entire velocity distribution over the plate.

The procedure adopted in setting up the pressure distributions was to initially adjust the roof to give, crudely, the required static pressure distribution along the plate, measured from the plate static tappings via a multitube manometer. Fine adjustment of the roof was then implemented by measuring the freestream velocity distribution, with a hot wire, and adjusting the roof accordingly.

Four different roof settings were used to illustrate the effects of favourable, zero and adverse pressure gradients. All the roof settings gave reasonably linear velocity distributions over the test length of the plate except for the favourable gradient setting which, due to the tunnel geometrical constraints, was non-linear in the region of the leading edge.

The pressure distributions expressed in terms of the pressure coefficient, C_p, are shown in fig. [2.5.1] along with the corresponding velocity distributions.

2.6 Hot Wire Instrumentation

DISA hot wire instrumentation was used consistently throughout the duration of this project. Miniature boundary layer probes (55P15) were connected via a probe support (55H21) and a 5 m length of coaxial cable to the (55M01) Main Unit fitted with a (55M10) Bridge operating in the constant temperature mode. A simplified schematic diagram of the constant temperature anemometer is shown in fig. [2.6.1].

In essence, the constant temperature anemometer consists of a Wheatstone bridge, with the probe wire serving as one of the bridge arms, and a servo amplifier. The bridge is in balance if the probe resistance and the adjacent bridge resistance Rv (fig. [2.6.1]) are equal, so a voltage applied to the top of the bridge will produce no out of balance, or error voltage across the bridge. Any flow over the probe will have the effect of cooling the wire, resulting in a small change in probe resistance which in turn produces an error voltage across the bridge. This is amplified in the servo amplifier and fed back to the bridge top, causing the bridge current to increase and the probe temperature to eventually return to its original value. The voltage which is fed to the bridge top to maintain the probe temperature can be related to the fluid velocity by calibration. The response of the system is optimised by subjecting the probe to a square wave input and adjusting the bridge gain and upper operating cut off frequency. Fine tuning is achieved by adjustment of the Q and L cable compensation potentiometers.

The voltage output from the constant temperature anemometer is non-linearly related to the fluid velocity over the probe. In order to obtain a linear relationship, the signal from anemometer is passed through a 55M25 Lineariser, which is basically an analogue computer that linearises the anemometer signal by means of a transfer function composed of exponential and square root terms. A pictorial representation of the non-linearised and linearised hot wire signal is shown in fig. [2.6.2] and an actual linearised calibration is shown in fig. [2.6.3].

A spectral analysis of the turbulence signal from a typical turbulent boundary layer shows that the turbulent energy is contained below a frequency of approximately 2 kHz , therefore the signal output from the lineariser is passed through the auxiliary unit (55D25) and filtered at a -3db cut off frequency of 2 kHz.

The signal from the auxiliary unit is then fed to a Digital volt meter (55D30) for measurement of mean velocity and an r.m.s voltmeter (55D35) for measurement of the r.m.s. value of the velocity fluctuation.

The vertical positioning of the probe was carried out remotely using the DISA sweep drive unit (52B01) in conjunction with a stepper motor (52C01) and traverse mechanism (55H01). A photograph of the instrumentation bank is given in fig. [2.6.4] and a schematic layout is shown in fig. [2.6.5].

2.7 Probe Linearisation

As indicated in the previous section, linearisation of the hot wire probe was achieved by means of the DISA (55M25) lineariser. This is a complex piece of apparatus with a fairly comprehensive set-up procedure. In order to simplify this linearisation procedure a computer program, for a BBC micro-computer, was developed that enabled a graphical output of the linearisation to be viewed on a monitor during the set-up procedure. This enabled new probes to be fairly quickly and accurately linearised. Details of this program and the set-up procedure are given in Appendix 2

The probes were linearised such that the hot wire output voltage corresponded to 1/10th of the fluid velocity. The freestream velocity, measured by the Hot wire, was checked against a pitotstatic reading before and after each traverse and if the hot wire velocity was in error by more than 2% the profile was rejected and the probe was recalibrated. Recalibration of a probe already in use involved measuring a set of velocities in the test range, against a pitotstatic and usually only minor adjustments to the "Gain High" and "Exponent Factor" settings on the lineariser was all that was required. It was found, however, that after a period of time, the stability of the probes deteriorated to a point where they developed such a significant drift in their calibration that they became unusable.

2.8 Intermittency Measurement

From the outset of the project it was obvious that one of the most important parameters to be measured was that of intermittency in the transition region. Intermittency was first measured by Townsend (1948) who used the term γ as the intermittency factor and defined it as the fraction of time a given signal is turbulent. For $\gamma = 0$ the flow is laminar all the time and for $\gamma = 1$ the flow is turbulent all the time.

Intermittency is observed in two quite different situations ie, in the breakdown of a laminar shear flow to turbulence, a process which normally occurs over an appreciable streamwise distance, and at the freestream interface of a fully turbulent shear flow where the interface of the turbulence fluctuates with time so that over an appreciable cross-stream distance, the flow alternates between turbulent and substantially irrotational motion. It is the former of these two situations which the present investigation is primarily concerned.

There are various methods by which the intermittency factor can be measured. One of the first methods used by Townsend (1948), Klebanoff (1955) and Sandborn (1959) was that of the flatness factor. The flatness for u' is given as:

$$\text{flatness factor} = \overline{u'^4} / (\overline{u'^2})^2 \qquad \text{..........} \qquad 2.1$$

As the probability distribution of the interface between the turbulent and non-turbulent fluid is approximately Gaussian, then near the wall, where the intermittency is unity, the flatness factor corresponds closely to the Gaussian value of 3.0. By considering the intermittency as an on/off process the value of γ can then be found from

$$\gamma = 3 / (\overline{u'^4} / (\overline{u'^2})^2) \qquad \text{..........} \qquad 2.2$$

Other methods developed along the lines of Corrsin & Kistler (1954), which are popular with more recent researchers, Sharma, Wells et al (1982), Murlis et al (1982), are usually termed on/off Velocity-intermittency methods. The basis of these methods is to modify the hot wire signal to enable distinct discrimination to be made between laminar and turbulent flow regimes. A schematic diagram of this process is shown in fig. [2.8.1]

Fiedler & Head (1966) have had some success in measuring the intermittency through a turbulent boundary layer using a photo-cell instead of a hot wire anemometer to obtain the basic signal. Smoke is introduced into the boundary layer and illuminated by a light normal to the surface making a cross-section of the boundary layer visible. The relative illumination of the boundary layer and free-stream are then detected by a photo cell and the output from this photo cell is passed through the same intermittency measuring circuitry as used for the hot wire signal shown in fig.[2.8.1 (b)].

More recently Murlis et al (1982) have developed a temperature-intermittency scheme using a cold-wire and a heated plate. The advantage of this is that the temperature in a heated flow is larger than that in the freestream everywhere within the turbulence, unlike velocity-intermittency schemes where the discriminating fluctuating velocity of the turbulence can be negative as well as positive and even the square of the fluctuating velocity component will have occasional zeros.

The latter two methods mentioned above have been developed for measurement of the intermittency distribution through a turbulent boundary layer and it is doubtful if they would be of any use when making intermittency measurements in a region of breakdown from laminar to turbulent flow.

For this reason, and the fact that hot wire instrumentation and a DISA APA system were readily available, an on/off velocity-intermittency system was developed for the measurement of intermittency for this investigation. A circuit diagram of the hot wire signal modifier is shown in fig. [2.8.1 (a)].

The signal modifier consists of 3 parts:

(i) Removal of the D.C. component of the hot wire signal leaving only the time dependent velocity signal.

(ii) Amplification and full wave rectification of the signal.

(iii) Removal of the zeros and smoothing to give an approximate square wave.

The signal from the signal modifier is then passed to the DISA comparitor (52B10) which is fed with a triggering level. The comparitor produces 5v time dependent pulses corresponding to the approximate square pulses produced by the signal modifier as shown in fig. [2.8.2 (a)]. This signal is then passed to an averaging D.V.M. which gives a reading of 5v for $\gamma = 1$ ie all the modified signal is above the triggering level, and a reading of Ov for $\gamma = 0$, ie all the modified signal is below the triggering level. Values in between Ov and 5v correspond to intermittency values between 0 and 1.

In practice the triggering level was set for each flow by visual observation, on a dual beam oscilloscope, of simultaneous traces of the modified hot wire signal and corresponding triggered signal from the DISA comparitor.

Arnal (1984) noticed that in high freestream turbulence and adverse pressure gradient flows the intermittency is less easily discriminated. This is because of high amplitude, but low frequency disturbances that are present in the laminar portion of the flow making the choice of an appropriate detection signal unclear. This problem was overcome by passing the "raw" hot wire signal through a 50-100 Hz HP filter, depending on the flow, before passing it to the signal modifier.

This effectively filters out the low frequency signal leaving prominent turbulent bursts which can easily be discriminated from the surrounding laminar flow as shown in fig. [2.8.2 (b)]. Fig. [2.8.2 (c)] shows a comparison between the filtered hot wire signal and the modified signal and as can be seen from this figure the "approximate" square wave pulses from the signal modifier correspond to the turbulent bursts from the filtered signal.

2.9 Measurements of Cf using a Preston tube

The Preston tube is essentially a circular total head and static tube pair, details of which are given in fig. [2.9.1]. The differential pressure measured between the two tubes can then be converted to a wall shear stress and skin friction coefficient using the calibration of Patel (1965).

$$\text{ie } y^* = 0.8287 - 0.1381x^* + 0.1437x^{*2} - 0.0060x^{*3} \quad \ldots\ldots\ 2.3$$

$$\text{for } 1.5 < y^* < 3.5$$

$$\text{or } y^* = 0.5x^* + 0.037 \quad \ldots\ldots\ 2.4$$

$$\text{for } y^* < 1.5$$

$$\text{where } x^* = \log_{10} \frac{\Delta P_p . d^2}{4\rho\nu^2} \quad \text{and } y^* = \log_{10} \frac{\tau_o . d^2}{4\rho\nu^2}$$

ΔP_p - Preston tube pressure differential

d - Preston tube external diameter

The local skin friction coefficient can then be calculated from:

$$Cf = \frac{2\ \tau_o}{\rho U_\infty^{2}} \qquad \ldots\ldots\ldots\ldots \qquad 2.5$$

Details of the Preston tubes used are given by Fraser (1979).

Only a limited number of measurements using the Preston tube were made throughout the duration of the experimental investigation. The values of skin friction coefficient obtained from these measurements were mostly used as an independent check on the values obtained directly from the universal turbulent boundary layer profile and from the correlations of Ludwieg and Tillman (1950) and White (1974). Details of these are given in Chapter 4.

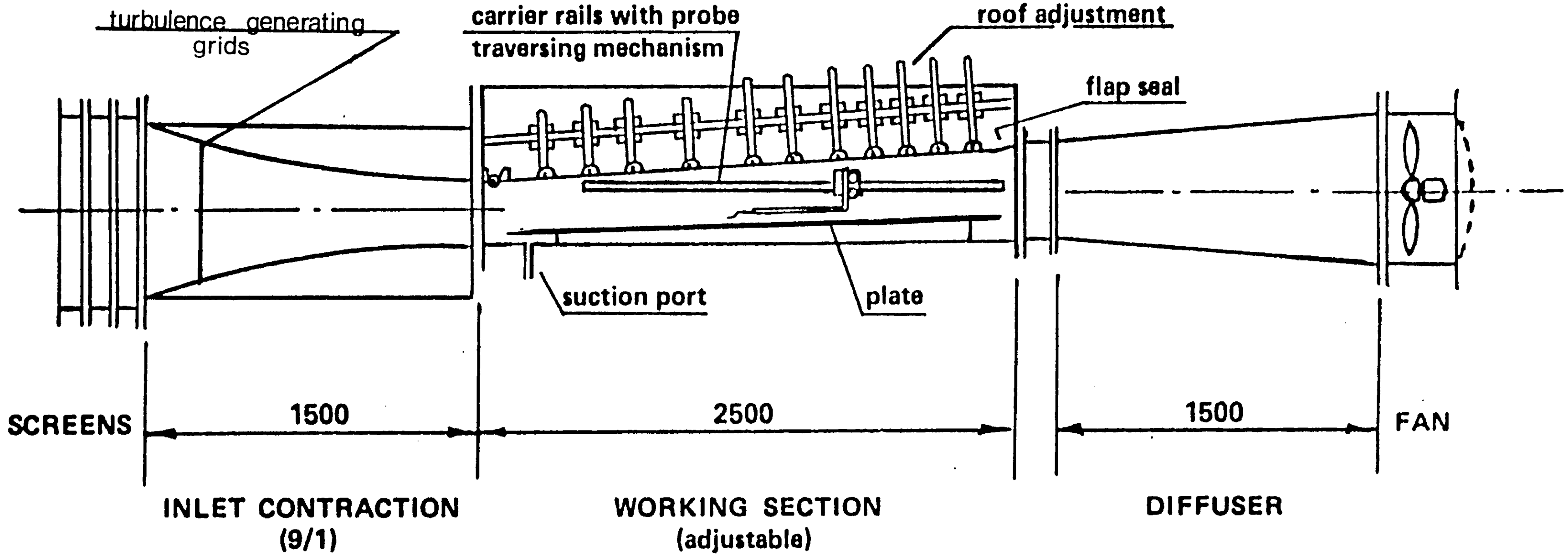

Fig. 2.1.1 Schematic layout of Boundary Layer Wind Tunnel

Fig. 2.1.2 Probe Traversing Mechanism

Fig. 2.2.1 Leading edge geometry

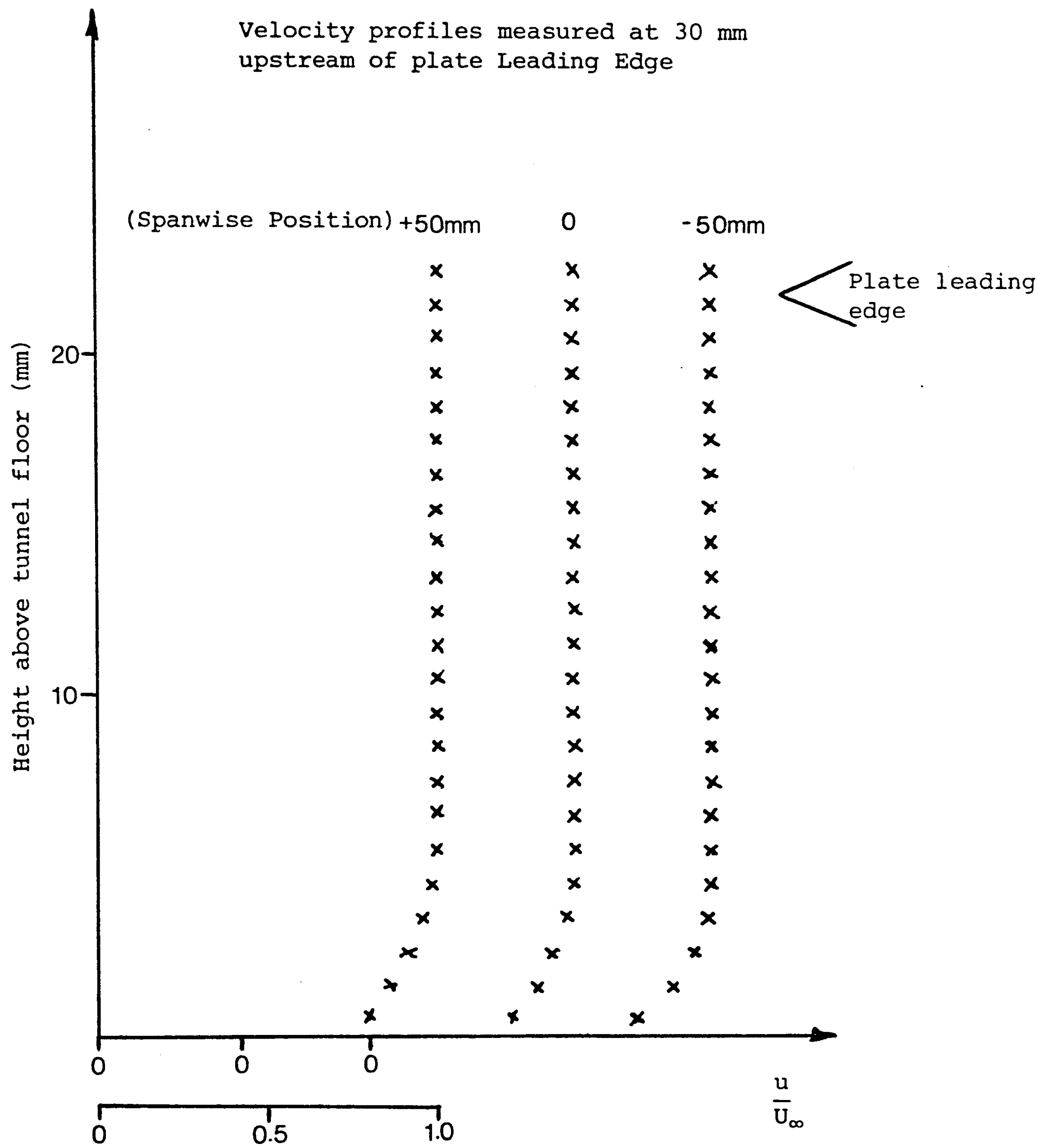

Fig. 2.2.2 Leading Edge Approach Velocity profiles

Plan View of flat plate

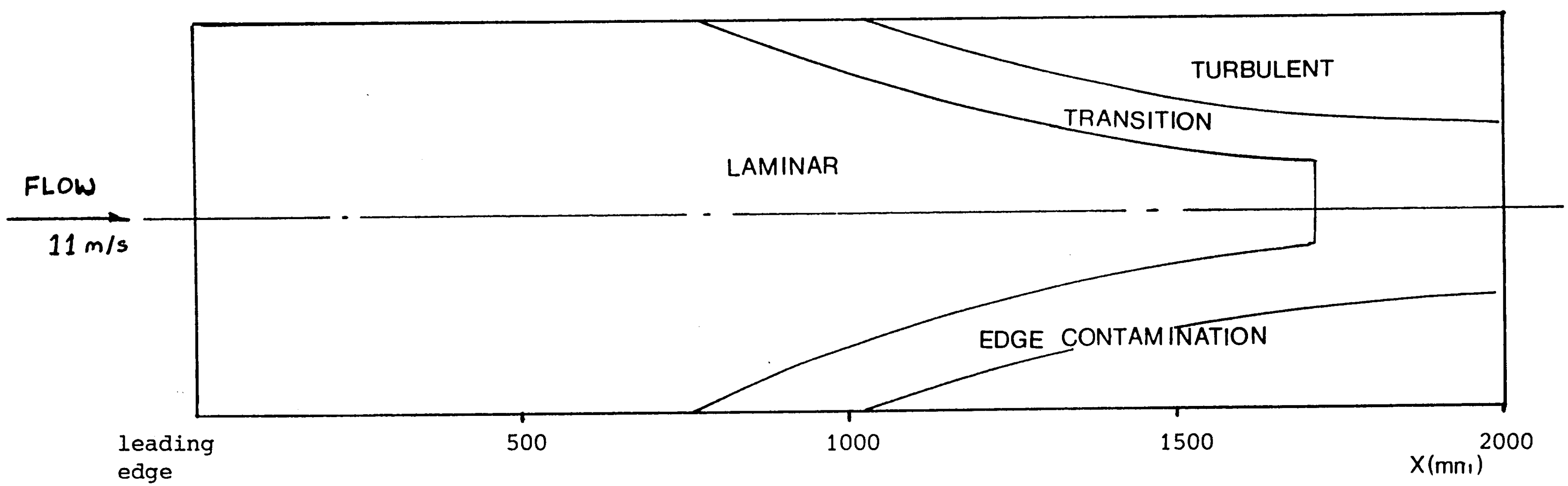

Fig. 2.3.1 Tunnel side wall disturbances

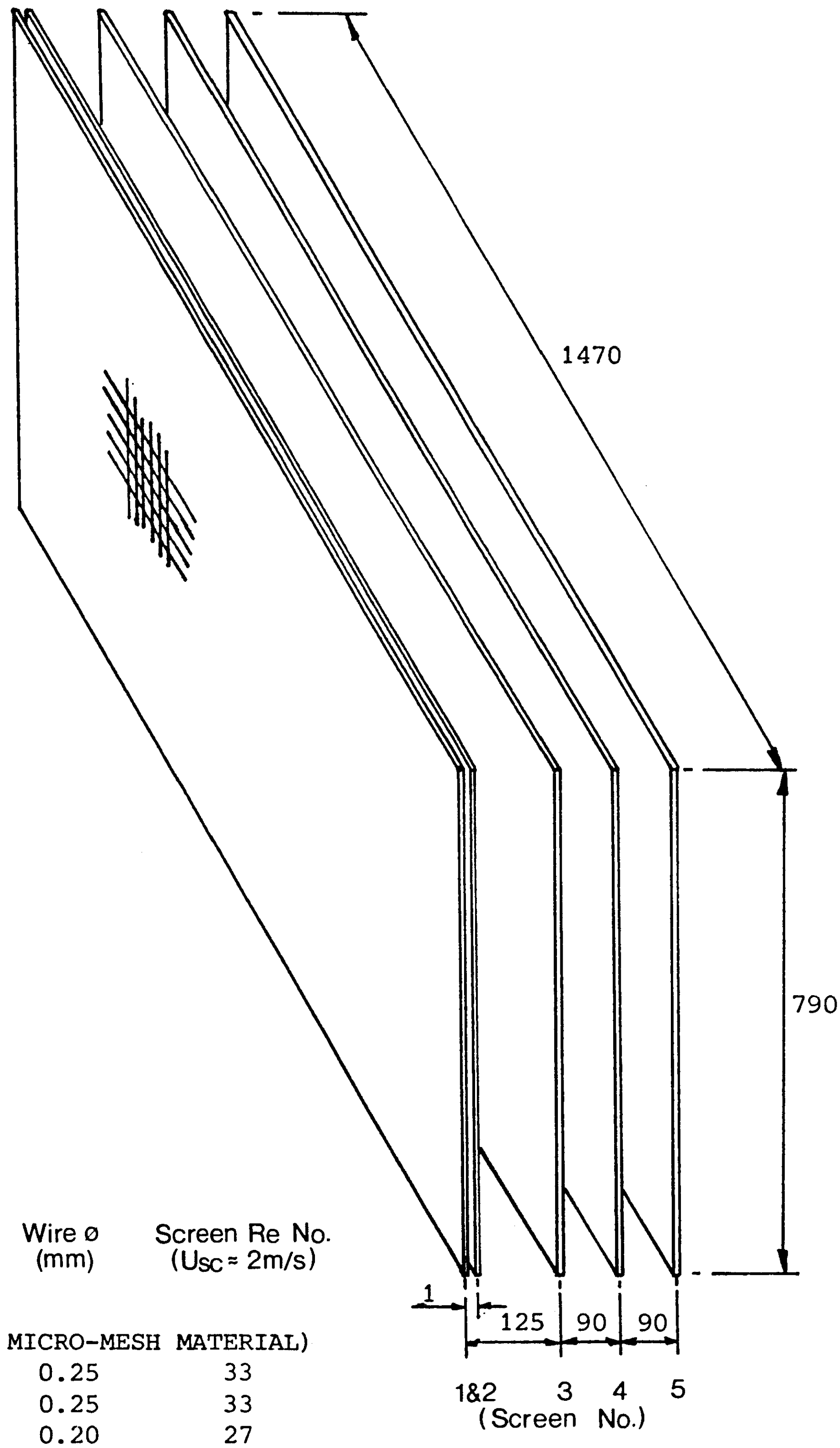

Screen No.	Mesh	Wire ø (mm)	Screen Re No. ($U_{SC} \approx 2m/s$)
1	(NYLON MICRO-MESH MATERIAL)		
2	20x20	0.25	33
3	20x20	0.25	33
4	30x30	0.20	27
5	40x40	0.15	20

Fig. 2.3.2 Turbulence Damping Screen Details

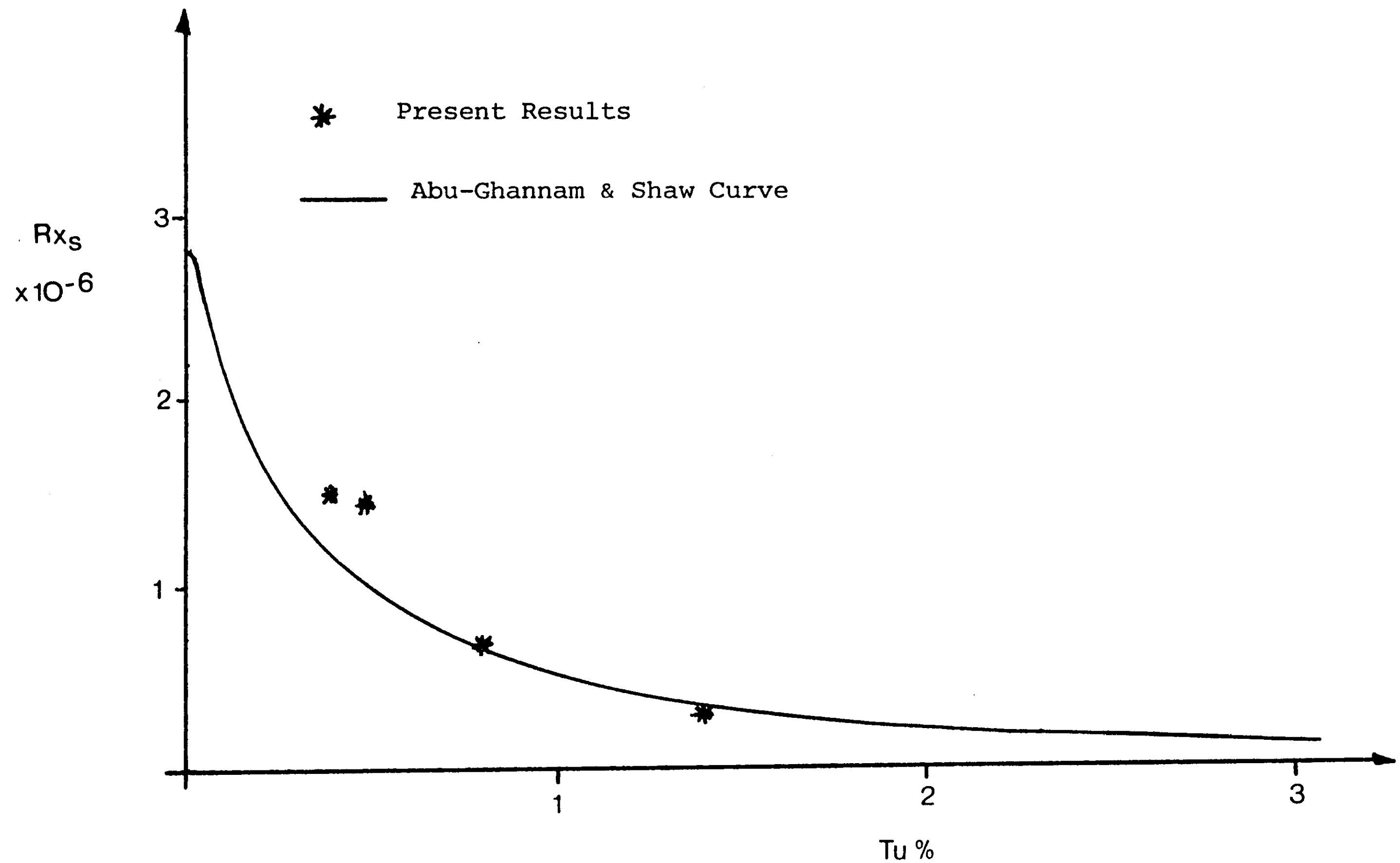

Fig. 2.3.3 Graph of Rx_S against Tu% for Zero Pressure Gradient Flows

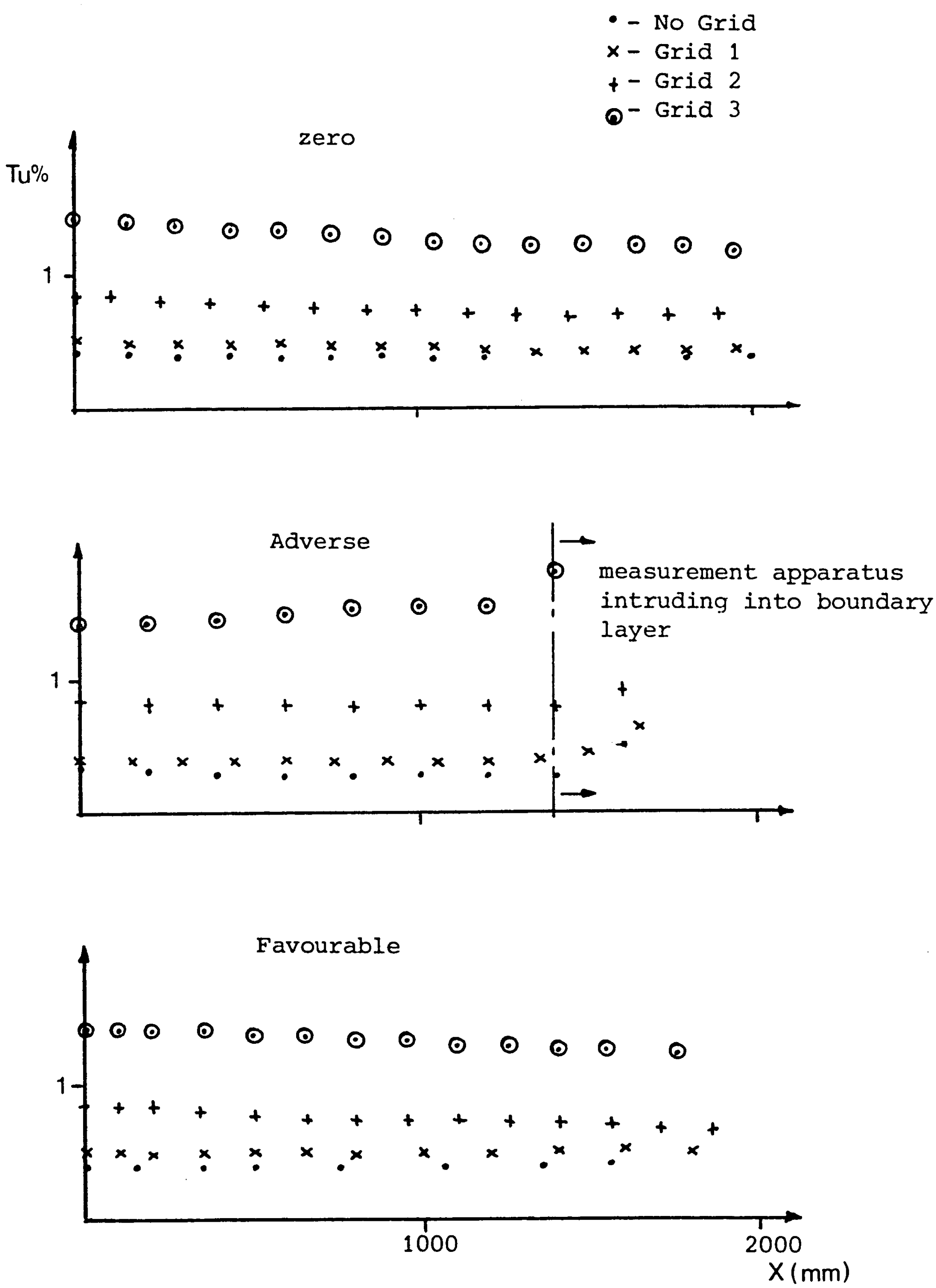

Fig. 2.4.1 Turbulence distributions along plate

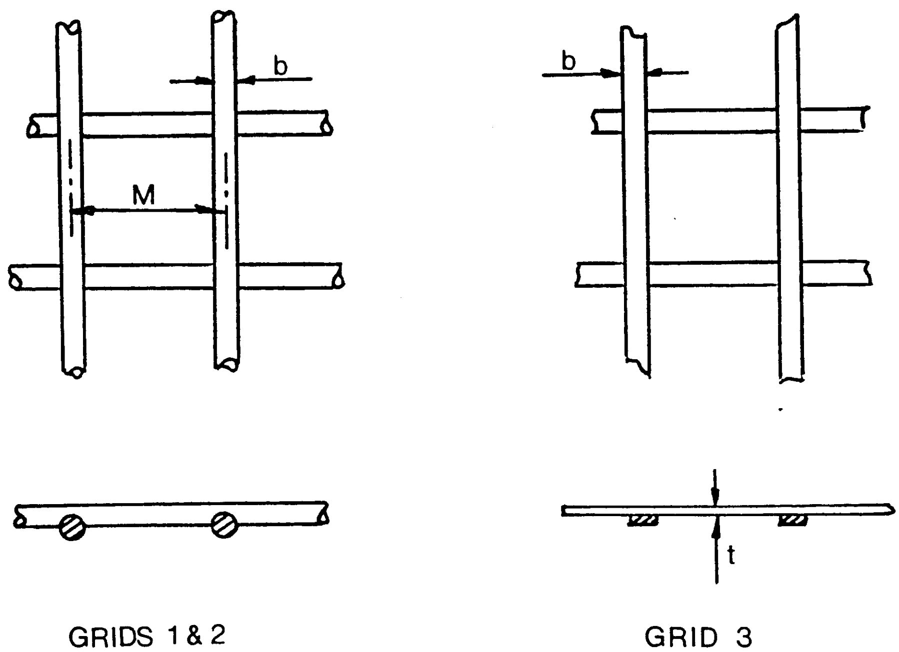

GRID No.	b	M	t	M/b	% Open Area
1	2.5	25	-	10	82
2	5.5	25	-	4.55	63
3	12.5	38	6.25	6.25	47

Fig. 2.4.2 Details of Turbulence Generating Grids

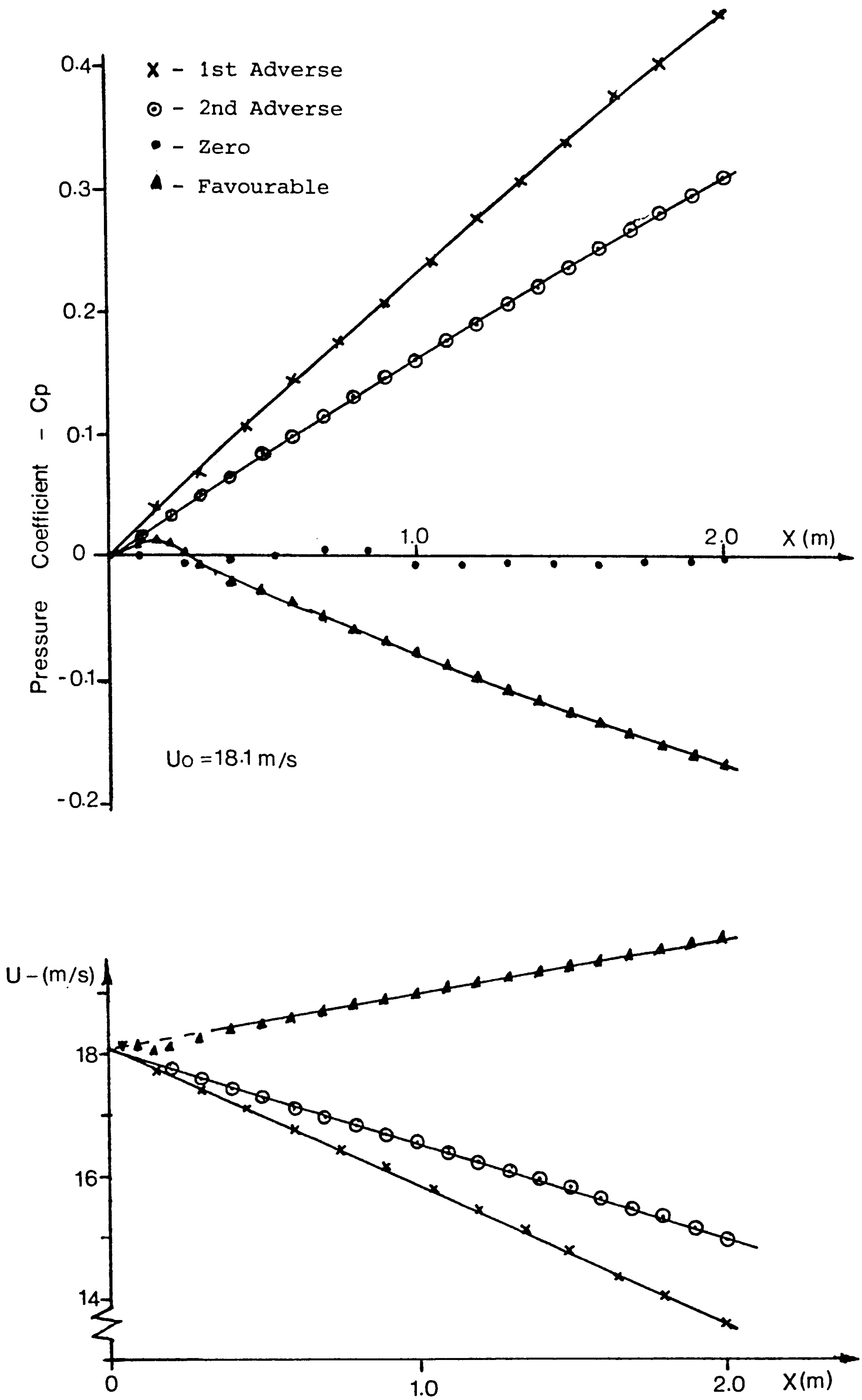

Fig. 2.5.1 - Details of pressure Gradients

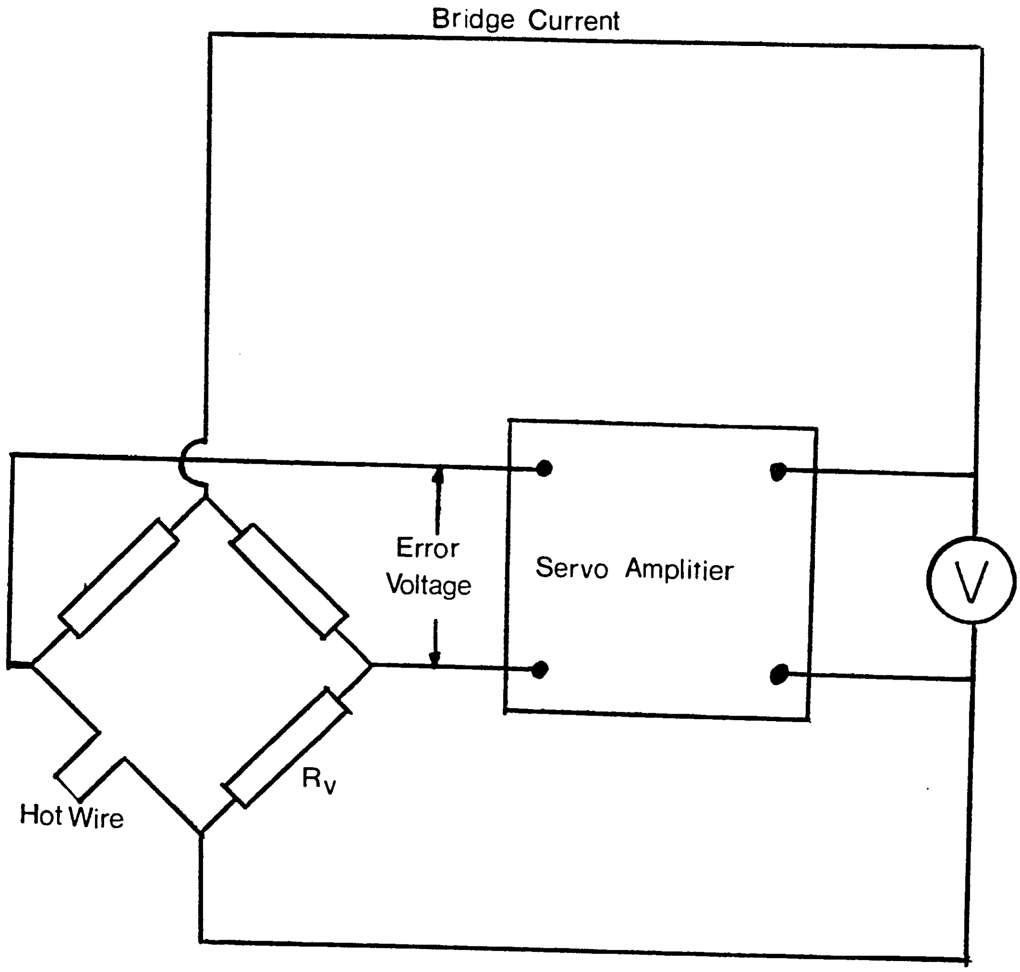

Fig. 2.6.1 Schematic diagram of Constant Temperature anemometer

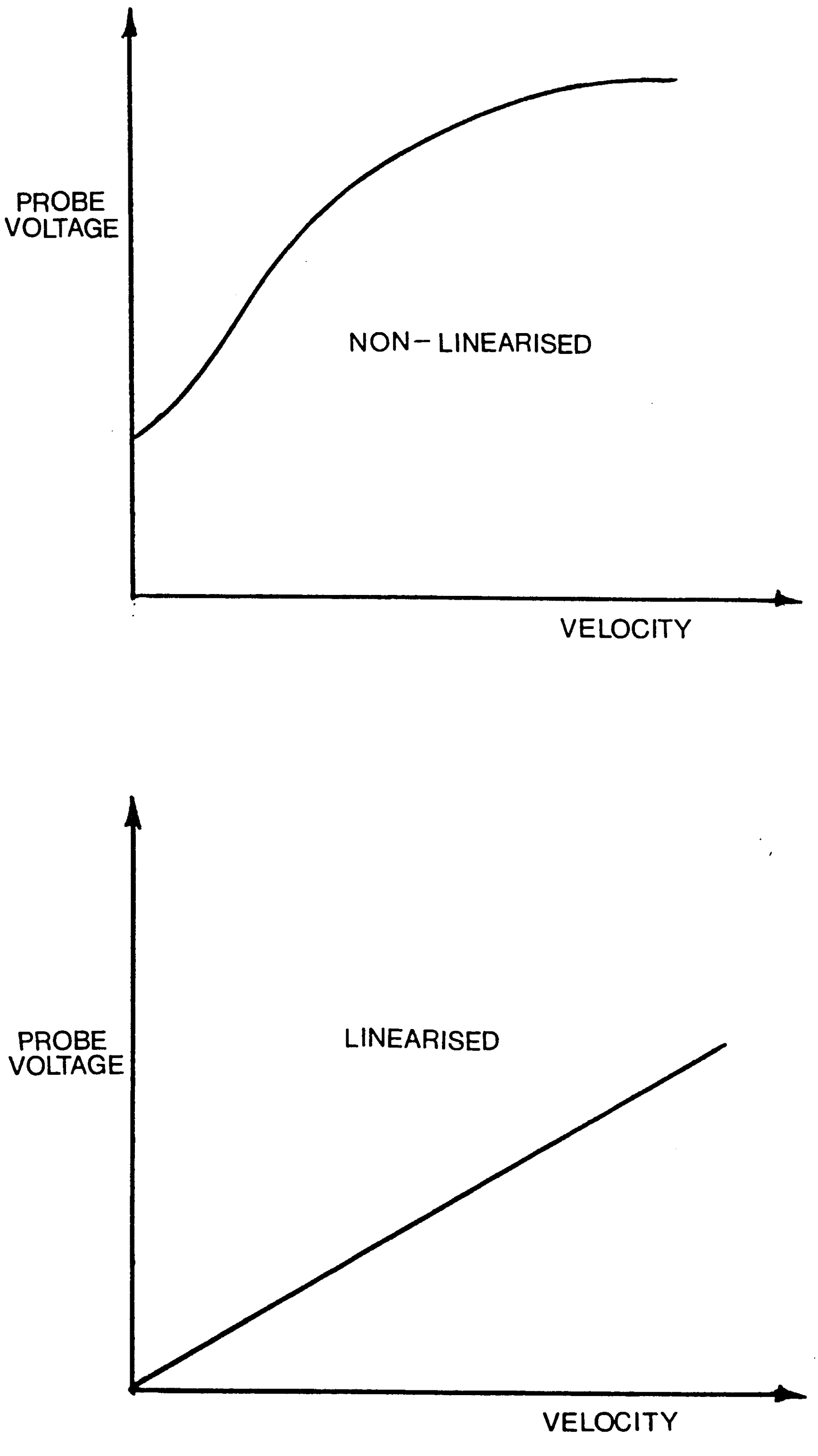

Fig. 2.6.2 Pictorial representation of linearised and non-linearised hot wire probes

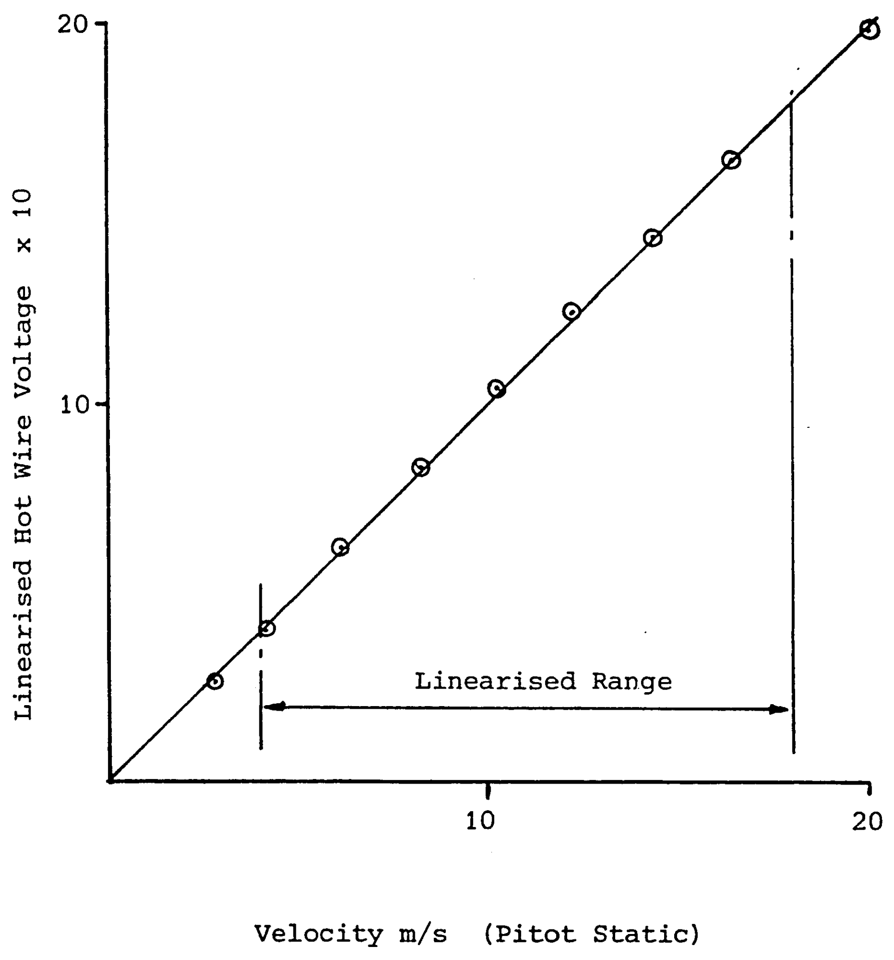

Fig. 2.6.3 Hot Wire Calibration Curve

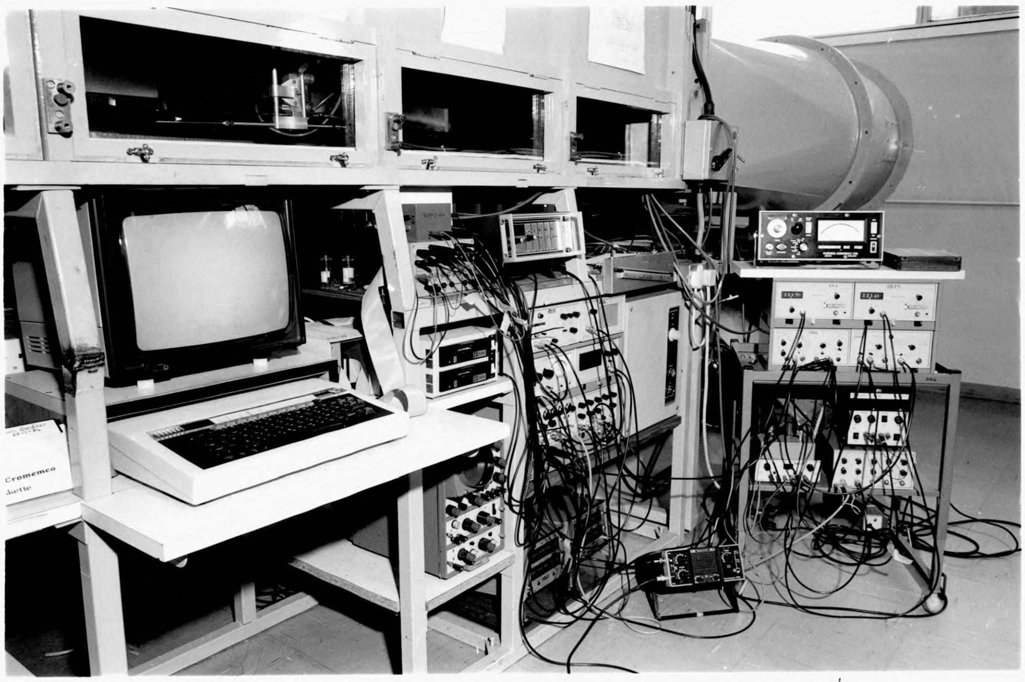

Fig. 2.6.4. Hot Wire Apparatus

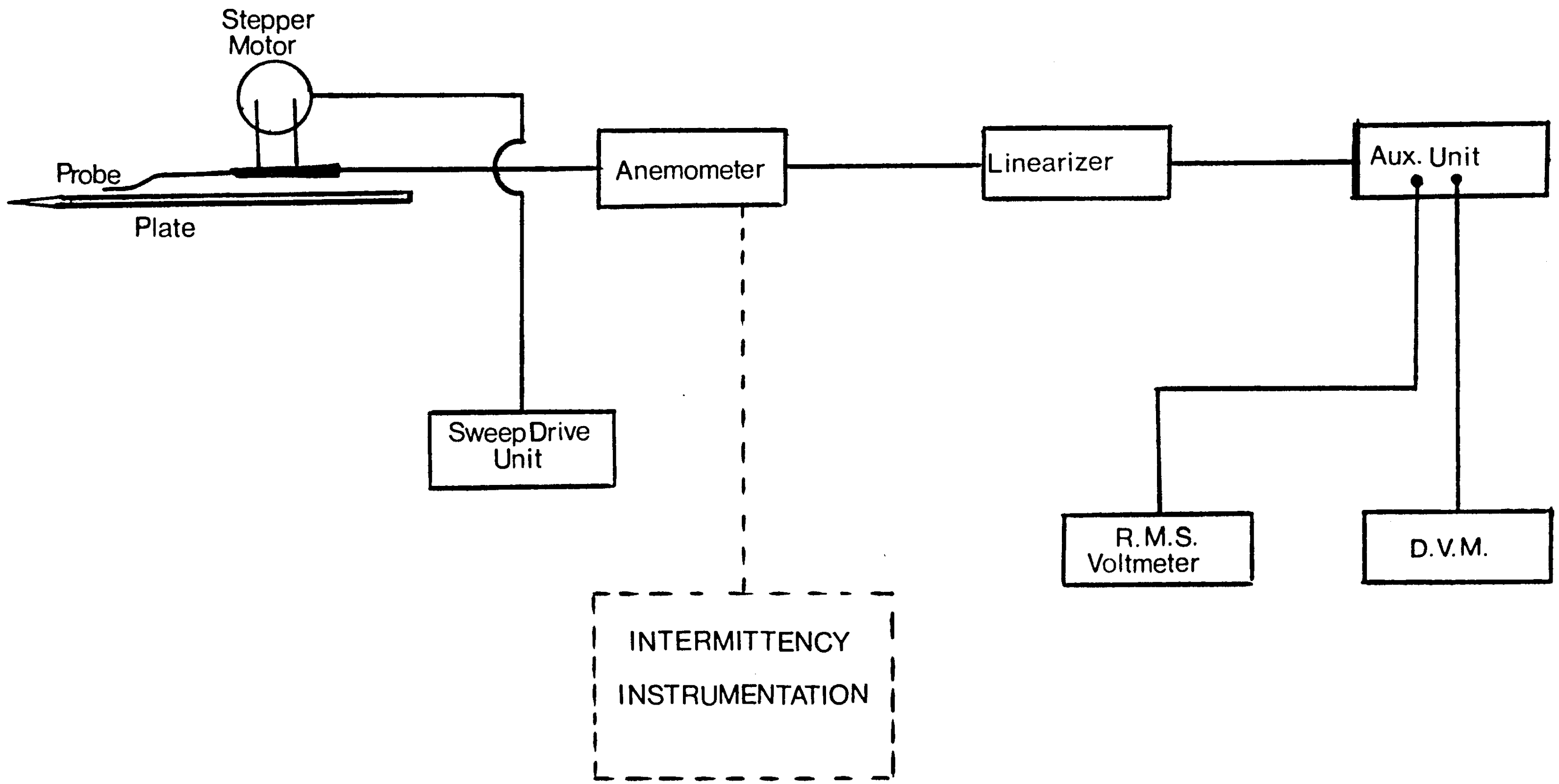

Fig. 2.6.5 Schematic layout of Hot Wire Apparatus

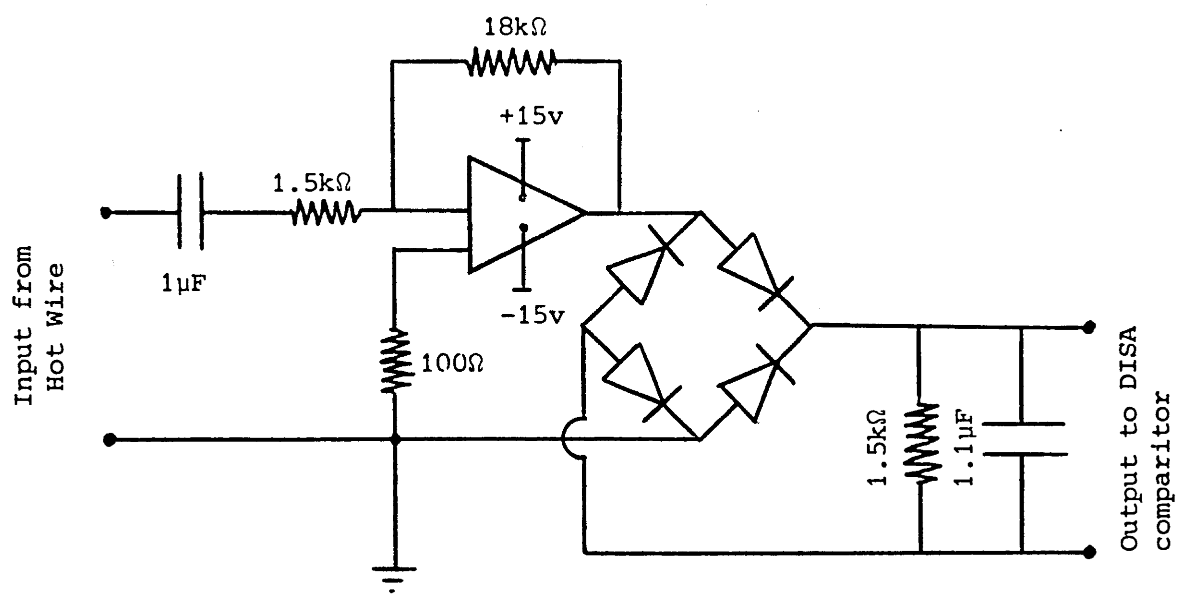

Fig. 2.8.1 (a) Circuit diagram of signal modifier

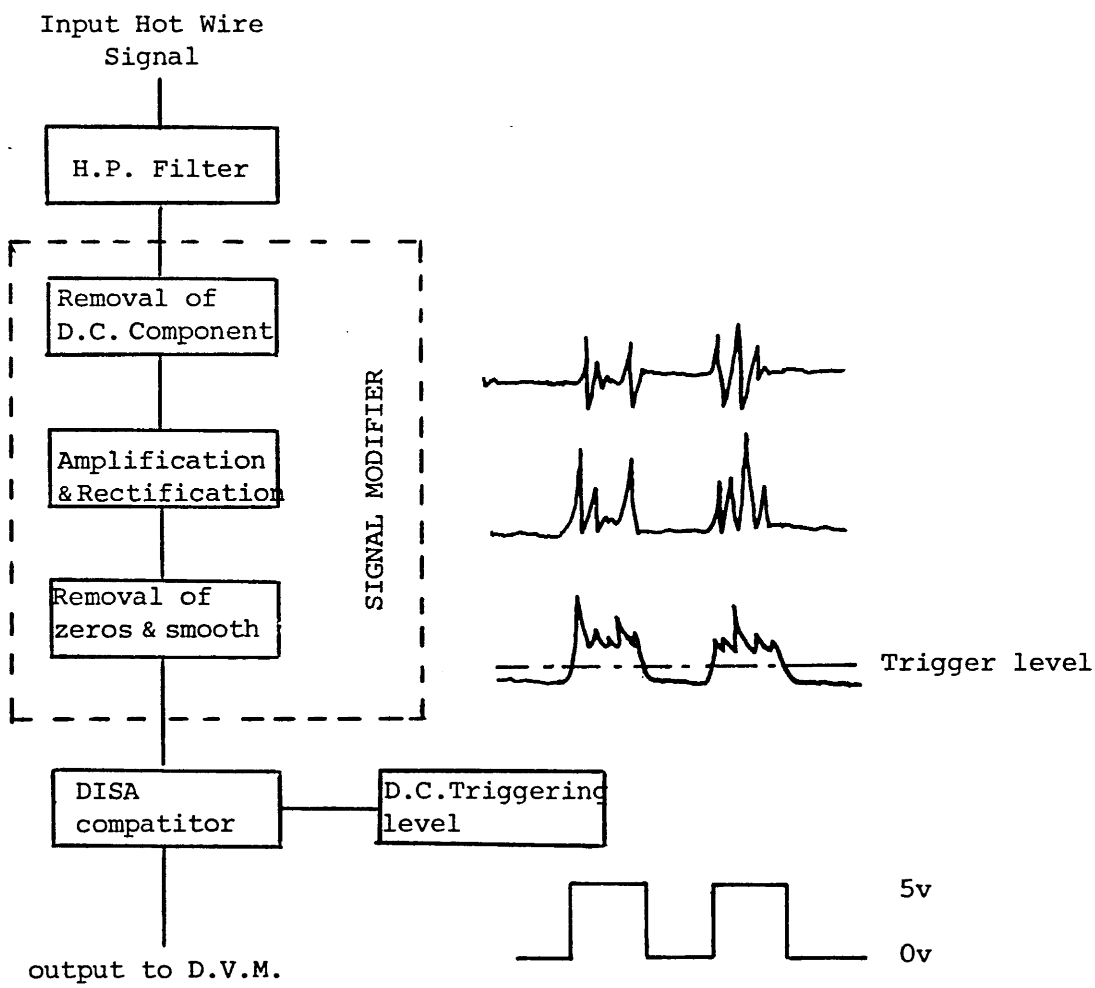

Fig. 2.8.1 (b) Schematic layout of intermittency meter with typical signal outputs

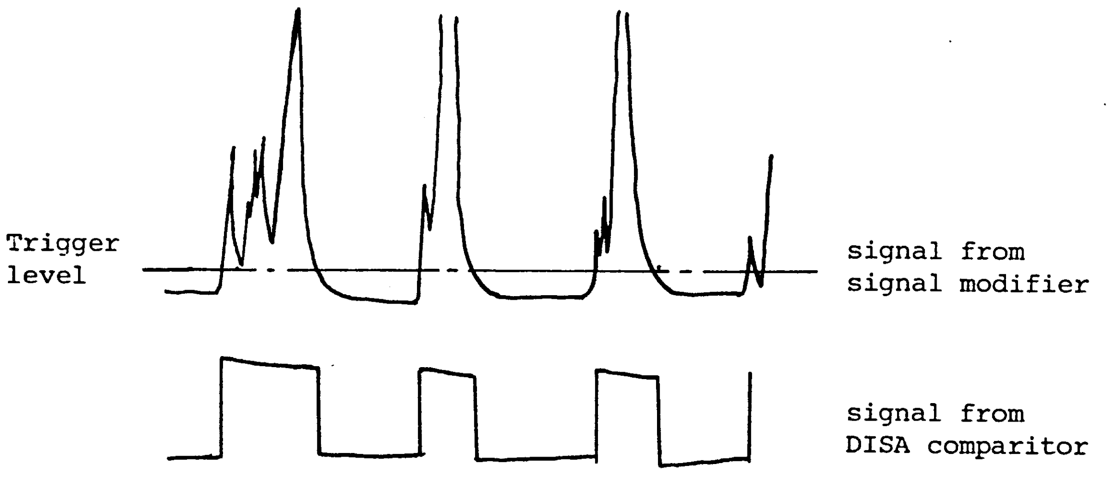

Fig. 2.82 (a) Comparison between modified signal and signal from DISA comparitor

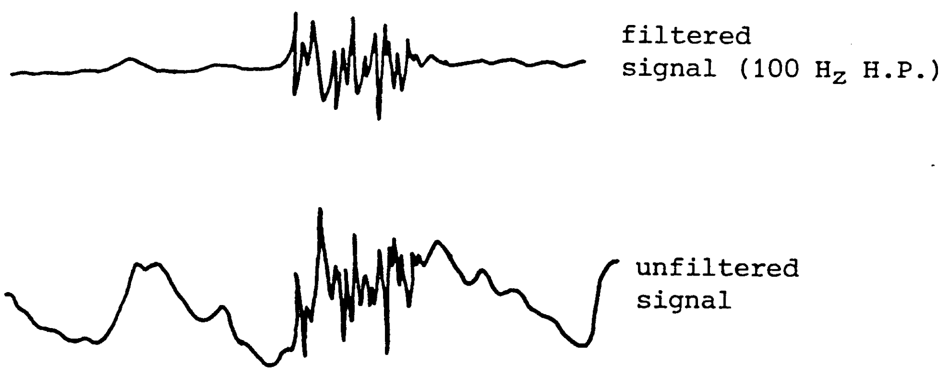

Fig. 2.8.2 (b) Comparison between filtered and unfiltered Hot wire signals

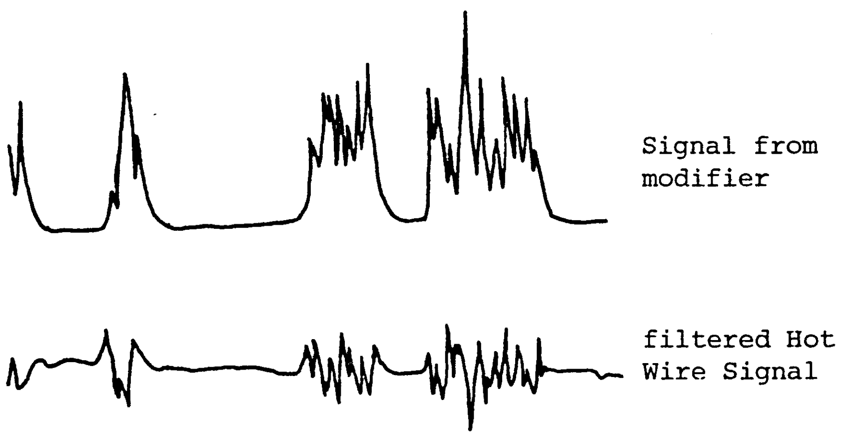

Fig. 2.8.2 (c) Comparison between signal from the intermittency signal modifier and the filtered Hot wire signal

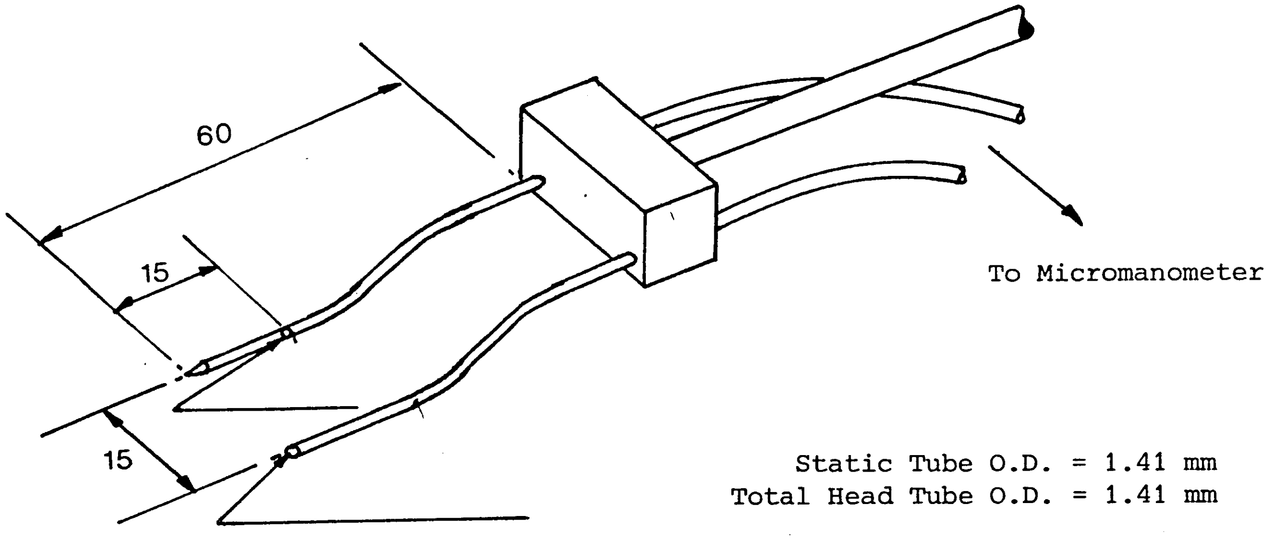

Fig. 2.9.1 <u>Details of Preston Tube</u>

CHAPTER 3

Microcomputer Data Acquisition and Control

3.1 Introduction

The microcomputer has, over the last decade, become an important element in measurement and control systems although, in the early stages of their development, microcomputers were regarded as nothing more than toys by "mainframe and mini" users. Their recent increase in stature has come as a result of improved speed and memory capability enabling the traditional engineering data logging and processing systems to be replaced by much more versatile microcomputer systems. The prime benefits of microcomputer based systems are that they can perform tests quickly with good repeatability and, as well as collecting data, can process this data with very little delay. The processed results can then be displayed using the inherent powerful graphics usually associated with good microcomputers, and a hard copy of the display can be obtained direct from the printer using a "screen dump" program or from a graph plotter connected to the microcomputer. A further advantage of microcomputer control and data acquisition systems is that alterations can normally be made easily by changing software to modify parameters rather than physically changing hardware.

The design and development of a microcomputer control and data acquisition system for application to experiments on transitional boundary layers, including the signal conditioning instrumentation and the computer hardware and software, is described in the following sections.

3.2 Transmission of Data

One of the first considerations in selecting a microcomputer to be used for a data acquisition system is how the data is to be acquired by the computer. There are various methods of passing information from instruments such as a DVM or signal generator to the microcomputer; one method is via a common digital transmission standard, for example the IEEE-488 bus which was developed to allow standardised interconnection of the increasing number of *intelligent* instruments used in laboratories. With this transmission standard the microcomputer becomes the *controller* capable of monitoring devices termed *listeners* which receive data over the IEEE-488 bus and *talkers* which transmit data on the bus. Another standard bus is the serial type RS232 which is normally associated with peripheral equipment such as VDUs and printers.

If the instrumentation, or microcomputer, is not equipped with an interface to allow connection to one of these standard bus structures but the instruments have analogue outputs related to the physical quantities being measured, then a cheaper and probably more common method of passing information to the microcomputer is via an analogue-to-digital converter or ADC. This device, as the name suggests, converts an analogue signal to a digital signal that can then be processed by the microcomputer. Many microcomputers now have built in *on board* ADCs but those that do not, usually have the facility to enable peripheral devices such as ADCs to be *added on* by direct connection to the machine's bus structure.

The DISA 5600 series hot wire anomometer equipment has an interface to allow digital information to be passed over the IEEE-488 bus but the 55M series described in Chapter 2, and used in this investigation has no such facility. It does however output voltages which are representative of the quantities being measured enabling measurements from this equipment to be passed to the computer via an analogue-to-digital converter.

3.3 Data Acquisition

The rate at which data acquisition systems function may range from daily sampling to sampling in short MHz bursts and will depend very much on the signal being analysed, the information required from the signal and the technique used to extract data from the signal. Arnal (1977), Shaw et al (1983) and Castro (1984) used very fast analogue-to-digital conversion techniques to store turbulent and transitional hot wire signals in the form of digital data in the computer memory with subsequent analysis of this data to give values of mean velocity, rms of the fluctuating velocity component and, in the case of transitional flows, intermittency. To ensure that the computer reconstructs the correct waveform from the digital data it is required that the sampling rate is at least twice as fast as the highest frequency component in the signal (Shannon sampling theorem), hence the need for very fast ADC when digitising turbulence signals which may have frequency components as high as 2 kHz. (Jarvis (1985) suggested that for most engineering purposes the sampling rate should be at least 5 times the highest frequency component in the signal).

The advantage of storing a complete digital signal is that, provided the data is stored in a retrievable form, further analysis of the signal can be performed at a later date without having to reconstruct and remeasure the flow.

Apart from the *expensive* fast ADC required, a disadvantage of this technique, especially when using microcomputers, is the large amount of computer storage required to store a small sample of a digitised turbulence signal. For example; in the experiments carred out by Shaw et al (1983) the signal is being sampled at 20 kHz and since each data point or digital number occupies 2 bytes of computer memory then the 32 k bytes of memory (RAM) available on the BBC microcomputer would be completely allocated after 0.8s. In a transitional flow this would hardly be enough time to obtain a representative sample of the signal for subsequent processing.

Another method of obtaining information such as rms of the fluctuating velocity, intermittency, etc from the hot wire signal, which is more suited to the microcomputer, is to first pass the hot wire signal to analogue type instruments which measure the physical quantities required and output related voltages. The output voltages can then be passed, after conditioning, to the microcomputer via an analogue to digital converter as before. To increase the accuracy of this method a large number of samples from each device can be averaged with only the mean value being stored in the computer memory. The mean value of the fluid velocity can also be obtained by this method directly from the linearised hot wire signal by sampling at frequencies which can be much lower than those suggested by the Shannon Sampling Theory, Arnal (1977). The reason for this is the *quasi-steady* nature of the hot wire signal from a transitional or turbulent flow, ie *the frequency and amplitude of the signal are non-uniform but the signal does have a time steady average value.* Therefore, provided the sample frequency is regular and a reasonable number of values are averaged, an accurate value of mean velocity will be obtained even for low sample rates.

When using a microcomputer this method has the advantage of addressing very little RAM for the storage of data as only mean values are actually committed to memory. The sampling rate does not need to be very fast as the signal is not being digitised, therefore cheaper ADCs can be used and can be accessed in a high level language such as BASIC giving the added advantage of simplifying the software.

Initial tests in a turbulent jet flow using the DISA 55M series equipment and a Cromenco Z - 2D microcomputer fitted with two different types of analogue-to-digital converters were conducted to confirm that reliable mean values of velocity and rms of the fluctuating velocity could be obtained from the hot wire signal in a highly turbulent flow using fairly slow sample rates.

The two analogue-to-digital converters used were a 12 bit dual slope integrating converter and an 8 bit successive approximation type converter. The 12 bit 3D INLAB R-12ADS dual slope converter is an integrating type and operates by charging a capacitor for a fixed time interval then a clock and binary counter are used to count the time taken for the capacitor to discharge. The conversion rate of this type of converter is very slow. The converter being used has a conversion rate of only 5 Hz, but an advantage of this method, due to the integrating effect of the converter, is that the influence of high noise levels on a signal are eliminated.

The successive approximation converter operates on an entirely different principle. This is a counter type converter and its main components are a counter, a comparitor and a Digital to Analogue Converter (DAC). When an analogue signal is fed into the converter the counter starts to count and passes a digital value to the DAC, starting with the most significant bit (MSB). The output from the DAC, is then compared to the analogue signal being measured and if the signal is greater than the output from the DAC the "1" in the MSB of the counter is retained. If the signal is lower then the "1" in the MSB of the counter is removed. This process is repeated until the DAC output compares with the analogue input signal. This type of converter has a much faster rate of conversion than the integrating type described above, typically 100 ms, but when accessing the ADC in Basic using the CROMEMCO Z - 2D micro, the maximum sample rate is only 30 Hz.

The initial investigation using the apparatus shown in fig. [3.3.1] with the 8 bit successive approximation converter demonstrated that the principle of averaging mean values from analogue devices by digitally sampling and averaging their outputs could be used successfully as excellent agreement was achieved between the instrument analogue displayed value and those obtained from the microcomputer, with the ADC system.

Surprisingly when using the 12 bit integrating ADC, the results obtained were poor. The values obtained by digitally sampling and averaging the signal were consistently below those read directly from a voltmeter. It was thought that this lack of agreement was due to the large conversion time required by this converter and it was concluded that this converter would be of little use when measuring rapid fluctuating signals, such as the signal from a hot wire probe in a turbulent flow.

3.4 Choice of microcomputer

As the microcomputer chosen was to be dedicated to this project, the main constraints on the choice were the cost, availability, and the fact that it was to be interfaced to the DISA 55M series hot wire equipment already available within the department. Although the Z - 2D cromemco microcomputer, used for the initial turbulent jet study described in the previous section, is a very powerful microcomputer which has the facility to be programmed in a number of high level languages such as FORTRAN and ALGOL as well as the usual micro language BASIC, it was not considered suitable for this project mainly because it was extensively used by undergraduates. This made it essentially unavailable, but it was also rejected because of its large physical size, the fact that it was not particularly reliable and had only modest graphics.

A wide range of smaller but more suitable microcomputers, which are relatively inexpensive, are now available on the market; one such computer is the BBC Microcomputer. Because of its growing popularity in educational establishments and the fact that it has an on board 4 channel, 12-bit analogue to digital converter and an easily accessible 8-bit user port to facilitate the control of peripheral devices, it seemed a natural choice. The BBC microcomputer also has the advantage of an extended high level BASIC with excellent file handling facilities and colour graphics. A further asset of the machine is the ease by which commercially available hardware can be *added-on* to the computer, as areas of memory called *FRED* and *JIM*, addressed within the range &FCOO to &FDFF have been specifically reserved for such additions. Communication with these *add-ons* is via the 1M Hz expansion bus where the term 1 MHz simply refers to the speed at which it operates.

A disadvantage of the BBC microcomputer is the limited amount of RAM. This can be overcome however, by using a "dump-CHAIN-retrieve" routine. The BBC BASIC CHAIN command enables a program which is stored on disc to be called from a program being run in the computer memory. The procedure would be to dump relevant data from the initial program to disc, then CHAIN an extension program which is loaded into the machine memory over the original program. This extension program can then retrieve the data and continue with the analysis.

A complete microcomputer system based on the BBC-B microcomputer with a CUMANA 40/80 track switchable double disc drive, an EPSON FX-80 printer and a MICROVITEC colour monitor was purchased at a price of approximately £1100 (1983 prices) and incorporated into the wind tunnel test facility fig. [3.4.1]

Due to the unsuitability of the BBCs on board ADCs, see section (3.5), it was subsequently found necessary to extend this system by adding the BEEBEX Eurocard mini rack system fitted with the CUBAN-8 DAC card at a further cost of approximately £400. This system is described in detail in section [3.6].

3.5 Accessing Signals on the BBC micro

After the BBC microcomputer had been purchased it was discovered that the built in four channel analogue to digital converter was an integrating type converter which had been shown previously (see Section 3.3) to be unsuitable for measurements in highly turbulent or rapid fluctuating flows. However the BBC *single slope* integrating converter, as described by Bannister & Whitehead (1985), operates at a rate twenty times faster than the (3D INLAB-R12ADS) *dual slope* integrating converter previously tested. For this reason it was decided to persevere further with the BBC on board converters with the knowledge that if problems were encountered more suitable add on ADC systems are available for use with the BBC microcomputer. The four ADC channels available on the BBC micro are accessed in high level BASIC by the command ADVAL (N) where N is the channel number, 1 to 4. This returns a 16 bit value with the four least significant bits set to zero and the true 12 bit number associated with the analogue signal can be obtained by ADVAL (N) DIV16. In actual fact, because of the low reference voltage (1.8V) and the high noise level on the ADC chip, only a 9-bit value can be obtained with any confidence (Beverley 1984). This is not a problem however, as initial tests showed 8-bit resolution to be satisfactory for measurements in turbulent flows although Beverley also showed that greater accuracy could be achieved at the expense of conversion time, if machine code averaging routines are used to reduce the standard deviation of the readings.

The speed at which conversion takes place on a single channel is 10 ms, although this cannot be realised if more than one channel is being used as conversion has to be complete at every channel before the values of any one channel can be read, effectively giving an overall conversion time of 40 ms if all channels are being used. The reason for this is that when the ADVAL command is made the four channels are scanned in reverse order and the values at each channel are not available until the end of conversion on the last channel has been sensed using ADVAL (0). For example; consider the program below to read in 10 values from each channel.

```
10 FOR K = 1 TO 10
20 REPEAT UNTIL ADVAL (0) DIV256 = 1
30 CH1%(K) = ADVAL (1) DIV16
40 CH2%(K) = ADVAL (2) DIV16
50 CH3%(K) = ADVAL (3) DIV16
60 CH4%(K) = ADVAL (4) DIV16
70 NEXT K
```

The REPEAT UNTIL statement ensures that conversion at channel 1, and hence all other channels since they are being scanned in reverse order, is complete before the values are available for reading. Channels can be switched off using the *FX16 command which will effectively speed up the scan rate and hence the rate at which values are available for reading. *FX16,1 will initialise channel 1 only, hence a sample rate of approximately 100 Hz ie 10 ms conversion can be achieved; *FX16,3 will initialise channel 3 but will also switch on channels 1 and 2 therefore a sample rate of approximately only 30 Hz can be achieved if three channels are being used. When accessing the ADC channels in BASIC therefore, channel 1 is the only channel which can sample at rates close to the conversion rate of 10 ms. The rate at which additional channels can be sampled will be a 10 ms multiple of the number of channels switched on.

The ADC conversion rate can be increased further by switching the ADC chip from 12 bit mode to 8 bit mode giving a conversion rate of 4 ms per channel but this is very rarely used because the inherent error present in the 12 bit reading which reduces it to having only 9 bit accuracy is equally bad in the 8 bit reading reducing it to 5 or 6 bit accuracy (Beverley 1985). By far the most serious failing of the on board ADC system, and one which is very difficult to overcome, is the fact that the machine reference voltage, specified at 1.8v, is not constant. When the machine used for this project is powered up, the reference voltage has a value of 1.91v but over a period of about four hours this reduces by about 6% to a value of approximately 1.8v and still does not hold steady at this value but drifts between 1.8v and 1.83v. This is obviously not acceptable for precision data acquisition systems, although it can be allowed for in the software by continually feeding in the measured reference voltage. This is somewhat inconvenient and can introduce unnecessary errors.

After all these problems had been identified the author developed a distinct lack of confidence in the on board BBC-ADC system. This was justified when incorporating the on board ADC into the data acquisition system as it was found that a steady mean value of velocity could not be obtained from the hot wire signal of a steady freestream flow even when averaging 1000 values at the maximum sample rate. For this reason, and the previously mentioned problems associated with the BBC-ADC port, a more effective data acquisition system was obtained employing a separate interface which connects directly into the microcomputer bus structure.

3.6 Accessing Signals using the BEEBEX Eurocard Extension

The interface chosen to enhance the data acquisition system was that termed BEEBEX, supplied by Control Universal of Cambridge, and is a general purpose Eurocard extension unit for the BBC micro. When incorporated into a mini rack system this becomes an extremely versatile method of expanding the BBC micro as a number of Eurocards which include analogue to digital converters, digital to analogue converters, digital i/o, heavy duty industrial opto-isolated i/o etc, become available as hardware extensions. The BEEBEX Eurocard mini rack is plugged into the 1 MHz expansion bus on the BBC micro and is controlled through a specific byte in memory reserved for the BEEBEX system. This is the last byte in the area of memory called FRED and is addressed at &FCFF.

As initial tests had shown that 8-bit accuracy was sufficient for the purpose of this investigation, it was decided to use 8-bit resolution analogue-to-digital conversion Eurocard termed CUBAN-8 for the use with the BEEBEX system. This card was developed jointly by Control Universal and Paisley College Microelectronics Educational Development Centre, see Ferguson et al (1981) for details. The CUBAN-8 card has 16 analogue input channels, 1 analogue output channel, 16 digital i/o channels contained in two 8-bit user ports, termed PORT A and PORT B, and four control lines, all available via a 40 way socket on the edge of the card. To simplify connection to these channels an interface was built which transfers the channel from the 40 way edge socket to 4 mm jack plug sockets. This interface is shown in fig. [3.6.2]. The CUBAN-8 ADC is a successive approximation type, shown previously to be suitable for measurements in a turbulent flow, with an accuracy of ±½ bit and, when using BBC BASIC to access the ADC, has a sample rate of 500 Hz. (The conversion rate of the ADC is specified as 10,000 Hz but this cannot be realised when sampling in BASIC. To achieve sample rates close to the specified conversion rate machine code programs would have to be used).

The easiest method of accessing the CUBAN-8 card,with BBC software for reading data from a particular bit on an output port is to utilise a *sideways ROM* fitted into one of the spare sockets under the Keyboard of the BBC micro. Such a control ROM is supplied by Control Universal and is enabled in the software by the command *IO. When the *IO is initialised, other sideways utility ROMS, if fitted, such as the Disk Operating System are disenabled. Therefore, to use the SAVE, LOAD and CHAIN commands the Disk Operating System must be reinitialised using *DISK. The concept of *IO is that any area of memory outside the BBC micro is treated in the same way as a disc file using OPENUP, PTR# (position pointer), BGET# (Get Byte), BPUT# (Put Byte). When the PAGE and BLOCK switches (see fig. [3.6.2] for location of the PAGE & BLOCK switches on the CUBAN-8 Card) are set to Ø and C then the card is accessed by

```
A% = OPENUP"CU-DAC8 &CØØØ"
```

(the % symbol indicates integer values)

Consider the program overleaf to read in 10 values from channel 1, then 10 values from channel 5.

```
1Ø 10                            - initiate *10 ROM

2Ø CLOSE#Ø                       - precautionary-close all
                                   opened files

3Ø A% = OPENUP"CU-DAC8 & CØØØ    - access CUBAN-8 card

4Ø PTR#A% = 1                    - set pointer to channel 1,
                                   pointer will stay at channel 1
                                   until moved to another channel

5Ø FOR K = 1 to 1Ø

6Ø Value %(K) = BGET#A%          - Get value from channel 1

7Ø NEXT

8Ø PTR#A% = 5                    - set pointer to channel 5

9Ø FOR K = 1 to 1Ø

1ØØ Value%(K) = BGET#A%          - Get value from channel 5

11Ø NEXT
```

The BEEBEX Eurcard system, accessed in BASIC with a sample rate of 500 Hz, was found to be completely satisfactory for the measurements of the flow variables and was a valuable addition to the data acquisition and control system developed.

3.7 Control of the hot wire probe position

The hot wire probe is positioned via a traverse mechanism and stepper motor connected to a DISA (52B01) Sweep Drive Unit (SDU) which is capable of being stopped during a sweep by closing an external switch. The CUBAN-8 card is fitted with a 6522 VIA which contains the 16 i/o digital channels in the form of two 8-bit user ports termed PORT A and PORT B and computer control of the SDU is achieved via the LSB of PORT B. When the LSB is set high a reed relay is energised and the switch closes to stop the SDU. The opposite occurs when the LSB is set low. Details of the reed relay interface are given in fig. [3.7.1].

Initially, the direction in which information is to travel over the bi-directional port has to be set up and this is done via the port Data Direction Register (DDR). Setting all the bits of the DDR to 1 (or High) causes all the bits of the user port to behave as outputs, and setting all bits of the DDR to Ø (or Low) causes all the bits of the user port to behave as inputs. A combination of inputs and outputs can be obtained by setting the relevant bits of the DDR to either 1 or Ø.

For this application the LSB of Port B has to be set to output and this is done by placing a 1 in the LSB of the DDR. In acutal fact all the bits of the user port were set to output by placing a 1 in every bit of the DDR, ie passing the value 255 to the DDR, but the status of the higher 7 bits of Port B is irrelevant as they are not used.

As before if the PAGE and BLOCK switches are set to Ø and C then PORT B of the CUBAN 8 card is addressed as

"BUS &C000"

and the corresponding DDR is addressed as

"BUS &C002"

A program to set all bits of PORT B as output, and output a logic '1' on the LSB is as follows:

```
1Ø*IO                        - enable control ROM
2ØCLOSE#Ø                    - precuationary: close all files
3Øddr%=OPENUP"BUS&COØØ2"     - access DDR
4ØBPUT#ddr%,225              - set all bits of user port to output
5ØCLOSE#ddr%                 - close DDR
6ØPb%=OPENUP"BUS&CØØØ"       - access port B
7ØBPUT#Pb%,1                 - output logic 1 or high level on LSB
                               Port B
```

3.8 Conditioning of signals to suit the BEEBEX system

The fundamental measurements to be made in the present work are those of mean velocity, rms of the fluctuating velocity, intermittency and position normal to the plate surface. These measurements are obtained by sampling the analogue signal outputs from the relevant DISA hot wire instrumentation and passing them to the BBC micro via the CUBAN-8 ADC. To ensure the full range of the ADC is used, ie the full 255 bits for a maximum input of 2.5v, and also that the ADC is not overloaded, the maximum reading expected from each instrument must be conditioned to approximately 2.5v. This is done by passing the analogue outputs from the DISA instrumentation to a FYLDE modular instrumentation rack containing Op. Amps having x0.1 and x1 switched gains with a x10 variable control and digital display monitor.

mean velocity:- The mean velocity is obtained by sampling and averaging the linearised hot wire signal which has been passed through a 2 kHz L.P. filter to eliminate electrical noise.

It is worth noting at this stage the reason why the hot wire signal is linearised directly using the DISA (55M25) analogue lineariser instead of linearising the probes within the computer software. It is known that the calibration of a hot wire probe adheres to Kings Law, equation 3.1:

$$\rho^2 = \rho_o + Bu^{\frac{1}{2}} \quad \ldots\ldots\ldots\ldots \quad 3.1$$

where ρ is the voltage from the hot wire anemometer

ρ_o and B are constants

Therefore, it would have been a fairly simple task to linearise the probes within the software by a least square fit of Kings law to a set of calibration points in order to obtain the constants ρ_o and B. With the constants known this law can then be used to convert averaged values of voltage, obtained directly from sampling the non-linearised hot wire signal, to values of mean velocity.

However, in transitional boundary layer flows this presents problems which arise from the fact that the voltage readings from the hot wire signal are averaged before they are linearised. Dhawan and Narasimha (1957) pointed out that in a transitional flow the mean velocity obtained from averaging instrumentation is not the same as the true mean velocity. This is because the transitional mean velocity is a composite consisting of an intermittency weighted proportion of the laminar and turbulent velocity components, ie

$$\overline{u}_t = (1 - \gamma)\ \overline{u}_L + \gamma \overline{u}_T \ \ldots\ldots\ldots\ldots \qquad 3.2$$

In the case of a pitot tube, which is an averaging instrument, where the reading is proportional to the pressure, ie u^2 then

$$\overline{u}_{p_t} = \{(1- \gamma)\ \overline{u}_L^{\,2} + \gamma \overline{u}_T^{\,2}\}^{\frac{1}{2}} \ \ldots\ldots\ldots\ldots \qquad 3.3$$

which is not the same as the true mean velocity given in 3.2. The same difficulty is extended to measurements using a non-linearised hot wire probe where the reading from the hot wire anemometer is basically proportional to $u^{1/4}$. This difficulty is overcome if the signal from the hot wire is linearised directly by passing it through the DISA 55M25 lineariser thereby obtaining a voltage reading which is directly proportional to the fluid velocity, enabling the signal to be sampled and averaged to give a true mean velocity.

The signal from the hot wire was linearised such that the voltage output from the DISA 55M25 lineariser was equivalent to 1/10th of the fluid velocity. The maximum velocity expected in the planned experiments was approximately 20 m/s which would correspond to an output of 2v from the lineariser, therefore to use the full range of the ADC the output from the lineariser was passed through an amplifier, on the FYLDE instrumentation rack, set at a value of x1.25. A digital value of 255 as read by the computer will now correspond to a fluid velocity of 20 m/s and to convert this digital value back to a velocity for use with the computer software for subsequent processing or display a calibration constant is required which is calculated from

$$\text{max. fluid velocity} = \text{calibration constant} \times 255 \quad \ldots\ldots\ldots\ldots \quad 3.4$$

in this case

$$\text{calibration constant} = \frac{20}{255} = 0.07843 \text{ (m/s)/bit}$$

rms of velocity fluctuation - The rms of the velocity fluctuation is obtained by passing the linearised hot wire signal through the DISA 55D35 RMS voltmeter which has a twelve position rotary switch to select a number of measurement ranges varying from Ø to 1 mv to Ø to 300v fsd and has an analogue output of 1v for fsd which is linearly related to these ranges. The analogue output value can increase to a value of 1.2v if the scale is overloaded, ie the incorrect range is selected, and for this reason the specified output voltage of 1v for fsd is not conditioned to 2.5v, to utilise the full range of the ADC, but only conditioned to 2v to prevent an overload condition damaging the ADC.

The signal is conditioned, as before, by passing it through an amplifier on the FYLDE instrument rack set to a value of x2 giving a digital value of 204 for fsd of the rms meter. The calibration constant is calculated depending on the range selected.

$$\frac{\text{rms range}}{\text{x10}} = \frac{\text{calibration}}{\text{constant}} \times 204 \quad \ldots\ldots\ldots\ldots \quad 3.5$$

(the factor of 10 multiple of the rms range is to convert the rms voltage to an rms velocity since the voltage is linearised to correspond to 1/10th of velocity).

Intermittency - Intermittency was measured using the apparatus shown in fig. [2.8.1] and described in section 2.8. Unfortunately the averaging DVM used for visual display of the intermittency function does not have an analogue output therefore the signal from the DISA 52B10 comparitor, which outputs discrete 5v square pulses, was passed to a true integrator DISA 52B30 set on a low integration time (0.5s). The signal from the true integrator outputs a maximum value of 5v for $\gamma = 1$ therefore the signal from this was conditioned, by passing it through a x0.5v amplifier, to give a maximum output of 2.5v utilising the full range of the ADC and preventing overload. A digital value of 255 as read by the computer will correspond to an intermittency of 100% or $\gamma = 1$ and the calibration constant can be calculated as shown previously.

Vertical Positioning of the hot wire probe - The position of the probe above the plate is determined from the output voltage of the DISA 55D35 Sweep Drive Unit which is basically a variable D.C. ramp generator, the output of which is made proportional to the linear displacement of hot wire probe via a stepper motor and traverse mechanism, fig. [2.1.2]. Calibration of the sweep drive unit, fig. [3.8.1] gives a linear relationship between the voltage and the displacement.

$$y = y_o + K(V - V_o) \quad \ldots\ldots\ldots\ldots \quad 3.6$$

where y is the vertical displacement, in mm, corresponding to V, the displacement voltage and the suffix "o" denotes the datum values. From the calibration on fig. [3.8.1] the value of K = 10.52 mm/volt and as the maximum traverse of the probe in the wind tunnel working section is limited by geometry to approximately 50 mm, the position signal was passed through a x0.5 amplifier giving a maximum displacement of 52.5 mm corresponding to a digital value of 255 as read by the computer. The calibration constants for reconversion of the digital value to position can be calculated from this as before.

A schematic layout of the complete Data acquisition and control apparatus is shown in fig. [3.8.2].

3.9 Development of Data Acquisition and Control Software

This section details the development of the software for the basic data-acquisition and control system used for the measurement of the mean velocity profiles as well as two data acquisition programs for the measurement of the intermittency and freestream turbulence distributions along the plate.

Data acquisition and control code for measurement of mean velocity profiles - The object was, for a particular location on the plate surface and mainstream velocity, to measure the flow variables - mean velocity, rms of the fluctuating velocity and intermittency - at specified step increments through the boundary layer, measured relative to a datum, until the freestream velocity was reached. The probe datum position was set manually using a scaled block placed behind the probe and viewing the probe and block through a cathetometer from outside the tunnel working section. The software was developed to automatically control the experiment from this datum point until a complete boundary layer traverse had taken place.

Firstly the output voltage from the DISA Sweep Drive Unit was read, via the ADC, to determine the digital value corresponding to the probe datum and all other probe positions were calculated relative to this. A number of readings of mean velocity, rms of velocity fluctuation and intermittency were then accessed by the computer, via the ADC, from the relevant instruments before their averages were stored in specified arrays and the probe was moved to the next position. The probe movement was controlled, as described in more detail in section 3.7, by outputting a control signal via the LSB of user port B on the CUBAN-8 6522 VIA. Setting this bit low switches on the sweep drive unit while setting it high switches off the sweep drive unit. Therefore, once all the values have been stored, the LSB of port B is set low thus moving the probe. While the probe is moving the output voltage from the sweep drive unit is monitored by the microcomputer until the output exceeds the value of the datum plus the specified step increment and at this point the LSB of port B is set high and the probe traverse is stopped. The BASIC code for this is:-

```
10 BPUT#Pb,0                                  - LSB of Port B Set Low
20 REPEAT UNTIL BGET#0> (Datum+Step Inc)      - read in value from
                                                channel 0 until > (LIMIT)
30 BPUT#Pb,1                                  - LSB of Port B Set High
```

The actual position in which the probe stopped is then determined by reading in and averaging a number of values of output voltage from the sweep drive unit. The flow variables are then read in again and, once averaged values of each variable have been stored, the probe is moved to the next position. This continues until the freestream velocity is reached, sensed by three consecutive values of mean velocity being within ±0.5% of each other, and the probe traverse is stopped. The freestream velocity is then determined by averaging the mean velocities at the last three positions and the boundary layer thickness is estimated, as the y value corresponding to 99.5% of the freestream velocity, by a linear interpolation routine. Data such as ambient pressure and temperature, distance of the probe from the plate leading edge and spanwise probe position are fed in interactively at the start of the program. This data along with values of the freestream velocity, the boundary layer thickness and values of $^{y}/_{\delta}$, $^{u}/_{U_\infty}$, γ, and rms velocity obtained for each step increment are printed out and then dumped to a disc file. A typical printout of this data is shown in fig. [3.9.1]. A graphics program is then 'CHAINed' which retrieves the data from the disc file and displays the mean velocity data on axes of $^{y}/_{\delta}$ against $^{u}/_{U_\infty}$ along with the Blasius and $^{1}/_{7}$th Power Law profiles for comparison purposes, as illustrated in fig. [3.9.2].

Because of the contrasting shape of the velocity profiles in laminar and turbulent boundary layer flows the program provides the facility to choose the step increments for the upper and lower regions of the boundary layer. These step increments are fed in interactively at the start of the program.

To increase the accuracy at the flow variables 100 values of position, 5000 values of mean velocity (corresponding to a 10s sample time), 1000 values of rms velocity and 1000 values of the intermittency factor were averaged before storing the mean values for one particular point. This takes in excess of 15 seconds and for a typical boundary layer, with say 20 step increments, a complete traverse would take approximately 5 minutes.

A flow diagram of this program is shown in fig.[3.9.3] and a printout is included in Appendix 5

Data acquistion Codes for streamwise freestream turbulence and intermittency distributions - Two data acquisition and operator interactive programs, which do not involve any element of control, were developed to give large sample times for obtaining accurate values of freestream turbulence and intermittency. The intermittency program prompts the operator to position the probe close to the place surface and input the streamwise position of the probe then press RETURN for the values to be read in from the intermittency instrumentation. (10,000 values are read in and averaged giving a mean value of intermittency over a period of approximately 20 seconds). Once the values have been read in and the average value stored in an appropriate array the program prompts the operator to move the probe to the next measurement station and press RETURN again, to read in the values. This continues until the operator is satisfied the run is complete and then presses the 'C' key for this data to be dumped to disc. The data is stored on disc in the form of x and γ values and can be retrieved at any time for subsequent processing.

The freestream turbulence distribution program operates in a similar manner but for this case the probe is placed in the freestream and the rms of the velocity fluctuation and the mean velocity are read in and the freestream turbulence is calculated from

$$T_u = \frac{\sqrt{\overline{u'^2}}}{U_\infty} \times 100$$

A printout of both these programs is given in Appendix 5

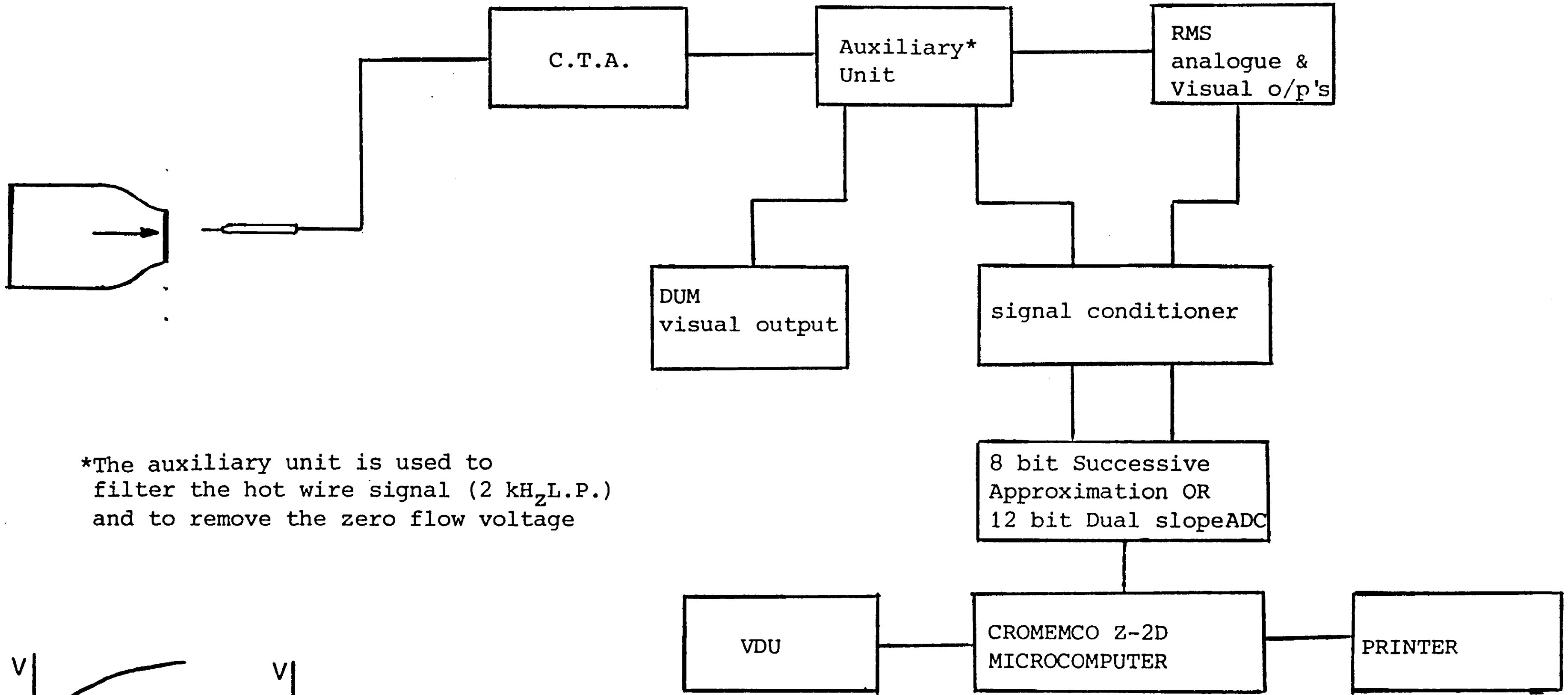

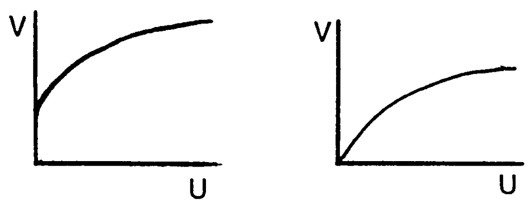

Fig. 3.3.1 Schematic layout of turbulent jet flow test

Fig. 3.4.1 Photograph of tunnel working section with BBC System below

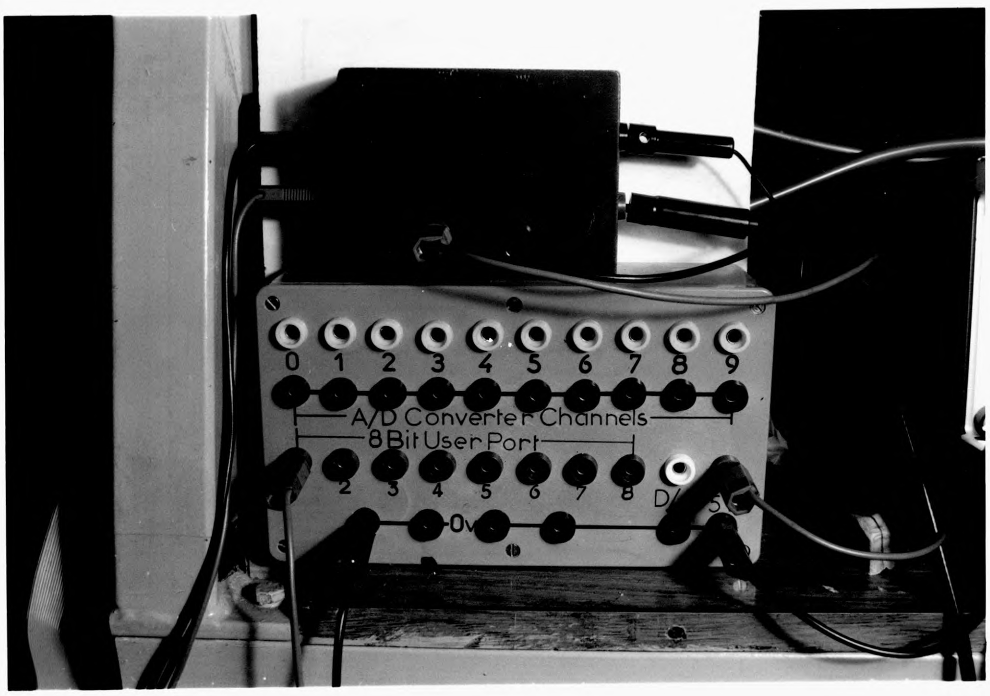

Fig. 3.6.2 CUBAN-8/4mm socket interface

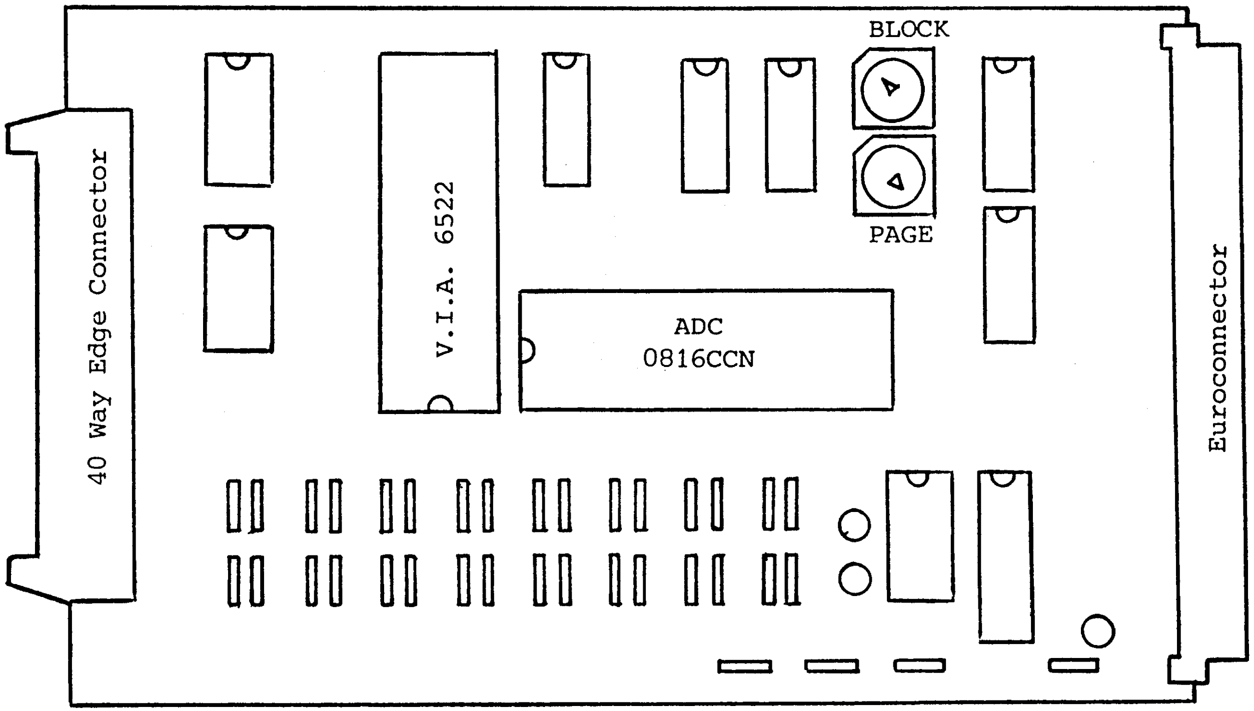

Fig. 3.6.1 Schematic layout of CUBAN-8 card showing position of PAGE and BLOCK

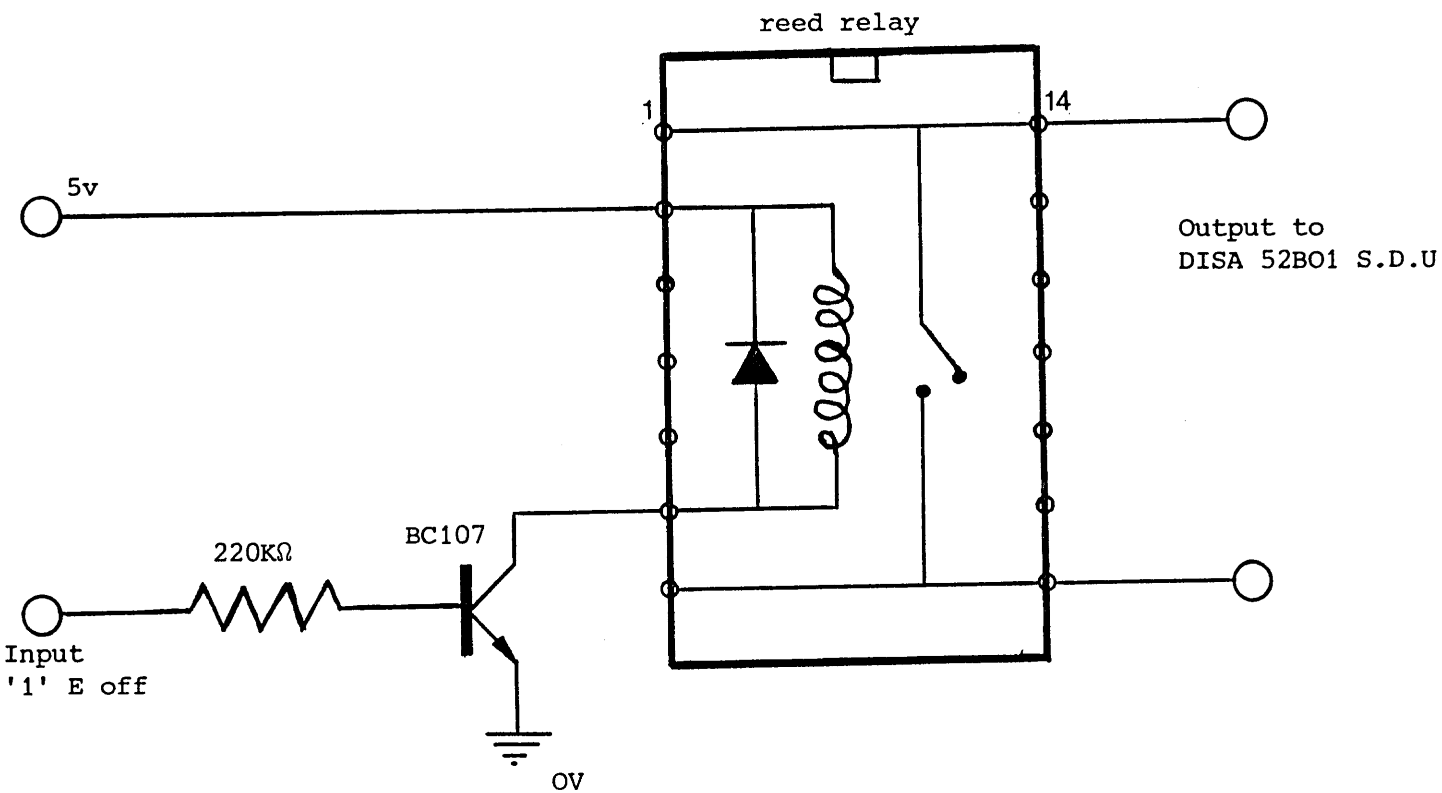

Fig. 3.7.1 stepper motor on/off interface

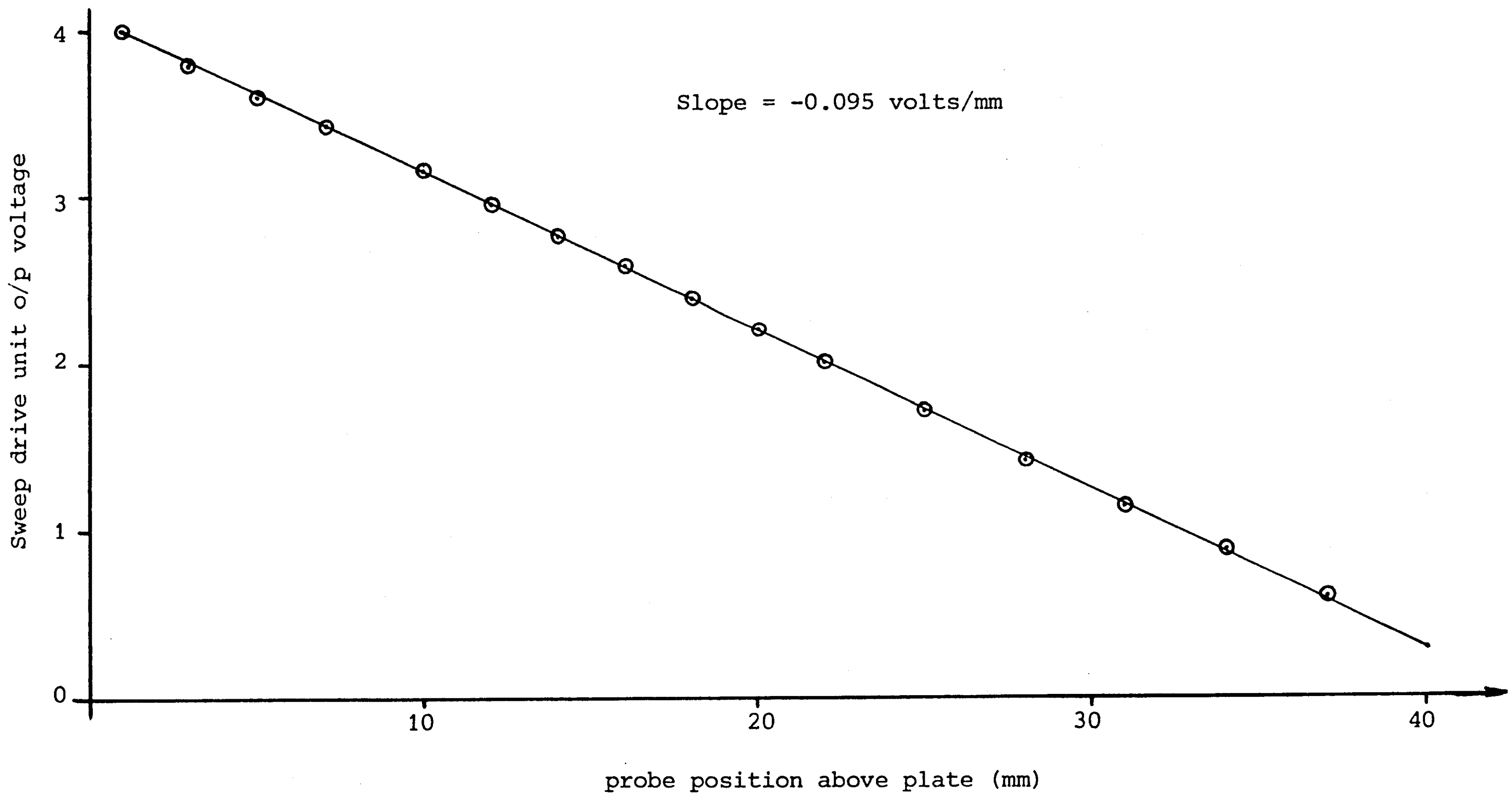

Fig. 3.8.1. <u>Calibration of DISA 52B01 sweep Drive Unit</u>

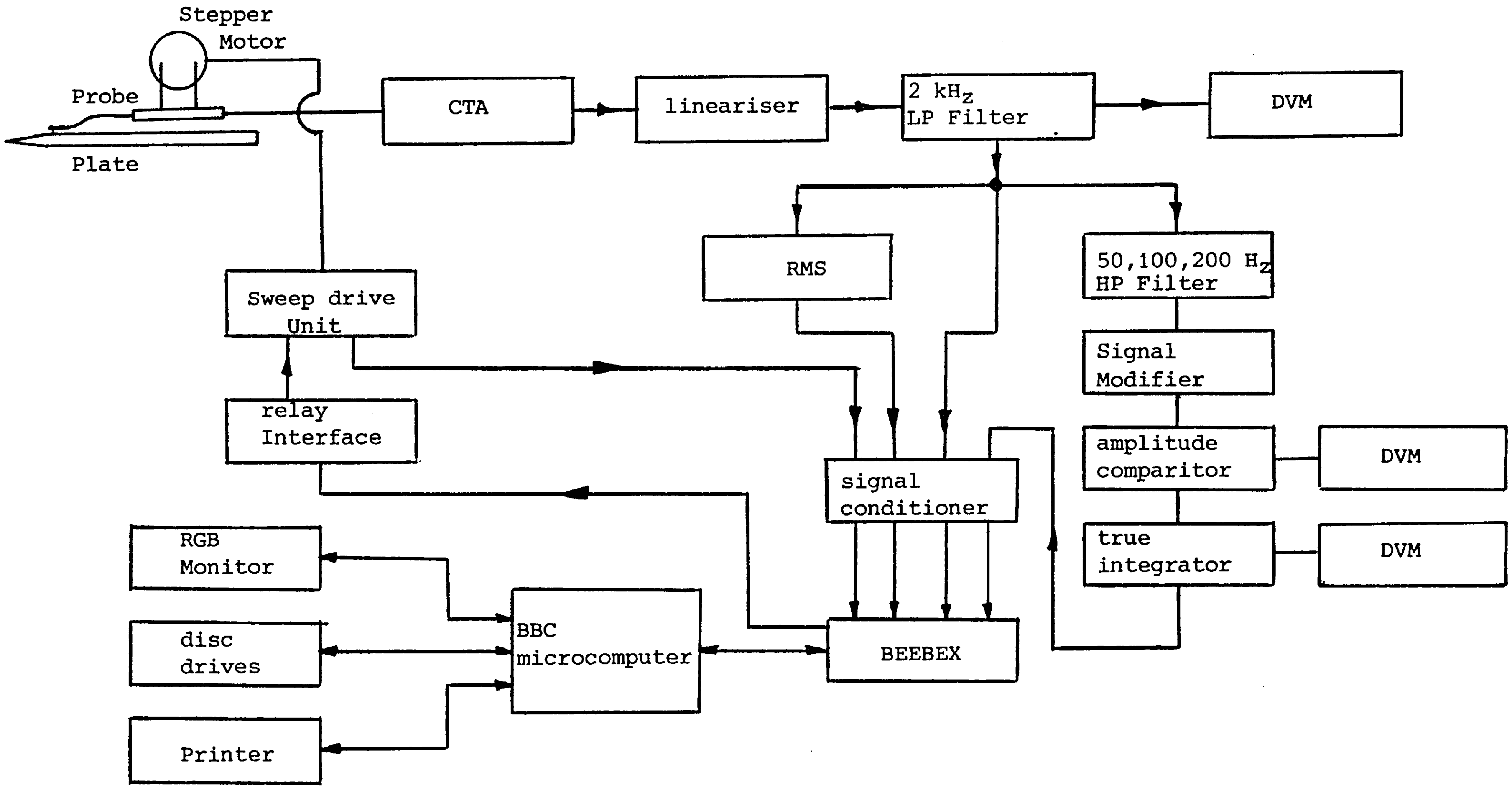

Fig. 3.8.2 Schematic Layout of Data Acquisition and Control System

Velocity m/s	Y-Pos. mm	Intermittency γ	RMS-Vel. m/s
10.588	0.5	0.98	1.4
12.54	1.34	0.98	1.18
13.227	1.89	0.98	1.1
13.923	2.72	0.98	1.07
14.409	3.36	0.97	1.03
14.81	3.96	0.97	1.01
15.289	4.82	0.97	0.97
15.564	5.32	0.96	0.96
16.075	6.22	0.94	0.91
16.392	6.87	0.92	0.88
16.555	7.51	0.9	0.85
16.897	8.23	0.85	0.81
17.178	8.92	0.76	0.75
17.679	10.4	0.52	0.63
18.142	11.88	0.29	0.54
18.465	13.47	0.1	0.43
18.426	14.95	3E-2	0.29
18.568	16.57	0	0.26
18.607	18.04	0	0.21
18.601	19.48	0	0.19

DIST.FROM L.E.=1000mm SPANWISE LOCATION =0mm

APPROX. EDGE OF BOUNDARY LAYER = 13.18mm

FREE STREAM VELOCITY = 18.59mm

n	y (mm)	Vel. m/s	u/uinf	y/d	RMS	Gama
1	0.5	10.588	0.569	3.8E-2	1.4	0.98
2	1.34	12.54	0.674	0.102	1.18	0.98
3	1.89	13.227	0.711	0.143	1.1	0.98
4	2.72	13.923	0.749	0.206	1.07	0.98
5	3.36	14.409	0.775	0.255	1.03	0.97
6	3.96	14.81	0.797	0.3	1.01	0.97
7	4.82	15.289	0.822	0.366	0.97	0.97
8	5.32	15.564	0.837	0.404	0.96	0.96
9	6.22	16.075	0.865	0.472	0.91	0.94
10	6.87	16.392	0.882	0.521	0.88	0.92
11	7.51	16.555	0.89	0.57	0.85	0.9
12	8.23	16.897	0.909	0.624	0.81	0.85
13	8.92	17.178	0.924	0.677	0.75	0.76
14	10.4	17.679	0.951	0.789	0.63	0.52
15	11.88	18.142	0.976	0.901	0.54	0.29
16	13.47	18.465	0.993	1.022	0.43	0.1
17	14.95	18.426	0.991	1.134	0.29	3E-2
18	16.57	18.568	0.999	1.257	0.26	0
19	18.04	18.607	1.001	1.369	0.21	0
20	19.48	18.601	1	1.478	0.19	0

EYEBALL AVE OF INTERMITTENCY AT y/d=0.2 = 0

AVE. OF INTERMITTENCY VALUES BELOW (y/d=0.2)= 0.98

Fig. 3.9.1 Printout from Data Acquisition & Control Prog.

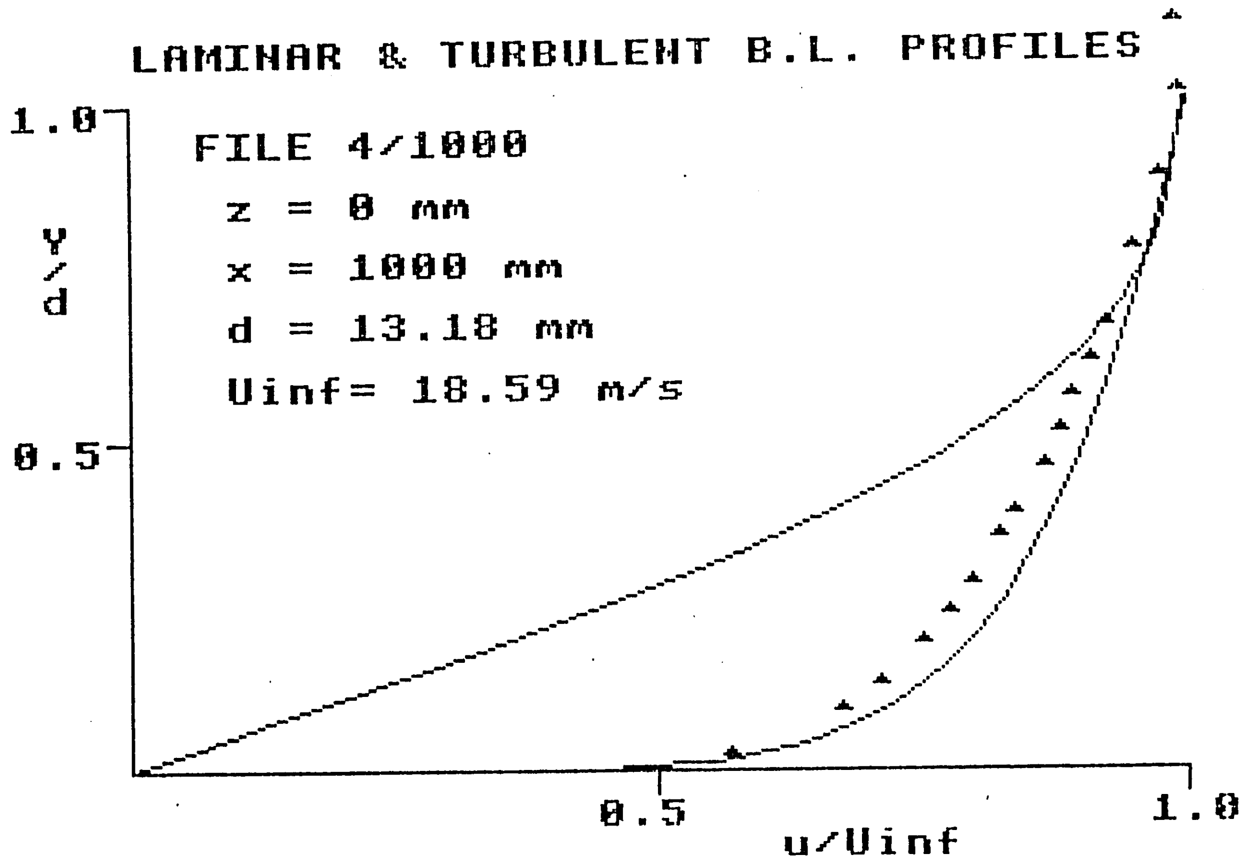

Fig. 3.9.2 Dump from $y/_{\delta vs}$ $u/_{U_\infty}$ graphics program

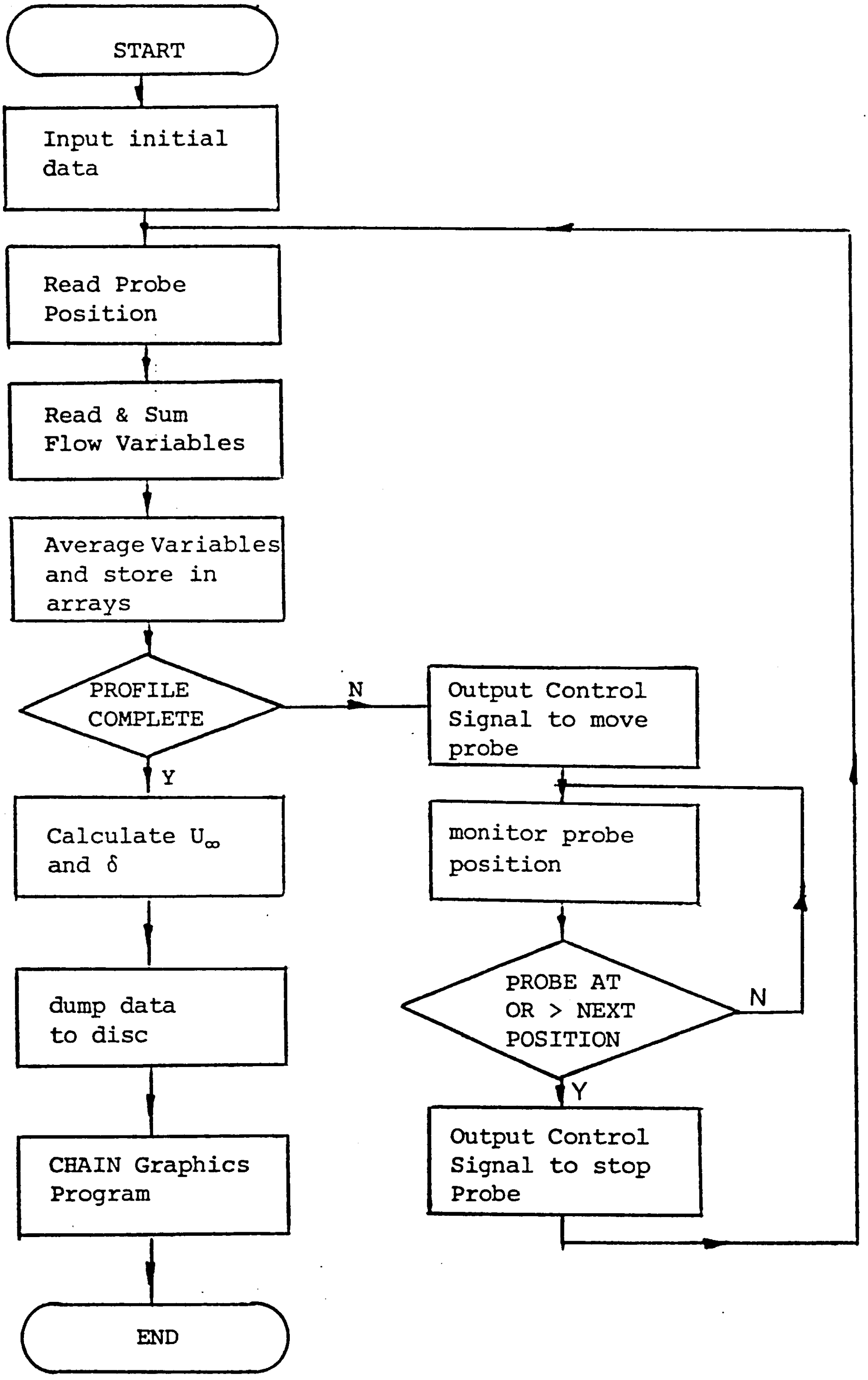

Fig. 3.9.3 Flow Diagram of Data Acquisition and Control Program

CHAPTER 4

Data Reduction and Theoretical Considerations

4.1 Introduction

In this chapter, the methods used for reducing the mean velocity profile data for the laminar, turbulent and transitional boundary layers are presented along with some estimation of the errors involved. The technique used for determining the start and end of the transition region is discussed and compared to methods used by other researchers. Also, the early development of the turbulent boundary layer, associated with transitional boundary layers, is considered with reference to low Reynolds number effects. Finally, the two dimensionality of the boundary layer flows are examined and the momentum balance technique for testing two dimensionality is described.

4.2 Reduction of Laminar Mean Velocity Profiles

The Pohlhausen (1921) solution for the laminar boundary layer, in arbitrary pressure gradients, is based on the assumption that the laminar boundary layer velocity profile can be represented by a fourth order polynomial of the form.

$$\bar{u}/U_\infty = A\left(y/\delta\right) + B\left(y/\delta\right)^2 + C\left(y/\delta\right)^3 + D\left(y/\delta\right)^4 \qquad 4.1$$

A least squares technique was used to fit a polynomial through the data points of u/U_∞ against y/δ and with the constants known the boundary layer integral parameters δ^*, θ and δ^{**} were easily obtained by direct integration of the respective functions. The shape factors H_{12} and H_{32} immediately follow from the integral parameters. (In actual fact it was found that a third order polynomial was sufficient to fit the data. Therefore, this was used in preference to a fourth order polynomial as it simplified the software). To determine the wall shear stress from the profile data available, use was made of the fact that in the laminar layer the shear stress is directly proportional to the rate of strain.

ie $$\tau_0 = \mu \, {}^{\partial \overline{u}}/_{\partial y} \qquad 4.2$$

and in the region $0 < {}^{\overline{u}}/_{U_\infty} \leqq 0.45$ the slope ${}^{d\overline{u}}/_{dy}$ is approximately linear. The shear stresses was determined therefore, by averaging the slope of all the data points in this region. The thickness of the boundary layer was defined as the y value corresponding to $\overline{u} = 0.995\ U_\infty$ and was determined via a linear interpolation routine. A typical printout from this analysis is shown in fig. [4.2.1] and a fit of the third order polynomial to a set of data is shown in fig. [4.2.2]. A printout of the program used for this analysis is given in appendix 5.

4.3 Reduction of turbulent mean velocity profiles

The analysis of Coles (1968), as applied to the data presented at the Standford Conference, Coles & Hirst (1968), was used for the reduction of the turbulent mean velocity profiles measured. A brief description of this analysis is given below.

It is generally accepted that the turbulent boundary layer consists of an inner and outer region. In the inner region, which contains but extends far beyond the laminar sublayer, viscous and turbulent stresses are important, while in the outer region the turbulent stresses dominate. A schematic representation of the turbulent boundary layer is shown in fig. [4.3.1].

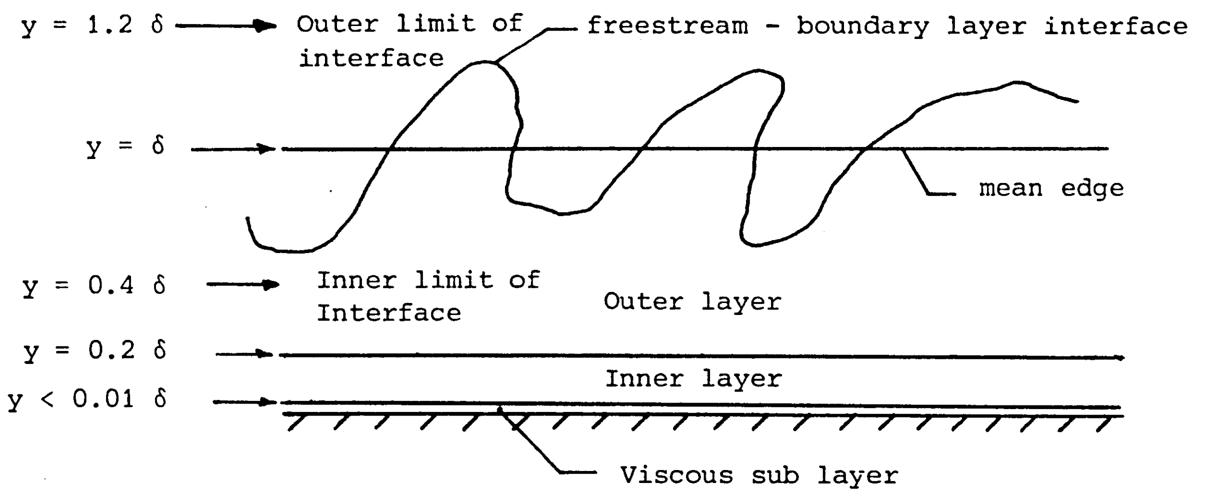

Fig. 4.3.1 Schematic representation of a turbulent boundary layer

In the viscous sublayer, which accounts for approximately 1% of the total shear layer thickness, viscous forces dominate and the mean velocity profile can be approximated by:

$$\bar{u}/u_\tau = \frac{y u_\tau}{\nu} \qquad 4.3$$

or

$$u^+ = y^+$$

Outside this viscous sublayer the analysis of Coles assumes that the turbulent boundary layer can be modelled by two separate wall and wake functions. This is shown schematically below in fig. [4.3.2].

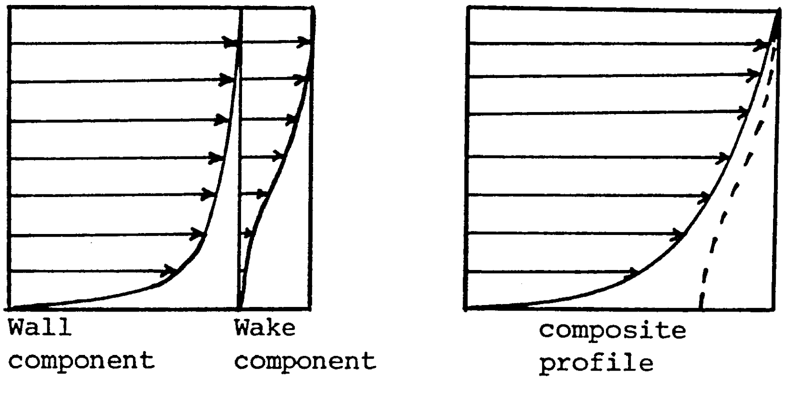

Fig. 4.3.2 Schematic representation of wall and wake components taken from Coles (1968)

The wall function can be obtained from Prandtl's mixing length concept assuming that the mixing length ℓ is proportional to y close to the wall (ie $\ell = ky$) and that the wall shear stress $\tau_0 = \rho\ell \cdot \left(\frac{\partial u}{\partial y}\right)^2$ remains constant.

$$\therefore \quad \tau_0 = \rho\, k^2 y^2 \left(\frac{\partial \bar{u}}{\partial y}\right)^2 \qquad \ldots\ldots \; 4.4$$

$$\frac{\partial \bar{u}}{\partial y} = \frac{u_\tau}{ky} \qquad \ldots\ldots \; 4.5$$

which integrates to give

$$\bar{u} = \frac{u_\tau}{k} \ln(y) + \text{constant} \qquad \ldots\ldots \; 4.6$$

or in non-dimensional form

$$\frac{\bar{u}}{u_\tau} = \frac{1}{k} \ln \frac{y u_\tau}{\nu} + C \qquad \ldots\ldots \; 4.7$$

Equation 4.5 can also be derived from dimensional analysis arguments. Cebeci & Bradshaw (1977) & Bradshaw (1972).

The constants k and C are wholly empirical and their values will be discussed later in section 4.5.

The wake function was obtained by relating the outer mean velocity profile to the inner profile and defining the function such that it represented the deviation from the law of the wall (ie equation 4.7).

The form of the wake function obtained by Coles (1956) was

$$W = 2 \sin^2 \left({}^{\pi}/_{2} \cdot {}^{y}/_{\delta}\right) \qquad \ldots\ldots \; 4.8$$

Therefore the composite turbulent boundary layer outside the viscous sub layer, (normally outside $\frac{yu_\tau}{\nu} > 50$) is:

$$\bar{u}/u_\tau = 1/k \quad \ln\left[y\,\frac{u_\tau}{\nu}\right] + C + {}^{2\Pi}/_k \, \sin^2\left({}^{\pi}/_2 \cdot {}^{y}/_\delta\right) \qquad \ldots\ldots \; 4.9$$

where Π is a wake parameter related to the strength of the wake function. The strength of the wake function $\Delta\, \bar{u}/u_\tau$ was defined by Coles as the maximum deviation of the velocity profile from that obtained by equation 4.7 at the edge of the boundary layer (ie at $y = \delta$) and can be calculated from:

$$\Delta\left(\frac{\bar{u}}{u_\tau}\right) = \left(\frac{\bar{u}}{u_\tau}\right) - \frac{1}{k}\ln \quad [y+] \; + C = \frac{2\Pi}{k} \qquad \ldots\ldots \; 4.10$$

The analysis of Coles assumes that the law of the wall is universally valid in the region $100 \leqq y+ \leqq 300$ irrespective of the freestream turbulence or any external pressure gradient acting on the boundary layer. (In strong adverse pressure gradient ie flows close to separation the law of the wall breaks down and the above will not apply). Therefore, equation 4.7 was iterated to obtain an optimum value of u_τ for each data point within the specified region and the averaged value obtained was taken as representative of the particular velocity profile being analysed. The fitting region used by Coles was altered to $y+ > 30$ and $y/_\delta < 0.2$, on the suggestion of Murlis et al (1982), to account for the low Reynolds number flows associated with the present work. The boundary layer thickness, δ, was then determined from the data by the linear interpolation routine used previously for the laminar profile analysis. With these two values known, ie u_τ and δ the value of Π can be obtained from equation 4.9. Coles used a set of standard integrals for the integral parameters within the viscous sub-layer ie from y = 0 to y+ = 50. These were

$$\int_0^{50} \left[\frac{\bar{u}}{u_\tau}\right] d\left[\frac{yu_\tau}{\nu}\right] = 540$$

$$\int_0^{50} \left[\frac{\bar{u}}{u_\tau}\right]^2 d\left[\frac{yu_\tau}{\nu}\right] = 6546$$

$$\int_0^{50} \left[\frac{\bar{u}}{u_\tau}\right] d\left[\frac{yu_\tau}{\nu}\right] = 82770$$

Equation 4.9 is then assumed to continue the integration from y+ = 50 to some point in the log-law region. This point was taken to be the third data point ie y+(3) in the analysis. In some cases the value of y+(3) was actually less than 50 and for these cases the first data points are automatically deleted and the data renumbered. Integration from the third data point to the freestream was carried out by a parabolic fitting routine using a modified Simpson's rule. A parabola was fitted through three adjacent points, and the integrals from the first to second and from the second to third points are computed. The central point is then moved one point outward and the process repeated. The two values for each interval are then averaged providing an element of smoothing for the integrals. The integrals of

$\left(\bar{u}/U_\infty\right)$, $\left(1 - \bar{u}/U_\infty\right)$, $\left(\bar{u}/U_\infty\right)^2$ and $\left(\bar{u}/U_\infty\right)^3$ obtained

in this manner are appropriately combined to obtain the required integral thicknesses.

The wall shear stress, τ_0 was calculated from the value of u_τ obtained from the profile analysis, ie from velocity profile measurements in the logarithmic region.

$$\tau_0 = \rho\, u_\tau^2 \qquad \ldots\ldots \quad 4.11$$

and the skin friction coefficient follows from

$$Cf = \frac{2\,\tau_0}{\rho\, U_\infty^2} = 2\left(\frac{u_\tau}{U_\infty}\right)^2 \qquad \ldots\ldots \quad 4.12$$

The justification for using the log-law region for calculation of u_τ is that the log-law is extraordinarily insensitive to the variation of freestream turbulence and pressure gradient effects. Evidence for its applicability is provided by the quality of the fit of the present profiles, and of the vast amount of data presented at the standard conference, to the universal logarithmic law.

The value of Cf can also be obtained by substitution of the shape faction, H_{12} and momentum thickness, θ from the profile analysis into any one of a number of correlations of the form

$$Cf = f(R_\theta, H_{12})$$

Two such correlations are those of Ludwieg & Tillman

$$Cf = 0.246 R_\theta^{-0.268} \exp(-1.561 H_{12}) \qquad \ldots\ldots \quad 4.13$$

and a curve fit due to White for the skin friction relation derived from the wake integrations of Coles formula - equation 4.9.

$$Cf = \frac{0.3\exp(-1.33 H_{12})}{(\log_{10} R_\theta)^{(1.74+0.31 H_{12})}} \qquad \ldots\ldots \quad 4.14$$

Preston tube measurements were also made, for a limited number of profiles, mainly for comparison with the values obtained by the methods mentioned above.

Taking the log-law values obtained from the velocity profiles as a reference, the deviation of the skin friction as measured by the other methods are

	(zero pressure gradient)		(Adv press gradient)
	Tu=0.5%	Tu=1.5%	Tu=1.5%
Ludwieg/Tillman	-2.2%	-0.6%	+1.0%
White-Coles	-5.8%	-4.0%	-3.25%
Preston tubes	-3.4%	-1.15%	-5.24%

A computer printout from the velocity profile analysis is given in fig. [4.3.3] and the universal turbulent boundary layer velocity profile is shown for a typical set of data along with the composite profile, defined by equation 4.9, in fig. [4.3.4]. A printout of the program used for the analysis is included in appendix 5

4.4 Estimation of errors in boundary layer integral thicknesses

When linearising the signal from a hotwire probe using the DISA 55M25 lineariser there is an inherent parabolic error, usually with a maximum close to the centre of the linearised region and tailing off to zero at the maximum and minimum velocities, as shown in fig. [4.4.1].

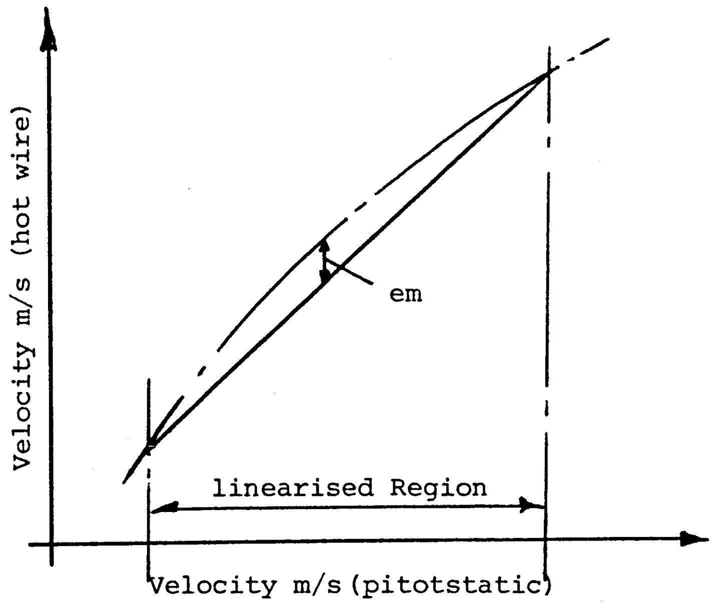

Fig. 4.4.1 Lineariser error

This is only a very small error, usually of the order +1%, and as can be seen from an actual probe calibration, fig. [2.6.3], it is barely detectable. However, the error analysis in Appendix 1 shows that for a maximum error, em, of +1% the corresponding error in displacement and momentum thickness are -2.52% and -2.24% respectively for a $^1/_7$th power law turbulent velocity profile and -0.93% and -0.78% respectively for a parabolic laminar type velocity profile. Possible error introduced into the boundary layer thicknesses which can be associated with the curve fitting and integration techniques, described in the previous two sections, are very difficult to define. For the laminar analysis, since the polynomial is integrated directly, all the likely error can be attributed to the fit of the polynomial to the data. As in most cases the polynomial fits the data very well, the errors are assumed to be minimal. For the turbulent boundary layer the analysis is the same as that used at the Stanford Conference. This is a well tested method and is considered to be as good, if not better than any other methods available. Fraser (1979) compared integral thicknesses obtained by the Stanford Conference method with those obtained by planimeter measurements and found agreement to be within 0.7%.

4.5 Approach to equilibrium and low Reynolds number effects

The present investigation, although mainly concerned with the development of the transitional boundary layer, is also related to the early development of the turbulent boundary layer and the low Reynolds number effects associated with this early development. In order to explain the low Reynolds number effect, reference is made to the approach of a constant pressure turbulent boundary layer towards equilibrium conditions. Initially though, it is necessary to define an equilibrium turbulent boundary layer.

Bradshaw (1972) described a turbulent boundary layer as being in equilibrium if the generation of Reynolds stresses by interaction with the mean flow and existing Reynolds stresses is equal to the destruction of the Reynolds stresses by viscous forces. In contrast, self preserving boundary layers (often misleadingly called equilibrium layers) are defined by Townsend (1965) as those in which distributions of the flow quantities, ie Reynolds stresses, mean velocity etc have the same form at all distances from the flow origin differing only in common scales of velocity and length. The importance of self preserving flows is that rates of change of velocity and length scales can be predicted with no more specific assumption about the nature of turbulent motion than that the large scale motion is independent of fluid viscosity.

Clauser (1954) found that constant pressure turbulent boundary layers possessed a set of similar profiles when expressed in terms of the velocity defect. ie

$$\frac{U_\infty - u}{u_\tau} = f\left({}^{y}/_{\delta}, \Pi\right) \qquad \ldots\ldots \quad 4.15$$

(This can be obtained from equation 4.9 by setting $\overline{u} = U_\infty$ at $y = \delta$ and subtracting the resultant equation from 4.9). He also reasoned that since such a set of profiles existed then the turbulent boundary layer in a constant pressure flow was indeed in equilibrium, (equilbrium layers in the Clauser sense are actually self preserving layers). Clauser went on to show, with some considerable experimental effort, that a turbulent boundary layer with variable pressure gradient but constant history, expressed in terms of the pressure gradient parameter, $\beta = \frac{\delta^*}{\tau_o} \cdot \frac{du}{dx}$, also possessed such a set of similarity profiles. From this he concluded that such layers were also in turbulent equilibrium since the gross properties of the boundary layer could be expressed in terms of a single parameter: eg

$$\frac{U_\infty - \overline{u}}{u_\tau} \equiv f\left({}^{y}/_{\delta}, \beta\right) \qquad \ldots\ldots \quad 4.16$$

From equations 4.15 and 4.16 it can be seen that Π and β must be related and that Π and β must be constant in an equilibrium boundary layer. Coles (1962) found $\Pi \cong 0.55$ for a constant pressure boundary layer at Reynolds numbers, based on the momentum thickness, above 5000, but at Reynolds numbers below this the velocity defect factor $\Delta\, {}^{\overline{u}}/_{u_\tau} = {}^{2}/_{k}\Pi$ was Reynolds number dependent.

Coles expressed this dependency through the wake function Π which has been conveniently curve fitted by Cebeci & Smith (1974) as:-

$$\Pi = 0.55\ [1-\exp(-0.243Z^{0.5} - 0.298Z)] \qquad \text{...... 4.17}$$

$$\text{where } Z = \left({}^{R_\theta}/_{425} - 1 \right)$$

Simpson (1970) on the other hand correlated the velocity data in the outer similarity law by varying the Von Karman constant, k, and the additive constant in the law of the wall. From this he suggested that the Von Karman constant was Reynolds number dependant and should be replaced by the term Ω

$$\Omega = 0.4 \left({}^{R_\theta}/_{6000} \right)^{-1/8} \qquad \text{...... 4.18}$$

for $R_\theta < 6000$.

In order to settle the controversy, Huffman and Bradshaw (1972) after critically reviewing the available literature and examining the low Reynolds number effect, reached the conclusion that k was in fact constant, (equal to 0.41) and that the additive constant could be considered mildly Reynolds No. dependant. The Reynolds number effect was attributed to the affect of the turbulent-irrotational interface on the outer law of the wall and was substantiated by the fact that no such effects were present in duct flows which do not have such an interface. This in effect vindicates the observations of Coles (1962).

Since Huffman & Bradshaw concede that the additive constant, C, can vary and does in fact increase for R_θ values below approximately 1000, the value of 5.2, as suggested by Murlis (1975) and used by other researchers since then eg Castro (1984), Fraser (1980), was adopted for C. This value was used in preference to the usual value of 5.0, as the present investigation is associated with the early development of the turbulent boundary layer and consequently R_θ values less than 1000 are fully expected.

Although the above low Reynolds number effect has been described for the special case of a constant pressure turbulent boundary layer, which is approaching equilibrium, all turbulent boundary layer flows with R_θ values less than approximately 5000 will be subject to this effect.

4.6 Transitional mean velocity profiles

The transitional boundary layer is characterised by regions of laminar and turbulent flow with the mean velocity at any height in the boundary layer defined by a *near wall* intermittency weighted average of the laminar and turbulent velocity contributions ie

$$\overline{u}_t = (1 - \overline{\gamma})\ \overline{u}_L + \overline{\gamma}\overline{u}_T$$

Dhawan & Narasimha (1957) noted that although γ varies across the boundary layer, for the purposes of the profile calculation, the value of γ measured close to the wall, $^{y}/_{\delta} < 0.2$, gives sufficiently accurate results for the whole profile. The intermittency distribution through the boundary layer, characterised by the variation $\gamma(y)$, has only a secondary influence on the transition flow, $\overline{\gamma}(x)$ being the significant property. Since the transitional boundary layer is a composite consisting of laminar and turbulent velocity components, neither of the two analyses described in sections 4.2 and 4.3 are strictly applicable. However, since they are both purely numerical techniques, with a polynomial being fitted to the data in the laminar analysis and a curve fitting and integration technique used for the bulk of the data in the turbulent analysis, true transition integral thicknesses can be representatively obtained. To enable the decision as to which analysis should be used a computer program was developed to display the measured data graphically, in ordinates $^{y}/_{\delta}$ vs $^{\bar{u}}/_{U_\infty}$, along with the third order polynomial fit to the data, on the R.G.B. monitor. If the polynomial was a good fit to the data, usually the case for values of $\bar{\gamma} < 0.5$ where the boundary layer is dominantly laminar, the laminar analysis is used, otherwise the turbulent analysis is selected.

The skin friction coefficients calculated from these analyses, in the transitional boundary layer, will not give representative transitional values. The laminar analysis assumes equation 4.2 to be valid and does not account for the substantially larger contribution from the turbulent regime to the overall skin friction in the transitional boundary layer, hence the skin friction will be underestimated. Similarly in the turbulent boundary layer the skin friction coefficient will be overestimated.

In attempt to give a better account of the transitional local skin friction coefficients Fraser (1980) developed an empirical relation in the form

$$Cf_t = f(R_\theta, H_{12}, \bar{\gamma}) \qquad \ldots\ldots \quad 4.19$$

This relationship was devised from the observations of Emmons (1951) that the skin friction coefficient could be represented by

$$Cf_t = (1 - \bar{\gamma})\ Cf_L + \bar{\gamma}\ Cf_T \qquad \ldots\ldots \quad 4.20$$

The laminar skin friction component was obtained from the Thwaites (1949) solution and the turbulent component was derived by equating the turbulent velocity profile described by a power law, with the exponent n free, to the log-law relation given by 4.7 which was assumed to be universally valid at y+ = 100.

This gives after some algebraic manipulation:

$$Cf_t = \frac{2\ell_1(\lambda_\theta)}{R_{\theta L}}(\bar{\gamma}-1) + 2\bar{\gamma}\left[\left(\frac{R_{\theta T}\,K}{100}\right)^{\frac{2}{(H_T-1)}} \times \frac{H_T\ (H_T+1)}{(H_T-1)}\right]^{\frac{-2(H_T-1)}{(H_T+1)}} \quad \ldots.\ 4.21$$

The laminar and turbulent component values cannot obviously be determined from experimental measurements in the transitional boundary layer. Therefore the values of $R_{\theta t}$ and H_t are used in the formula and were found to give reasonable results. (See Fraser (1979) for a complete derivation of 4.21).

4.7 Determination of start and end of transition

For the purpose of the present study a reliable method of determining the position of the start and end of transition is of paramount importance. The method adopted was to place the hot wire probe close to the plate surface and pass the signal from the hot wire anemometer to the intermittency measurement apparatus. The start of transition was defined as the x position corresponding to a reading of $\gamma = 0.01$ and the end of transition as the x position corresponding to a reading of $\gamma = 0.99$. The signal from the hot wire anemometer was also passed to an oscilloscope and a loud speaker to provide audible and visual detection of the appearance of turbulent bursts or *spots*.

The method of detection of transition is very important as different techniques can give widely varying results for the position of start and end of transition. Hall & Gibbings (1972) noted that it would not be unreasonable to expect scatter of ±5% in the value of R_{θ_s} due to the different detection methods. The present method is likely to give R_{θ_s} values lower than those obtained by the common surface pitot method used by Hall & Gibbings and many others. However, the author suggests that the present method is more reliable and repeatable as it measures the intermittency function directly and does not lend itself to the degree of estimation required by other techniques. Sharma et al (1982) used a similar technique of measuring the intermittency function directly using flush mounted hot film probes, but they defined the start of transition at $\gamma = 0.1$ which would give values of R_{θ_s} higher than those presented here. Provided the method used by other researchers is noted, then a comparison of results can be made by estimating the affect that the detection method has on determining the transition position.

4.8 Flow two dimensionality

Most of the boundary layer prediction methods assume that the flow is two dimensional in order to simplify the fundamental Navier-Stokes equations governing fluid motion, and enable a solution to be achieved. However, many of the early researchers, when obtaining data to validate such prediction methods, paid very little attention to the two-dimensionality of the flow and merely assumed this to be the case. In practice however, it is very difficult to obtain two dimensionality especially in adverse pressure gradients. In 1954 Clauser reported, after much experimental effort in obtaining a two dimensional boundary flow in an adverse pressure gradient, quote - *"we came to have great respect for the ease with which air can move laterally in boundary layers subject to adverse pressure gradients"*. Since the 1968 Standford Conference the importance of obtaining good quality two dimensional test flows has been realised and various methods have been developed to assess the quality of the flow with regard to two dimensionality, Fraser (1986). One such method, which has been used in the present work, is the momentum balance principle. This method was used to assess the two dimensionality of the flows at the Standford Conference and consists basically of integrating with respect to x, the von Karman momentum equation in the form given below

$$\frac{d\,(U_\infty^2\theta)}{dx} + \frac{\delta^*}{2}\,\frac{d(U_\infty^2)}{dx} = \tau_0/\rho \qquad \ldots\ldots\ 4.24$$

normalising and integrating from $x = x_i$ to $x = x$, where subscript i denotes initial value, results in

$$\frac{U_\infty^2\theta}{(U_\infty^2\theta)_i} - 1 + \tfrac{1}{2}\int_{x_i}^{x}\frac{\delta^*}{\theta_i}\,d\left[\frac{U_\infty}{U_{\infty i}}\right]^2 = \int_{x_i}^{x}\left[\frac{U_\tau}{U_{\infty i}}\right]^2 d\left[\frac{x}{\theta_i}\right] \qquad \ldots\ 4.25$$

A computer program was used to determine the values of the left and right hand side of equation 4.25 using input data of x, θ, u_τ, U_∞ and Cf at various spanwise positions along the plate centre-line. The modified Simpsons rule described in section 4.3 was used to evaluate the integral terms and give a degree of smoothing to the data. Any lack of agreement between left and right hand sides of equation 4.25, termed PL & PR respectively, indicating a lack of two dimensionality of the flow, assuming the input values of θ, Cf, u_τ and U_∞ are confidently known.

Flow divergence is represented by PR being greater than PL and flow convergence is represented by PL being greater than PR. The momentum balances of three test flows in favourable, zero and adverse pressure gradients are shown in fig. [4.8.1]. Excellent agreement indicative of good two dimensionality is obtained in the zero and favourable pressure gradient cases with only a very slight convergence detectable. The adverse pressure gradient, as expected, is not as good as the other two cases but is still better than normally accepted two dimensional flows such as Weighardt's flat plate flow, presented at the Standford Conference as one of the better two dimensional flows.

The slight convergence of the flows is thought to be caused by the side wall contamination as described in section 2.3.

FILE 32/1200

DATA FOR LAMINAR BOUNDARY LAYER VELOCITY PROFILE

DISTANCE FROM LEADING EDGE = 1200 mm

SPANWISE LOCATION = 0 mm

FREE STREAM VELOCITY = 10.51 m/s

AIR TEMPERATURE =20 Deg.C ATMOSPHERIC PRESSURE =765 mmHg

Y mm	U m/s	Y/d	u/uinf	RMS	eta
0.5	1.86	0.103	0.177	0.1	0.383
0.87	3.37	0.179	0.321	0.17	0.665
1.04	4.03	0.214	0.383	0.15	0.795
1.24	4.8	0.256	0.457	0.19	0.951
1.47	5.51	0.303	0.524	0.2	1.126
1.86	6.68	0.384	0.636	0.24	1.427
2.09	7.22	0.431	0.687	0.24	1.602
2.32	7.75	0.478	0.737	0.24	1.776
2.45	8.06	0.505	0.767	0.28	1.877
3.14	9.2	0.647	0.875	0.22	2.404
3.57	9.68	0.736	0.921	0.18	2.735
3.96	10.01	0.816	0.952	0.16	3.032
4.58	10.35	0.944	0.985	0.11	3.508
5.01	10.44	1.033	0.993	7E-2	3.839
5.62	10.49	1.159	0.998	5E-2	4.307
6.05	10.51	1.247	1	5E-2	4.634
6.68	10.53	1.377	1.002	5E-2	5.117

RMS ERROR OF FIT = 1.15061622E-2

LAMINAR BOUNDARY LAYER INTEGRAL PARAMETERS

APPROX EDGE OF BOUNDARY LAYER	= 4.85 mm
DISPLACEMENT THICKNESS	= 1.61 mm
MOMENTUM THICKNESS	= 0.67 mm
ENERGY THICKNESS	= 1.05 mm
SHAPE FACTOR H12	= 2.42
SHAPE FACTOR H32	= 1.58
MOMENTUM TH. REYNOLDS NO.	= 468
DISPLACEMENT TH. REYNOLDS NO.	= 1135
SKIN FRICTION COEFF.	= 1.034E-3
WALL SHEAR STRESS	= 6.9E-2 N/mm^2

Fig. 4.2.1 Printout from laminar analysis program

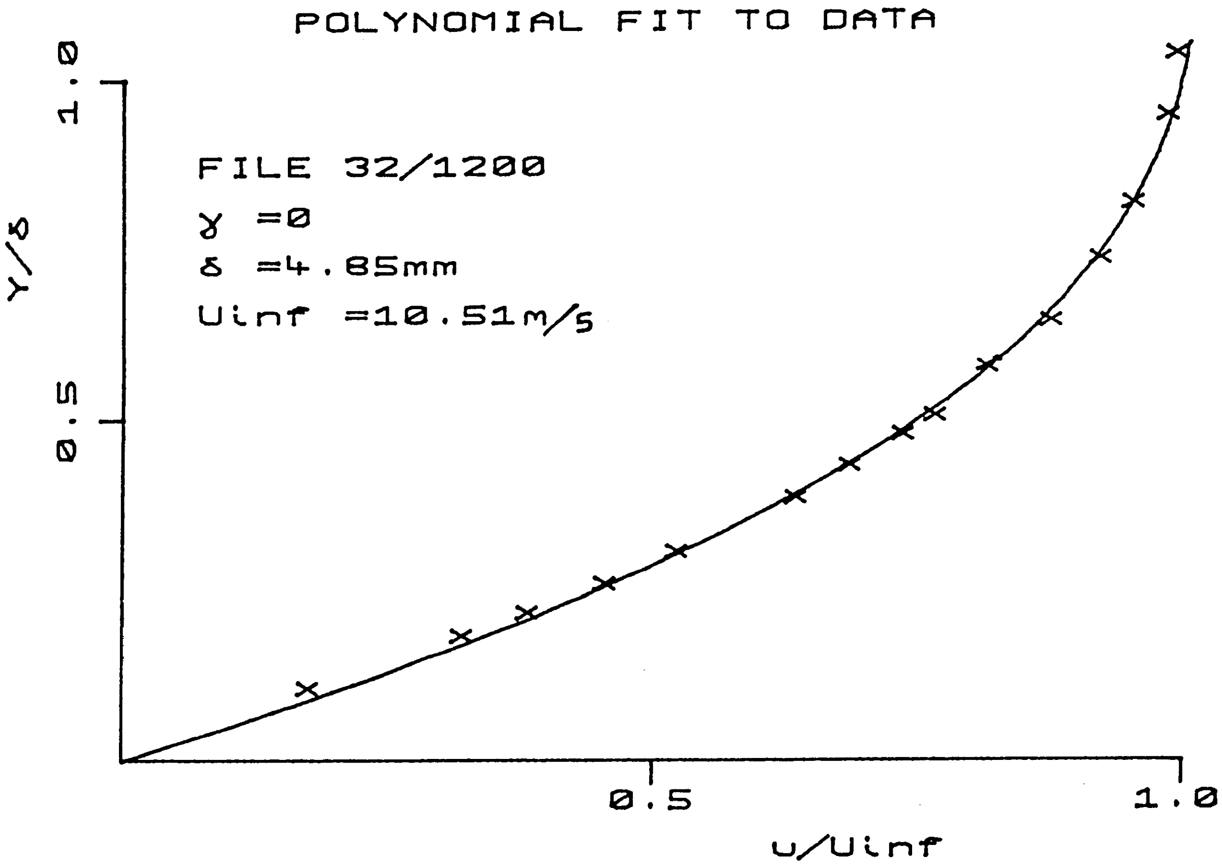

Fig. 4.2.2 Polynomial fit to data

FILE FB/1200

DATA FOR TURBULENT BOUNDARY LAYER VELOCITY PROFILE

DISTANCE FROM L.E. = 1200 mm

SPANWISE LOCATION = 0 mm

FREESTREAM VELOCITY = 15.9 m/s

AIR TEMPERATURE = 21 Deg.C ATMOSPHERIC PRESSURE = 753 mmHg

Y-mm	Y/d	U/Uinf	RMS vel.
0.505	1.9E-2	0.454	1.41
1.09	4.1E-2	0.548	1.24
1.968	7.4E-2	0.609	1.12
2.872	0.108	0.641	1.12
3.669	0.138	0.669	1.09
4.467	0.168	0.688	1.09
5.318	0.2	0.714	1.07
6.222	0.234	0.728	1.07
6.993	0.263	0.744	1.06
8.615	0.324	0.776	1.06
10.503	0.395	0.806	1.03
12.364	0.465	0.841	0.96
13.96	0.525	0.866	0.94
15.848	0.596	0.889	0.9
17.789	0.669	0.916	0.84
19.623	0.738	0.938	0.75
21.272	0.8	0.953	0.68
23.107	0.869	0.968	0.6
24.968	0.939	0.981	0.53
26.882	1.011	0.992	0.46
28.531	1.073	0.997	0.4
30.366	1.142	1.001	0.32
32.041	1.205	1.002	0.28

yplus	Uplus	Resid.	Udef.
20.21	11.838	-0.694	14.237
43.61	14.289	-0.119	11.786
78.711	15.879	3.1E-2	10.195
114.876	16.714	-5.7E-2	9.361
146.786	17.444	7.6E-2	8.631
178.696	17.939	9.1E-2	8.135
212.734	18.617	0.344	7.457
248.898	18.982	0.326	7.092
279.745	19.399	0.458	6.675
344.628	20.234	0.784	5.841
420.149	21.016	1.083	5.058
494.606	21.928	1.597	4.146
558.426	22.58	1.953	3.494
633.946	23.18	2.244	2.894
711.594	23.884	2.666	2.19
784.987	24.458	3	1.617
850.935	24.849	3.194	1.225
924.328	25.24	3.384	0.834
998.784	25.579	3.534	0.495
1075.368	25.866	3.64	0.209
1141.316	25.996	3.626	7.8E-2
1214.709	26.1	3.578	-2.6E-2
1281.72	26.126	3.473	-5.2E-2

TURBULENT BOUNDARY LAYER INTEGRAL PARAMETERS

APPROX. EDGE OF BOUNDARY LAYER = 26.59 mm

DISPLACEMENT THICKNESS = 4.747 mm

MOMENTUM THICKNESS = 3.332 mm

ENERGY THICKNESS = 5.825 mm

SHAPE FACTOR H12 = 1.424

SHAPE FACTOR H32 = 1.748

MOM. TH. REYNOLDS No. = 3475

DISP. TH. REYNOLDS No. = 4950

cf (LUD/TILL) = 2.994E-3
cf (LOG-PLOT) = 2.942E-3
cf (COLES-FORM) = 2.86E-3

WALL FRICTION VELOCITY = 0.61 m/s

WALL SHEAR STRESS = 0.442 N/m^2

WAKE PARAMETER PI = 0.794

Fig. 4.3.3 Printout from turbulent analysis program

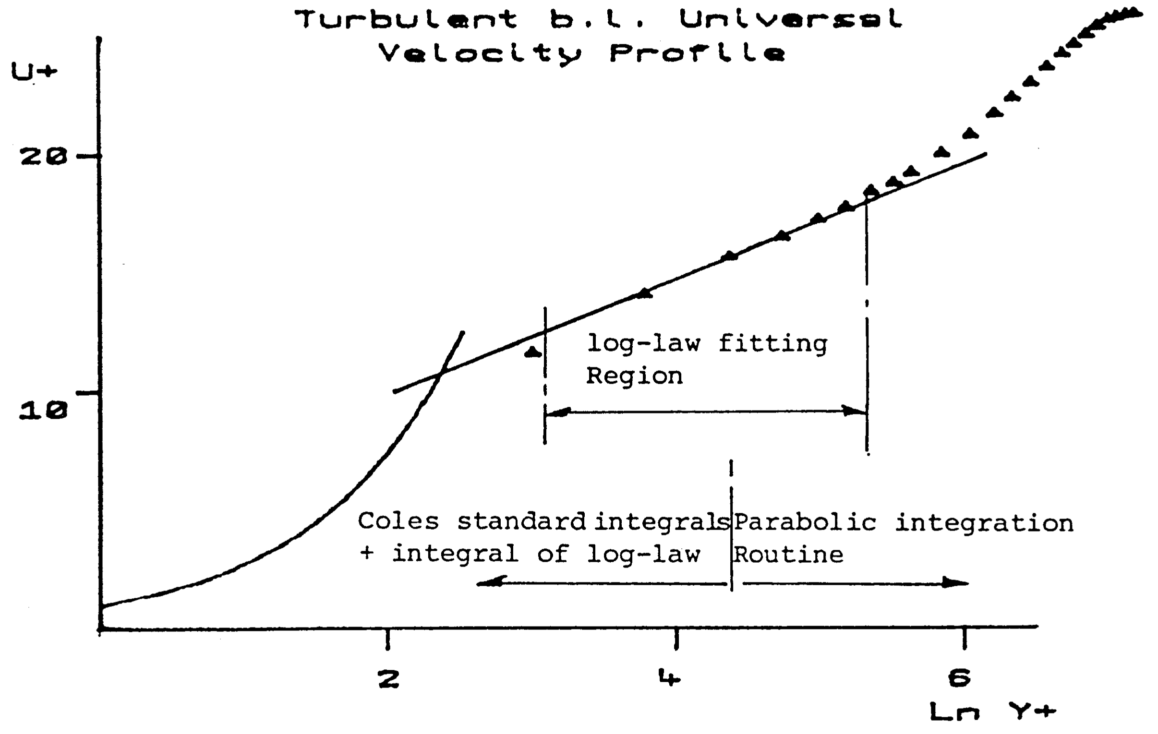

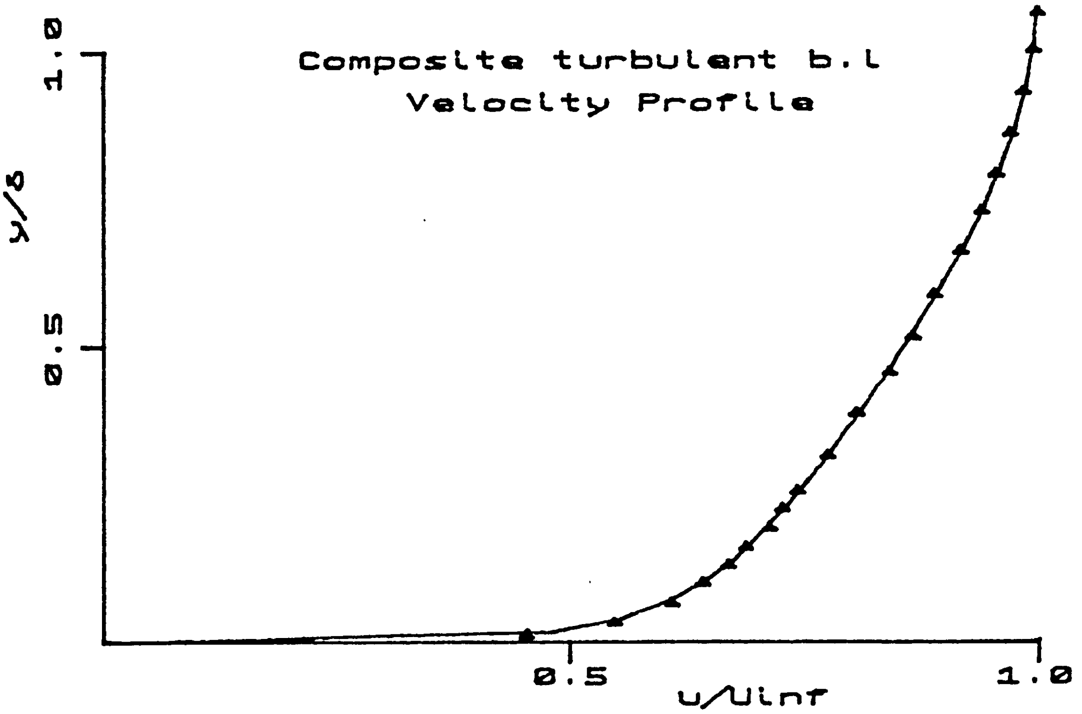

Fig. 4.3.4 Universal and Coles Composite turbulent boundary layer Velocity profiles

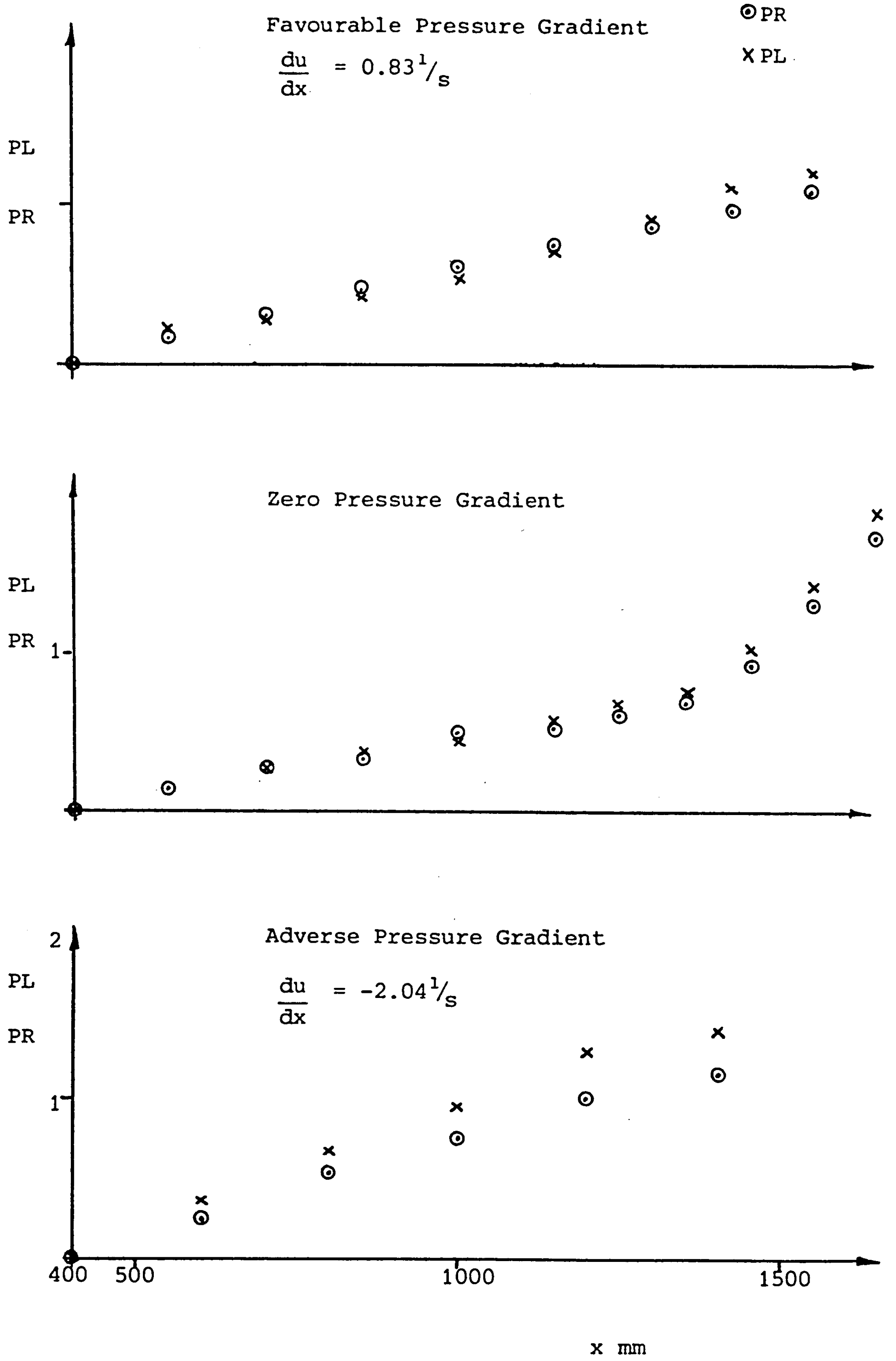

Fig. 4.8.1 Flow Two Dimensionality by the Momentum Balance Principle

CHAPTER 5

Development of Data Acquisition, Control and Data Reduction Software Package

5.1 Introduction

This chapter describes the development of a complete software package, related to the measurement and processing of boundary layer velocity profile data, for use with the BBC microcomputer. The function of the package is twofold; firstly to gather data from the experiments and dump this data to a disc file for permanent storage and secondly, to retrieve data from the disc files for subsequent analysis and display. The programs described in the previous two chapters for the data collection (Chapter 3) and data reduction (Chapter 4) from the basis of the package.

The package was developed specifically for use with a CUMANA double disc drive unit. Each drive of this unit has a double head enabling both sides of a disc to be used and, as each side of a disc has a storage capacity of approximately 200 k bytes, the facility makes available 800 k bytes of storage space. The top and underside of the lower disc and top and underside of the upper disc are numbered 0, 2, 1 and 3 respectively. The disc filing system (DFS) refers to the disc sides as *drives* ie drives 1 and 3 are sides 1 and 3 of the upper disc and drives 0 and 2 are sides 0 and 2 of the lower disc. Drive Ø is called the BOOT drive as the BBC has an auto BOOT facility which allows a short introductory program, stored in the BOOT file, to be automatically loaded into the machine from drive Ø, and run by simultaneously depressing the SHIFT and BREAK keys.

Because of the limited amount of RAM available on the BBC micro the software package takes the form of a number of programs each dedicated to a specific task. The programs are interlinked using the BBC CHAIN command which enables one program to automatically load and run another program. The complete software package is stored on a master disc which is inserted into the lower drive of the disc drive unit leaving the upper drive, ie drives 1 and 3, free for the storage of raw data.

5.2 Running the Software Package

To augment the following description of the software package reference should be made to the flow diagram fig. [5.2.1]

The package is initiated by the auto boot facility (ie depressing the SHIFT & BREAK keys simultaneously) which immediately runs a BOOT program to CHAIN the program called PROGSEL. This program is used for the initial selection of whether:

1. an existing file is to be read; or
2. a new file is to be created.

Option 1 If an existing file is to be read the name of the file and the drive number that the file is stored on are required and are fed in interactively from the keyboard. The name of the data file being read is then stored on disc, in a file called DATA. The name of the file can then be passed between programs by reading the file DATA at the beginning of each program. This streamlines the package as it eliminates the need for the file name to be typed in when a continuation program is CHAINed.

Option 2 If a new file is to be created the data acquisition and control program described in Section 3.9 is called and a boundary layer traverse is initiated. On completion of the traverse the raw data is dumped to a designated disc and the specified file name is stored in the file DATA as before.

A graphics program is then called which displays either the newly acquired data, or the data from a specified existing file, on axes of y/δ and u/U_∞ along with the laminar Pohlhausen and turbulent $1/7$ power law velocity profiles for comparison. A hard copy of this display can be obtained by calling a *screen dump* program which causes the EPSON FX-80 printer to copy the graphics displayed on the RGB Monitor. (fig. [3.9.2] shows a screen dump printout of a graphical display.)

Once the data has been displayed a decision on which analysis is to be used for the reduction of the raw velocity profile data is required. There are three options available:-

Option 1 - laminar analysis If this option is chosen the laminar analysis program described in section 4.2 is called and the reduced data is printed out on the RGB monitor. A hard copy can be obtained from the EPSOM printer, see fig. [4.2.1] No further analyses or displays are available from this stage.

Option 2 - turbulent analysis If this option is chosen the turbulent analysis program, described in section 4.3, is called and the reduced data is available as before (a printout of this reduced data is shown on fig. [4.3.2]). From this stage a plot of the data on the turbulent universal velocity profile can be obtained by dumping the Calculated u+, y+ data to a disc file, then calling the appropriate graphics program and retrieving the data from the file. A hard copy of this plot can be acquired by calling the screen dump program as described previously. No further analysis or displays are available from this stage.

Option 3 - transitional analysis If this option is chosen a further decision on whether to use the laminar type analysis $\gamma \leqq 0.5$ or the turbulent type analysis $\gamma \geqq 0.5$ is required. The difference between the actual laminar and turbulent analysis described in sections 4.2 and 4.3 and the transitional versions of these programs is that the heading titles have been altered and the transitional skin friction value obtained from equation 4.21 is included in the analysis. The γ (y) distribution is also printed out and the near wall intermittency value is calculated by averaging the γ (y) values at all positions below $^{y}/_{\delta} = 0.2$, and is used for the solution of equation 4.21.

No further options are available and the program ends.

5.3 Special features of the package

After conducting an experiment, the data collected by the data acquisition and control program is dumped to a specified disc and the file is given a name. The data would normally be dumped to the upper disc, ie drive 1 or drive 3. If the specified drive is either full of data or the drive catalogue is full (the drive catalogue is capable of holding information on only 32 files) then the computer will sense an error code and terminate the program, thereby losing the collected data before it has been dumped to disc for permanent storage. To prevent this, the error code is intercepted within the software and the message, "Disk full-select another drive" is printed to screen. The data is then held in the computer memory until another drive has been specified or a new disc has been inserted into the drive unit. The program then down loads the data onto the new disc or alternative drive.

As all the package programs are stored on a Master disc, inserted into the lower drive, and the raw data files are stored on discs which are inserted into the upper drive, then switching between drives automatically within the software is necessary for smooth operation of the package. The drives can be selected within the software by the command *DR.X, but the X has to be an integer between 0 and 3 (eg *DR.1) and cannot be left as a free variable. For example the computer will not understand the following.

```
1Ø  X = 3
20  *DR.X
```

To overcome this a small procedure was developed to enable a variable, say D, for example, to select a specified drive:-

```
10  DEFPROC Drive (D)     - define procedure
20  IF D = Ø THEN *DR.Ø
30  IF D = 1 THEN *DR.1    select drive using
                           value of variable D
40  IF D = 2 THEN *DR.2
50  IF D = 3 THEN *DR.3
60  ENDPROC               - end procedure
```

Everytime a drive is to be selected by a variable the above procedure is simply called.

The drive number, on which the raw data file is stored, is passed between programs using one of the special variables A% to Z% on the BBC micro. These variables once specified are retained in the computer memory until they are overwritten or the computer is switched off. The BREAK or even CTRL/BREAK fuctions do not affect these variables.

To illustrate how data file names and drive numbers are passed between programs the following example, which can be considered as the end on one program and the start of a continuation program, is described.

Assume that the data file is stored on drive 3 and that the value D%, used to pass the drive number between programs, has been set to 3 at an earlier stage.

```
1ØØØ PROCDrive (D%)        - select drive 3

1Ø1Ø Ch%=OPENOUT'DATA'     - open file DATA for output to disc

1Ø2Ø PRINT#Ch%,NAME$       - put character string in NAME$
                             to file 'DATA'
1Ø3Ø CLOSE#Ch%             -

1Ø4Ø *DR.Ø                 - select drive Ø

1Ø5Ø CHAIN "Next prog"     - load next program from drive Ø
                             and RUN

  1Ø REM next program      -

  2Ø PROCDrive (D%)        - select drive 3

  3Ø Ch%=OPENIN'DATA'      - open file for input to computer
                             from file
  4Ø INPUT#Ch%,NAME$       - read character string in
                             NAMES from file DATA
  5Ø Close#Ch%             - close file
```

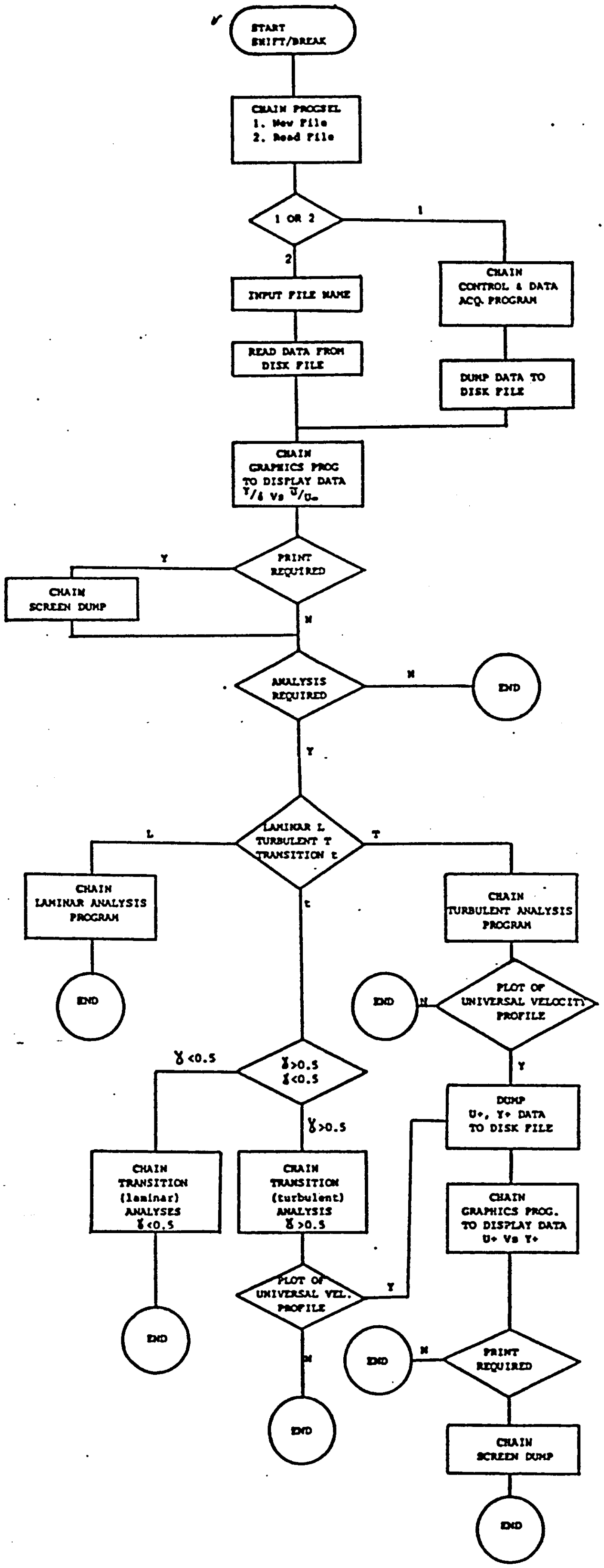

Fig. 5.2.1 Flow Diagram of Software Package

CHAPTER SIX

Details of Experiments and Discussion of Results

6.1 Introduction

With regard to the stated objectives a series of experimental flows were set up to investigate the influence of freestream turbulence and pressure gradient on the position and extent of the transition region in a boundary layer developing from the leading edge of a smooth flat plate. These flows are described in detail in this chapter and the results extracted from each flow are discussed and compared with alternative source data. The present method of defining the streamwise intermittency distribution through a transition region is compared to those of Abu-Ghannam & Shaw (1980) and Dhawan & Narasimha (1957) and statistical similarity of transition regions in zero and non-zero pressure gradients is observed. The transition length data acquired from the experiments is ultimately used to obtain a correlation which can be used to predict the combined effect of freestream turbulence and pressure gradient on the extent of the transition region.

6.2 Description of experimental flows

For each of the experimental flows the boundary layers were allowed to develop naturally from the leading edge of a smooth flat plate without the influence of external tripping devices such as vibrating ribbons, trip wires, surface roughness etc, to promote transition. The only factors considered to influence transition being the freestream turbulence level and the streamwise pressure distribution within the tunnel working section.

The natural test section turbulence level was approximately 0.35%. Three higher turbulence levels were generated by the insertion of various turbulence generating grids at a distance upstream from the leading edge, giving in all four test section freestream turbulence distributions. Details of these grids are given in section 2.4. For each grid the freestream turbulence distributions along the plate are remarkably constant as can be seen from fig. [2.4.1]. This is due to the positioning of the grids at a distance far upstream from the leading edge of the plate within the tunnel contraction, see fig. [2.1.1], allowing the grid generated turbulence to decay to an almost constant value before the flow reaches the plate leading edge.

Only the longitudinal component of the velocity fluctuation ie u' has been considered when calculating the freestream turbulence intensity. However, due to the constancy of the freestream turbulence distributions along the plate it is assumed that the turbulence is isotropic ie:-

$$Tu = \frac{1/3\sqrt{\overline{u'^2} + \overline{v'^2} + \overline{w'^2}}}{U_\infty} = \frac{\sqrt{\overline{u'^2}}}{U_\infty} \times 100 \qquad \text{........ 6.1}$$

No measurements of the v' and w' Velocity components were made to justify this but Blair (1980) showed that by the time grid generated turbulence had decayed to an almost constant value the three constituent fluctuating velocity components u', v' and w' were approximately equal. Fig. [6.2.1] which is a reproduction of fig. (31) from Blair (1980) supports this premise.

Blair also observed, in accordance with Baines and Peterson (1951), that the turbulence levels generated for each grid configuration were constant at a specific streamwise location, regardless of the freestream velocity. This agrees well with the freestream turbulence generated from the three grids used in this investigation as is shown in fig. [6.2.2]. A spectral analysis of the freestream turbulence levels generated by the various grids used for this investigation showed that in each case the bulk of the turbulence energy was contained at frequencies below 2 kHz. This is normal for grid generated turbulence, Meier & Kreplin (1980). The length scales of the freestream turbulence levels were also measured using a DISA-APA system and a similar set up to that used by Meier & Kreplin, to obtain auto-correlations for the turbulence generated by each grid. This showed that the streamwise length scales varied from 4 mm for grid 1 to 12 mm for grid 3. These values are similar to those obtained by Abu-Ghannam & Shaw (1980) who concluded that such a range of length scales would have a negligible effect on the position of the transition region. The conclusion from these measurements was that the various test section freestream turbulence levels generated for this investigation were concurrent with standard classical grid generated turbulence.

The pressure gradients were introduced by adjusting the variable height roof, as described in section 2.5, and are shown expressed in terms of pressure coefficient Cp in fig. [2.5.1]. The tunnel working section geometries were set up to give linear velocity distributions ie constant velocity gradients. Four roof settings were arranged to give, when expressed non-dimensionally, four velocity gradients ie a zero gradient $\frac{d\left(U/U_O\right)}{d\left(X/L\right)} = 0$, two adverse gradients $\frac{d\left(U/U_o\right)}{d\left(x/L\right)}$ =-0.23 & $\frac{d\left(U/U_o\right)}{d\left(x/L\right)}$ = -0.15 and a favourable gradient $\frac{d\left(U/U_o\right)}{d\left(x/L\right)}$ = 0.094. When expressed non-dimensionally in terms of $\frac{d\left(U/U_o\right)}{d\left(x/L\right)}$ the velocity gradients are independent of the tunnel reference velocity and are approximately constant for each roof setting. (Slight variations in the velocity distributions can be detected when the flow reference velocity and freestream turbulence are altered. This is due to the varying rates of growth of the tunnel boundary layers but amount to a variation of less then 3% from the mean in the worst case.) The mean velocity distributions for each roof setting are plotted in terms of $\left(U_\infty/U_o\right)$ and $\left(x/L\right)$ in fig. [6.2.3].

In all, twenty three flows were investigated each having a different combination of freestream turbulence and pressure gradient. Details of each of these flows are given in table 6.1 and are described briefly below.

Flows 1→4 are zero pressure gradient flows with freestream turbulence levels ranging from 0.35% to 1.40%. In order to position the transition region within the working area of the plate these flows had to be tested at the maximum tunnel reference velocity of, nominally, 18 m/s. Even at this maximum tunnel reference velocity the measured end of transition for the two lower freestream turbulence flows, ie flows 1 and 2, occurs just beyond the *safe* working area of the plate and in consequence are thought to occur prematurely in both cases.

Flows 5 → 12 are adverse pressure gradient flows. The working section geometry for these flows were set for the first *non-dimensional* adverse velocity gradient. Flows 5 to 8 are tested at the maximum tunnel reference velocity of 18 m/s while flows 9 to 12 are tested at a reduced reference velocity of nominally 10 m/s, giving two velocity gradients ie $dU/dx = -2.2s^{-1}$ and $dU/dx = -1.2s^{-1}$. Each flow was a different combination of velocity gradient and freestream turbulence. The relevant areas of interest for each of these flows occurs well within the safe working area of the plate.

Flows 13 → 20 are also adverse pressure gradient flows but with the working section geometry altered to give the second *non-dimensional* adverse pressure gradient. These flows were tested, as before, at tunnel reference velocities of nominally 18 m/s and 10 m/s giving two further velocity gradients $dU/dx = -1.4s^{-1}$ and $dU/dx = -0.75s^{-1}$.

Flows 21 → 23 are favourable pressure gradient flows. Unfortunately because of the tunnel geometrical constraints the adjustable roof had to be lifted above the level of the contraction outlet, in the region of the plate leading edge, to obtain a favourable pressure gradient within the tunnel working section, see fig. [6.2.4] below.

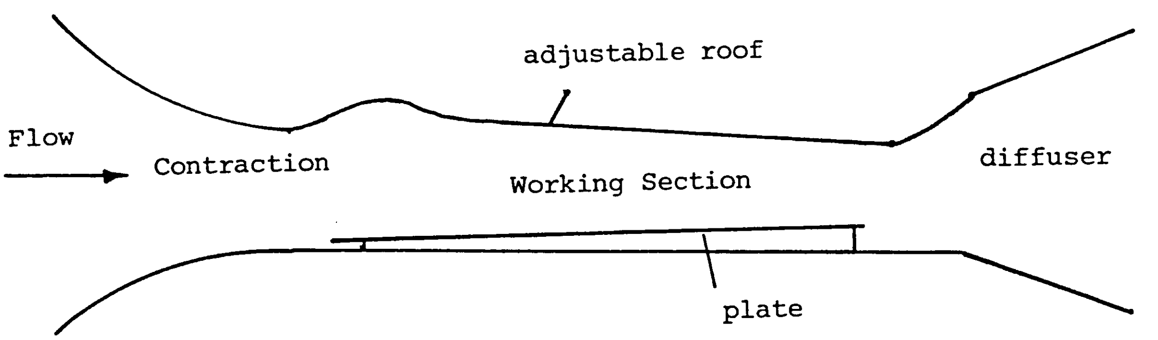

Fig. 6.2.4 Cross-section through tunnel Showing roof setting for favourable pressure gradients

Consequently as the flow enters the working section it is subjected to a fairly strong adverse pressure gradient, before it impinges on the plate leading edge and over the initial 150 mm of the plate surface. Due to the effect of this initial adverse pressure gradient the high freestream turbulence level flow (ie the flow with Grid 3 in position - Tu 1.4%), becomes transitional within the first 100 mm of the plate surface. This is far earlier than would have been expected had it been possible to set up a favourable pressure gradient over the entire length of the plate. For this reason no measurements are presented for grid 3 flows for the favourable pressure gradient case. Transition for flows 21, 22 and 23 begins well downstream of the initial adverse pressure gradient and disturbances within the boundary layer amplified by the initial adverse pressure gradient (though not enough to promote transition) are likely to have been damped out by the calming influence of the favourable pressure gradient, Schubauer & Skramstad (1948). However it would be reasonable to expect the initial adverse pressure gradient to have some detrimental effect on the boundary layer which is likely to promote early transition. The favourable pressure gradient flows described above were tested at the tunnel maximum reference velocity of 18 m/s to ensure that, at least the start of transition would be positioned within the plate safe working area. Disappointingly only in flow 21 (Tu 0.8%) did the end of transition occur within this region. The end of transition for flows 22 and 23 occurs well outwith the safe working area and as a consequence it is likely that the length of the transition region is shorter than would normally be expected.

Bearing in mind the observations overleaf the data available from the favourable pressure gradient flows, with the present experimental facility, is very limited.

6.3 Flow Measurements

For each of the twenty three flows described a series of measurements were made; these were:-

(i) Hot wire boundary layer traverses at regular streamwise intervals, along the centre line of the plate, measuring the mean velocity, rms velocity, and intermittency distribution through the boundary layer perpendicular to the plate.

(ii) The streamwise intermittency distribution along the plate centreline.

(iii) The streamwise freestream turbulence distribution.

(iv) The streamwise freestream velocity distribution.

The position of the start and end of transition were also noted and the velocity profiles at or very close to these positions were measured for each flow. This enabled measured values of integral thicknesses to be obtained at the start and end of transition.

A summary of the relevant data extracted from each flow is given in table 6.2. The freestream turbulence levels given in this table are the values at the position of start of transition ie

$$T_{u_S} = \frac{\sqrt{\overline{u_S'^2}}}{U_{\infty S}} \times 100 \qquad \ldots\ldots\ldots\ 6.2$$

although they vary very little, if at all, from the nominal values given in table 6.1 measured at the position of the plate leading edge.

A limited number of measurements from various other flows supplementary to the twenty three flows described in section 6.2 were made. These flows were tested at low tunnel reference velocities (U_o = 5 m/s for the adverse gradients and U_o = 10 m/s for the favourable gradient) and the only data extracted from them was the position of the start of transition. For this reason these flows were not numbered but when data from such a supplementary flow is presented on a diagram the relevant parameters are given alongside the plotted point.

6.4 Description of the transition process

Since the experiments of Schubauer & Skramstad (1948) it has generally been accepted that the breakdown process from laminar to turbulent motion, within a boundary layer, involves the amplification of small two dimensional disturbances superimposed on the laminar flow (ie Tollmein-Schlichting waves). At some critical Reynolds number the Tollmein Schlichting waves become unstable and grow as they move downstream eventually breaking down into *bursts* of random fluctuation characteristic of turbulent flow. These *bursts* occur in small localised regions in the form of turbulent spots, first observed by Emmons (1950), and grow in size as they travel downstream until they coalesce into a fully developed turbulent boundary layer. The region between the first occurrence of these turbulent spots and the position at which they merge to form a fully turbulent boundary layer is termed the transition region. Arnal et al (1977), Schubauer & Klebanoff (1956), Emmons (1950) and many others since have observed that the flow within a transition region alternates between the laminar and turbulent flow states. Although separate laminar and turbulent velocity components were not measured in this investigation, evidence to support this can be gleaned from measurements of the instantaneous velocity within a transitional boundary layer. Fig. [6.4.1] shows oscilloscope traces of the instantaneous velocities measured by a hot wire probe placed both near to the wall, and in the outer region of a transitional boundary layer. With the probe placed close to the wall (Trace (a)) the signal shows an increase in mean level as a turbulent region is encountered, and with the probe placed in the outer region of the boundary layer (Trace (b)) the signal shows a decrease in mean level as a turbulent region is encountered.

These observations are consistent with the sketch of the mean laminar and turbulent velocity profiles shown in this figure. At $y < y_c$ the turbulent component of mean velocity is greater than the laminar component and at $y > y_c$ the laminar component of the mean velocity is greater than the turbulent component. The implication here is that the transitional boundary layer consists of laminar and turbulent mean velocity components qualitatively similar to those shown in fig. [6.4.1].

Confirmation of this physical model is given by both Wygnanski et al (1976) and Arnal et al (1977). These researchers used conditional sampling techniques to measure the constituent profiles in and out of turbulent spots and verified that the component profiles within a transition region were characteristic of mean laminar and mean turbulent velocity profiles.

This model of the transition region can be used to describe the continuous growth of the mean boundary layer properties, through transition, from typical laminar to typical turbulent values: The process of transition involves an increase in momentum, displacement and energy thicknesses; a decrease in the displacement thickness shape factor H_{12} and a slight, but significant, increase in energy thickness shape factor, H_{32}. The skin friction coefficient also increases from a laminar to a turbulent value over the length of the transition region.

Typical distributions of the boundary layer parameters through a transition region are shown in fig. [6.4.2]. The points plotted on this figure are experimental points and the lines are mean lines drawn through the experimental data.

6.5 Start of transition - Correlations

The point at which a laminar boundary layer first becomes unstable (point of instability) is normally expected to lie upstream of the experimentally observed point of transition (ie the point at which turbulent bursts first appear) and the distance between these two points is dependent on the degree of amplification of disturbances within the boundary layer and the type of disturbance present in the freestream. Although a fair amount of success has been adhered in predicting the influence of various effects on the limit of stability, Schlichting (1979); to date no rational explanation from first principles is available for predicting the onset of turbulence, ie the transition point.

In order to obtain a practical solution to the prediction of the transition point, researchers have been striving to obtain realistic correlations which are applicable to as wide a range of practical situations as possible. To achieve this the factors which influence the position of transition must be identified and the major effects incorporated into the correlation. Two such effects which have been correlated with some success are the influence of freestream turbulence and pressure gradient on the transition point. In the absence of a pressure gradient it is known that increasing the freestream turbulence level will advance the onset of transition. This effect has been fairly well correlated by a number of researchers; two such correlations due to Van Driest and Blumer (1963) and Hall and Gibbings (1972) for zero pressure gradient flows are shown in fig. [6.5.1]. Plotted on this figure is the present data from the zero pressure gradient flows (FLOWS 1 → 4) which compare favourably with the correlations. Both correlations are similar and show that the effect of freestream turbulence on the position of transition (defined in terms of R_{θ_S} in fig. [6.5.1]) asymptotes to an almost constant value as Tu increases, the bulk of the effect being contained within the region $0 \leq Tu > 2\%$. A more recent correlation by Abu-Ghannam and Shaw (1980) is also shown on fig. [6.5.1] represented by a chain dotted line. This correlation is almost identical to that of Hall and Gibbings except that it has been modified to asymptote to the Tollmein-Schlichting stability limit $R_\theta = 163$, rather than the value of $R_\theta = 190$ used by Hall and Gibbings, to fit the wider range of data supplied by Brown and Burton (1978) and Martin et al (1978) for freestream turbulence levels up to 9.2%.

The correlations of Abu-Ghannam & Shaw, Van Driest & Blumer and others such as those due to Dunham (1972) and Seyb (1972) were developed further to take into account the combined effect of freestream turbulence and pressure gradient on the location of the transition point. It seems generally agreed that the effect of pressure graident can be best correlated against R_{θ_S} and Tu, when expressed in terms of a non-dimensional pressure gradient parameter, the most common being the Thwaites (1949), or modified pohlhausen parameter $\lambda_\theta = \frac{\theta^2}{\nu}\frac{dU_\infty}{dX}$; although recently the acceleration parameter $K = \frac{\nu}{U_\infty^2}\frac{dU_\infty}{dX}$ has become popular for quantifying the strength of favourable pressure gradients. See Brown & Martin (1976) and Blair (1982). The merits of these two parameters will be discussed in a later section.

Data from the present study is shown plotted against the most recent of these correlations, ie that of Abu-Ghannam and Shaw, on fig. [6.5.2]. For adverse pressure gradients, ie $\lambda_\theta < 0$ all the correlations mentioned previously shown the same general trend but for favourable pressure gradient $\lambda_\theta > 0$ the correlations of Dunham (shown as a chain dotted line in fig. [6.5.2]) and Seyb are in marked disagreement with the Abu-Ghannam & Shaw correlation, both showing a rapid increase in R_{θ_S} with increasing λ_θ.

The limited amount of favourable pressure gradient data from the present study and that of Blair (1982) would appear to substantiate the correlation of Abu-Ghannam & Shaw.

The value of R_{θ_s} gathered from the adverse pressure gradient flows in the present investigation generally lie below those forecast by Abu-Ghannam & Shaw's correlation. Two reasons for this are:-

(i) The method of detecting transition in the present work locates the start of transition very close to the appearance of the first turbulent bursts which is likely to be upstream of pointed located by Abu-Ghannam & Shaw because of the different detection techniques used (see section 4.7 for more detail). For this reason values of R_{θ_s} obtained by Abu-Ghannam & Shaw are likely to be higher than those obtained here for similar flow conditions.

(ii) The adverse pressure gradients were arranged to be effective directly from the plate leading edge, therefore, any leading edge disturbances would be amplified by the amplifying effect of the adverse pressure gradient and may lead to a breakdown of the laminar boundary layer at values of R_{x_s} less than would normally be expected. In retrospect it may have been advantageous to arrange a fairly strong favourable pressure gradient in the vicinity of the plate leading edge (say over the first 50 mm, or so, of the plate surface). This would have had the beneficial effect of damping any leading edge disturbances.

The correlation proposed by Abu-Ghannam & Shaw is based on a wide range of experimental data so there would be no justification to *tune* the correlation to give a better fit to the present data. However, having identified the above effects the present data is fairly reasonable and when compared to the actual data of Abu-Ghannam & Shaw it is within acceptable experimental scatter.

6.6 Statistical similarity of transition regions

As previously described in section 6.4 the transition region is composed of intermittent regions of laminar and turbulent flow. The turbulence originating in the form of small spots which grow downstream and eventually coalesce to form a completely turbulent flow regime.

Emmons (1951), who pioneered the concept of turbulent spots, introduced a spot source density function to describe the production of these spots and related this to the probability of the flow being turbulent at any time, ie the intermittency function γ. Dhawan & Narasimha (1957) argued that the spot source density function should have a maximum value at some point, which can be considered as the experimentally measured point of transition, and that downstream of this point the turbulence probability could be defined by the unique relation

$$\gamma = 1 - e^{A\xi^2} \qquad \ldots\ldots\ldots \quad 6.3$$

where $\xi = (x - x_s)/\lambda$ is a normalised streamwise co-ordinate in the transition region and λ is a measure of the extent of the transition region.

Dhawan & Narasimha showed that the distribution of intermittency was universal on the $\overline{\gamma}$ (ξ) plot irrespective of the physical length of the transition region. This was supported by the earlier work of Schubauer & Kelbanoff (1956) who gave rise to the concept of the statistical similarity of transition regions. In contrast to Dhawan & Narasimha, Schubauer & Klebanoff normalised the streamwise intermittency distribution ($\overline{\gamma}$) to the normal distribution function, matching the curve at $\overline{\gamma} = 0.5$ using the normalised streamwise co-ordinate $\zeta = (x - \overline{x})/\sigma$. Where σ, the standard devitation, is a measure of the extent of the transition region and $\overline{x}$ is the distance from the leading edge to the point where $\overline{\gamma} = 0.5$.

In both papers mentioned overleaf, the intermittency distributions were measured only in zero pressure gradients and both make the observation that it does not necessarily follow that transition regions will exhibit the same distribution of $\overline{\gamma}$ in the presence of a pressure gradient.

The present investigation makes use of the work by Schubauer & Klebanoff, in assuming the value σ to be representative of the transition length. A computer program was written to calculate the mean value of σ from the experimentally measured $\overline{\gamma}$ (x) distribution stored in a disc file. For computational convenience the normal distribution or Gaussian integral curve was represented by a polynomial approximation to the curve, ie equation 6.4.

$$\overline{\gamma} = \tfrac{1}{2}[1 + \frac{\zeta}{|\zeta|}(0.8273\ |\zeta| - 0.096\ |\zeta|^2 - 0.073\ |\zeta|^3 + 0.0165\ |\zeta|^4)] \qquad \ldots\ldots\ldots \quad 6.4$$

$$\text{where} \quad \zeta = \frac{x - \overline{x}}{\sigma} \qquad \ldots\ldots\ldots \quad 6.5$$

(Care has to be taken of the singularity point at $\zeta = 0$)
The polynomial approximation to the normal distribution is shown on fig. [6.6.1]. To the scale of this diagram no difference between the two is detectable.

The procedure for determing the standard deviation of the intermittency distribution was to firstly obtain the value of $\overline{x}$, the location of the $\overline{\gamma} = 0.5$ point. This was done by fitting a least squares straight line to all the experimentally measured points in the region $0.75 < \overline{\gamma} > 0.25$, as the distribution is approximately linear in this region, and determining $\overline{x}$ from the resulting straight line equation. Using the experimentally obtained values of $\overline{\gamma}$ for each point the value of ζ is determined by iteration of equation 6.4 and substitution of this value into equation 6.5 gives the value of σ for each point. The average value of σ is then taken to be representative of the complete distribution. The experimental $\bar{\gamma}$ (x) data is then converted to $\bar{\gamma}$ (ζ) data using the calculated values of $\bar{x}$ and average σ value. These experimental points are then plotted graphically on the display monitor and compared to the normal distribution represented by equation 6.4.

Assuming x_s is measured at $\gamma = 0.01$ and x_e is measured at $\gamma = 0.99$ then the corresponding normalised co-ordinate (ζ) for the start and end of transition will be -2.30 and +2.30 respectively. The length of the transition region can therefore be related to the standard deviation σ by the relation

$$x_l = 4.6\sigma$$

or non-dimensionally

$$R_{x_l} = 4.6R_\sigma \qquad \text{........} \quad 6.6$$

The experimentally measured value of $x_l = (x_s - x_e)$ is plotted against the value of x_l calculated from equation 6.6 in fig. [6.6.2]. Excellent agreement between the measured value of x_l and that obtained from equation 6.6 can be seen from this figure.

Fig. [6.6.3 (a)] shows the intermittency data from the present experimental flows plotted separately for the adverse, zero and favourable pressure gradient cases, against the γ (ζ) distribution. Figs. [6.6.3 (b)] and [6.6.3 (c)] shown the same data plotted in the γ (ξ) distribution of Dhawan & Narasimha and the γ (η) distribution of Abu-Ghannam & Shaw. It can be seen from these figures that the present method of defining the intermittency distribution is superior to the other two methods mentioned overleaf. The reason for this lack of agreement between the present distribution, $\gamma(\zeta)$ and the $\gamma(\xi)$ and $\gamma(\eta)$ distributions of Dhawan & Narasimha and Abu-Ghannam & Shaw respectively, is that the latter two distributions use x_s as the datum length, whereas $\bar{x}$, used in the present method is more readily defined. Also the parameters used for normalising the transition co-ordinates ξ and η, by Dhawan & Narasimha and Abu-Ghannam & Shaw are defined by only two points in the transition region. The normalising parameter, σ, used in the present method is calculated for each data point and an average value is used to define the distribution.

From fig. [6.6.3 (a)] and fig. [6.6.2], it can be seen that neither the pressure gradient nor the freestream turbulence has any influence in the intermittency distribution when expressed in terms of γ and ζ. This is consistent with the observations of Abu-Ghannam & Shaw. However, it is likely that if the pressure gradient was to alter drastically within the transition region (eg if it were to change sign) then the intermittency distribution expressed in terms of $\gamma(\zeta)$ might not follow the normal distribution curve shown in fig. [6.6.1].

6.7 The effect of freestream turbulence on transition length (zero pressure gradient)

As described in the previous sections the degeneration of the flow from the laminar to the turbulent state is not instantaneous but occurs over a finite length. Although a number of researchers have conducted experiments to determine the influence of various effects on the point at which this degeneration begins, see section 6.5, very little information is available on the influence of the various parameters on the extent of the transition region.

A popular method of obtaining the transition length is to use the *very* approximate relationship of Dhawan & Narasimha who defined the Reynolds number, based on the transition length parameter λ, as a function of the length Reynolds number at the start of transition, equation 6.7.

$$R_\lambda = 5 R_{x_s}^{0.8} \qquad \text{........} \qquad 6.7$$

From the data presented by Dhawan & Narasimha, Dunham (1972) observed that the total transition length, x_l, could be related to the length parameter λ by the relationship

$$x_l = 3.36\lambda \qquad \text{........} \qquad 6.8$$

Therefore, modifying Dhawan & Narasimha's original relationship to give the transition length, results in:-

$$R_{x_l} = 16.8\ R_{x_s}^{0.8} \qquad \text{........} \qquad 6.9$$

Dunham further modified this using the Blasius relation $R_\theta = 0.664\sqrt{R_x}$, to

$$R_{x_l} = 31.8\ R_{\theta_s}^{1.6} \qquad \text{........} \qquad 6.10$$

for zero pressure gradient flows. Debruge (1970) proposed a similar correlation to that of Dhawan & Narasimha, merely adjusting the constant and power terms to fit his particular range of data.

$$R_\lambda = 0.005\ R_{x_s}^{1.28}$$

Even as recently as 1980, Abu-Ghannam & Shaw used an unmodified version of Dhawan & Narasimha's original correlation to determine the extent of the transition region and used this as the basis for calculating the boundary layer development through the transition region.

However, Dhawan & Narasimha stated orginally that their proposed correlation was no more than speculative due to the considerable degree of scatter of the experimental data (disguised by a log-log plot, in Fig. 5 of Dhawan & Narasimha's original paper). They also suggested that a family of R_λ v's R_{x_s} curves, each depending on the specific agency causing transition, would be more realistic.

The present approach to defining the transition length is somewhat different to the Dhawan & Narasimha approach in that the effects influencing the transition length are directly correlated to a transition length Reynolds number based on the length parameter σ, ie

$$R_\sigma = \frac{U_{\infty s}\ \sigma}{\nu} \qquad \text{........ 6.11}$$

(The length parameter λ can be related to σ by the relationship $\lambda = 1.37\sigma$). This new approach is however, consistent with the implications of Dhawan & Narasimha's relationship ie equation 6.7.

The present correlation for the effect of freestream turbulence on the transition length in zero pressure gradient flow is shown on fig. [6.7.1]. (R_σ is correlated to the local value of freestream turbulence at the transition point although as described earlier the freestream turbulence level is almost constant over the entire length of the plate). Also plotted on this figure is the present data and that of previous workers. Unfortunately transition length/freestream turbulence level data is very scarce for zero pressure gradient flows and is almost non-existent for non-zero pressure gradient flows, in the presently available literature.

The available data is best correlated by:-

$$R_{\sigma} = \left[270 - \frac{250\ T_u^{3.5}}{(1 + T_u^{3.5})}\right] \times 10^3 \qquad \ldots\ldots\ldots \quad 6.12$$

The upper limit for R_{σ} was obtained from Schubauer & Skramstad (1947). Schubauer & Skramstad showed that R_{x_S} reached an upper limit at a freestream turbulence level of about 0.1% and decreasing the freestream turbulence below this value had no further effect on R_{x_S}. The value of R_{x_l} was also constant in this range but did increase from $0.1 < Tu > 0.25$. However, flows with freestream turbulence levels of less than 0.25% are probably of limited practical significance, excepting the case of free flight, so the value of $R_{\sigma} = 270 \times 10^3$ obtained from Schubauer & Skramstad, for flows with $Tu < 0.1$, was taken to be the upper limit and is held constant at this value until $Tu = 0.25$ is exceeded. At this point there is a rapid decrease in R_{σ} with increasing freestream turbulence, eventually asymptoting to a lower limiting value, as implied by Abu-Ghannam & Shaw and Hall & Gibbings, of $R_{\sigma} = 20 \times 10^3$. This concept of a lower limit is thought to be reasonable as transition is always expected to occur over some finite length.

6.8 Combined effect of freestream turbulence and adverse pressure gradient on transition length

Whereas it is possible to eliminate the effect of freestream pressure distribution enabling the independent effect of freestream turbulence to be examined, it is not possible, due to the natural level of freestream turbulence present in all wind tunnels, to separate the effect of freestream turbulence from pressure distribution in non-zero pressure gradient flows. In consequence only the combined influence of the two effects on the transition length can really be examined. However, for the present investigation the pressure gradients were all arranged to give constant velocity gradients and the freestream turbulence levels attributed to each flow were nominally constant over the plate working length. Each flow could therefore be specified by a single value of velocity gradient, dU_∞/dX, and freestream turbulence level, Tu. It was thus possible to compare the effect of varying dU_∞/dX on the transition length and location for a range of constant freestream turbulence flows and also to compare the effect of varying Tu on the transition length and location for a range of constant velocity gradient flows. Figs. [6.8.1], [6.8.2] and [6.8.3] were constructed, therefore to give an *indication* of the separate effects. (The dotted lines drawn through the data on these figures serve to highlight the effects and are not meant to imply any specific relationship).

From fig. [6.8.1] it can be seen that the effect of increasing the velocity gradient at a constant value of freestream turbulence has the effect of advancing the onset of transition and, to a greater extent, advancing the position at which transition ends, ie the position where the flow becomes fully turbulent. Hence increasing $\frac{dU_\infty}{dx}$ has the effect of decreasing the transition length. This substantiates the observations of Schubauer & Klebanoff (1956) and Tani (1969). From this figure it can also be seen that the influence of increasing the velocity gradient (ie the adverse gradient becoming more negative) on the position of the start of transition is less significant as the freestream turbulence level is increased.

Fig. [6.8.2] shows the effect of increasing freestream turbulence level in a constant velocity gradient flow. As can be seen from this figure the effect of increasing freestream turbulence appears to increase the transition length. This effect is most significant for low freestream turbulence levels, below 1%, and tends to fade for higher turbulence levels and may in fact reverse to give a decrease in transition length with further increase in freestream turbulence level.

This can be explained by examination of fig. [6.8.3] as follows: At low freestream turbulence levels approximately below 1% slight increases in the value of freestream turbulence have a marked effect in advancing the onset of transition but appear to have less of an effect on the end of transition. This is due to the fact that the end of transition has already been advanced to, perhaps, a more stable position by the effect of the adverse velocity gradient and is not likely to be advanced further by low freestream turbulence levels or small changes in freestream turbulence. However at higher freestream turbulence levels ($Tu \geqq 1.0$) the effect on the advancement of the transition point by increasing the freestream turbulence level becomes less significant until, as in the case of zero pressure gradient flows, further increase in Tu causes no further advancement of the start of transition. As this asymptotic position is approached the lengthening effect of increasing Tu will decrease and may in fact reverse if the rate at which the end of transition is advancing due to increasing Tu is greater than that of the start of transition. At some point both the position of the start and end of transition will reach their respective minimum limiting values where further increase in Tu will result in no further effect on transition length.

6.9 The effect of favourable pressure gradient on transition length

Although a considerable amount of experimental effort was expended in setting up and making measurements in favourable pressure gradient flows, the effect of the velocity gradient on transition length can only be examined for one single flow (ie Flow 21). The other favourable velocity gradient flows (Flows 22 & 23 and various other supplementary flows) are either severely affected by the adverse pressure gradient in the region of the plate leading edge, see section 6.2, or the end of transition occurs beyond the safe working region of the plate. However from flow 21 and the zero pressure gradient counterpart, flow 3, (both with a freestream turbulence level of 0.8%), it can be seen that the effect of introducing a favourable velocity gradient is to delay the start of transition and to a greater extent delay the end of transition, hence increasing the transition length. This effect is shown in Fig. [6.9.1] and as would be expected is opposite to the effect observed in adverse velocity gradient flows. Unfortunately no comments can be made as to the effect of freestream turbulence on the transition length in favourable velocity gradient flows as there is insufficient data.

6.10 Correlating the combined influence of freestream turbulence and pressure gradient on transition length

As described in the previous section there is only one favourable pressure gradient flow (Flow 21) for which transition length data can be confidently extracted. For this reason the correlation presented here is limited to zero and adverse gradient cases but could possibly be modified to account for favourable gradients if reliable data becomes available.

The major obstacle in correlating experimental data is in defining adequate non-dimensional parameters which are sufficient in independent variables to describe the problem. The present transition length data and that of previous researchers appears to correlate fairly well in terms of the transition length Reynolds Number R_σ, and the local value of freestream turbulence at the start of transition Tu_S, as shown in fig. [6.7.1]. To correlate the transition length data in adverse pressure gradients the present approach was to modify this correlation using some parameter, involving the velocity gradient, which would describe the effects outlined in section 6.8. This approach has been used in the past by other researchers to correlate the position of the onset of transition in non-zero pressure gradient flows. The most popular parameter to account for pressure gradient effects being the modified Pohlhausen/Thwaites parameter, $\lambda_\theta = \frac{\theta^2}{\nu} \frac{dU_\infty}{dx}$, although other parameters such as the acceleration parameter $K = \frac{\nu}{U_\infty^2}\frac{dU_\infty}{dX}$ and a non-dimensional velocity gradient parameter $\frac{d\,^{U_\infty}/_{U_o}}{d\,^{x}/_{L}}$, have been used by other researchers such as Brown & Burton (1978) and Blair (1982).

A fairly recent paper by Brown & Burton (1976) and discussion by Gibbings and Slanciauskas & Pėdisius, reviews the merits of the modified Pohlhausen/Thwaites parameter, λ_θ and the acceleration parameter, K. Brown & Burton suggest that K is a more suitable parameter than λ_θ for correlating pressure gradient effects mainly because it is composed of independent variables which are directly measurable and therefore more readily useable by the design engineer. This is obviously an advantage, but a distinct disadvantage of this parameter is that it does not, through any of its component variables, account for the history of the flow. The present author suggests that λ_θ is a more suitable parameter for correlating the effects of freestream turbulence and pressure gradient on the position and extent of transition for the following reasons:

(a) to some degree the history of the flow is taken into account through the inclusion of the boundary layer momentum thickness as a variable;

(b) when using a local value of λ_θ at the start of transition or perhaps an averaged value of λ_θ as suggested by Granville (1953) and Abu-Ghannam & Shaw (1980), the parameter is influenced by both the freestream turbulence and velocity gradient;

(c) more important is the fact that the present transition length data appears to correlate well in terms of R_σ, Tu and λ_θ.

The correlation presented on fig. [6.10.1] uses the local value λ_{θ_S} although an averaged value of λ_θ from the origin of the boundary layer to the point of transtion would account further for previous flow history. However with the linear velocity gradients used in this investigation the λ_θ distribution is almost linear, therefore such an average would merely result in halving the local values at the start of transition. Abu-Ghannam & Shaw actually found no improvement in their correlation by using a mean value of λ_θ defined by

$$\lambda_\theta = \frac{1}{x_S - x_O} \int_{x_O}^{x_S} \lambda_\theta \, dx \qquad \text{........ 6.13}$$

but did in fact find an improvement in correlation when using the extreme value of λ_θ ie the local maximum value of λ_θ. For the present experimental flows λ_θ (extreme) will always occur at the start of transition ie $\lambda_{\theta\,(extreme)} = \lambda_{\theta_S}$.

It may seem rather speculative to relate the transition length to local values at the start of transition but the degree of correlation would appear to justify this speculation. The final correlation shown in fig. [6.10.1] is represented by

$$R_\sigma = \left[270 - \frac{250\ Tu^{3.5}}{1 + Tu^{3.5}}\right] \left[\frac{1}{1+1710(-\lambda_\theta)^{1.4} \exp -\sqrt{1+Tu^{3.5}}}\right] \times 10^3 \quad 0<\lambda_\theta>-0.04 \qquad \text{........ 6.14}$$

$R_\sigma = 20 \times 10^3 \quad \lambda_\theta <-0.04$

It may appear that this correlation does not illustrate the effect described in section 6.8, that at low freestream turbulence levels increasing Tu increases the transition length. However as suggested previously in this section the parameter λ_θ accounts for the combined freestream turbulence and pressure gradient effect. Increasing freestream turbulence advances the onset of transition and hence reduces λ_{θ_S}, which is indicated in the correlation by an increase in R_σ at low values of Tu. At higher freestream turbulence levels (say above 1%) the effect of increasing freestream turbulence on θ_s is small, however λ_θ will still reduce but not to the extent that R_σ increases, as at the higher levels of freestream turbulence the direct effect of Tu is having a dominant effect in reducing R_σ.

The limit of $R_\sigma = 20 \times 10^3$ at $\lambda_\theta < -0.04$ was specified to fit the present adverse pressure gradient data and to correspond to the limit in the zero pressure gradient correlation of R_σ and Tu.

The experimentally measured values of R_σ are plotted against those obtained from equation 6.14 on Fig. [6.10.2]. Fig. [6.10.3] shows the experimentally measured values of R_λ plotted against those obtained from the Dhawan & Narasimha correlation (equation 6.7). Comparison of these two figures shows the marked improvement of the present correlation over that of Dhawan & Narasimha for the present data. Unfortunately, very little alternative source data is available in the present literature which can be plotted on this correlation. It is hoped, however, that this work will show other researchers that it is possible to correlate the transition length, expressed non-dimensionally as a transition length Reynolds number, directly in terms of external influences such as freestream turbulence and pressure gradient. Also it is hoped that this will stimulate other researchers to producing a wider range of suitable data and that the correlation can then be tuned or modified to suit a wider range of practical situations.

FLOW NO	Roof Setting	U_o (m/s)	$\frac{d\ U_\infty/U_o}{d\ x/L}$	$\frac{du}{dx}$ L=2000mm	Tu% (Nominal)
1	ZERO	18.2	Ø	Ø	0.35
2		18.25	Ø	Ø	0.45
3		18.0	Ø	Ø	0.75
4		18.6	Ø	Ø	1.40
5	1st ADVERSE	18.4	-0.235	-2.15	1.40
6		18.5	-0.240	-2.20	0.80
7		18.3	-0.240	-2.20	0.40
8		18.4	-0.240	-2.20	0.30
9		10.7	-0.225	-1.20	1.40
10		10.4	-0.225	-1.20	0.80
11		10.0	-0.225	-1.15	0.40
12		10.1	-0.230	-1.20	0.30
13	2ND ADVERSE	18.5	-0.150	-1.40	1.35
14		18.3	-0.150	-1.40	0.75
15		18.0	-0.150	-1.35	0.40
16		18.0	-0.150	-1.35	0.30
17		10.3	-0.145	-0.75	1.35
18		10.3	-0.150	-0.80	0.80
19		10.1	-0.150	-0.75	0.40
20		10.1	-0.150	-0.75	0.30
21	FAV.	18.4	0.095	0.90	0.80
22		18.0	0.095	0.85	0.50
23		17.9	0.10	0.90	0.40

Table 6.1 Test Flow details

Flow No	U_o (m/s)	Tu_s%	$\frac{dU_\infty}{dx}$	X_s (mm)	X_c (mm)	(a) θ_s (b.l) (mm)	(b)* θ_s (Tani) (mm)	θ_e (mm)	λ_θ $\frac{\theta_s^2}{\nu}\frac{dU_\infty}{dx}$	σ (mm)	λ (mm)
1	18.2	0.35	0	1300	1775	0.70	0.70	1.29	0	102	130
2	18.25	0.40	0	1250	1685	0.61	0.68	1.23	0	88	115
3	18.0	0.78	0	500	1225	0.43	0.44	1.23	0	156	145
4	18.6	1.30	0	150	585	0.26	0.24	0.86	0	95	105
5	18.4	1.32	-2.15	30	310	-	0.11	0.60	-0.0017	66	95
6	18.5	0.84	-2.20	175	480	0.27	0.27	0.85	-0.011	62	88
7	18.3	0.38	-2.20	315	560	0.35	0.36	0.89	-0.019	55	72
8	18.4	0.30	-2.20	280	410	0.36	0.34	0.75	-0.18	30	34
9	10.7	1.40	-1.20	130	525	0.31	0.30	1.20	-0.007	93	115
10	10.4	0.74	-1.20	375	575	0.51	0.53	1.15	-0.022	46	60
11	10.0	0.38	-1.15	505	650	0.60	0.64	1.35	-0.031	31	34
12	10.1	0.30	-1.20	430	530	0.57	0.59	0.52	-0.029	25	25
13	18.5	1.35	-1.40	100	460	-	0.20	0.78	-0.0034	79	80
14	18.3	0.77	-1.40	270	700	0.33	0.33	1.02	-0.01	99	125
15	18.0	0.38	-1.35	490	750	0.44	0.46	0.75	-0.19	62	70
16	18.0	0.30	-1.35	675	980	0.50	0.54	1.65	-0.021	64	80
17	10.3	1.35	-0.75	260	750	0.45	0.43	1.33	-0.009	113	138
18	10.3	0.77	-0.80	525	1000	0.66	0.64	1.40	-0.020	106	150
19	10.1	0.40	-0.75	875	1065	0.72	0.88	2.00	-0.040	42	54
20	10.1	0.34	-0.75	820	1275	0.68	0.80	2.20	-0.024	100	145
21	18.4	0.80	0.90	525	1325	0.43	0.43	1.30	0.01	170	225
22	18.0	0.50	0.85	1425	1800	0.69	0.67	1.18	0.027	84	105
23	17.9	0.40	0.90	1390	1875	0.70	0.66	1.24	0.028	104	135

Table 6.2 Results Summary

*(a) Calculated from measured velocity profile

(b) predicted by Tani's (1954) method

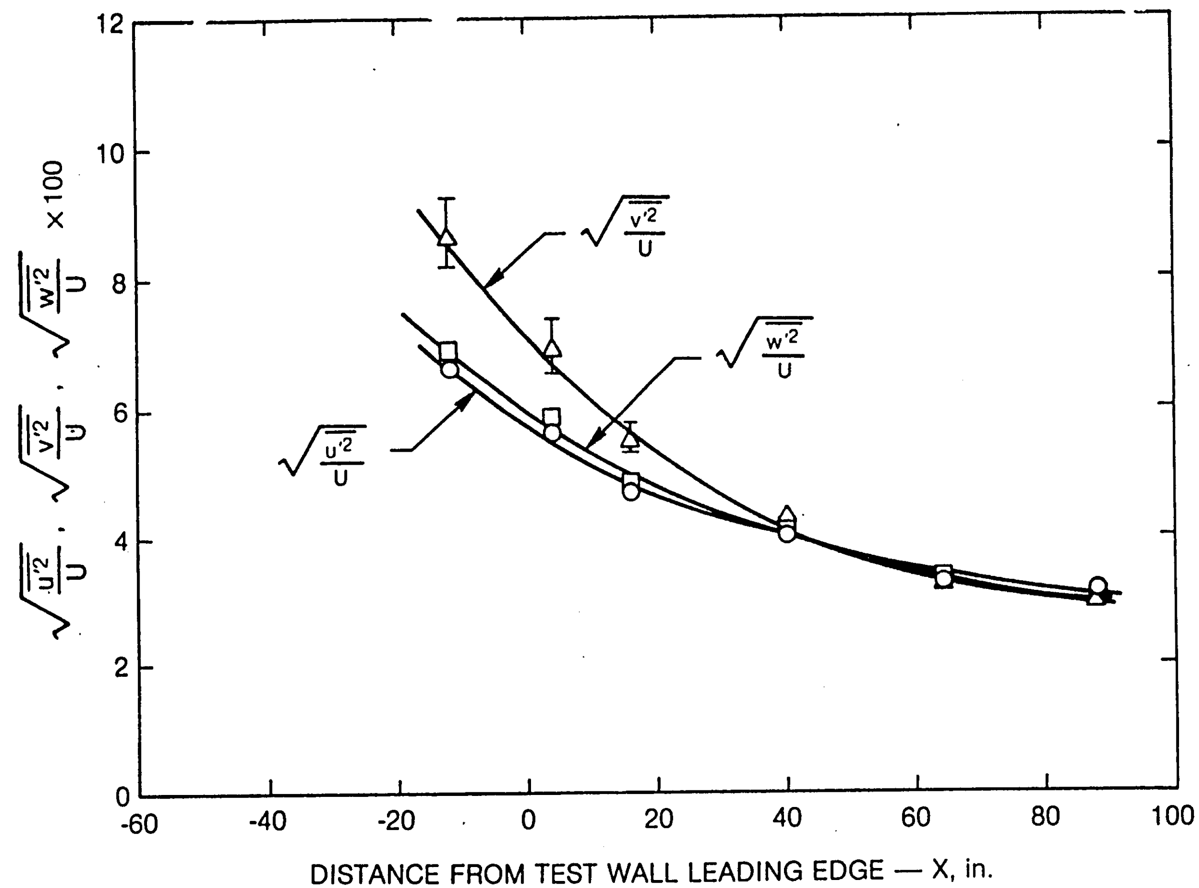

Fig. 6.2.1 <u>Streamwise distribution of freestream turbulence components (reproduction from Blair (1980))</u>

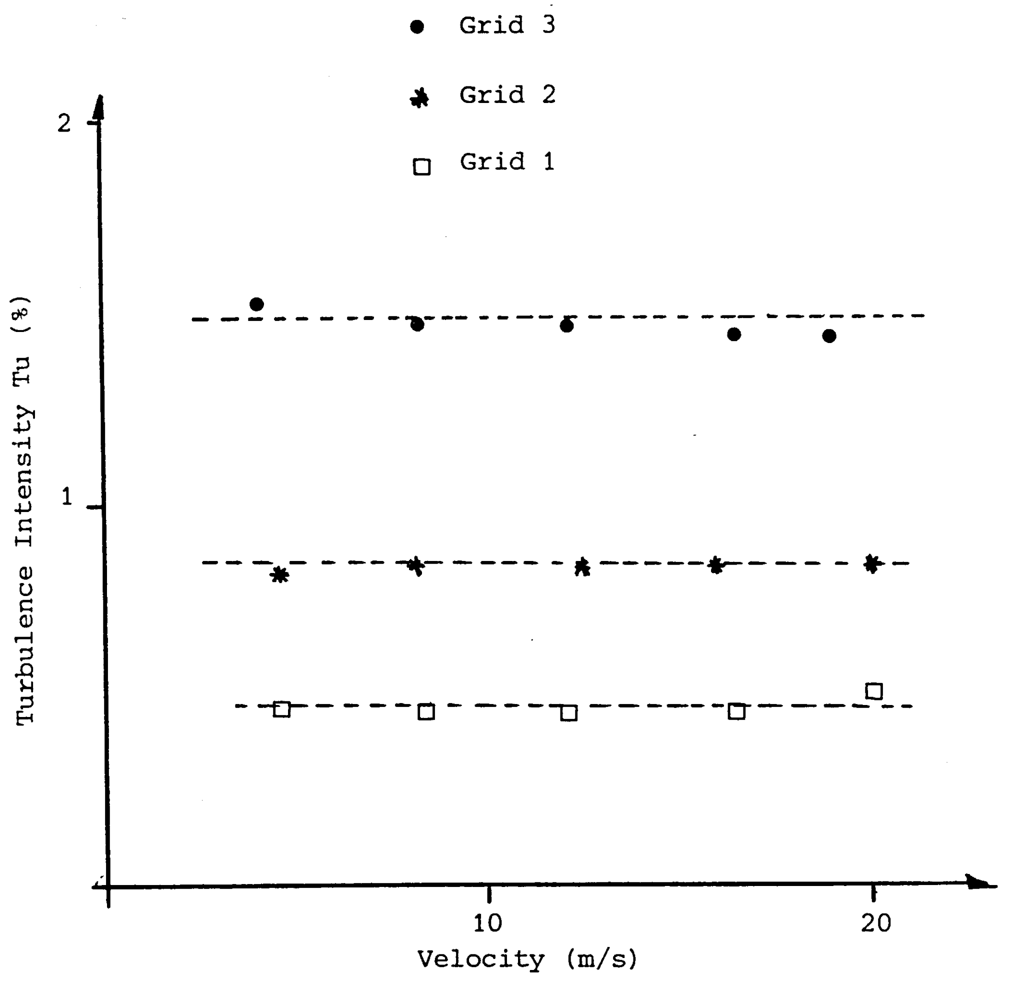

Fig. 6.2.2. <u>Turbulence intensity as a function of velocity</u>

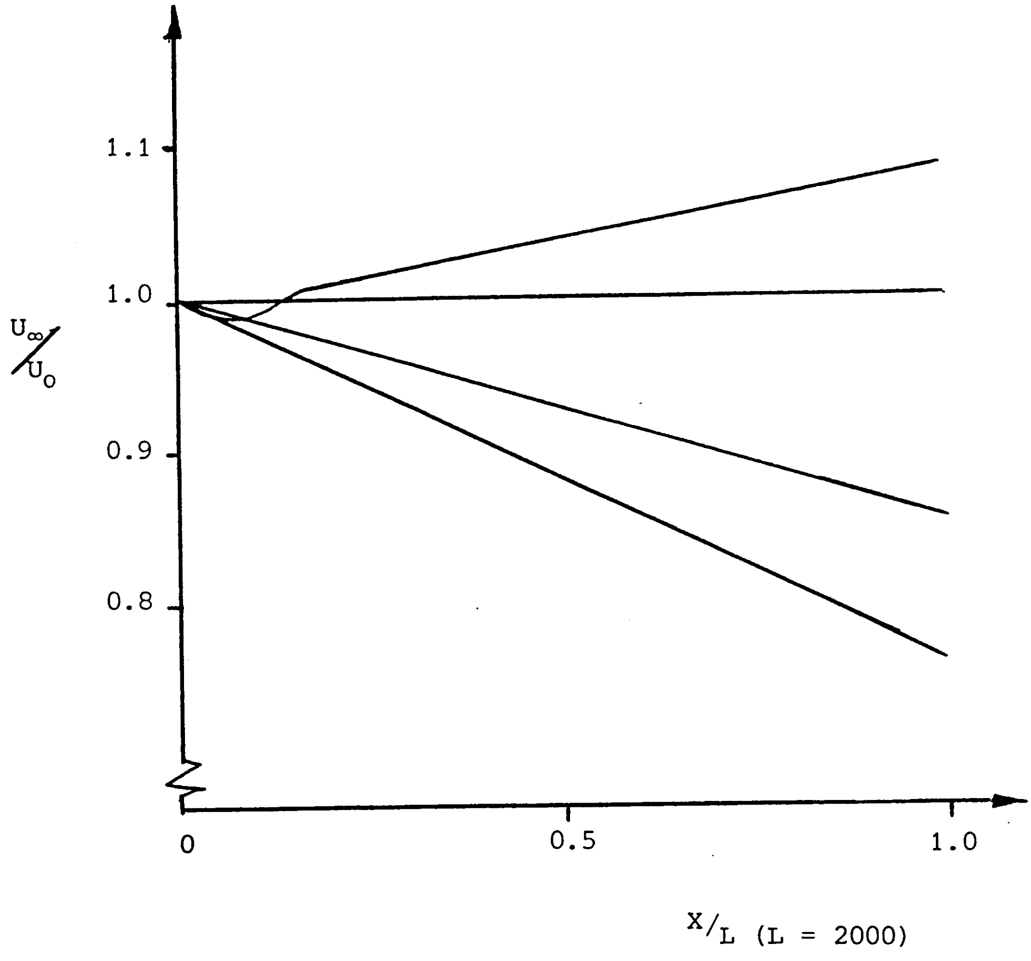

Fig. 6.2.3. Mean freestream velocity distributions for the four working section geometries tested

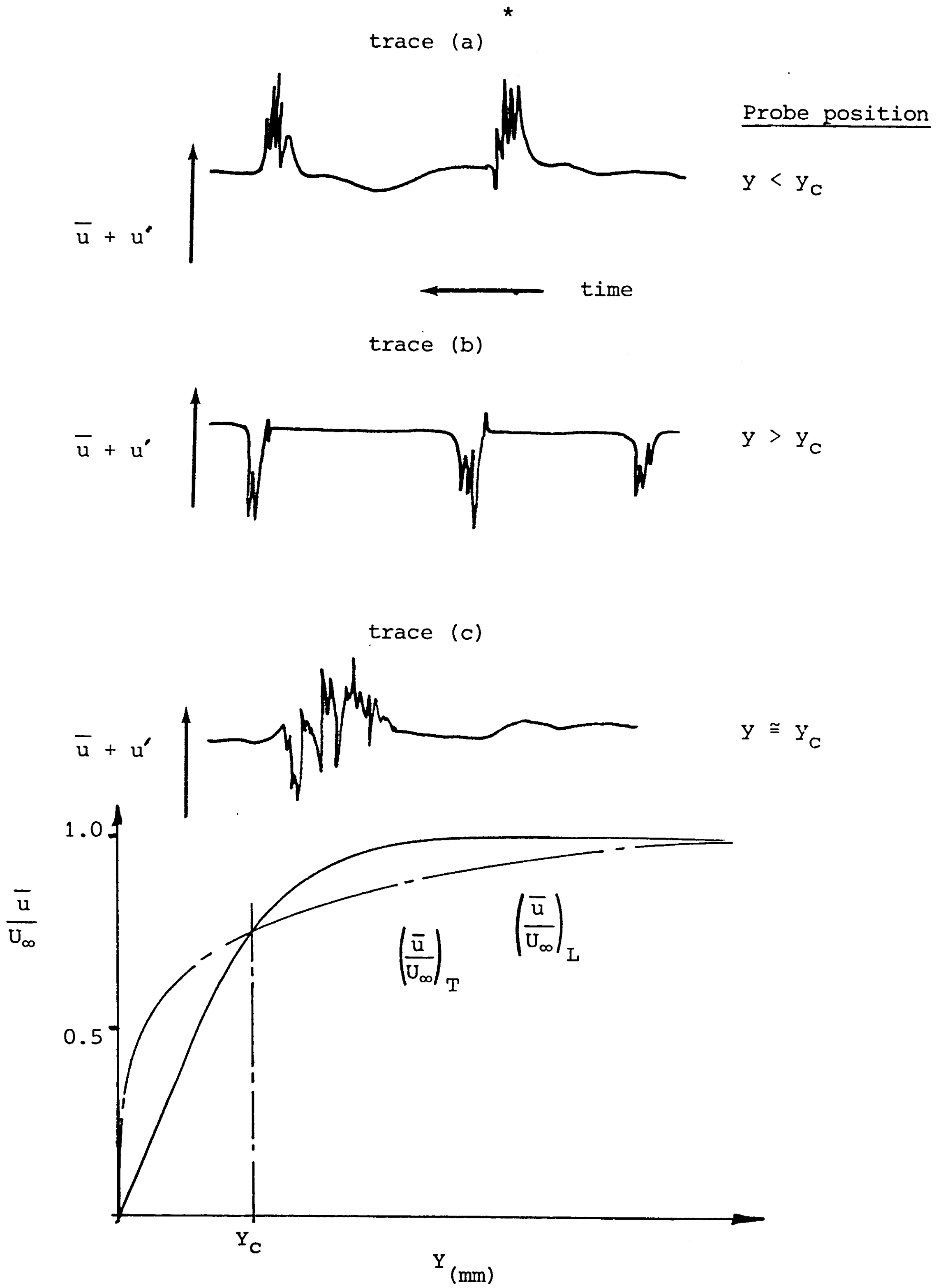

*The above traces were traced from photographs of a storage oscilloscope screen.

Fig. 6.4.1 Instantaneous velocity within a transitional boundary layer ($\gamma \cong 0.1$)

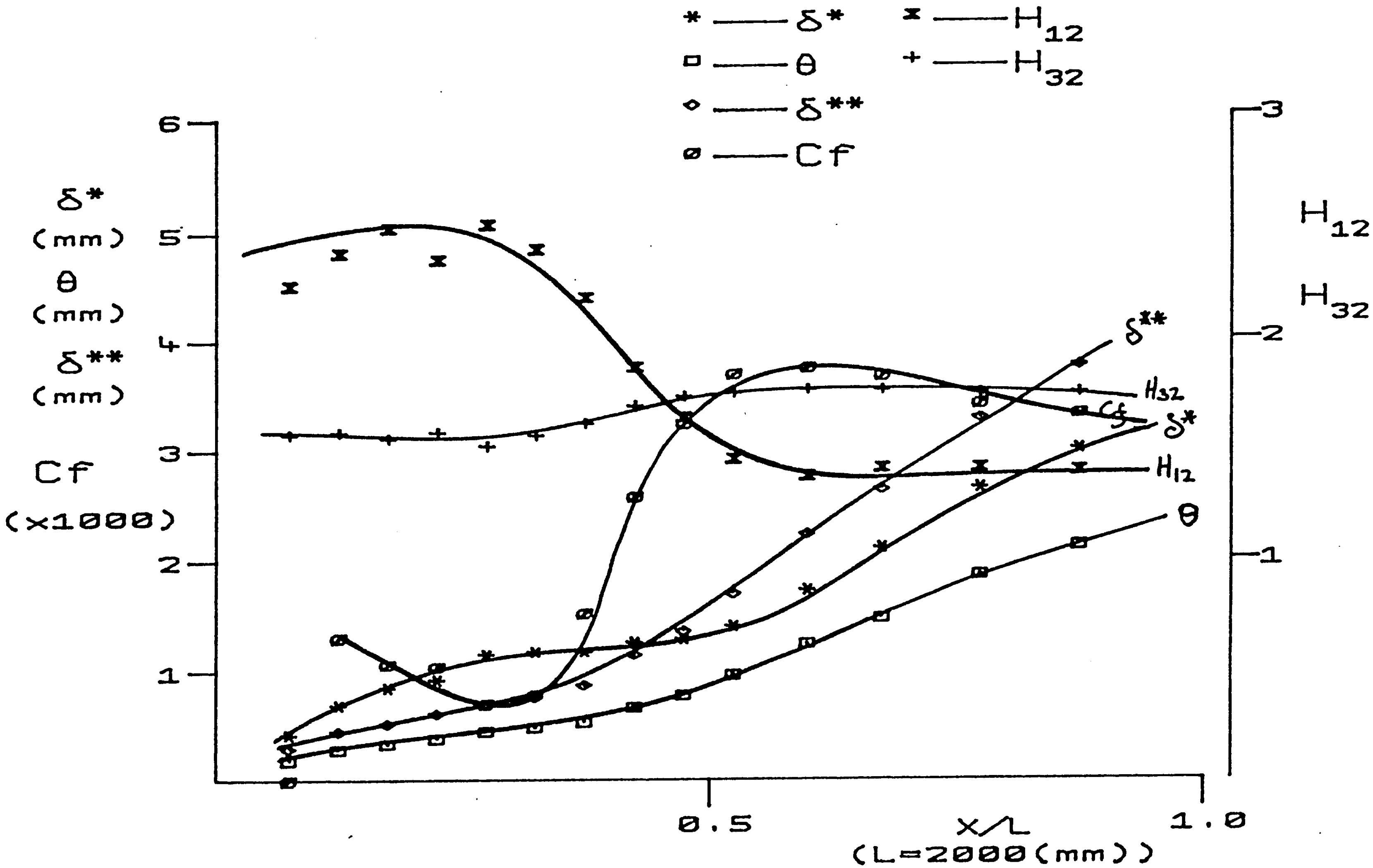

Fig. 6.4.2 Development of boundary layer through transition

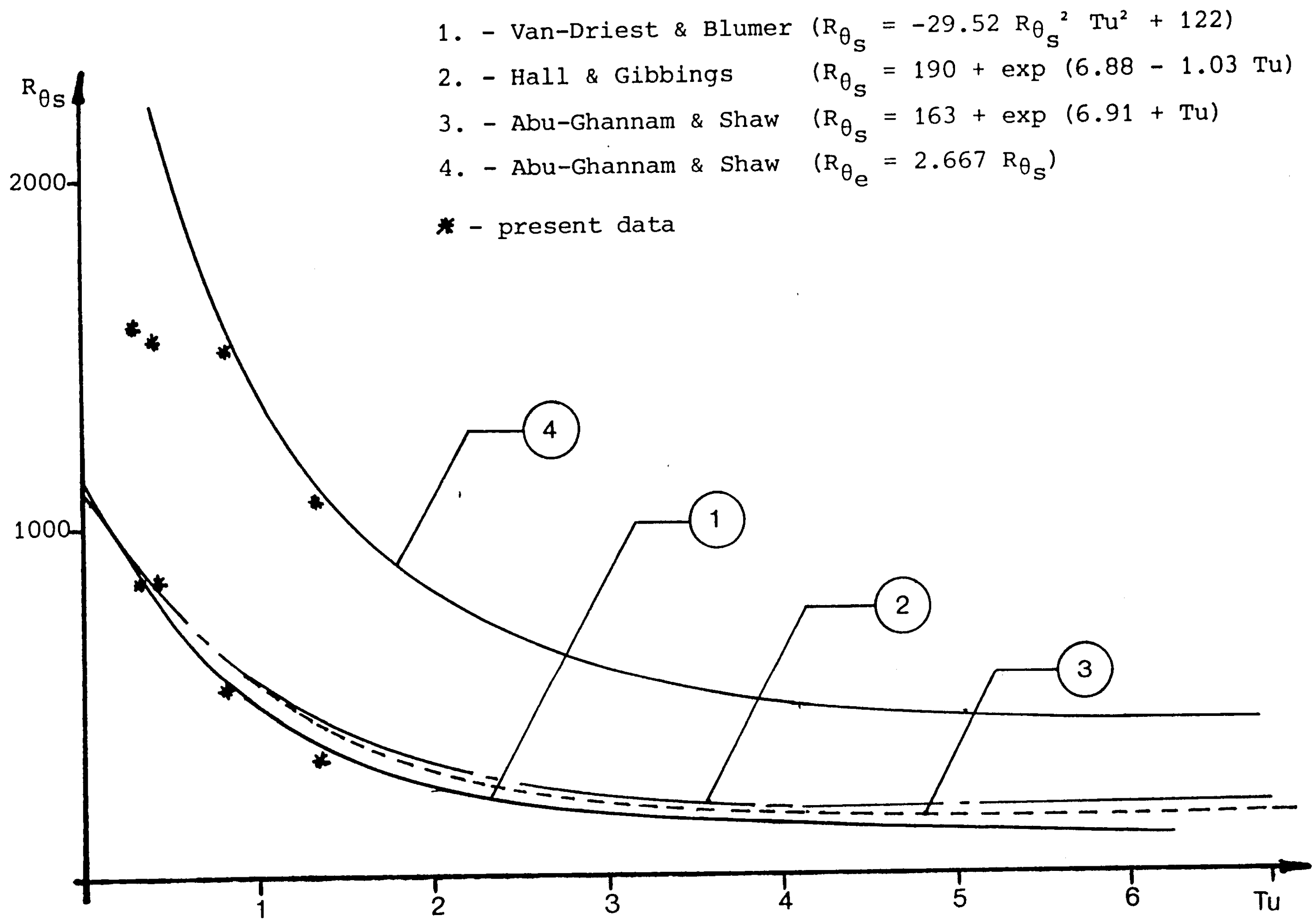

Fig. 6.5.1 <u>Start of transition correlations (zero pressure gradient)</u>

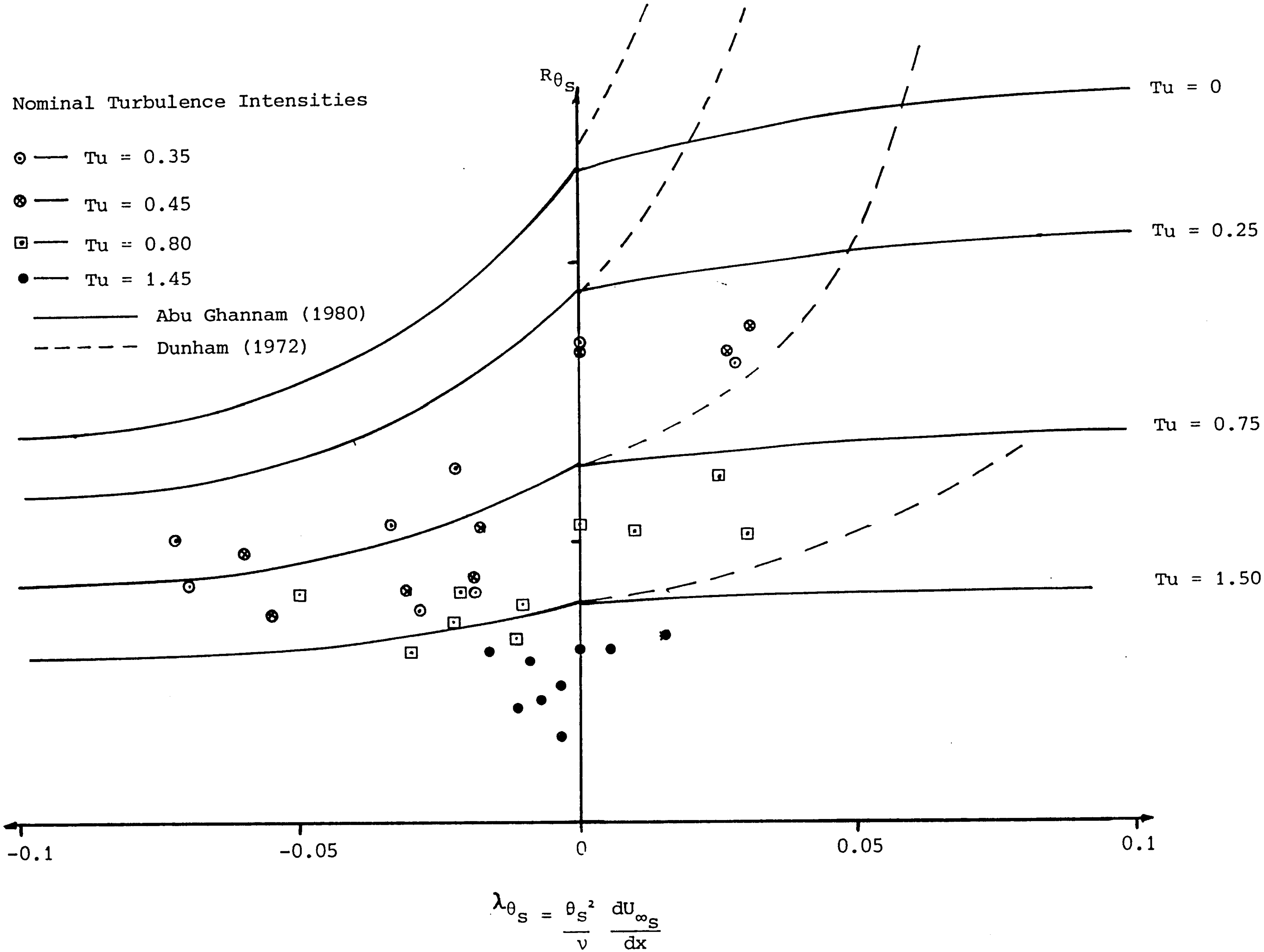

Fig. 6.5.2. Abu-Ghannam & Shaw correlation for R_{θ_s} in non-zero pressure gradient flows

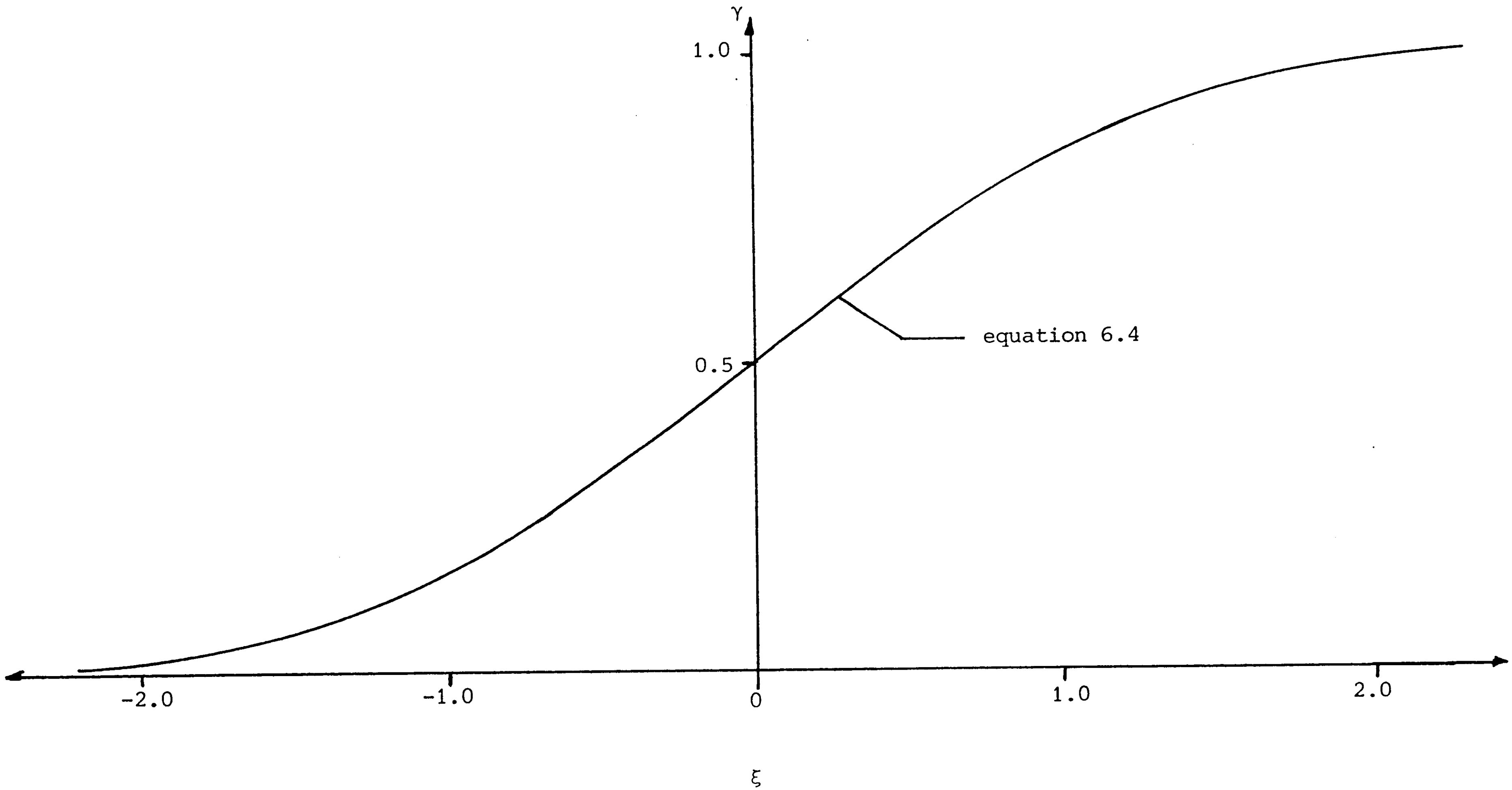

Fig. 6.6.1. Polynomial approximation to normal distribution

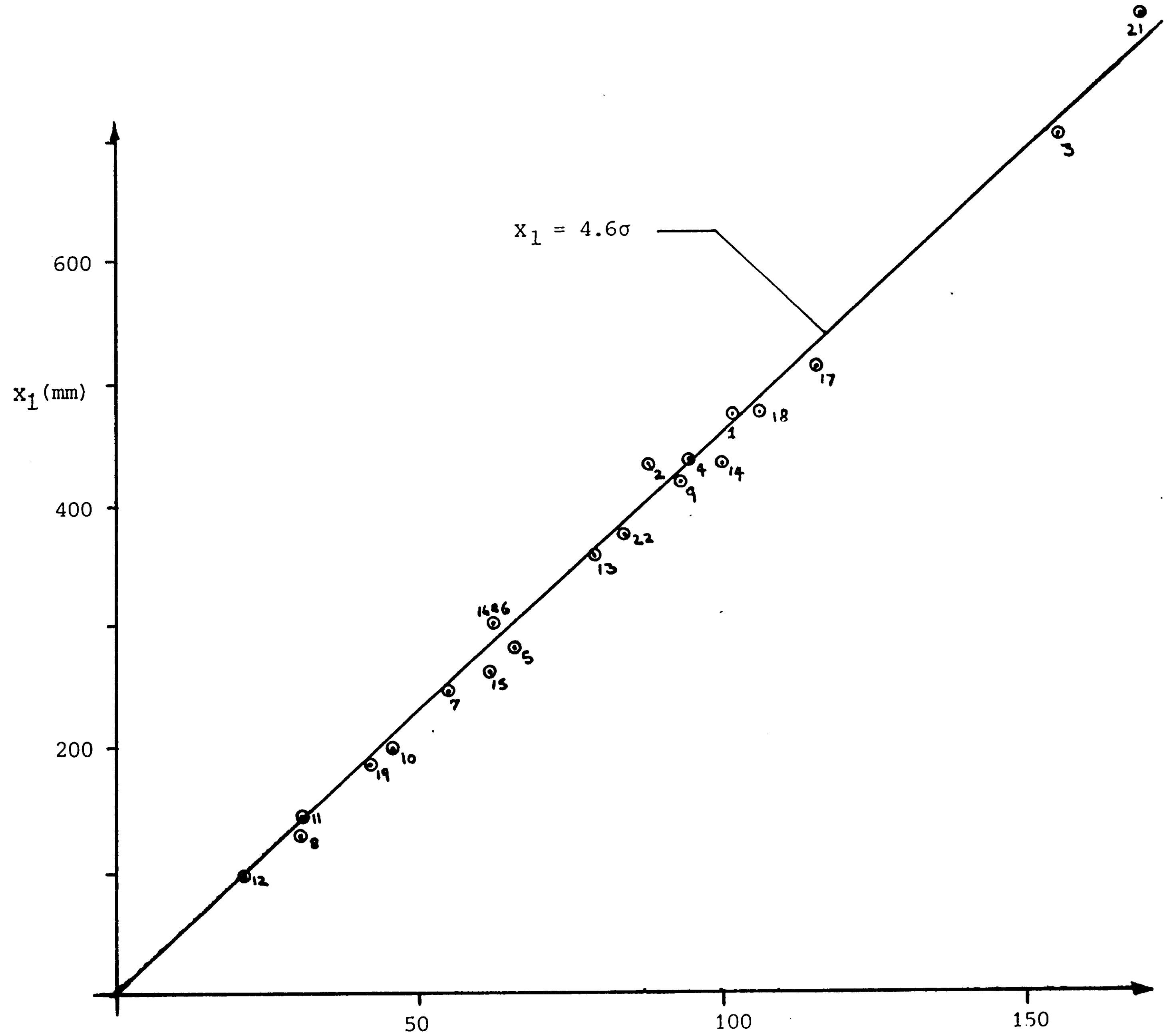

Fig. 6.6.2. Plot of X_1 against σ σ(mm)

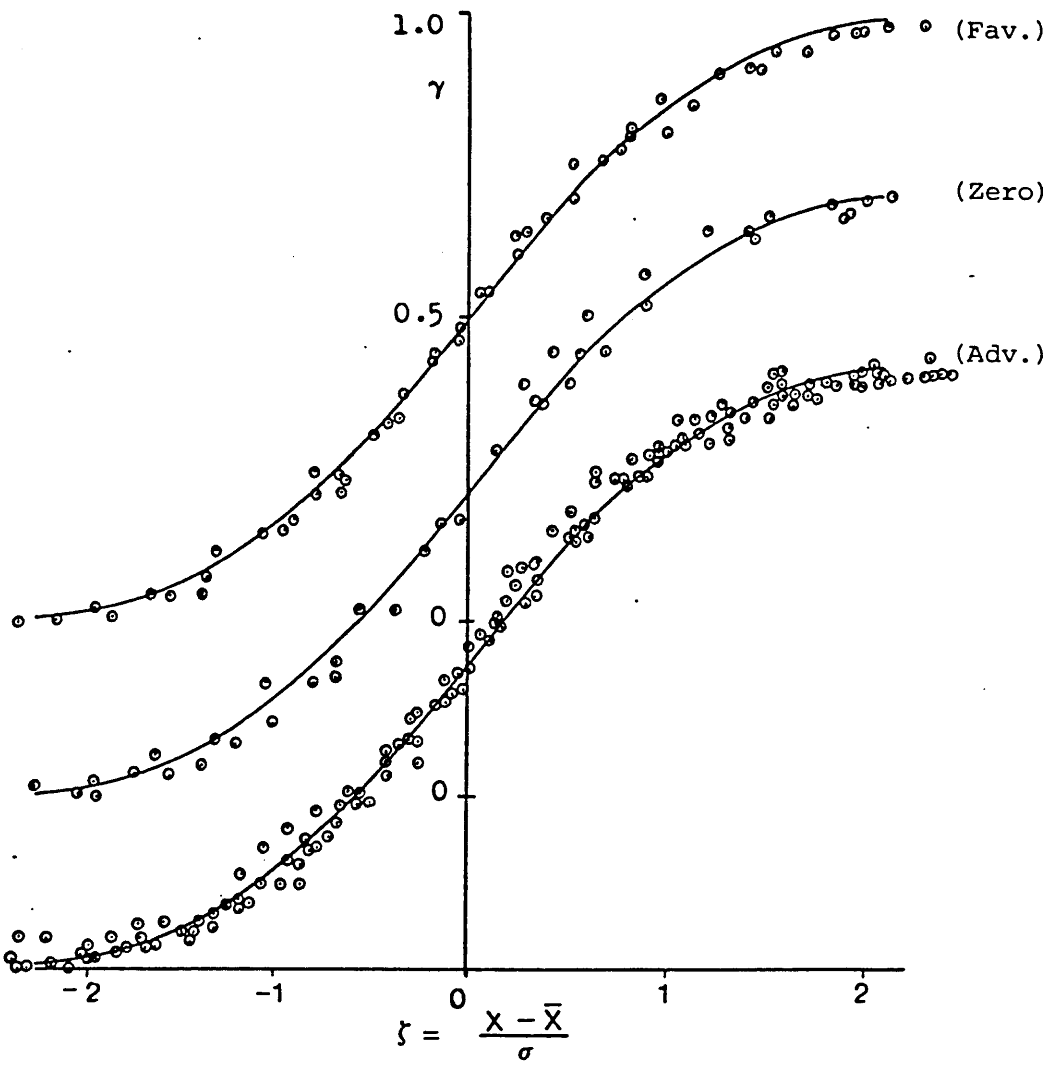

Fig. 6.6.3. (a) present γ vs ζ Intermittency distribution

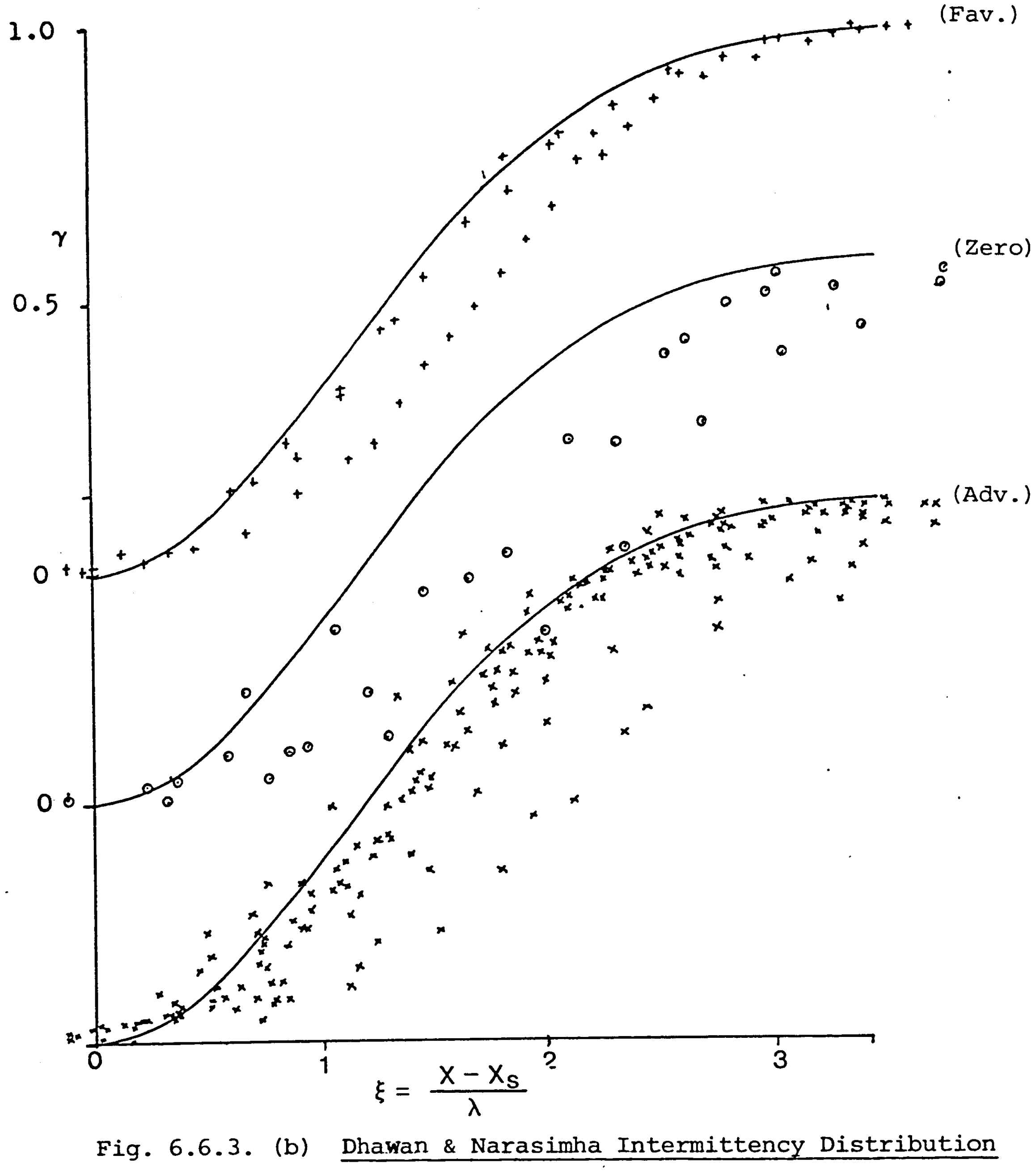

Fig. 6.6.3. (b) Dhawan & Narasimha Intermittency Distribution

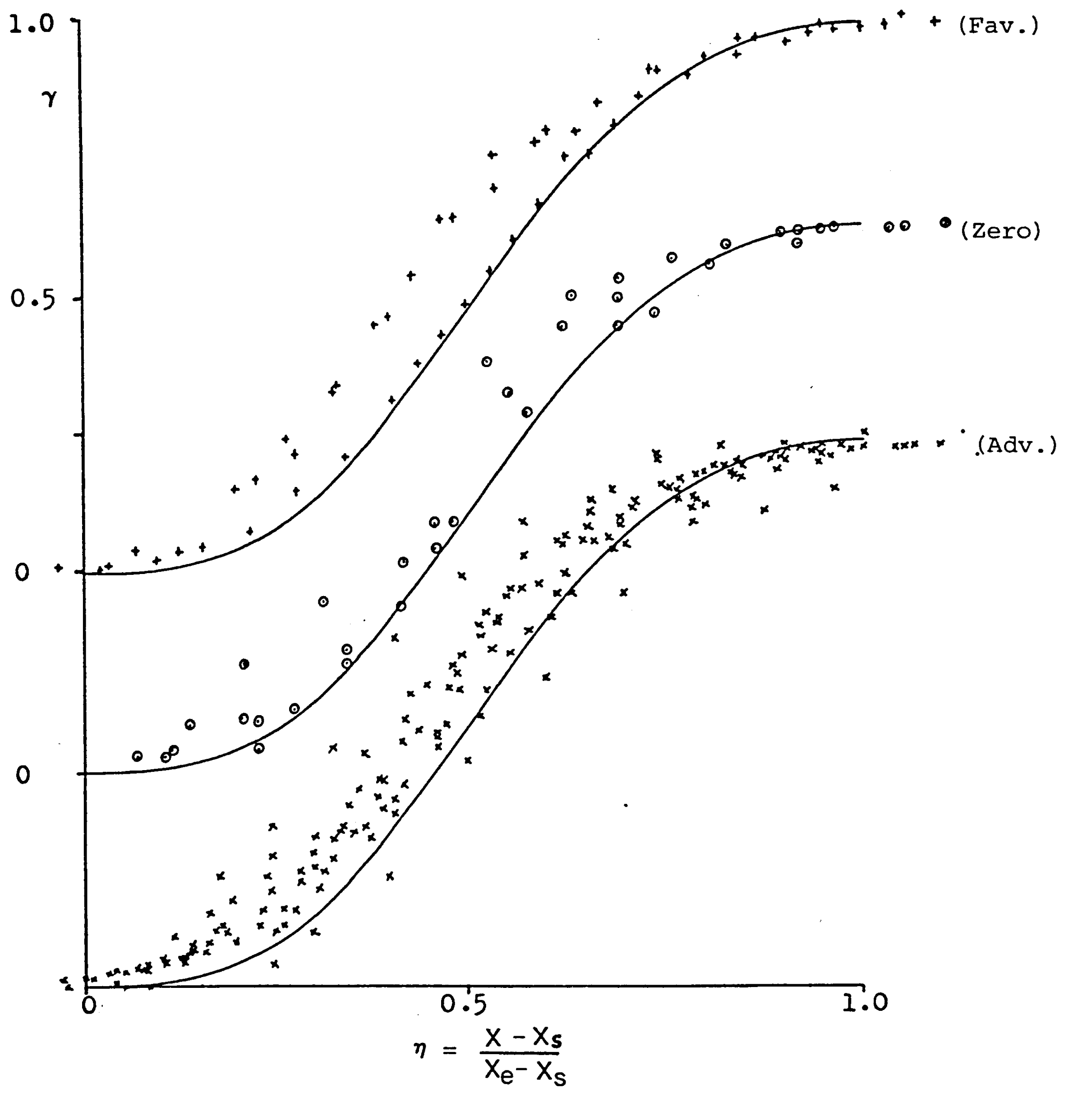

Fig. 6.6.3. (c) Abu-Ghannam & Shaw Intermittency Distribution

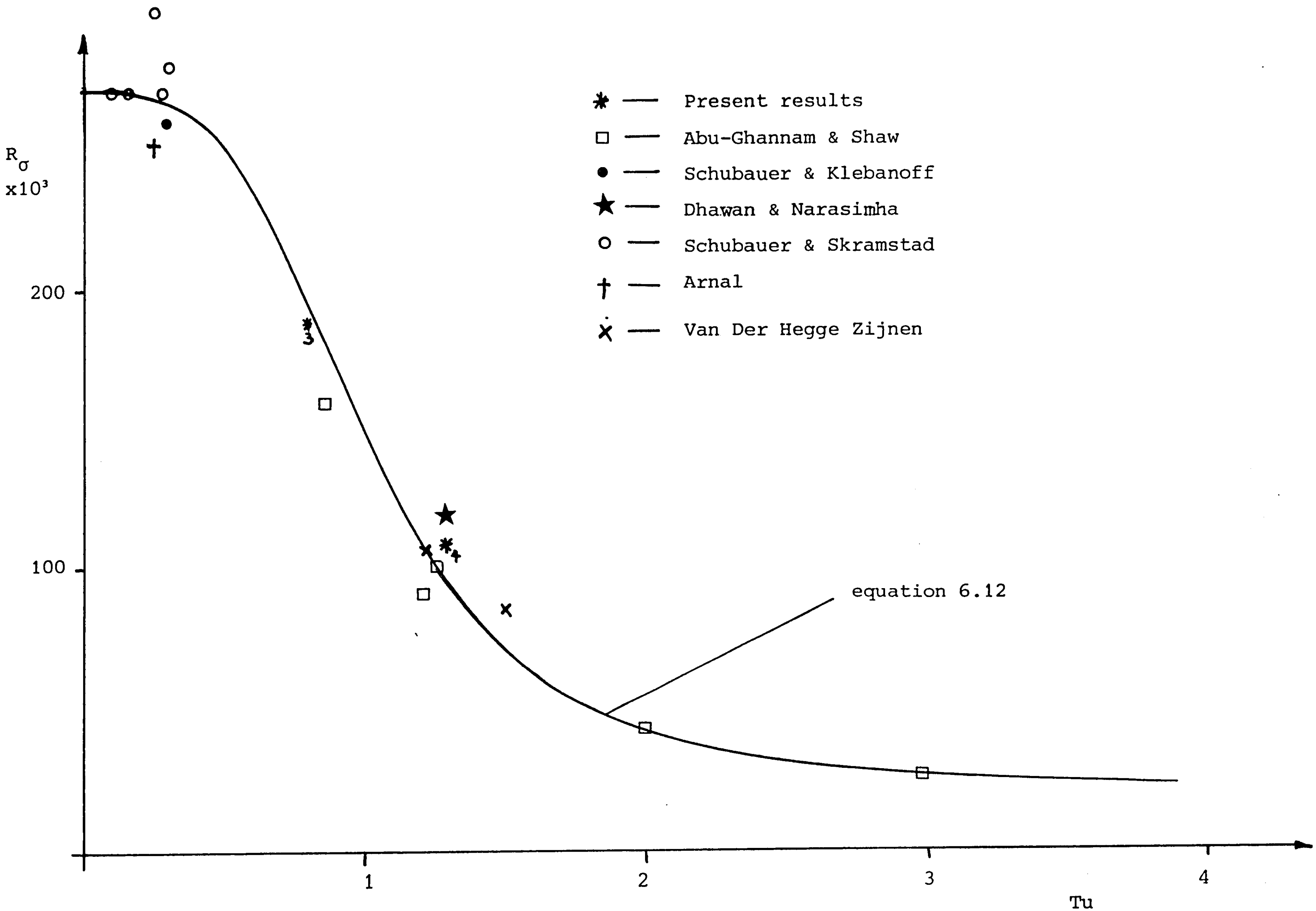

Fig. 6.7.1. Present zero pressure gradient correlation

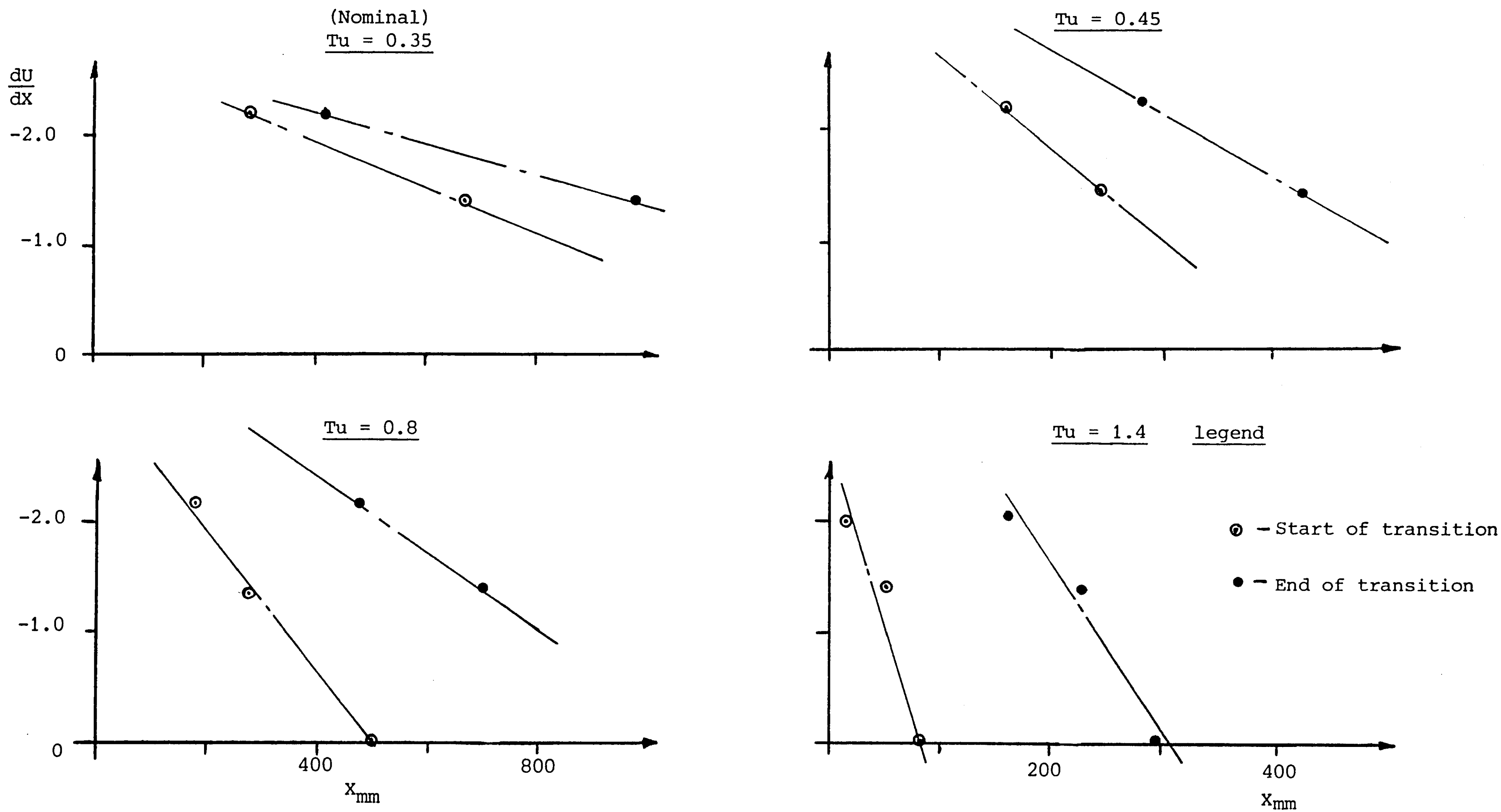

Fig. 6.8.1. Velocity gradient effect on transition length ($U_o \cong 18$m/s for all cases)

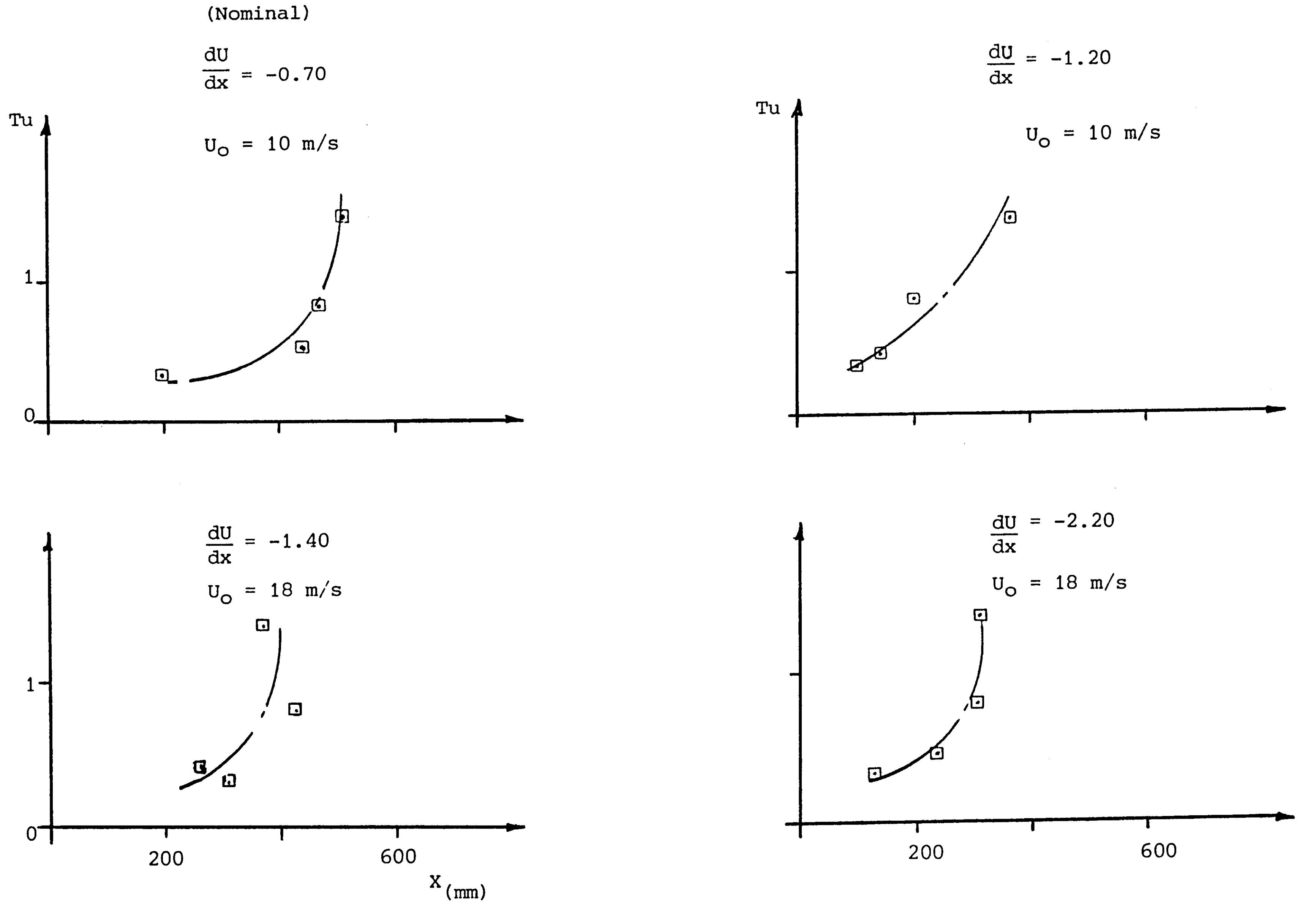

⊡ - transition length (mm)

Fig. 6.8.2. Effect of freestream turbulence on transition length for constant vecloity gradients

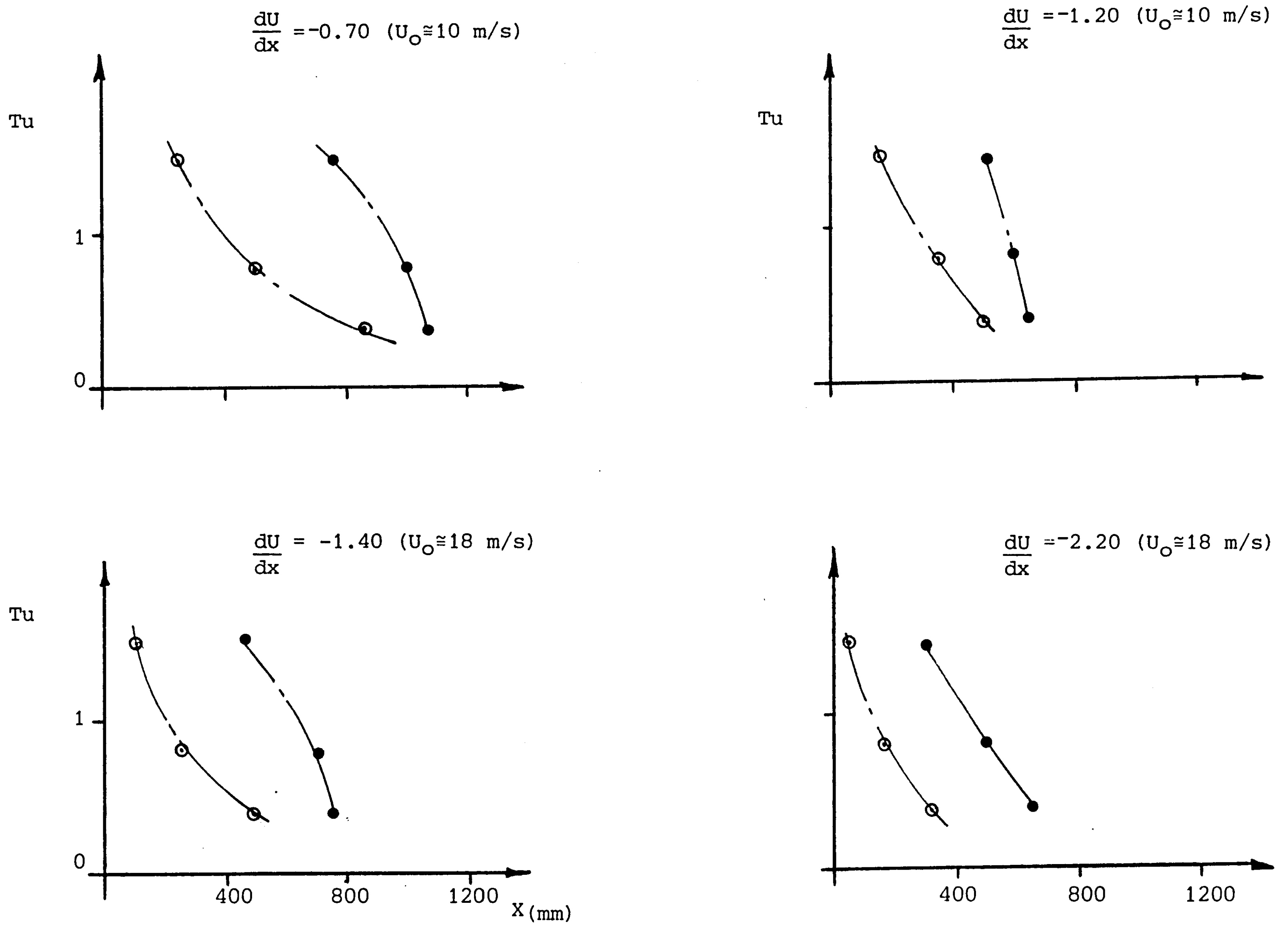

Fig. 6.8.3. Effect of freestream turbulence on start and end of transition for constant velocity gradient

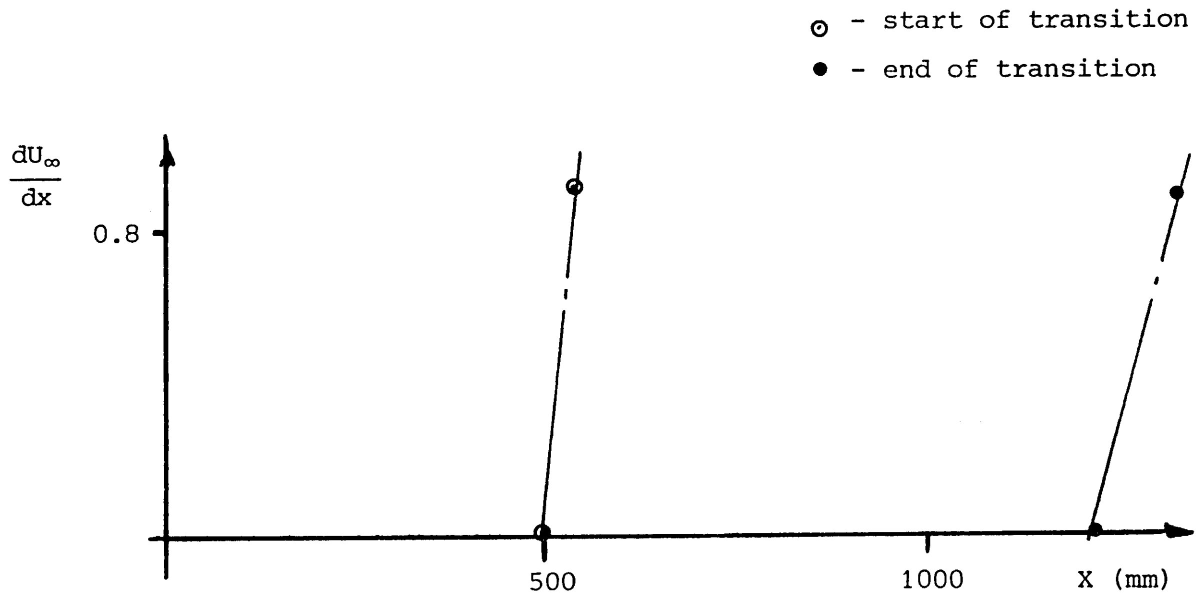

Fig. 6.9.1. Effect of fav velocity gradient on transition length

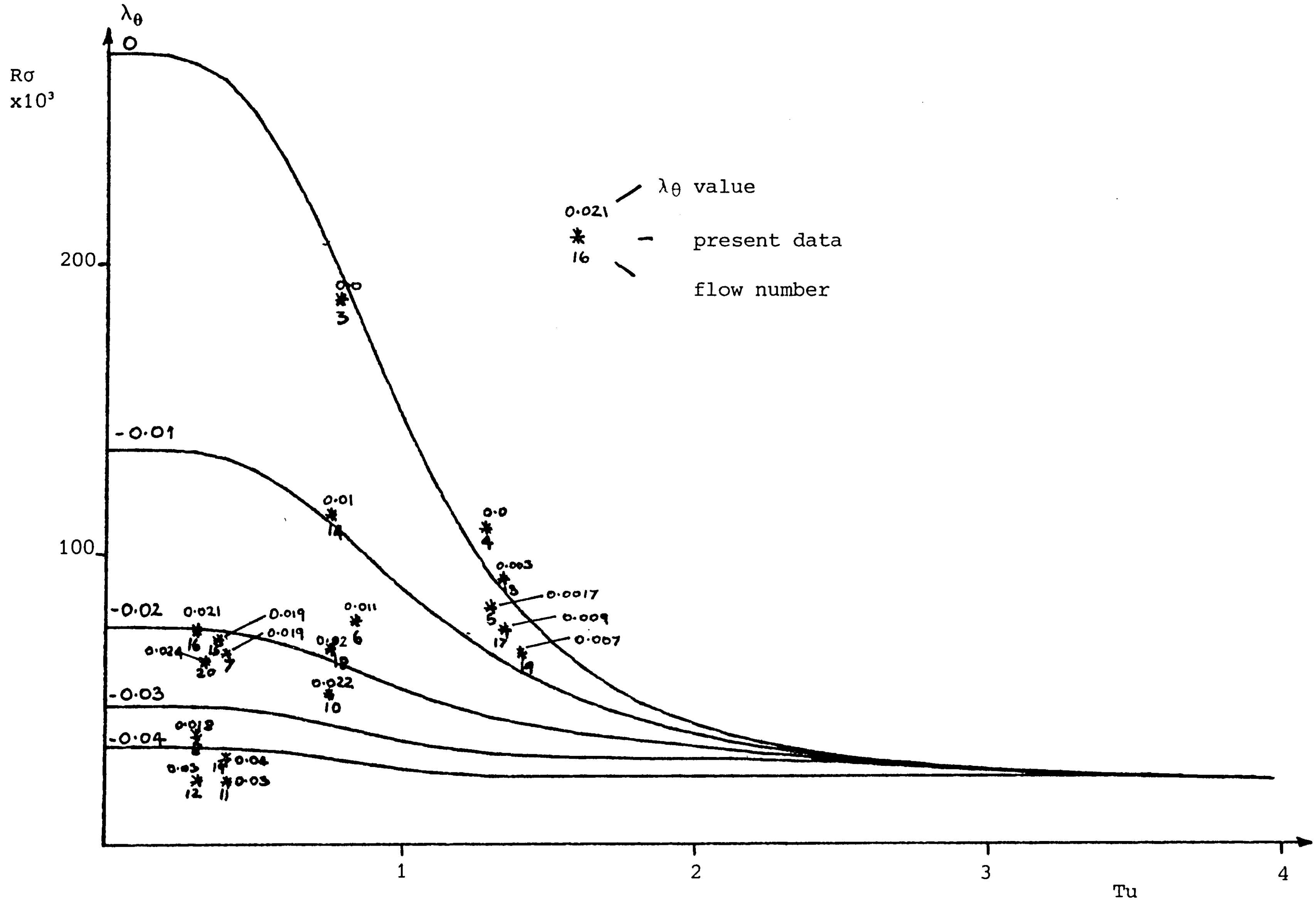

Fig. 6.10.1. Present correlation - combined effect of freestream turbulence and pressure gradient on transition length

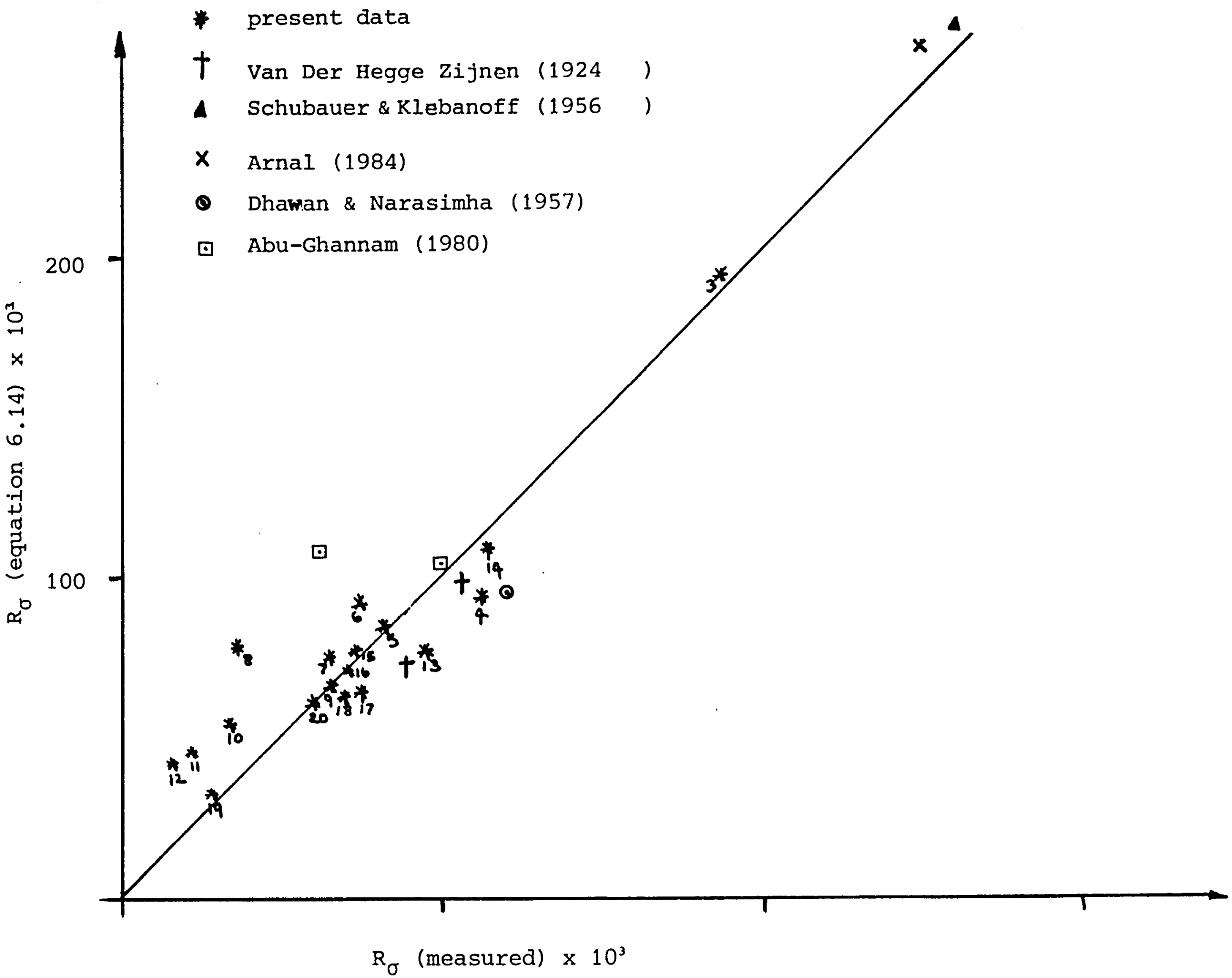

Fig. 6.10.2 <u>R_σ (equation 6.14) against R_σ (measured)</u>

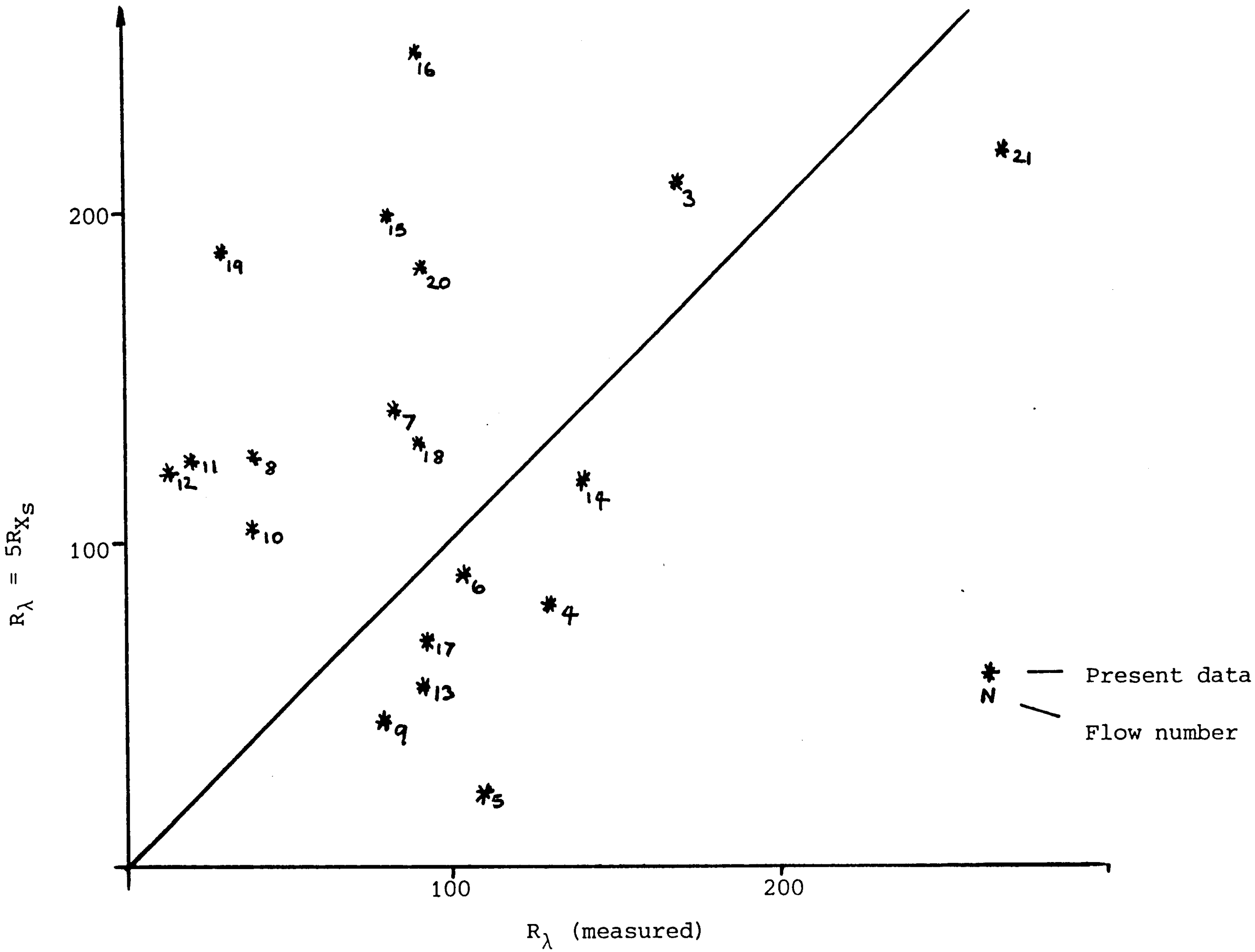

Fig. 6.10.3 Present Data Compared with Dhawan & Narasimhas' Production

CHAPTER SEVEN

Prediction of the Transition Boundary layer development

7.1 Introduction

Early methods for predicting the development of a boundary layer over a surface frequently ignored the transition region by assuming transition to occur abruptly at a specific point, normally chosen close to the centre of the transition region (see Rotta 1962). However, if the transition region occupies a high percentage of the surface, as in the case of flow over a turbine blade, the gradual change of the mean flow properties from the laminar to turbulent values is obviously of great importance for a reliable assessment of the boundary layer development to be made.

This is realised in the more recent prediction methods of McDonald & Fish (1973), Forrest (1977) and Abu-Ghannam & Shaw (1980). The former two methods are differential methods which solve the basic partial differential equations and ultimately results in predicted mean velocity profiles. These are then integrated numerically to give the boundary layer parameters. The method of Abu-Ghannam & Shaw is wholly empirical and is dependent on correlations of the mean flow parameters through transition.

The present method is different from the above techniques in that established integral methods for the laminar and turbulent boundary layers are used in conjunction with an intermittency modelled transition region. The advantage of this technique lies in the computational simplicity of integral prediction techniques and in the fact that the number of empirical correlations have been reduced to a minimum.

The two integral methods selected were those of Tani (1954), for the laminar boundary layer and Alber (1968), for the turbulent boundary layer. Alber's method was selected as it was reported to be one of the best methods presented at the Stanford Conference, Kline et al (1968) and Tani's method was selected as it was compatible with Alber's method, both being dissipation integral techniques. Both these methods are described in detail in Appendix 4.

In actual fact the transition model presented in this chapter is not dependent on the methods used for predicting the laminar and turbulent boundary layer components, provided that the methods predict the relevant flow parameters adequately. A comparison of the transition model using the methods of Thwaites (1949), for predicting the laminar boundary layer and Green et al (1977), for the turbulent boundary layer, is made between that of the Tani/Alber combination and is shown in fig. [7.4.8].

A complete boundary layer prediction scheme along with a fairly extensive graphics package was programmed to run on the same BBC micro-computer that was used for the data acquisition and control. The prediction scheme computes the development of the boundary layer from the leading edge of a plate through transition to the turbulent state. The input data was kept to a minimum and for arbitrary calculations the correlations of Abu-Ghannam & Shaw and that of the present author, equation 6.14 were used to define the onset of transition and the extent of the transition region respectively.

The transition model described below was then used to predict the development of the flow parameters through transition. A comparison of this model with a selection of the present data and that of Schubauer & Klebanoff (1956), Dhawan & Narasimha (1957) and Abu-Ghannam & Shaw is shown in figs. [7.4.1 → 7.4.8]

7.2 Transition model

As described in the previous chapter the flow within a transition region alternates between the laminar and turbulent flow states; the fraction of time spent in turbulent motion being governed by the intermittency function. The present intermittency function, which has been shown to be applicable in both zero and moderate non-zero pressure gradients, is defined by equation 6.4 in terms of the co-ordinates

γ versus ζ

Using this function the transition region is defined within the range $-2.3 < \zeta < 2.3$ corresponding to $0.01 < \overline{\gamma} < 0.99$. Therefore, provided the start and length of the transition region are defined, equations 6.4, 6.5 and 6.6 can be used to compute $\overline{\gamma}$ at any arbitrary position within the transition region.

Following Dhawan & Narasimha (1957) the mean transitional velocity profiles are represented by an intermittency weighted average of the separate laminar and turbulent components:

$$\left(u/U_\infty\right)_t = (1 - \overline{\gamma}) \left(u/U_\infty\right)_L + \overline{\gamma} \left(u/U_\infty\right)_T \qquad \ldots\ldots\ldots \quad 7.1$$

The boundary layer parameters through transition are defined as

$$\delta^*_t = \int_0^{\delta_t} \left\{1 - \left(u/U_\infty\right)_t\right\} dy \qquad \ldots\ldots\ldots \quad 7.2$$

$$\theta_t = \int_0^{\delta_t} \left\{ \left({}^{u}/_{U_\infty} \right)_t \left[1 - \left({}^{u}/_{U_\infty} \right)_t \right] \right\} dy \qquad \ldots\ldots\ldots \quad 7.3$$

$$\text{and } H_t = {}^{\delta^*_t}/_{\theta_t} \qquad \ldots\ldots\ldots \quad 7.4$$

where δ_t is the transitional boundary layer thickness and is taken as δ_L or δ_T whichever is the greatest.

Evaluation of these integrals using equation 7.1 results in

$$\delta_t = (1-\bar{\gamma})\ \delta^*_L + \bar{\gamma}(\delta^*_T) \qquad \ldots\ldots\ldots \quad 7.5$$

$$\theta_t = (1-\bar{\gamma})\ \{(1-\bar{\gamma})\,\theta_L - \bar{\gamma}\delta^*_L\} + \bar{\gamma}\{\bar{\gamma}\theta_T - (1-\bar{\gamma})\,\delta^*_T\} + 2\bar{\gamma}(1-\bar{\gamma})\ F\ (\delta_t) \qquad \ldots\ldots\ldots \quad 7.6$$

$$\text{where } F\ (\delta_t) = \int_0^{\delta_t} \left\{ 1 - \left(\frac{u}{U_\infty}\right)_L \left(\frac{u}{U_\infty}\right)_T \right\} dy$$

Further, the skin friction coefficient through transition can be represented by:

$$Cf_t = (1-\bar{\gamma})\ Cf_L + \gamma Cf_T \qquad \ldots\ldots\ldots \quad 7.7$$

An additional boundary layer parameter predicted by this model is the energy thickness δ^{**}, which is defined as

$$\delta_t^{**} = \int_0^{\delta_t} \left\{ \left({}^{u}/_{U_\infty} \right)_t \left[1 - \left({}^{u}/_{U_\infty} \right)_t^2 \right] \right\} dy \qquad \ldots\ldots\ldots \quad 7.8$$

evaluation of this integral results in

$$\delta^{**}_t = (1-\bar{\gamma})\ \{(1-\bar{\gamma})^2\,\delta^{**}_L + \bar{\gamma}(\bar{\gamma}-2)\,\delta^*_L\} + \bar{\gamma}\{\bar{\gamma}^2\delta^{**}_T + (\bar{\gamma}^2-1)\,\delta^*_T\ 3\bar{\gamma}(1-\bar{\gamma})\,Q(\delta_t) \qquad \ldots\ldots\ldots \quad 7.9$$

$$\text{where } Q\ (\delta_t) = \int_0^{\delta_t} \left\{ 1 - \left(\frac{u}{U_\infty}\right)_t \left(\frac{u}{U_\infty}\right)_L \left(\frac{u}{U_\infty}\right)_T \right\} dy$$

The derivation of this equation is given briefly in Appendix 3.

The energy thickness shape factor is then given by

$$H_{32_t} = \frac{\delta_t^{**}}{\theta_t} \qquad \ldots\ldots\ldots \quad 7.10$$

Evaluation of the mixed integral terms F (δ_t) and Q (δ_t) in equations 7.6 and 7.9 requires the laminar and turbulent mean velocity profiles to be fully specified.

mean laminar velocity profile

The Pohlhausen fourth-order polynomial velocity profile is assumed for the laminar mean velocity profile.

$$\left(\frac{u}{U_\infty}\right)_L = 2\left\{\left(y/\delta_L\right) - 2\left(y/\delta_L\right)^3 + \left(y/\delta_L\right)^4\right\} + \frac{\lambda_p}{6}\left\{\left(y/\delta_L\right) - 3\left(y/\delta_L\right)^2 + 3\left(y/\delta_L\right)^3 - \left(y/\delta_L\right)^4\right\} \quad \ldots\ldots\ldots \quad 7.11$$

$$\text{where } \lambda_p = \frac{\delta_L{}^2}{\nu}\,\frac{dU_\infty}{dX} \quad \ldots\ldots\ldots \quad 7.12$$

Tani's method for predicting the laminar boundary layer does not output the boundary layer thickness δ. However the term λ_θ ie

$$\lambda_\theta = \frac{\theta_L{}^2}{\nu}\,\frac{dU_\infty}{dX} \quad \ldots\ldots\ldots \quad 7.13$$

is available and is related to λ_p through the Pohlhausen relationship.

$$\lambda_\theta = \lambda_p\left\{\frac{37}{315} - \frac{\lambda_p}{945} - \frac{\lambda_p^2}{9072}\right\} \quad \ldots\ldots\ldots \quad 7.14$$

The curve fits of Fraser (1979) are used to recast the subject of the above equation ie

$$\lambda_p = 10\,\lambda_\theta\{\lambda_\theta^2\,(6600\,\lambda_\theta - 543) + (7 + 31\,\lambda_\theta)\} \quad \ldots\ldots\ldots \quad 7.15$$

For $\lambda_\theta > 0$

$$\lambda_p = \lambda_\theta\,\{73 + 109\,\lambda_\theta + 790\,\lambda_\theta^2\} \quad \ldots\ldots\ldots \quad 7.16$$

For $\lambda_\theta < 0$

The boundary layer thickness δ_L can then be obtained from equation 7.14.

mean turbulent velocity profile

The turbulent mean velocity profile is represented as a power law:

$$\left(\frac{u}{U_\infty}\right)_T = \left({}^{y}/_{\delta_T}\right)^{1/n} \qquad \ldots\ldots\ldots \quad 7.17$$

The exponent n being related to the turbulent velocity profile shape factor by

$$n = \frac{2}{H_T - 1} \qquad \ldots\ldots\ldots \quad 7.18$$

and the thickness δ_T represented by

$$\delta_T = \frac{\theta_T\, H_T\, (H_T + 1)}{H_T - 1} \qquad \ldots\ldots\ldots \quad 7.19$$

7.3 The computational model

The computational model was written in BBC BASIC and requires a minimum of input data to predict the development of a boundary layer from the leading edge of a body. The following input data is required:

(a) The freestream velocity distribution;

(b) The freestream turbulence level, Tu;

(c) The plate length, L;

(d) The reference velocity, U_0;

(e) The ambient pressure and temperature.

For computational convenience the freestream velocity distribution is input in the form

$$\frac{U_\infty}{U_0} = E\left({}^{x}/_{L}\right)^{P} + A + B\left({}^{x}/_{L}\right) + C\left({}^{x}/_{L}\right)^{2} + D\left({}^{x}/_{L}\right)^{3} \ldots\ldots \quad 7.20$$

which covers a convenient range of test flow conditions.

The method of Tani (1954) is then used to calculate the laminar boundary layer parameters from the leading edge through to the end of the transition region. Hence the values of Cf_L, δ^*_L, θ_L and δ^{**}_L are available throughout the transition region. The turbulent boundary layer calculation commences from the point at which transition starts through to the end of the plate. Therefore, the turbulent boundary layer parameters Cf_T, δ^*_T, θ_T and δ^{**}_T are also available throughout the transition region. These values along with the numerical integration of the terms $F(\delta_t)$ and $Q(\delta_t)$ are then used to obtain the transition boundary layer parameters Cf_t, δ^*_t, θ_t and δ^{**}_t from equations 7.7, 7.5, 7.6 and 7.9 respectively.

To start the turbulent calculation initial values of δ^*_T, Π and Cf_T are required. Whites skin friction correlation (equation 4.14), which requires the input of R_θ and H_T, is used to estimate the initial skin friction coefficient. Due to numerical difficulties the calculation could not be started at the flow origin ie $\theta_T = 0$ therefore, the assumption that $\theta_T = \theta_{Ls}/3$ is made for the starting value of θ_T at the point of transition. (Surprisingly the calculation procedure is relatively insensitive to the starting value of θ_T). Following the work of Wygnanski et al (1976), who measured velocity profiles within turbulent spots, the initial shape factor is set to H = 1.5. With initial values of Cf_T, θ_T and H_T defined, δ^*_T and Π are calculated from

$$\delta^*_T = \theta_T H_T \qquad \ldots\ldots\ldots \quad 7.21$$

$$\Pi = 0.8\ (\beta_T + 0.5)^{0.75} \qquad \ldots\ldots\ldots \quad 7.22$$

where $\beta_T = \frac{2\ \delta_T^*}{Cf_T\ U_\infty} \frac{dU_\infty}{dx}$

Unlike the laminar boundary layer the turbulent boundary layer mean flow parameters are effected by the magnitude of the turbulence level in the freestream. The empirical correlations of Bradshaw (1974) are incorporated into the turbulent calculation procedure to account for this effect ie:

$$\theta_{Tu} = \frac{\theta}{1 + 0.05\ Tu}$$

$$H_{Tu} = H\ [1 - 0.01\ Tu]$$

$$Cf_{Tu} = Cf\ [1 + 0.032\ Tu]$$

where subscript Tu denotes the freestream turbulence corrected value.

No empirical relationship exists for the effect of freestream turbulence on the energy thickness. This should be realised when comparing the predicted values of δ^{**} with the experimental data. However, for the range of freestream turbulence levels investigated the effect of the freestream turbulence is likely to be small as can be seen from the above equations.

The empirical correlation of Abu-Ghannam & Shaw (1980) which gives the momentum thickness Reynolds number at the start of transition as a function of the local pressure gradient parameter, λ_θ, and the freestream turbulence level, Tu, is included in the computational model to define the position at which transition commences. This correlation is given as:

$$R_{\theta_s} = 163 + \exp\left\{ f(\lambda_\theta) - f(\lambda_\theta) \frac{Tu}{6.91} \right\} \qquad \ldots\ldots\ldots \qquad 7.22$$

where

$$f(\lambda_\theta) = 6.91 + 12.75\ \lambda_\theta + 63.64\ (\lambda_\theta)^2 \quad \text{for } \lambda_\theta < 0$$

and

$$f(\lambda_\theta) = 6.91 + 2.48\ \lambda_\theta - 12.27\ (\lambda_\theta)^2 \quad \text{for } \lambda_\theta > 0$$

The correlation due to the present author, equation 6.14 is then used to define the transition length. This equation is repeated below for completeness of this section.

$$R_\theta = \left[270 - \frac{250\ Tu^{3.5}}{1 + Tu^{3.5}} \right] \left[\frac{1}{1 + 1710\ (-\lambda_\theta)^{1.4}\ \exp \sqrt{1 + Tu^{3.5}}} \right] \times 10^3$$

At present the model is restricted to zero and adverse pressure gradient flows as the transition length correlation is only applicable to such flows.

The computation model also incorporates a fairly extensive graphics package which can be used to compare the quality of the prediction to experimental data or merely to observe the prediction of the boundary layer parameters in the case of an arbitrary calculation.

The graphics software was written to enable a hard copy of the screen graphics to be obtained from a graph plotter which is controlled through the BBC microcomputer user port. Such printouts are shown in figures 7.4.1 → 7.4.8.

7.4 Model Performance

The validity of the model presented in this chapter was tested against a sample of the present data and the data of Dhawan & Narasimha (1957), Schubauer and Klebanoff (1956) and Abu-Ghannam & Shaw (1980). To make a fair assessment of the transition length correlation (equation 6.14), the experimentally measured position of the transition onset was read in as part of the input data.

Figures 7.4.1 (a) and 7.4.5 (b) show the predicted and measured boundary layer integral parameters and the mean velocity profiles for a representative sample of the present flows and also for the zero pressure gradient flow of Schubauer and Klebanoff. As can be observed from these figures the computational model predicts the boundary layer integral parameters and the velocity profiles very well for both the zero and adverse pressure gradient cases presented in the figures. Although the boundary layer velocity profiles and integral parameters have been predicted exceptionally well for the flow of Schubauer and Klebanoff the skin friction coefficient prediction is slightly lower than the experimentally measured values. However, due to difficulty in measuring the skin friction in a transitional flow, not too much emphasis should be placed on this observation.

Figures 7.4.6 and 7.4.7 show the present prediction against the experimentally measured data of Abu-Ghannam & Shaw for both a zero and an adverse pressure gradient flow. The zero pressure gradient flow is well predicted by the model, with the exception of the skin friction coefficient which again is slightly low, although not markedly so. The distribution of the skin friction through the transition region for the adverse pressure gradient flow of the Abu-Ghannam & Shaw has been poorly represented by the model.

The reason for this lies, not in the transition model itself, but in the fact that the transition length has been predicted approximately 30% less than the experimentally measured value.

As mentioned in section 7.1 the integral methods used to compute the component laminar and turbulent parameters for the transition model are not important provided they are reliable and well established methods. Fig. [7.4.8] shows the transition model described in section 7.2, against the data of Dhawan & Narasimha, using two different combinations of integral methods for the computation of the component laminar and turbulent boundary layer parameters. The two combinations are

(i) Tani/Alber used for the previous predictions.

(ii) Thwaites/Green et al - Thwaites (1949) method being used for the laminar boundary layer computation and Green et al (1977) lag entrainment method being used for the turbulent boundary layer computation.

As can be seen from this figure the transition model performs equally well irrespective of the combination chosen.

In general the transition model predict the flows very well but the method is crucially dependent on the accurate prediction of the onset and extent of the transition region. This is not peculiar to this particular method but would be as important for any method which uses transition onset and length correlations as a basis.

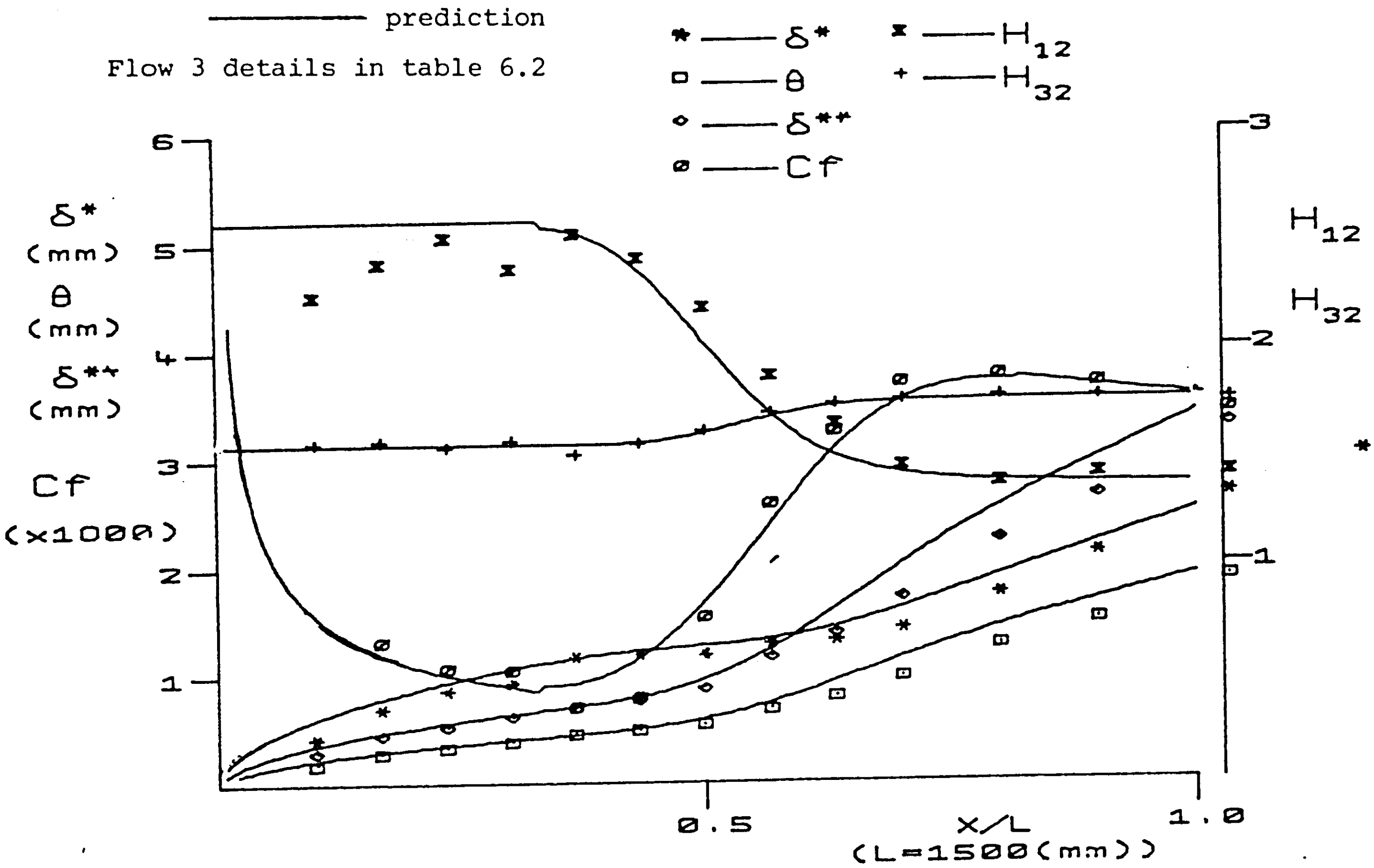

Fig. 7.4.1 (a) Boundary layer prediction of present Flow 3

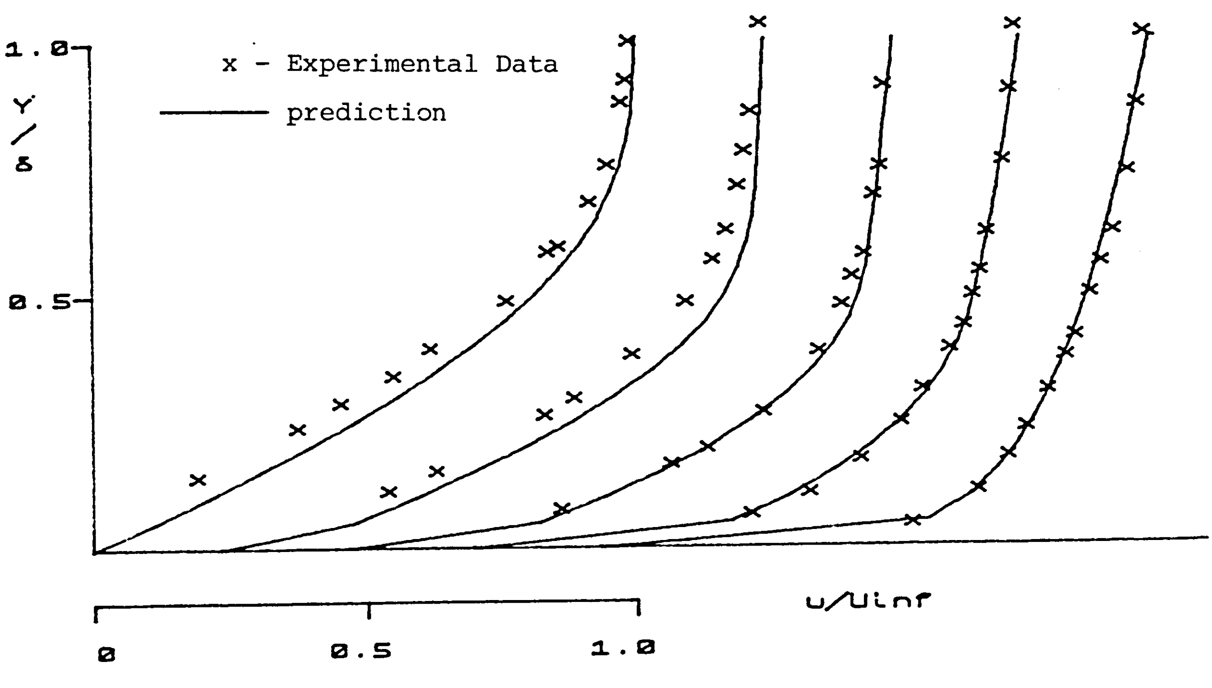

Fig. 7.4.1 (b) Predicted mean velocity profiles through transition

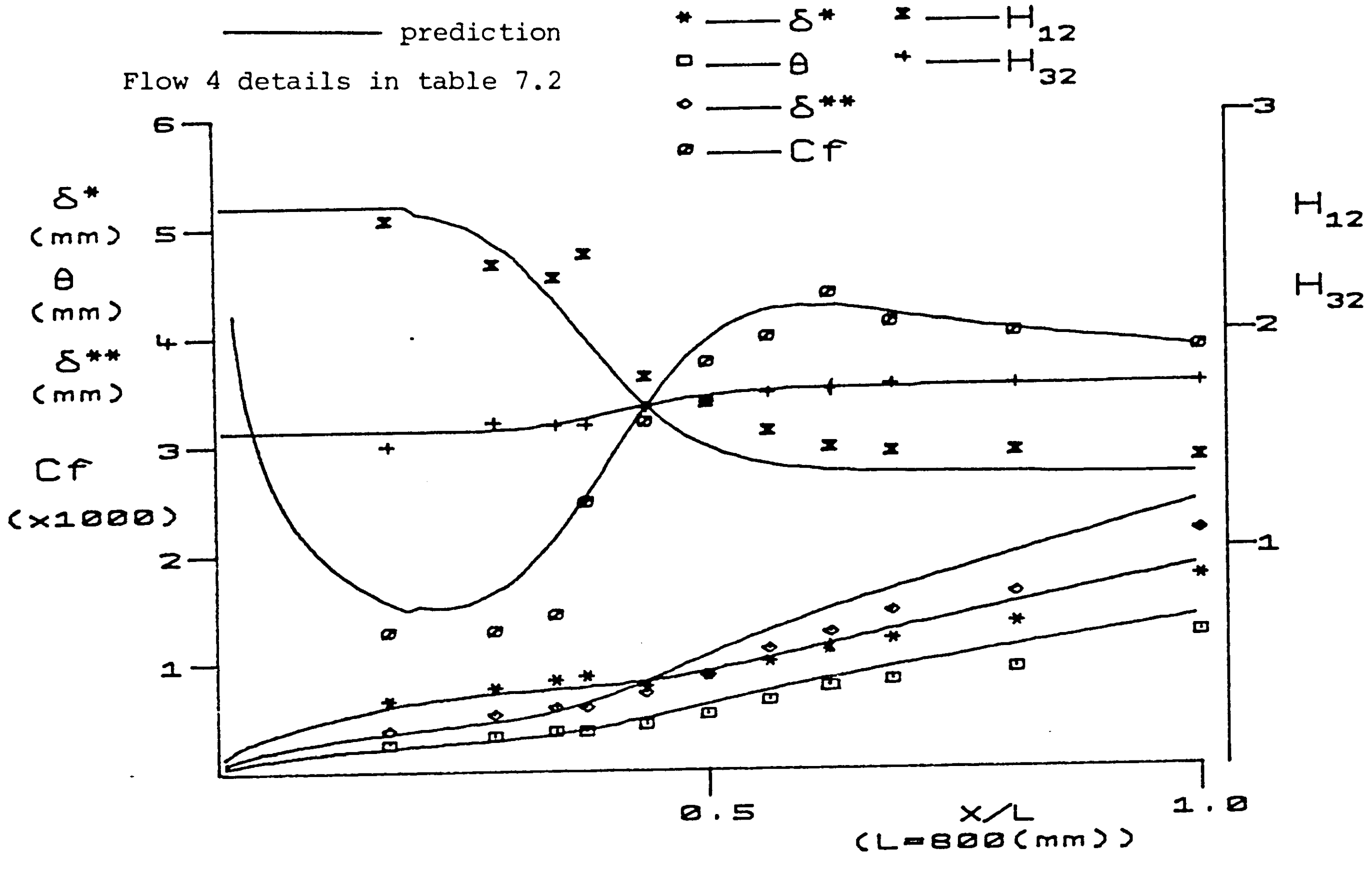

Fig. 7.4.2 (a) Boundary layer prediction of present Flow 4

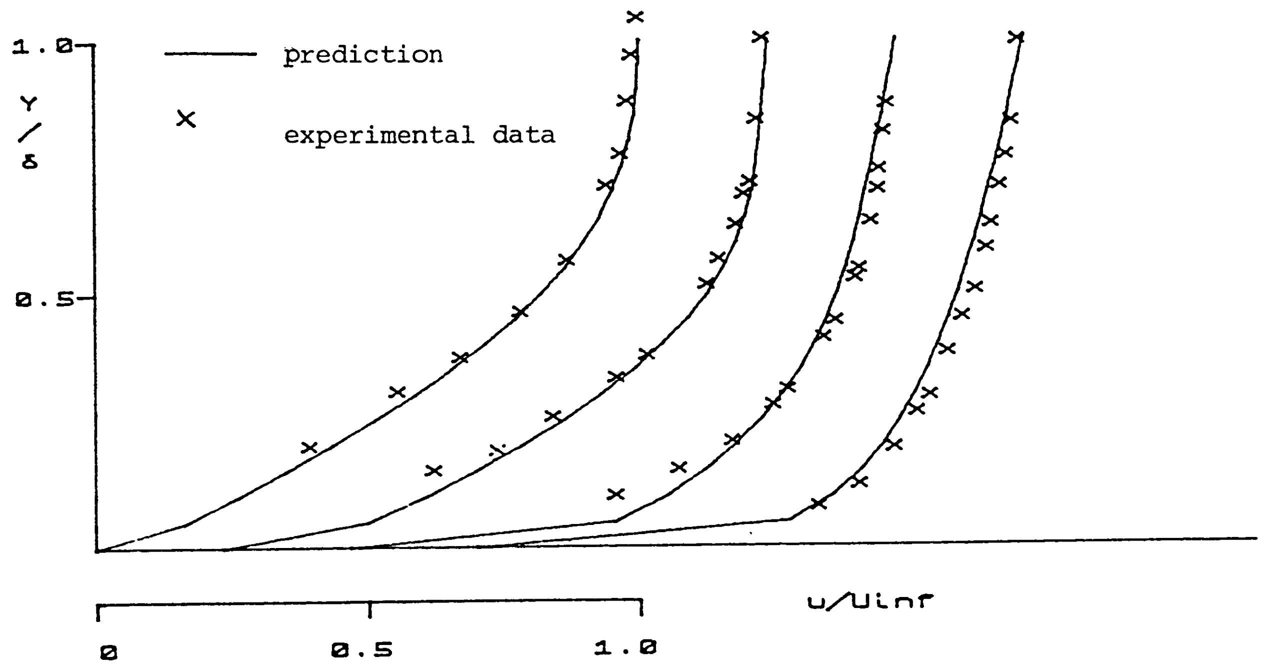

Fig. 7.4.2 (b) Predicted mean velocity profiles through transition

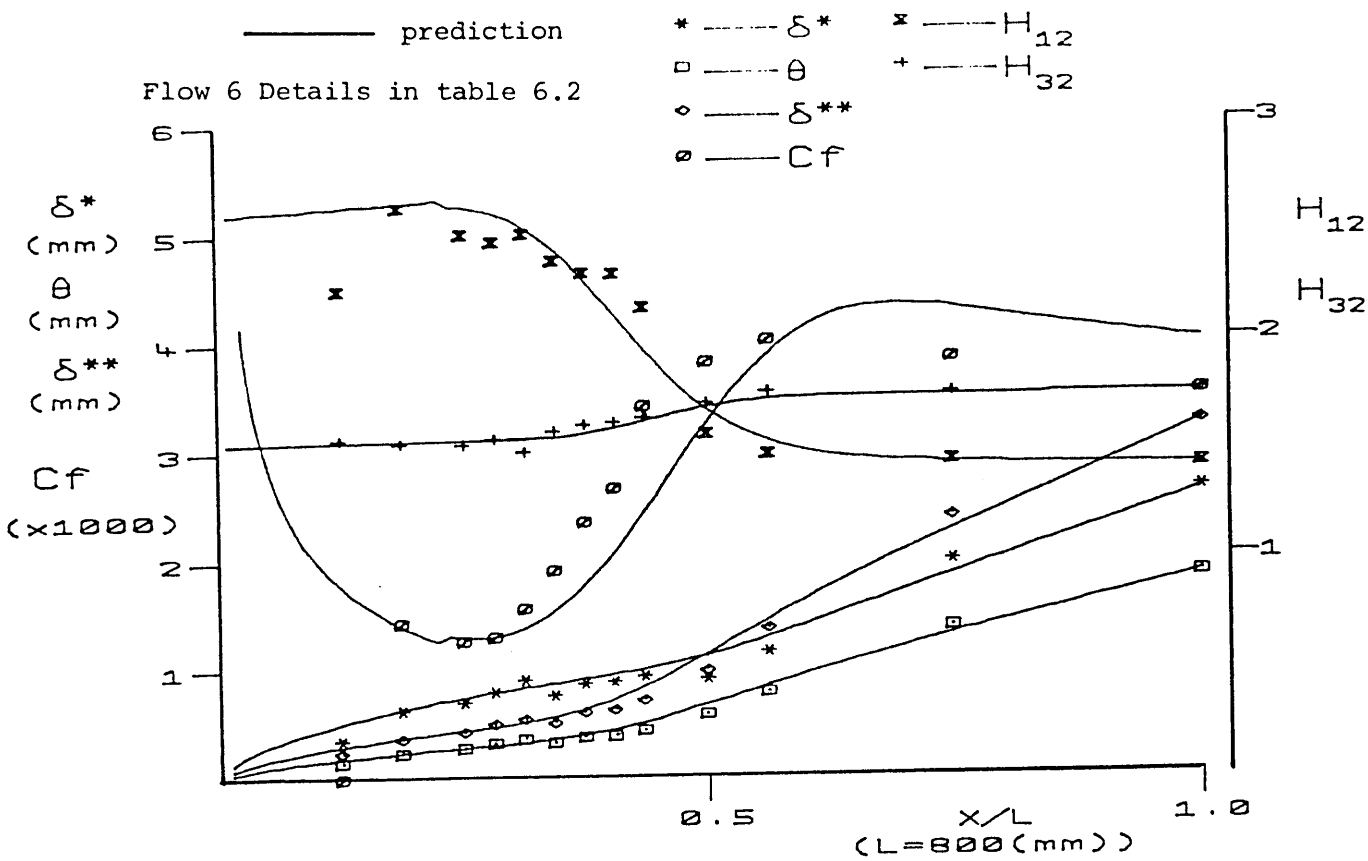

Fig. 7.4.3 (a) Boundary layer prediction of present Flow 6

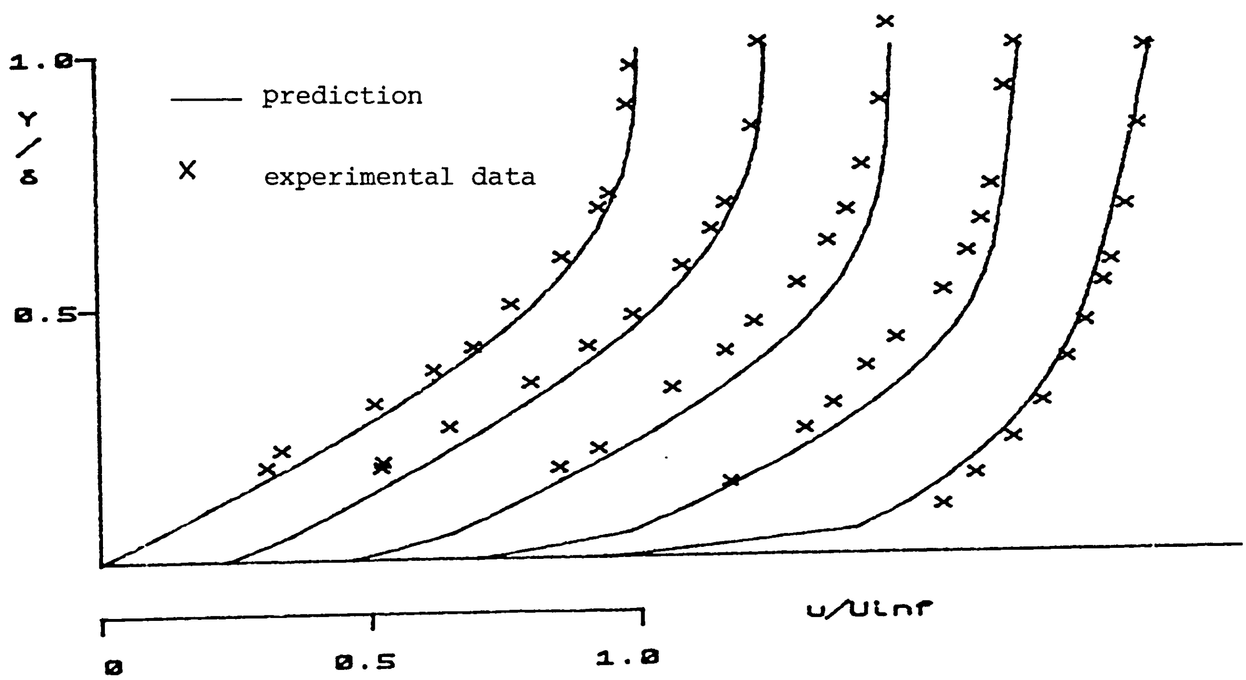

Fig. 7.4.3 (b) Predicted mean velocity profiles through transition

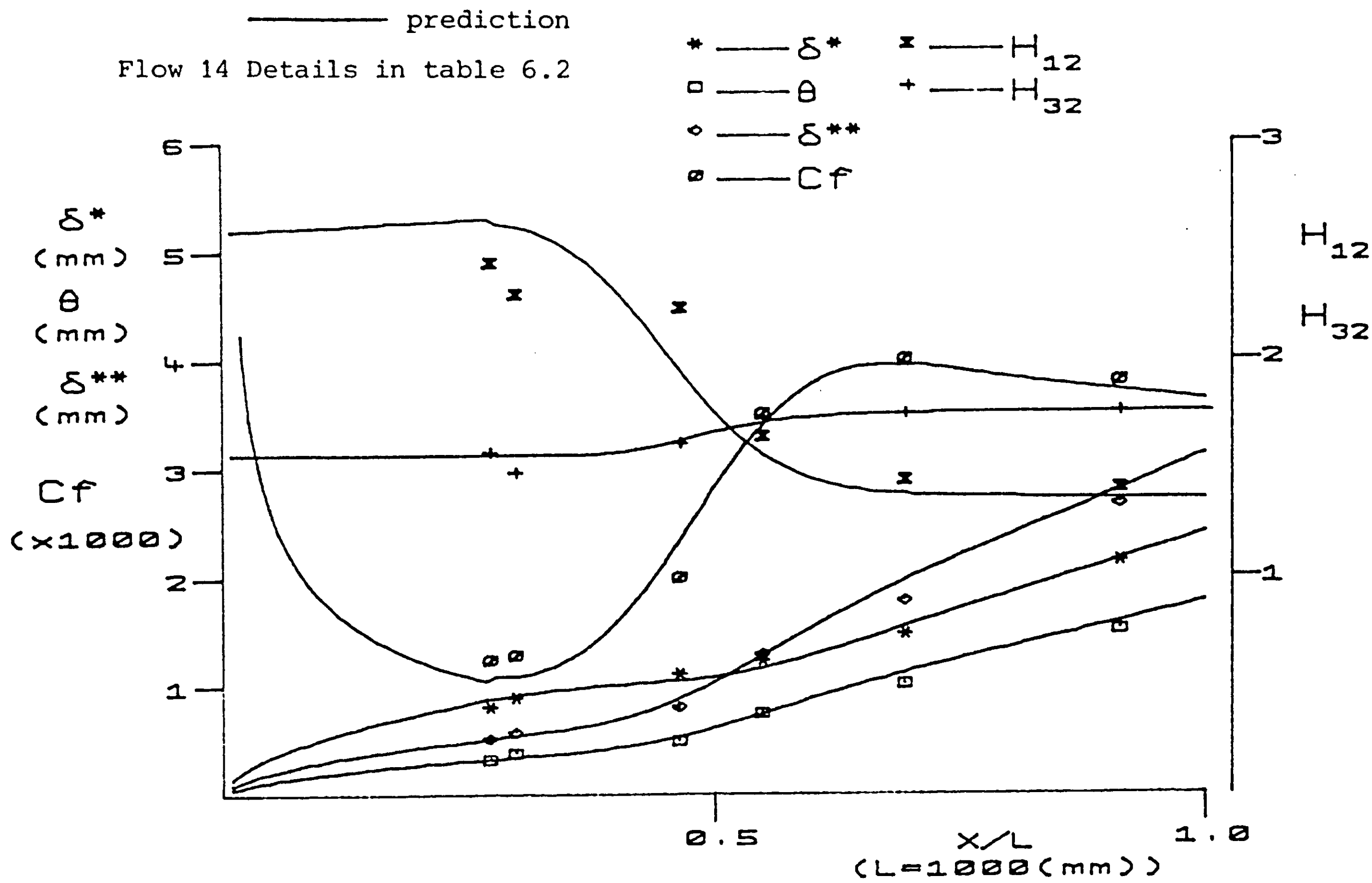

Fig. 7.4.4 (a) Boundary layer prediction of present Flow 14

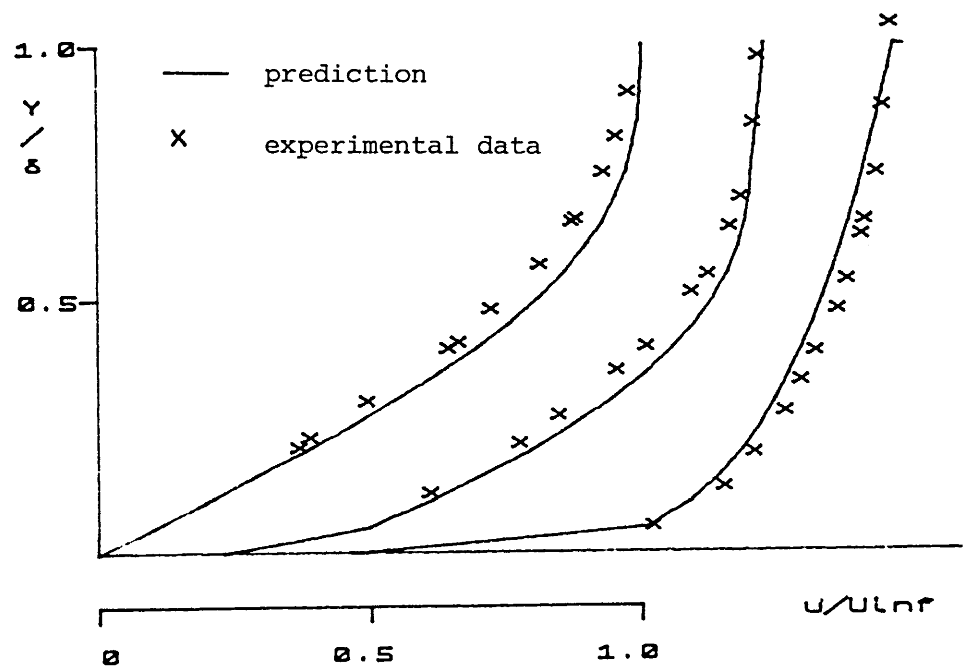

Fig. 7.4.4 (b) Predicted mean velocity profiles through transition

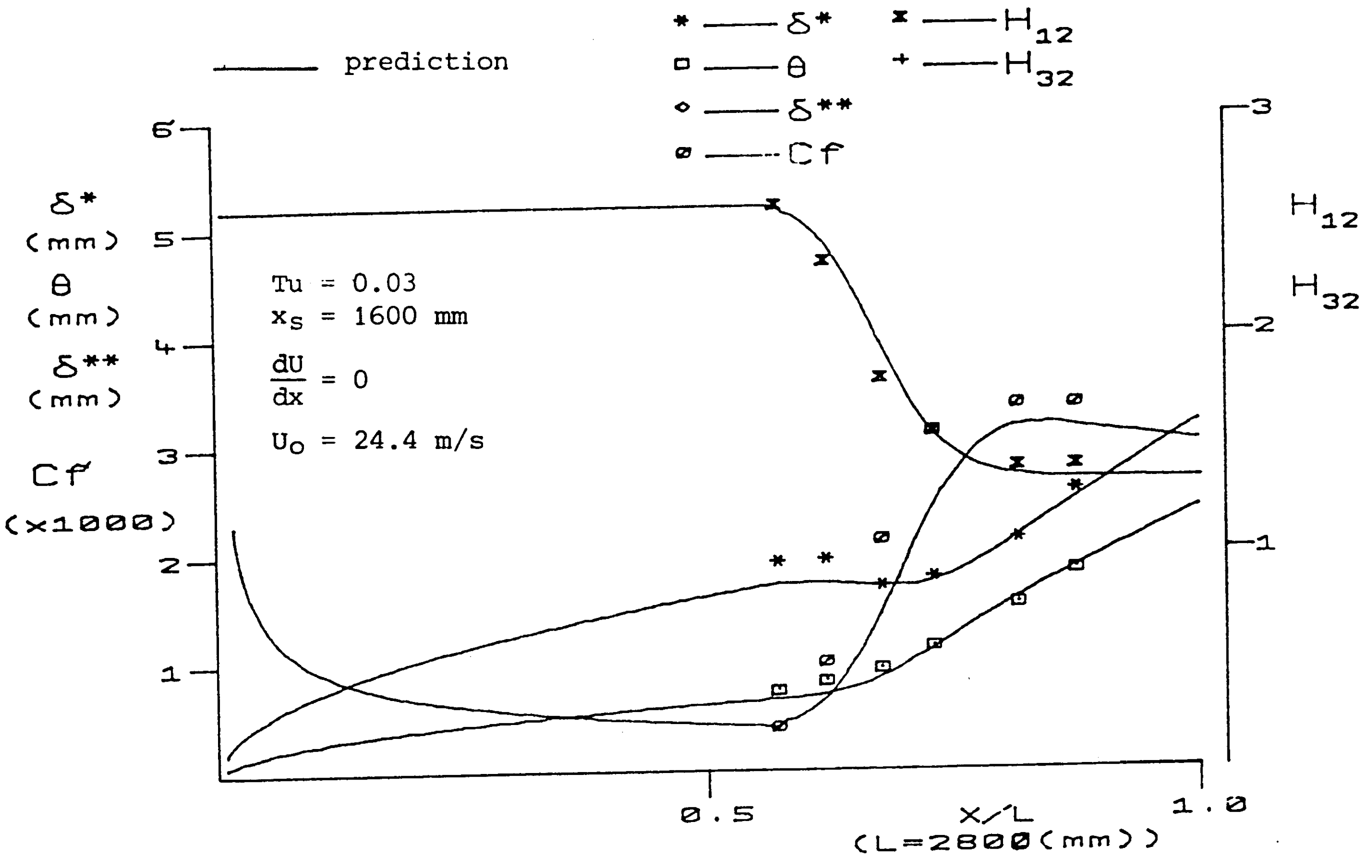

Fig. 7.4.5 (a) Boundary layer prediction of Schubauer & Klebanoff (1956) zero pressure gradient flow

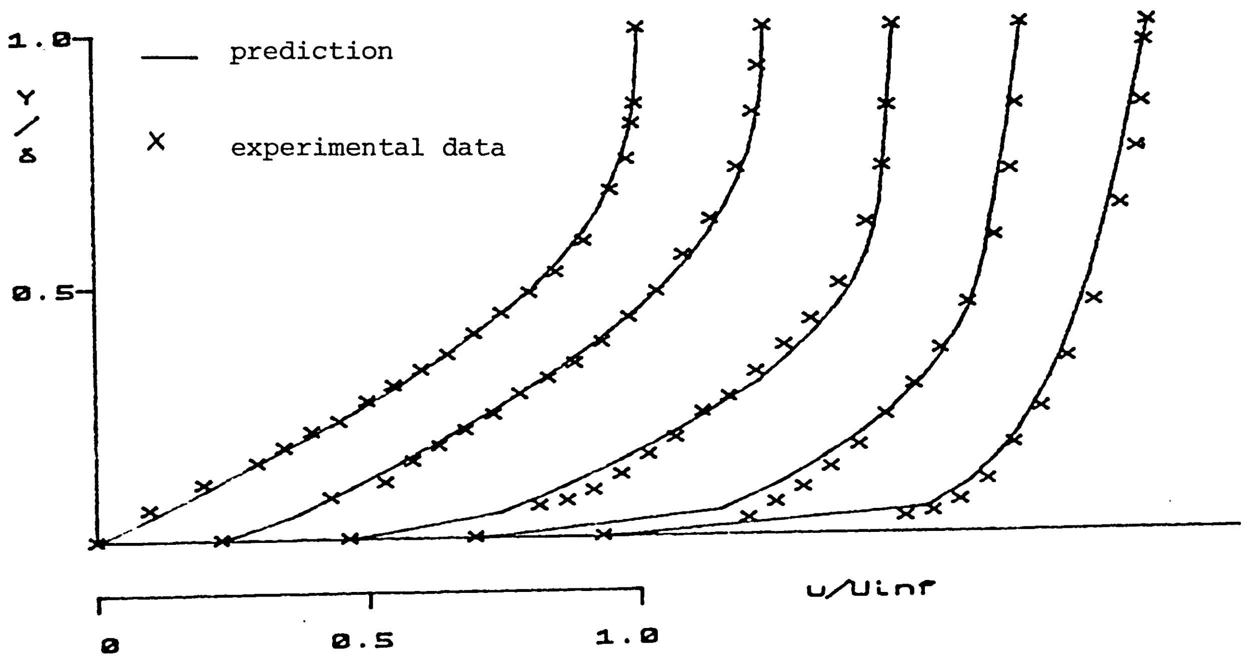

Fig. 7.4.5 (b) Predicted mean velocity profiles through transition

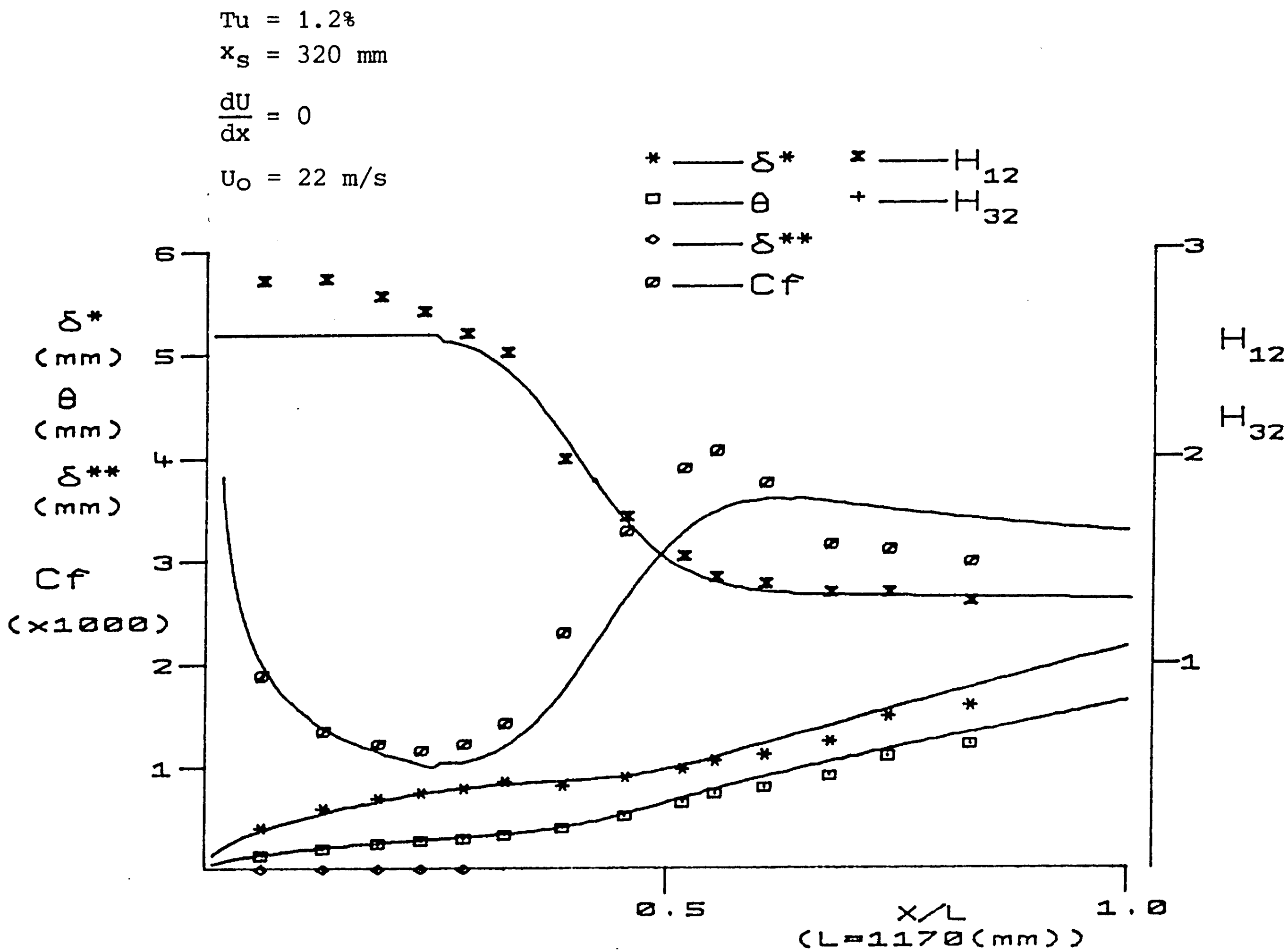

Fig. 7.4.6 Boundary layer prediction of Abu-Ghannam & Shaw (1980) zero pressure gradient flow

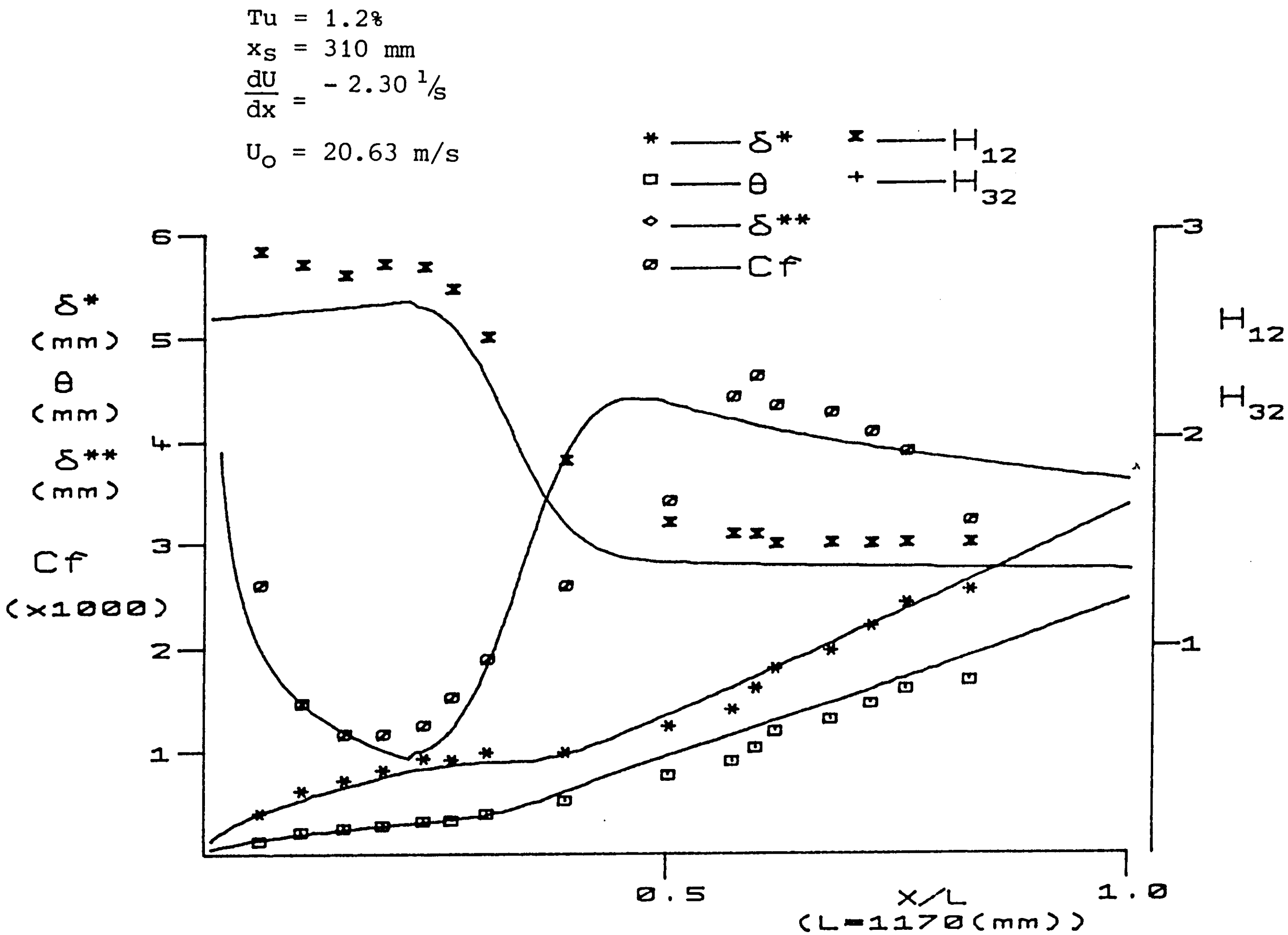

Fig. 7.4.7 Boundary layer prediction of Abu-Ghannam & Shaw (1980) Adverse pressure gradient flow

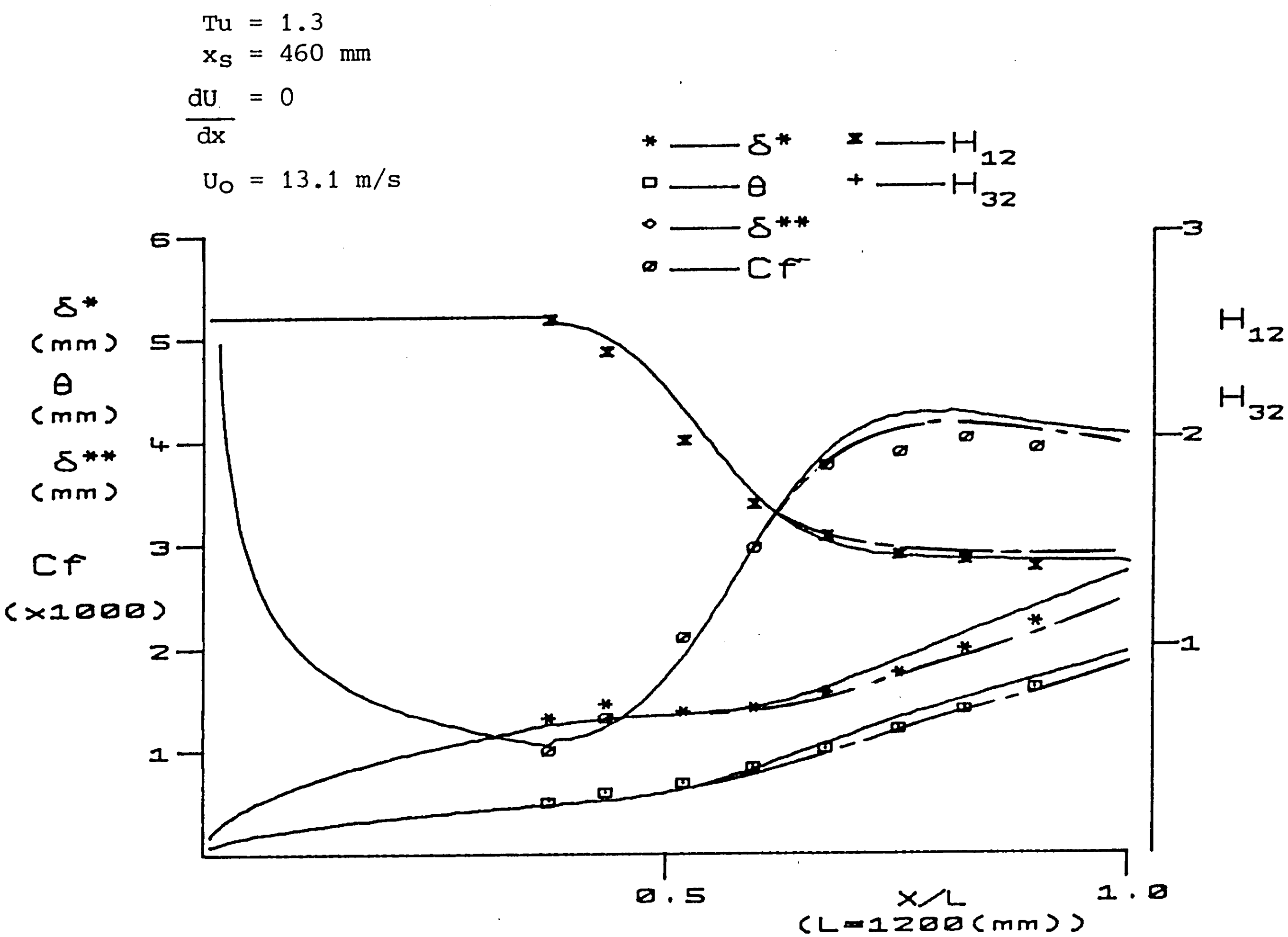

——— Tani/Alber
– – – Thwaites/Green

Fig. 7.4.8 Boundary layer prediction of Dhawan & Narasimha (1958) zero pressure gradient flow

CONCLUSIONS

1. The data acquisition and control system, based on the BBC microcomputer with BEEBEX Eurocard extension, was found to be completely satisfactory for the measurement of the mean flow variables in the laminar, turbulent and transitional boundary layers. The addition of this system, with analogue input and control, greatly enhanced the rate at which reliable data could be gathered and analysed. A further benefit lies in the ability to store the prime data in an organised manner for subsequent manipulation and graphical display. The data acquisition, control and data reduction software package developed, being interactively instructive, is extremely simple to use.

2. The flow over the test plate in the boundary layer wind tunnel facility has been improved to enable "free transition" values of R_{x_s} which concur with those of previous researchers.

3. A series of flows with different combinations of pressure gradient and freestream turbulence level were successfully set up and the boundary layer development for each case was recorded. Measurements were restricted to the plate centre line to remove the possibility of tunnel side wall effects influencing the results.

4. The system developed for measuring the intermittency function γ was very successful in giving reliable and repeatable measurements of the intermittency distribution $\overline{\gamma}(x)$ through the transition region.

5. The general boundary layer is well qualified by the *near wall* intermittency value. At intermittencies below $\overline{\gamma} = 0.01$ the mean flow is characteristically laminar and at intermittencies above $\overline{\gamma} = 0.99$ the mean flow is characteristically turbulent. At $\overline{\gamma}$ values between 0.01 and 0.99 the boundary layer is transitional and can be represented by an intermittency weighted function of the laminar and turbulent velocity components ie equation 7.1. The alternate switching process between the laminar and turbulent flow states within a transition region has been corroborated in a qualitative manner by observations of the instantaneous velocity signal within a transitional boundary layer, see fig. [6.4.1].

6. On the strength of the present data, the concept of statistical similarity of transition regions is shown to remain intact for moderate non-zero pressure gradients.

7. The mean intermittency distribution through a transition region is well represented by the normal distribution function and the statistical similarity is best illustrated when the intermittency $\overline{\gamma}$ is plotted against the normalised streamwise co-ordinate ζ.

8. With the transition region defined within the limits $0.01 < \overline{\gamma} < 0.99$ then the standard derivation σ of the intermittency data on the γ (ζ) distribution can be related directly to the transition length by equation 6.6 (see also fig. [6.6.2]).

9. The present results have shown that an adverse pressure gradient will promote early transition whilst a favourable pressure gradient will delay transition. This concurs with results from stability theory, Schlichting (1979), which indicate that adverse pressure gradients have a destabilising effect on the flow and that favourable pressure gradients have a stabilising effect.

10. For the present range of freestream turbulence levels tested, increasing the freestream turbulence has the effect of advancing the onset of transition. However, this effect becomes less significant with increasing adverse pressure gradient.

11. The length over which the breakdown process from laminar to turbulent flow occurs, ie the transition length, is greatly affected by both the freestream pressure distribution and the freestream turbulence level. In all cases the transition region is shortened by the influence of an adverse pressure gradient. From the present favourable pressure gradient/ transition length data available, it would appear that the transition length is increased by the influence of a favourable pressure gradient, however this observation is speculative as it is based on only one flow condition. In adverse pressure gradients, it has been shown that increasing the freestream turbulence, up to $Tu \cong 1\%$, has the effect of increasing the transition length. In this range, ie $0 < Tu < 1$, the freestream turbulence level has a greater effect in advancing the start of transition than the end of transition hence the overall transition length is increased. Increasing Tu above 1% reverses this trend, in consequence of the start of transition

approaching its asymptotic minimum position while the end of transition is still being significantly advanced.

12. A correlation which accounts for the combined effect of freestream turbulence and adverse pressure gradient on the transition length Reynolds number R_σ is presented. (Equation 6.14)

13. A general boundary layer integral prediction scheme for two-dimensional incompressible flows, which incorporates the new transition length correlation, has been developed. This prediction scheme uses existing integral techniques for the laminar and turbulent boundary layers in conjunction with an intermittency modelled transition region. The computational model was programmed to run on a BBC microcomputer and was tested against a representative sample of the present data and a number of flat plate test cases and is shown to model the development of the transitional boundary layer exceptionally well.

SUGGESTIONS FOR FUTURE WORK

A limitation of the present boundary layer prediction model is its inability to compute the development of a transitional boundary layer in a case where laminar separation is predicted within the transition region. This stems from the fact that accurate values of the laminar boundary layer parameters are required, in the computation procedure, through to the end of transition.

It has recently been brought to the author's attention that this limitation may present a problem when applying the present model to a flow with a velocity distribution typical of that which exists on the suction surface of a gas turbine blade. An interesting development of the present work would therefore be to set up conditions to simulate the flow over a turbine blade and to make detailed measurements of the boundary layer development on the test surface. [The present boundary layer wind tunnel, with perhaps a few minor modifications, would be capable of reproducing the type of velocity distribution required to simulate such a flow].

Two questions which immediately spring to mind, which may be elucidated by such an investigation:

(i) Does this predicted laminar separation actually occur within the transition region?

(ii) If it does occur, how can the effect be modelled and accounted for in a computational procedure?

To answer these questions, condition sampling techniques would have to be employed to measure the seperate laminar and turbulent velocity profiles in and out of turbulent patches within the transition region. This would necessitate the use of a fast data acquisition system capable of storing large amounts of data. Although the sample rate of the current BBC micro based system could be improved through the use of machine code routines, the limited amount of memory available would strictly limit its usefulness for such an investigation and therefore the present instrumentation would have to be enhanced by the addition of a more powerful microcomputer, possibly for example, the IBM PC with 512 K of available RAM.

Such an experimental program could also be extended to provide further data on the effect of local parameters on the location and extent of the transition region.

BIBLIOGRAPHY

Abu-Ghannam, B J & Shaw, R (1980) - "Natural Transition of Boundary Layers - The Effects of Turbulence, Pressure Gradient and Flow History". Jour Mech Eng Sci Vol 22, No 5 (1980)

Alber (1968) - "Application of an exact expression for the equilibrium dissipation integral to the calculation of turbulent non-equilibrium flows". Proc Computation of turbulent boundary layers, AFOSR-IFP, Stanford Conf (1968) Vol I pp 126 - 135

Arnal, D, Juillen, J C and Michel, R (1977) - "Analyse Experimentale et calcul de l'apparition et du developpement de la transition de la couche limite". AGARD conf Proc No 224, Laminar-Turbulent Transition, paper no 13, 1977. English Translation:- NASA TM 75325

Arnal, D (1984) - "Description and prediction of transition in two-dimensional incompressible flow". Parts I and II AGARD Report No 709 (1984)

Baines, W D & Peterson, E G (1951) - "An investigation of flow through screens". Trans. ASME, Vol 73, (1951)

Bannister, B R & Whitehead, M (1985) - "Interfacing the BBC microcomputer". Macmillan (1985) ISBN 0333371577

Beverly, P (1984) - "How to get full 12-Bit value from your ADC". ACORN USER March (1984)

Beverly, P (1985) - "Analogue Port Application" ACORN USER February (1985)

Blair, M F & Werle, M J (1980) - "The influence of freestream turbulence on the zero pressure gradient fully turbulent boundary layer". UTRC Report R80-914388-12 Sept (1980)

Blair, M F (1982) - "Influence of freestream turbulence on boundary layer transition in favourable pressure gradients". ASME Jour Eng Power Vol 104 (1982)

Blair, M F (1983) - "Influence of freestream turbulence on turbulent boundary layer heat transfer and mean profile development Parts I & II" ASME Jour Heat Tran Vol 105 (1983)

Bradshaw, P (1972) - "The understanding and prediction of turbulent flow". Aero Jour, July 1972

Bradshaw, P (1974) - "Effect of freestream turbulence on turbulent shear layers". Imp Coll Aero Rep 74 - 10 Oct (1974)

Brown, A & Burton R L (1978) - "The effects of freestream turbulence intensity and velocity distribution on heat transfer to curved surfaces". ASME Jour Eng Power Vol 100, (1978)

Brown, A & Martin, B W (1976) - "The use of velocity gradient factor as a pressure gradient parameter". Proc Instn Mech Engrs. Vol 190 (1976)

Castro, I P (1984) - "Effects of freestream turbulence on Low Reynolds number boundary layers". Tran ASME Vol 106 (1984)

Cebeci, T & Bradshaw, P (1977) - "Momentum transfer in boundary layers". McGraw-Hill (1977)

Cebeci, T & Smith, A M O (1974) - "Analysis of turbulent boundary layers". Academic Press (1974)

Clauser, F H (1954) - "Turbulent boundary layers in adverse pressure gradients". Jour Aero Sc 21, (1954)

Clauser, F H (1956) - "The turbulent boundary layer". Advances in App Mechs, vol 4 (1956)

Coles, D E (1956) - "The law of the wake in the turbulent boundary layer". Jour Fluid Mech, vol 1 (1956)

Coles, D E (1962) - "The turbulent boundary layer in a compressible fluid". Rand Rept, R-403-PR, Appendix A - "A manual of experimental bounday layer practice for low speed flow". (1962)

Coles, D E (1968) - "The young persons guide to the data" Proc Computation of turbulent boundary layers, AFOSR-IFP, Stanford Conf (1968) Vol II pp 1 - 53

Coles, D E & Hirst, E A (1968) - "Computation of turbulent boundary layers". AFOSR-IFP, Stanford Conf (1968)

Coles, D E & Savas, O (1979) - "Interaction for regular patterns of turbulent spots in a laminar boundary layer". Proc IUTAM Symposium on Laminar-Turbulent transition, (1979) pp 277 - 287 Eds Eppler & Fasel

Corrsin, S and Kistler, A (1954) - "The freestream boundaries of turbulent flows". N A C A Rep No 1244, (1954)

Crabtree, L F (1957) - "Prediction of transition in the boundary layer of an aerofoil". R A E, T N AERO 2491 (1957)

Debruge L (1970) - "A theoretical determination of convection heat-transfer coefficients during transition on the suction side of turbine aerofoils" AFAPL. TR-69-95, (1970)

Dhawan, S & Narasimha, R (1957) - "Some properties of boundary layer flow during the transition from laminar to turbulent motion". Jour Fluid Mech, Vol 3 (1958)

Dryden, H L (1936) - "Air flow in the boundary layer near a plate". NACA Report No 562

Dryden, H L (1956) - "Recent investigations of the problem of transition". Zeitschrift fur Flugwissenschaften Vol 4 (1956)

Dryden, H L & Schubauer, G B (1947) - The use of damping screens for the reduction of wind tunnel turbulence". Jour Aero Sci April (1947)

Dunham, J (1972) - "Prediction of boundary layer transition on turbomachinery blades". AGARD AG164, No 3 (1972)

East, L F (1972) - "Spatial variations of the boundary layer of a large low speed wind tunnel". Aero Jour 76, 1972

Emmons, H W (1951) - "The laminar turbulent transition in a boundary layer" Part 1 Jour Aero Sci Vol 18 (1951)

Fage, A & Preston, J H (1941) - "On transition from laminar to turbulent flow in the boundary layer" Proc Roy Soc Vol 144 No 2 (1941)

Ferguson, J D, Stewart J & Williams, P (1981) - "Interfacing microprocessors; Design, operation and application of a universal interface board". Wireless World Oct (1981) pp 34 - 39, November (1981) pp 59 - 62, December (1981) pp 71 - 75

Fiedler, H & Head, M R (1966) - "Intermittency measurements in the turbulent boundary layer". Jour Fluid Mech vol 25, part 4, (1959)

Forest, A W (1977) - "Engineering predictions of transitional boundary layers". AGARD conf Proc no 224, Laminar-turbulent transition, paper no 24 (1977)

Fraser, C J (1979) - "Boundary layer development from transition provoking devices" PhD thesis Dundee College of Technology (1979)

Fraser, C J & Milne, J S (1980) - "Boundary layer development from transition provoking devices". Int J Heat & Fluid Flow Vol 2 No 4 (1980)

Fraser, C J (1986) - "The assessment of boundary layer two dimensionality" Aero Jour (1986)

Fraser, C J, Milne J S & Gardiner, I D (1987) - "Application of a microcomputer for control, data acquisition and modelling in transitional boundary layer Studies". Proc 2nd Int Conf 'Microcomputers in Engineering' Swansea 7th - 10th April (1986) Eds Schrefler B A & Lewis R W

Fraser, C J, Gardiner, I D & Milne, J S (1987) - "A comparison of two integral techniques for the prediction of transitional boundary layer flow" Conference on numerical methods in laminar and turbulent flow July 6th - 10th, MONTREAL 1987

Gad-el-Hak, M, Blackwelder, R F & Riley, J J (1981) - "On the growth of turbulent regions in laminar boundary layers". Jour Fluid Mech, Vol 110 (1981)

Gazley, C (1953) - "Boundary layer stability and transition in subsonic and supersonic flow". Jour Aero Sci January (1953)

Granville, P S (1953) - "The caclulations of viscous drag on bodies of revolution". Navy Dept. The David Taylor model Basin Report 849, (1953)

Green, J E, Weeks, D J & Brooman, B G (1977) - "Prediction of turbulent boundary layers and Wakes in compressible flow by a lag entrainment method". Aero Res Coun, R & M No 3791, (1971)

Hall, D J & Gibbings, J C (1972) - "Influence of Stream turbulence and pressure gradient upon boundary layer transition". Jour Mech Eng Sci, Vol 14, No 2 (1972)

Hancock, P E & Bradshaw, P (1983) - "The effect of freestream turbulence on turbulent boundary layers" Tran ASME Vol 105 (1983)

Huffman, G D & Bradshaw, P - A note on Von Karman's constant in low Reynolds number turbulent flows. Jour Fluid Mech, Vol 53, part 1, (1972)

Jaffe, N A, Okamura, T T & Smith, A M O (1970) - "Determination of spatial amplification factors and their application to predicting transition". A I A A, vol 1 (1963)

Jarvis, J M (1985) - "Fast data acquistion and the Apple II and Sage microcomputers" Proc "Developments in measurements and instrumentation in Engineering" Hatfield, 11 - 13 September, 1985, pub. Mech Eng Pub Ltd, for I Mech E

Klebanoff, P S (1955) - "Characteristics of turbulence in a boundary layer with zero pressure gradient". N A C A, Tech note 3178, (1955)

Klebanoff, P S, Tidstrom, K D & Sargent, L M (1962) - "The three-dimensional nature of boundary layer instability" Jour Fluid Mech, vol 12, part 1 (1962)

Kline, S J (1966) - "Some remarks on turbulent shear flows" Proc Instn Mech Engrs Vol 180 pt 3 (1966)

Liepmann, H W (1943) - "Investigations of laminar boundary layer stability and transition on curved boundaries" NACA AC Rept No 3H30 (1943)

Ludwieg, H and Tillmann, W (1950) - "Investigation of the wall shearing stress in turbulent boundary layers" N A C A, Tech memo 1285 (1950)

Martin, B W, Brown, A & Garret, S E (1978) - "Heat transfer to a PVD rotor blade at high subsonic passage throat Mach numbers" Proc Inst Mech Engrs Vol 192 (1978)

McDonald, H & Fish, R W (1973) - "Practical calculations of transitional boundary layers", Int Jour Heat & Mass Transfer vol 16, No 9, (1973)

Meier, H V & Kreplin, H P (1980) - "Influence of freestream turbulence on boundary layer development" A I A A Jour Vol 18, No 1, (1980)

Michel, R (1951) - "Etude de la transition sur le profiles d'aile; establissement d'un critere de determination du point de transition et calcul de la trainee de propil en incompressible', ONERA rapport 1/1578A, 1951

Milne, J S, Fraser C J & Gardiner, I D (1985) - "A low-cost data acquisition and control system based on a BBC microcomputer", Proc: "Developments in measurements and instrumentation in Engineering" Hatfield 11 - 13 September 1985. Published by M E P for I Mech E

Mitchner, M (1954) - "Propagation of turbulence from an instantaneous point disturbance". Readers Forum, Jour Aero Sc, vol 21, No 5, 1954

Murlis, J, Tsai, H M & Bradshaw, P (1982) - "The structure of turbulent boundary layers at low Reynolds numbers" Jour, Fluid Mech Vol 122 (1982)

Orr, W M F (1907) - "The stability or instability of the steady motions of a perfect fluid and of a viscous liquid". Part 1: A perfect fluid; Part 2: A viscous liquid. Proc Roy Irish Acad 27, (1907)

Patel, V C (1965) - "Calibration of the Preston tube and limitations on its use in pressure gradients". Jour Fluid Mech, vol 23, part 1, 1965

Pohlhausen, K (1921) - "Zur naherungsweisen integration der differentialgleichung der laminaren reibungsschicht". Zeit fur ang. Math & Mech 1 (1921)

Prandtl, L (1904) - "On fluid motion at very small viscosity". Proc 3rd Int Math Cong. (Heidelberg)

Prandtl, L (1914) - "Der luftwiderstand von kugeln" Ges Wiss Gottingen, Math Phy Klasse (1914)

Preston, J H (1958) - "The minimum Reynolds number for a turbulent boundary layer and the selection of a transition device". Jour Fluid Mech, Vol 3, part 4, (1958)

Rayleigh, (Lord) (1880) - Sci Papers 1, 474, 1180; 3, 17, 1887; 4,197, 1913. see also: "On the stability of certain fluid motions". Proc London Math Soc 2, 57, 1880 and 19, 67, 1887, Sci Papers 1, 474 and 3,17. see also: Sci Papers 4, 203, 1895 and 6. 197 (1913)

Reshotko, E (1976) - "Boundary layer stability and transition" Ann Rev Fluid Mech Vol 8, (1976)

Reynolds, O (1883) - Phil Trans Roy soc 1883, or Collected Papers 2, 51, see also Sci Papers 2, 1883, see also "On the dynamic theory of incompressible viscous fluids and the determination of the criterion. Phil Trans Roy Soc (1895)

Rotta, J C (1962) - "Turbulent boundary layers in incompressible flow": Progress in Aero Sc vol 2, editors:- Ferri, A, Kuchemann, D and Sterne, L H G Pergamon Press (1962)

Sandborn, V A (1959) - "Measurements of intermittency of turbulent motion in a boundary layer", Jour Fluid Mech vol 6 (1959)

Schlichting, H (1979) - "Bondary layer theory" seventh edition. McGraw-Hill Book Company (1979)

Schubauer, G B & Klebanoff, P S (1956) - "Contributions on the mechanics of boundary layer transition", NACA Rep No 1289 and NACA TN 3489 (1956)

Schubauer, G B & Skramstad, H K (1942) - "Laminar boundary layer oscillations and stability of laminar flow", Nat Bur St, Res Rept 1772, 1943; see also NACA Rept 909, (1948)

Seyb, N J (1972) - "The role of boundary layers in axial flow turbomachines and the prediction of their effects" Proc AGARD Conf 164 (1972)

Sharma, O P, Wells, R A, Schlinker, R H and Bailey, D A (1982) - "Boundary layer development on turbuie airfoil suction surfaces" Trans ASME Vol 104 (1982)

Shaw R, Hardcastle, J A Riley, S & Roberts, C C (1983) - "Recording and analysis of fluctuating signals using a microcomputer" Int Conf on "The use of Micros in fluid engineering" BHRA June 7 - 8 (1983)

Simpson, R L (1970) - "Characteristics of the turbulent boundary layer", Jour Fluid Mech, vol 42, 1970

Smith, A M O & Gamberoni, N (1956) - "Transition, pressure gradient and stability theory", Proc 9th Int cong App Mech, 1956

Sommerfeld, A (1908) - "Ein beitrag zur hydrodynamischen erklarung der turbulenten flussig-keitsbeivegungen" Atti del 4, Cong Int dei Mat, vol 3, 1908

Tani, I (1954) - "On the approximate solution of the laminar boundary layer Equations" Jour Aero Sci Vol 21 (1954)

Tani, I (1969) - "Boundary layer transition" Ann Rev Fluid Mech Vol 1 (1969)

Taylor, G I - "Statistical theory of turbulence, 5. Effect of turbulence on boundary layer". Proc Roy Soc, London A 156, 1936; see also: "Some recent developments on the study of turbulence". Proc 5th Int cong App Mech, New York, 1938

Thwaites, B (1949) - "Approximate calculation of the laminar boundary layer", Aero Quarterly Jour vol 1, 1949

Tollmien, W (1929) - "Ueber die entstehung der turbulenz. 1. Mitteilung" Nachr Ger Wiss Gottingen, Math Phy Klasse, see also N A C A T M 1265, 1950

Townsend, A A (1948) - "Local isotrpy in the turbulent wake of a cylinder" Austr Jour Sci Res Vol 1 (1948)

Townsend, A A (1965) - "Self preserving flow inside a turbulent boundary layer" Jour Fluid Mech Vol 22, Pt 4 (1965)

Turner, A B (1971) - "Local heat transfer measurements on a gas turbine blade" Jour Mech Eng Sci Vol 13 No 1 (1971)

Van Driest, E R & Blumer, C B (1963) - "Boundary layer transition: free stream turbulence and pressure gradient effects" A I A A vol 1 (1963)

Van Ingen, J L (1956) - "A suggested semi-empirical method for the calculation of the boundary layer transition region" Rept V T H 74, Dept Aero & Eng, Inst of Tech, Delft, Holland (1956)

White, F M (1974) - "Viscous fluid flow", McGraw-Hill (1974)

Wygnanski, I, Sokolov M & Friedman, D (1976) - "On a turbulent spot in a laminar boundary layer", Jour Fluid Mech Vol 78, pt 4, (1976)

APPENDIX 1

Estimation of the experimental uncertainty in the measured boundary layer integral thicknesses

APPENDIX 1 Experimental uncertainty in integral thicknesses

A1.1 Error due to uncertainty in velocity measurement

As described in section 4.4, when linearising the signal from a hot wire probe using the DISA 55M25 lineariser there is an inherent parabolic error, usually with the maximum close to the centre of the linearised region and tailing off to zero at the maximum and minimum velocities, as shown in figure 4.4.1. The analysis which follows describes the effect such an error would induce on the boundary layer integral parameters in both a laminar (parabolic type velocity profile) and a turbulent ($^1/_7$ th. power type velocity profile) boundary layer

The error is assumed to be zero at both $(\bar{u}/U_\infty)=0$ and $(\bar{u}/U_\infty)=1$ with a maximum at $(\bar{u}/U_\infty)=0{\cdot}5$ as shown below :-

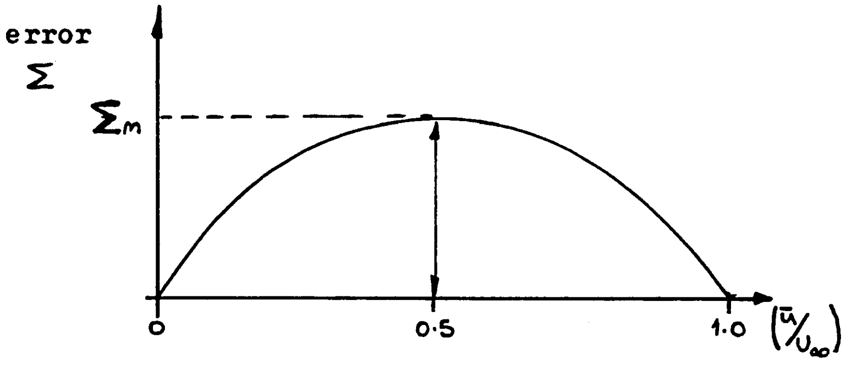

The error is represented by the parabola :-

$$\Sigma = A + B(\bar{u}/U_\infty) + C(\bar{u}/U_\infty)^2$$

Writing $U = (u/U_\infty)$ and applying the boundary conditions

(i) @ $U = 0, \Sigma = 0$

(ii) @ $U = 1, \Sigma = 0$

(iii) @ $U = 0{\cdot}5, \; d\Sigma/dU = 0, \; \Sigma = \Sigma_m$

results in the local error being represented by :-

$$\Sigma = 4\Sigma_m (U - U^2)$$

If this error is now introduced into the local velocity measurements ie.

$$U' = U + \Sigma U$$

then the error introduced into the displacement, momentum and energy thicknesses are respectively

$$\delta^{*\prime} = \int_0^1 (1 - U')\, d\eta \quad ; \quad \Theta' = \int_0^1 U'(1 - U')\, d\eta$$

and
$$\delta^{**\prime} = \int_0^1 U'(1 - U'^2)\, d\eta$$

Considering first the displacement thickness, δ^*

$$\delta^{*\prime} = \int_0^1 (1 - U - \Sigma U)\, d\eta$$

$$= \int_0^1 [1 - U - 4\Sigma_m (U - U^2) U]\, d\eta$$

$$= \int_0^1 (1 - U)\, d\eta - 4\Sigma_m \int_0^1 (U^2 - U^3)\, d\eta$$

$$\therefore \Delta\delta^* = \delta^{*\prime} - \delta^* = -4\Sigma_m \int_0^1 U^2 - U^3\, d\eta$$

Hence :-

$$\frac{\Delta \delta^*}{\delta} = \frac{-4\Sigma_m \int_0^1 (U^2 - U^3)\, d\eta}{\int_0^1 (1 - U)\, d\eta} \qquad \text{——— A1.1}$$

Considering now the momentum thickness, θ

$$\theta' = \int_0^1 \{(U + \Sigma U)\,[1 - (U + \Sigma U)]\}\, d\eta$$

$$= \int_0^1 \{[U + 4\Sigma_m (U - U^2) U]\,[1 - (U + 4\Sigma_m (U - U^2) U)]\}\, d\eta$$

$$= \int_0^1 \{[U + 4\Sigma_m U^2 - 4\Sigma_m U^3]\,[1 - U - 4\Sigma_m U^2 + 4\Sigma_m U^3]\}\, d\eta$$

Neglecting power terms in Σ_m results in :-

$$\theta' = \int_0^1 \{(U - U^2) + 4\Sigma_m U^2 - 12\Sigma_m U^3 + 8\Sigma_m U^4\}\, d\eta$$

$$\Rightarrow \quad \theta' = \theta + 4\Sigma_m \int_0^1 U^2 (1 - 3U + 2U^2)\, d\eta$$

$$\therefore \quad \Delta\theta = \theta' - \theta = 4\Sigma_m \int_0^1 U^2 (1 - 3U + 2U^2)\, d\eta$$

Hence :-

$$\frac{\Delta \theta}{\theta} = \frac{4\Sigma_m \int_0^1 U^2 (1 - 3U + 2U^2)\, d\eta}{\int_0^1 U (1 - U)\, d\eta} \qquad \text{——— A1.2}$$

Similarly if power terms in Σ_m are neglected then :-

$$\frac{\Delta \delta^{**}}{\delta^{**}} = \frac{4\Sigma_m \int_0^1 U^2 (1 - U + 3U^2 - 3U^3)\, d\eta}{\int_0^1 U (1 - U^2)\, d\eta} \qquad \text{——— A1.3}$$

Assuming a parabolic "laminar" velocity profile ie.

$$U = 2\eta - \eta^2$$

Substituting this into equations Al.1, Al.2, and Al.3 and evaluating, results in :-

$$\frac{\Delta \delta^*}{\delta} = -0{\cdot}92\,\Sigma_m$$

$$\frac{\Delta \theta}{\theta} = -0{\cdot}78\,\Sigma_m$$

$$\frac{\Delta \delta^{**}}{\delta^{**}} = -0{\cdot}70\,\Sigma_m$$

Substituting a $^1/_7$ th. power "turbulent" velocity profile into equations Al.1, Al.2 and Al.3 and evaluating, results in :-

$$\frac{\Delta \delta^*}{\delta} = -2{\cdot}5\,\Sigma_m$$

$$\frac{\Delta \theta}{\theta} = -2{\cdot}2\,\Sigma_m$$

$$\frac{\Delta \delta^{**}}{\delta} = -1{\cdot}9\,\Sigma_m$$

Therefore if the maximum error ie. Σ_m in the velocity measurements is 1% then the corresponding errors in δ^*, θ, & δ^{**} for a parabolic velocity profile would be -0.92%;0.78% and-0.70% respectively and -2.5%,-2.2% and -1.9% respectively for a $^1/_7$ th. power velocity profile. The negative sign shows that if the error Σ_m is positive then the integral thicknesses are underestimated. Figure Al.1.1 shows a parabolic profile with and without a 5% maximum error included (ie. Σ_m = 0.05)and figure Al.1.2 shows the corresponding profiles of $(1-U)$, $U(1-U)$ and $U(1-U^2)$

A1.2 Error due to uncertainty in y datum

A numerical error analysis assuming y/δ was under-estimated by 1% showed that the corresponding error in all the boundary layer integral thicknesses was approximately -1%. The y datum can be set, at the very worst, to an accuracy of $\pm$ 0.1 mm therefore, if the boundary layer thickness is small this may constitute a non-negligible error in the integral parameters (in a 10mm thick boundary layer the error in the integral thicknesses would, at worst, be 1% due to the uncertainty in setting the y datum). This error obviously diminishes as the boundary layer thickens

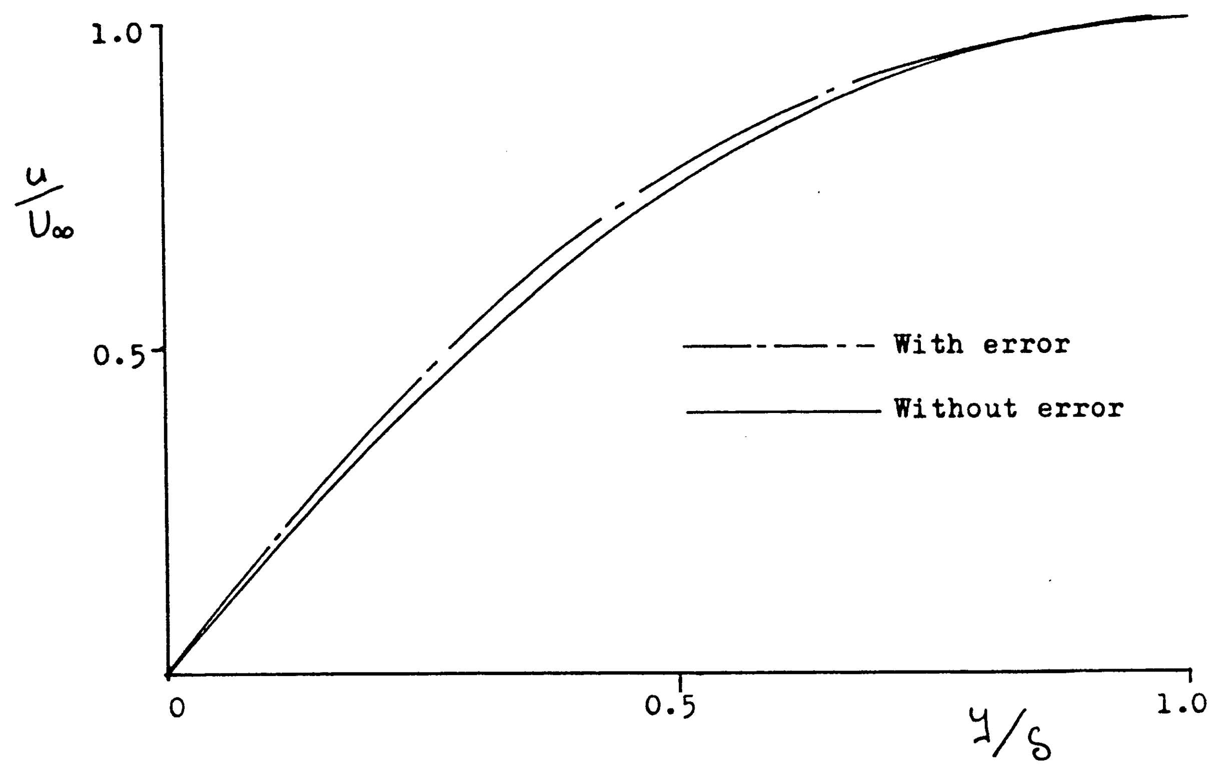

Figure A1.1.1 Velocity profile

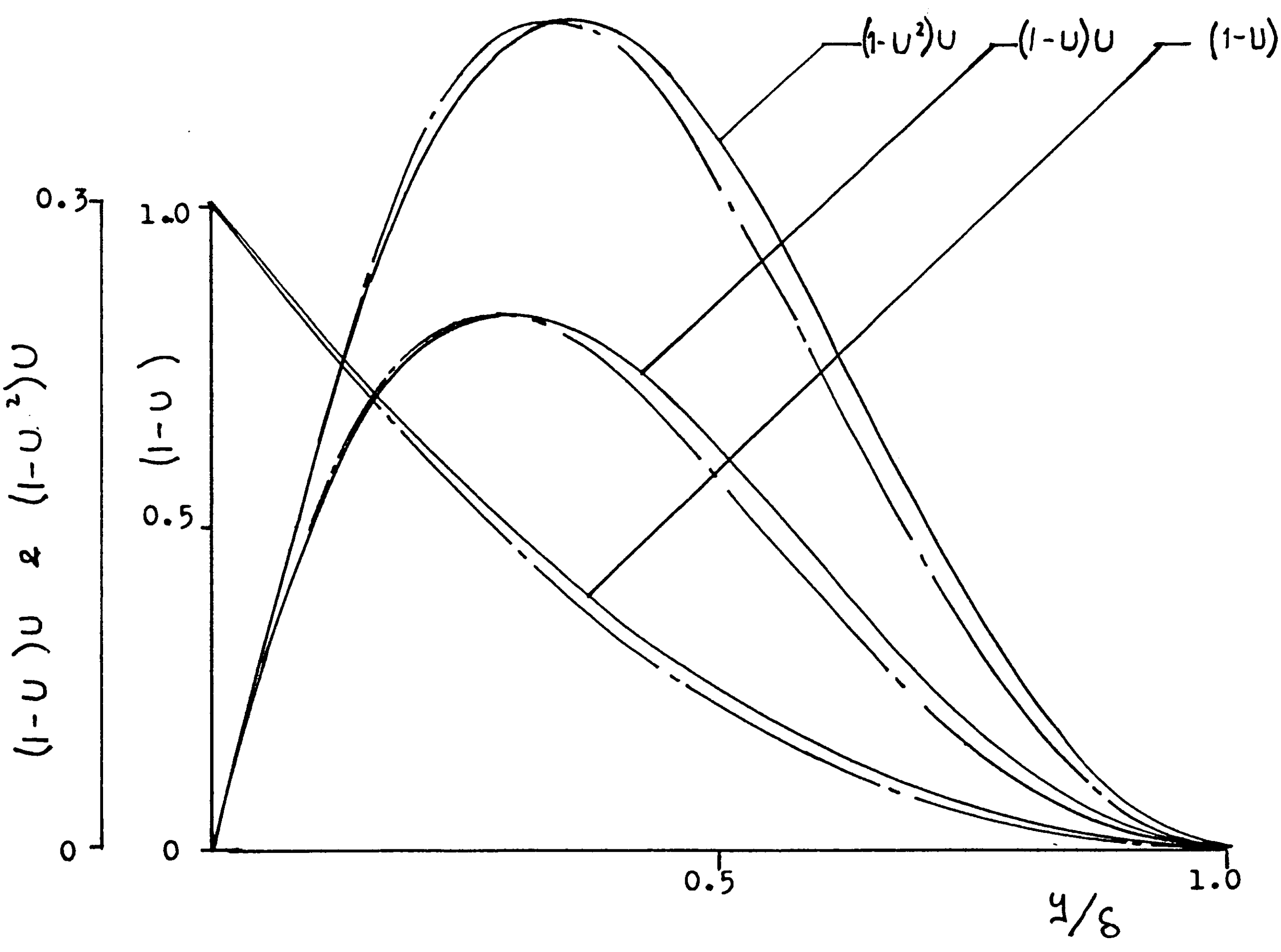

Figure A1.1.2

APPENDIX 2

Description of a microcomputer based system for setting up the DISA 55M25 lineariser

APPENDIX 2 Microcomputer based system for setting up the DISA 55M25 Lineariser

The procedure for linearising the signal from a hot wire probe using the DISA 55M25 lineariser is fairly complex and usually very time consuming. After the basic functions have been set, as described in the user manual, the signal from the probe is linearised via the 55M25 by a trial and error iterative process. The probe is first exposed to a known velocity at the high end of the calibration range and then the 'Gain High' control on the 55M25 is adjusted to give the required output on a digital voltmeter, DVM,(usually the voltage output from the lineariser is made to correspond to a convenient fraction of the flow velocity, in this case $^1/10$ th.). The probe is then exposed to a known velocity at the low end of the calibration range and if the reading on the DVM does not correspond to the relevant velocity the 'Exponent Factor' control, on the 55M25, is adjusted. The probe is then again exposed to the high velocity and the DVM reading is checked. This process continues until a satisfactory linearisation is achieved.

The problem with this procedure is that, although adjustment of the various controls on the 55M25 have varying degrees of influence on different regions within the calibration range, eg. the Gain High control affects the high velocity end of the range most significantly, each adjustment does in fact have some influence over the entire linearisation range. However the effect of such adjustments can only be assessed at one point at any one time. Therefore, for example when examining a reading on the DVM at the high end of the calibration range and making an adjustment to the Gain High control, there is no indication given of the effect this adjustment has on points at other positions within the linearisation region.

To overcome this problem and to speed up the linearisation process a microcomputer based system was developed which enabled a range of calibration points to be continuously fed into the lineariser input. The corresponding values output from the lineariser are then displayed on a monitor along with a line which corresponds to the 'ideal' linearised signal. The set up for this system is shown in figure A2.1 and a print out of the software required to run the system along with a flow diagram is given in figures A2.2 & A2.3. (The BUFFER between the DAC and the Signal Conditioner,shown in figure A2.1, was required to overcome impedance matching problems encountered).

Briefly, a set of calibration points are obtained from a single run of the tunnel, in the relevant velocity range (ie. raw hot wire voltages and corresponding pitotstatic readings). These values are then manually fed into the BBC microcomputer.After the points have been suitably conditioned, within the software, they are output to the lineariser via a Digital-to-Analogue Converter, DAC,and then retrieved from the lineariser via an Analogue-to-Digital Converter, ADC,in a closed loop. These points are continuously displayed on a graph of V_{in} (voltage into lineariser) against V_{out} (voltage out of lineariser), along with a line which corresponds to the 'ideal' linearised signal. The effect on each point of a single adjustment to the lineariser controls can then be viewed, almost immediately,and an optimum setting can fairly easily be obtained.

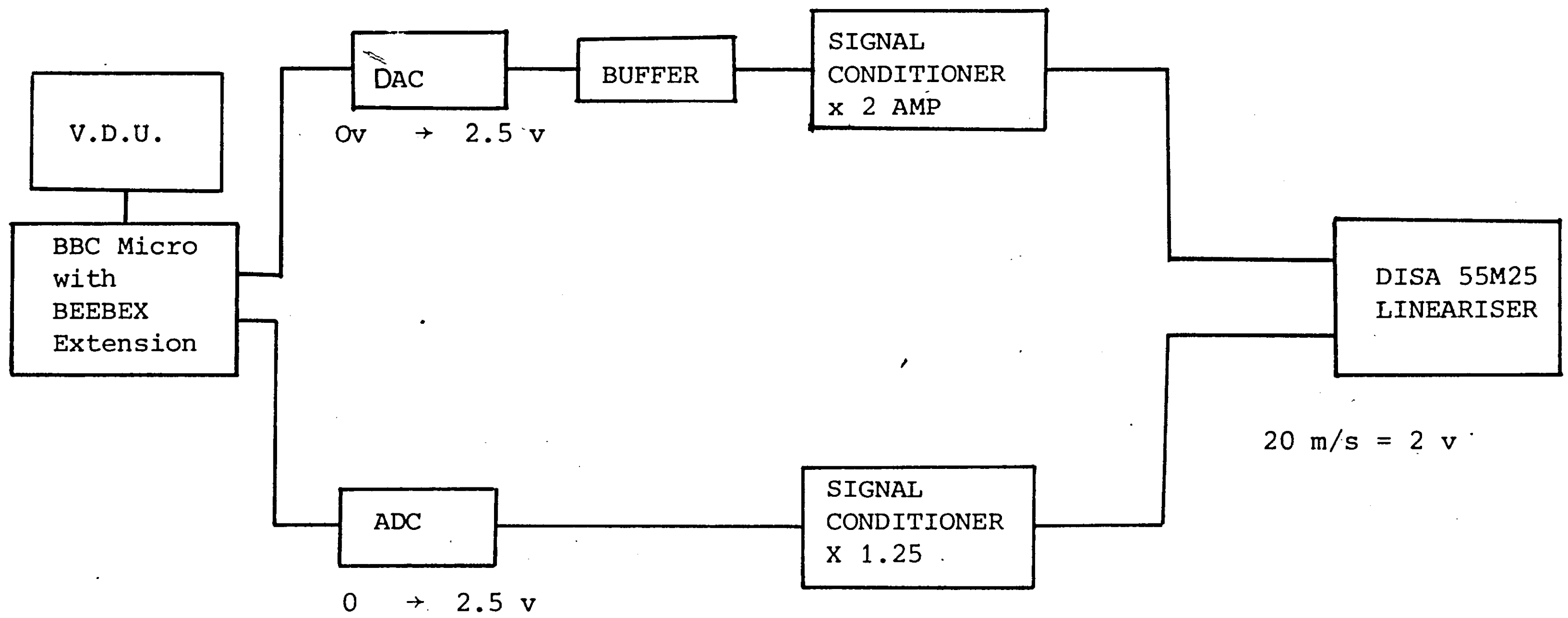

Fig. A.2.1 Schematic diagram of apparatus used for setting up the DISA 55M25 lineariser

```
10 CLOSE#0
20 MODE7
30 CLS
40 DIM P(11),Vbr(11),Vdac(11),Vadc(11)
50 DIM Voutpl(11),Vinpl(11)
60 REM PROB LIN.PROG
70 PRINTTAB(4,8)CHR$132"INPUT AIR TEMP IN DegC"
80 INPUTTAB(32,8) t
90 PRINTTAB(4,12)CHR$132"INPUT ATMOS. PRESS IN mmHg"
100 INPUTTAB(32,12) Z
110 Rho=0.46535*Z/(t+273)
120 CLS
130 PRINTTAB(0,2)CHR$133"INPUT CORRESPONDING H.W. VOLTAGES"
140 PRINTTAB(0,4)CHR$133"OPPOSITE THE DYNAMIC PRESSURES GIVEN"
150 PRINT:PRINT:
160  PRINTCHR$134"   Dynamic press.      H.W.Bridge"
170 PRINTCHR$134"       mmHg             Voltage"
180 X=0
190 FOR I = 1 TO 10
200 READ P(I)
210 PRINTTAB(8,10+X);P(I)
220 INPUTTAB(24,10+X) Vbr(I)
230 X=X+1
240 NEXT
250 MODE1
260 VDU 19,3,3,0,0,0
270 VDU 19,2,4,0,0,0
280 MOVE125,825:DRAW125,125:DRAW1225,125
290 VDU5
300 MOVE50,750:PRINT"V"
310 MOVE50,700:PRINT"i"
320 MOVE50,675:PRINT"n"
330 MOVE700,50:PRINT"V out"
340 MOVE50,850:PRINT"5v"
350 MOVE50,150:PRINT"2v"
360 MOVE125,90:PRINT"0v"
370 MOVE1215,90:PRINT"2v"
380 VDU4
390 Ydatum1=((Vbr(2)-2)*233.34)+125
400 Ydatum2=((Vbr(10)-2)*233.34)+125
410 Xdatum1=((SQR(2*9.81*P(2)/Rho)/10)*550)+125
420 Xdatum2=((SQR(2*9.81*P(10)/Rho)/10)*550)+125
430 MOVEXdatum1,Ydatum1
440 DRAWXdatum2,Ydatum2
450 *IO
460 A%=OPENUP "CU-DAC8 &C000"
470 FOR I= 1 TO 10
480 Vdac(I)=Vbr(I)*50.5
490 BPUT#A%,Vdac(I)
500 Vsum%=0
510 PTR#A%=8
520 FOR K = 1 TO 10
530 V%=BGET#A%
540 Vsum%=Vsum%+V%
550 NEXT
560 Vadc(I)=(Vsum%/10)*2/255
570 Vinpl(I)=((Vbr(I)-2)*233.34)+125
580 GCOL 0,1
590 Voutpl(I)=(Vadc(I)*550)+125
600 PLOT 69,Voutpl(I),Vinpl(I)
610 NEXT
620 TIME=0: REPEAT UNTIL TIME=50
630 FOR I=1 TO 10
640 PLOT 71,Voutpl(I),Vinpl(I)
650 NEXT
660 GOTO470
670 DATA 0,0.5,1.0,2.25,4.0,6.25,9.0
680 DATA 12.25,16.0,20.25
```

Figure A2.2 Print out of software for DISA 55M25 set up system

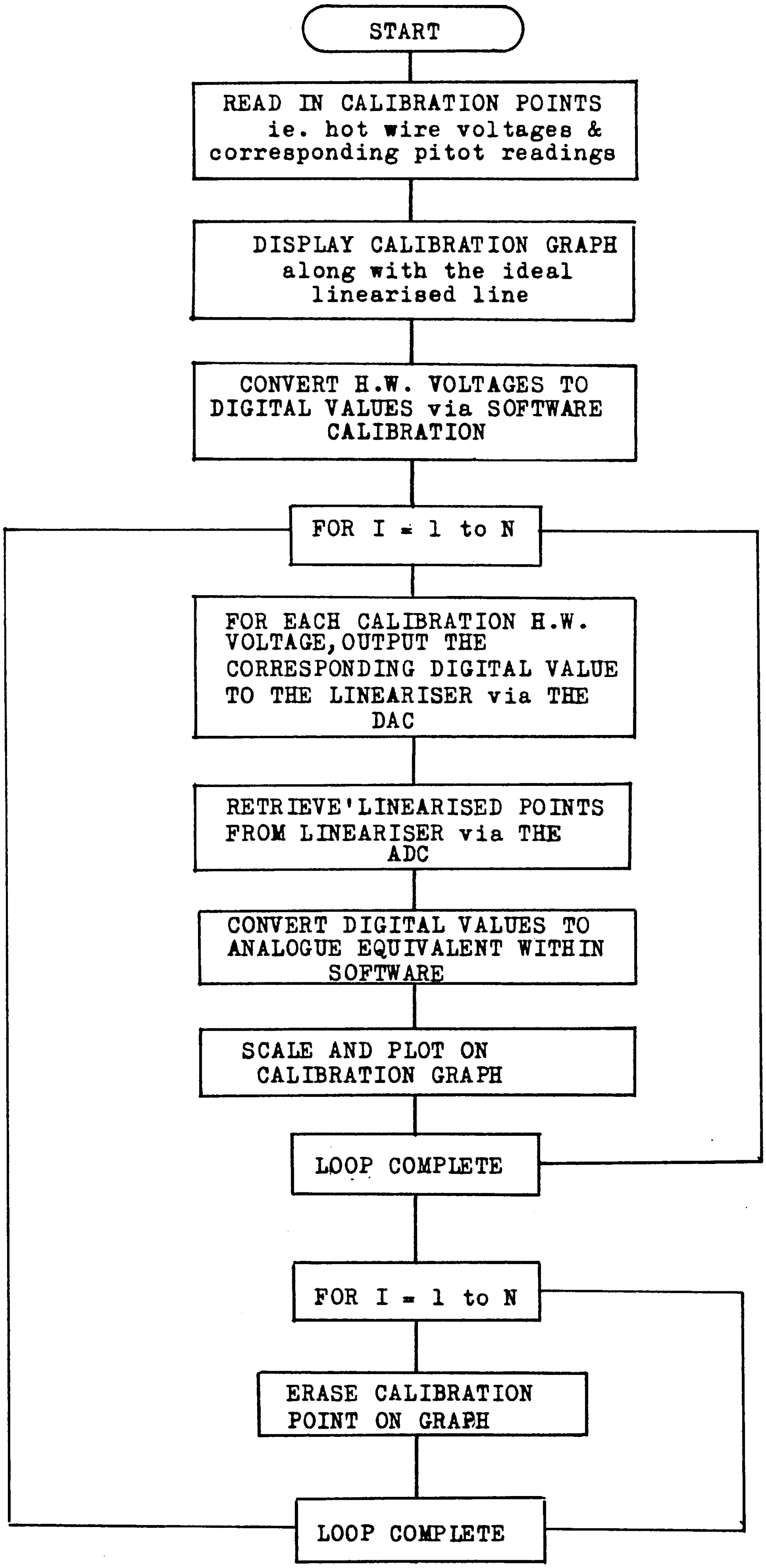

Figure A2.3 Software flow diagram

APPENDIX 3

Derivation of equation 7.9 for the energy thickness in a transitional boundary layer

APPENDIX 3 Derivation of δ_t^{**}

As described by Dhawan & Narasimha(1958) the transitional boundary layer mean velocity profile can be defined as :-

$$\left(\bar{u}/U_\infty\right)_t = (1-\bar{\gamma})\left(\bar{u}/U_\infty\right)_L + \bar{\gamma}\left(u/U_\infty\right)_T$$

Writing ;

$$U = \left(\bar{u}/U_\infty\right)$$

and defining ;

$$\delta^{**} = \int_0^{\delta} U\left[1-(U)^2\right] dy$$

then ;

$$\delta_t^{**} = \int_0^{\delta_t} \left[(1-\bar{\gamma})U_L + \bar{\gamma}U_T\right]\left[1-\{(1-\bar{\gamma})U_L + \bar{\gamma}U_T\}^2\right] dy \qquad \text{—— A3.1}$$

Considering terms in U_L only

$$\int_0^{\delta t} \left(U_L - U_L^3 + 3\bar{\gamma}U_L^3 - 3\bar{\gamma}^2U_L^3 - \bar{\gamma}U_L + \bar{\gamma}^3U_L^3\right) dy$$

$$= \int_0^{\delta t} \left[(1-\bar{\gamma})U_L - (1-\bar{\gamma})^3U_L^3\right] dy$$

adding and subtracting $(1-\bar{\gamma})^2 U_L$ gives:-

$$(1-\bar{\gamma})\int_0^{\delta t} \left[(1-\bar{\gamma})^2U_L - (1-\bar{\gamma})^2U_L^3 + U_L - (1-\bar{\gamma})^2U_L\right] dy$$

$$= (1-\bar{\gamma})\left\{(1-\bar{\gamma})^2\,\delta_L^{**} + \int_0^{\delta t}\left[U_L - (1-\bar{\gamma})^2U_L\right] dy\right\}$$

after some algebra ;

$$= (1-\bar{\gamma})\left\{(1-\bar{\gamma})^2\delta_L^{**} + (1-\bar{\gamma})^2\delta_L^{*} - \delta_L^{*} + \int_0^{\delta t}\left[2\bar{\gamma} - \bar{\gamma}^2\right] dy\right\}$$

$$= (1-\bar{\gamma})\left\{(1-\bar{\gamma})^2\delta_L^{**} + (1-\bar{\gamma})^2\delta_L^{*} - \delta_L^{*} + \bar{\gamma}(2-\bar{\gamma})\,\delta_t\right\} \qquad \text{—— A3.2}$$

From A3.1 considering terms in U_T only, ie.

$$\int_0^{\delta_t} (\gamma U_T - \gamma^3 U_T)\, dy$$

$$= \bar{\gamma} \int_0^{\delta_t} \left[\bar{\gamma}^2 (U_T - U_T^3) + U_T - \bar{\gamma}^2 U_T\right] dy$$

$$= \bar{\gamma} \left\{ \bar{\gamma}^2 \delta_T^{**} + \int_0^{\delta_t} (U_T - \bar{\gamma}^2 U_T)\, dy \right\}$$

$$= \bar{\gamma} \left\{ \bar{\gamma}^2 \delta_T^{**} + \int_0^{\delta_t} \left[\bar{\gamma}^2 (1 - U_T) + U_T - \bar{\gamma}\right] dy \right\}$$

$$= \bar{\gamma} \left\{ \bar{\gamma}^2 \delta_T^{**} + \bar{\gamma}^2 \delta_T^{*} + \int_0^{\delta_t} \left[U_T - \bar{\gamma}^2\right] dy \right\}$$

$$= \bar{\gamma} \left\{ \bar{\gamma}^2 \delta_T^{**} + \bar{\gamma}^2 \delta_T^{*} + \int_0^{\delta_t} \left[-(1 - U_T) + 1 - \bar{\gamma}^2\right] dy \right\}$$

$$= \bar{\gamma} \left\{ \bar{\gamma}^2 \delta_T^{**} + \bar{\gamma}^2 \delta_T^{*} - \delta_T^{*} + (1 - \bar{\gamma}^2)\, \delta_t \right\} \qquad \text{A3.3}$$

From A3.1 considering terms in $U_L U_T$ only, ie.

$$\int_0^{\delta_t} \left[-3\bar{\gamma} U_L^2 U_T + 6\bar{\gamma}^2 U_L^2 U_T - 3\bar{\gamma}^2 U_L U_T^2 - 3\bar{\gamma}^3 U_L^2 U_T + 3\bar{\gamma}^3 U_L U_T^2\right] dy$$

$$= -3\bar{\gamma}(1-\gamma) \int_0^{\delta_t} \left[(1-\bar{\gamma}) U_L^2 U_T + \gamma\, U_L U_T^2\right] dy$$

$$= -3\bar{\gamma}(1-\bar{\gamma}) \int_0^{\delta_t} \left[\left((1-\bar{\gamma}) U_L + \bar{\gamma} U_T\right) U_L U_T\right] dy$$

$$= -3\bar{\gamma}(1-\bar{\gamma}) \int_0^{\delta_t} \left[U_t U_L U_T\right] dy \qquad \text{Where } U_t = (1-\bar{\gamma}) U_L + \gamma U_T$$

$$= -3\bar{\gamma}(1-\gamma) \int_0^{\delta_t} \left[1 - 1 + U_t U_L U_T\right] dy$$

$$= -3\bar{\gamma}(1-\bar{\gamma})\delta_t + 3\gamma(1-\gamma) \int_0^{\delta_t} \left[1 - U_t U_L U_T\right] dy \qquad \text{A3.4}$$

Grouping A3.2,A3.3,A3.4 gives :-

$$\delta_t^{**} = (1-\bar{\gamma})\left[(1-\bar{\gamma})^2 \delta_L^{**} + (1-\bar{\gamma})^2 \delta^{*} - \delta^{*} + \bar{\gamma}(2-\bar{\gamma})\delta_t\right] +$$

$$\bar{\gamma}\left[\bar{\gamma}^2 \delta_T^{**} + \bar{\gamma}^2 \delta_T^{*} - \delta_T^{*} + (1-\bar{\gamma}^2)\delta_t\right] -$$

$$3\bar{\gamma}(1-\bar{\gamma})\delta_t + 3\bar{\gamma}(1-\bar{\gamma})\int_0^{\delta_t}\left[1 - U_t U_L U_T\right] dy$$

Considering all terms in δ_t ie.

$$(1-\bar{\gamma})\bar{\gamma}(2-\bar{\gamma})\delta_t + \bar{\gamma}(1-\bar{\gamma}^2)\delta_t - 3\bar{\gamma}(1-\bar{\gamma})\delta_t$$

$$= \left(3\bar{\gamma} - 3\bar{\gamma}^2 - \bar{\gamma}^3 + \bar{\gamma}^3 - 3\bar{\gamma} + 3\bar{\gamma}^2\right)\delta_t$$

$$= 0$$

Giving finally :-

$$\delta_t^{**} = (1-\bar{\gamma})\left[(1-\bar{\gamma})^2 \delta_L^{**} + \bar{\gamma}(\bar{\gamma}-2)\delta_L^{*}\right] +$$

$$\bar{\gamma}\left[\bar{\gamma}^2 \delta_T^{**} + (\bar{\gamma}^2-1)\delta_T^{*}\right] + 3\bar{\gamma}(1-\bar{\gamma})\int_0^{\delta_t}(1 - U_t U_L U_T)\, dy$$

APPENDIX 4

Integral prediction methods for laminar and turbulent boundary layers.

APPENDIX 4 Integral prediction methods for laminar and turbulent boundary layers

A4.1 Tani's(1954) method for laminar boundary layers

Tani's method makes use of both the momentum integral and energy integral equations in an approximate solution for the laminar boundary layer. Tani assumes that the velocity profiles belong to a one parameter family of curves but adopts a new profile parameter in favour of the usual Pohlhausen/Thwaites parameter, λ_θ . The relationship between the new profile parameter and λ_θ is derived from the momentum integral and energy integral equations and used in the solution.

The basic equations :-

The basic equations for a steady two dimensional, incompressible laminar boundary layer are :-

$$\partial u/\partial x + \partial v/\partial y = 0 \qquad \text{A4.1}$$

$$u\,\partial u/\partial x + v\,\partial u/\partial y = U_\infty\, dU_\infty/dx + \nu\, \partial^2 u/\partial y^2 \qquad \text{A4.2}$$

A4.1 and A4.2 are the continuity and momentum equations respectively

The momentum integral equation is obtained by integrating A4.2 from y = 0 to y = δ and results in :-

$$\frac{U_\infty}{\nu}\frac{d\theta^2}{dx} + 2\frac{\theta^2}{\nu}\frac{dU_\infty}{dx}\left(2 + \delta^*/\theta\right) = \frac{2\theta}{U_\infty}\left(\partial u/\partial y\right)_{y=0} \qquad \text{A4.3}$$

and the energy integral equation is obtained by multiplying A4.2 through by U_∞ and integrating w.r.t.y from y = 0 to y = δ resulting in :-

$$\frac{U_\infty}{\nu}\frac{d\delta^{**2}}{dx} + 6\frac{\delta^{**2}}{\nu}\frac{dU_\infty}{dx} = \frac{4\delta^{**}}{U_\infty^2}\int_0^\delta\left(\frac{\partial u}{\partial y}\right)^2 dy \qquad \text{A4.4}$$

Following Pohlhausen, Tani assumed a laminar velocity profile in the form :-

$$\frac{u}{U_\infty} = a_0 + a\, y/\delta + b\,(y/\delta)^2 + c\,(y/\delta)^3 + d\,(y/\delta)^4 \quad \text{— A4.5}$$

However in contrast to Pohlhausen the usual condition ;

$$y = 0 \; : \quad \frac{\partial^2 u}{\partial y^2} = -\frac{U_\infty}{\nu}\frac{dU_\infty}{dx}$$

which states that equation A4.2 is satisfied at the wall, is dropped so that the coefficient, a, remains undetermined. This coefficient is now adopted as the profile parameter and the velocity profiles are then represented by :-

$$\left(\frac{u}{U_\infty}\right) = (y/\delta)^2\left(6 - 8(y/\delta) + 3(y/\delta)^2\right) + a(y/\delta)(1 - y/\delta)^3 \quad \text{—— A4.6}$$

Tani then introduced the non dimensional quantities

$$\delta^*/\delta = D \;;\quad \theta/\delta = E \;;\quad \delta^{**}/\delta = F \quad \text{——— A4.7}$$

$$H_{12} = \delta^*/\theta \;;\quad H_{32} = \delta^{**}/\theta \quad \text{——— A4.8}$$

$$\frac{2\theta}{U_\infty}\left(\frac{\partial u}{\partial y}\right)_{y=0} = P \;;\quad \frac{4\delta^{**}}{U_\infty^2}\int_0^1 \left(\frac{\partial u}{\partial y}\right) dy = Q \quad \text{——— A4.9}$$

Using A4.7, A4.8 and A4.9, equations A4.3 and A4.4 can be rewritten in the form :-

$$\frac{U_\infty}{\nu}\frac{d\theta^2}{dx} + 2(2 + H_{12})\frac{\theta^2}{\nu}\frac{dU_\infty}{dx} = P \quad \text{——— A4.10}$$

$$\frac{U_\infty}{\nu}\frac{dH_{32}^2\theta^2}{dx} + 6\,\frac{H_{32}^2\theta^2}{\nu}\frac{dU_\infty}{dx} = Q \quad \text{——— A4.11}$$

where

$$D = \frac{2}{5} - \frac{a}{20} \quad \text{——— A4.12}$$

$$E = \frac{4}{35} + \frac{a}{105} - \frac{a^2}{252} \quad \text{——— A4.13}$$

$$F = \frac{876}{5005} + \frac{73}{5005}a - \frac{23}{5460}a^2 - \frac{a^3}{2860} \quad \text{——— A4.14}$$

$$P = 2aE \qquad \text{A4.15}$$

$$Q = \left\{\left(\frac{4}{35}\right)F\right\}\left(48 - 4a + 3a^2\right) \qquad \text{A4.16}$$

Tani also makes use of the approximation

$$\frac{\theta^2}{\nu} = \frac{0.44}{U_\infty^6}\int_0^x U_\infty^5\, dx \qquad \text{A4.17}$$

which is almost identical to Thwaites(1949) quadrature. However, Tani derived this form directly from the energy integral equation on the assumption that the variations in H_{32} and Q are sufficiently small for these parameters to be treated as constant.

θ^2/ν is determined explicitly from equation A4.17 hence λ_θ can then be obtained. But, since it is a and not λ_θ that is used as the parameter for the velocity profile, it is necessary to relate a to λ_θ

This is done by eliminating, $\frac{d\theta^2}{dx}$ from equations A4.10 and A4.11 and results in

$$\lambda_\theta\left(H_{12} - 1\right) = \frac{1}{2}\left(P - \frac{Q}{H_{32}^2}\right) + \lambda_\theta \frac{U}{H_{32}}\frac{dH_{32}}{dU_\infty} \qquad \text{A4.18}$$

<u>Method of solution :-</u>

As it stands equation A4.18 is not in a form suitable for solution. Therefore, using equations A4.13 and A4.14, equation A4.18 is rearranged to :-

$$a = \left\{\lambda_\theta\left(H_{12} - 1\right) + \frac{Q}{2H_{32}^2} - \frac{a^2}{105} + \frac{a^3}{252} - \lambda_\theta \frac{U}{H_{32}}\frac{dH_{32}}{dU}\right\}\left[\frac{35}{4}\right] \qquad \text{A4.19}$$

Also $H_{12} = D/E$; $H_{32} = F/E$ and Q are functions of the profile parameter, a ,and substitution of these functions, given by equations A4.12,A4.13,A4.14 and A4.16, into eguation A4.19 establishes the relationship between a and λ_θ

The value of θ^2/ν and hence $\lambda_\theta = \frac{\theta^2}{\nu}\frac{dU_\infty}{dx}$ is evaluated from step-by-step integration of the quadrature given by equation A4.17. Then, for a first approximation to the solution of equation A4.19 the term $\lambda_\theta \frac{U_\infty}{H_{32}} \frac{dH_{32}}{dU}$ is neglected and, at each integration step, the value of the profile parameter, α , is determined by iteration of the resulting equation. Using the values of α determined from the first approximation to the solution of A4.19, a curve fitting routine is employed to estimate the neglected term. This term is then included in the second approximation to the solution of equation A4.19 and so on.

With the profile parameter, α , evaluated at each step, the profile shape factors, H_{12} & H_{32} are calculated from :-

$$H_{12} = D/E \quad ; \quad H_{32} = F/E$$

The values of D, E and F being obtained from equations A4.12, A4.13 and A4.14 respectively. The values of momentum thickness, θ , obtained from the numerical integration of equation A4.17 are used to calculate the remaining boundary layer integral thicknesses δ^* & δ^{**} from equations A4.8

The skin friction coefficient, Cf, is obtained from equation A4.9 knowing :-

$$\tau_0 = \mu \left(\frac{du}{dy}\right)_{y=0}$$

and

$$Cf = \frac{2\tau_0}{\rho U_\infty^2}$$

then

$$Cf = \frac{P\nu}{\theta U_\infty}$$

For a zero pressure gradient flow ie. $\lambda_\Theta = 0$ equation A4.18 reduces to :-

$$P = Q/H_{32}^2$$

the solution of which is trivial and results in :-

$$\underline{a = 1{\cdot}857}$$

Other specific values of a which correspond to definite conditions are :-

(i) at a separation point ; $a = 0$

(ii) at a stagnation point ; $a = 4{\cdot}00$

A4.2 Alber's(1968) method for turbulent boundary layers

In general the boundary layer velocity profile employed in a turbulent boundary layer integral method is represented by a two parameter family of the form :-

$$u/U_\infty = f(\Pi, C_f, y/\delta)$$

For the basic boundary layer problem there are then three unknowns δ, Π and Cf and therefore three equations are required to solve for these unknowns. The three equations usually employed are :-

1. The momentum integral equation A4.3
2. Some local friction law
3. An auxiliary equation

The method of Alber uses the two parameter formulation of Coles(1956) for the local skin friction law ie.

$$\frac{u}{u_\tau} = \frac{1}{k} \ln \frac{y u_\tau}{\nu} + C + \frac{\Pi}{k} \sin^2\left(\frac{\pi}{2} \cdot y/\delta\right) \quad \text{——— A4.20}$$

and the energy integral equation, A4.4 as the auxiliary equation. By setting $u = U_\infty$ at $y = \delta$ and using the wake integration result

$$\frac{\delta^*}{\delta} = \frac{1+\Pi}{\lambda k} = \frac{\mathcal{S}(1+\Pi)}{k} \qquad \text{where } \lambda = 1/\mathcal{S} = \sqrt{2/c_f}$$

in A4.20 the following expression which relates Cf to δ^* and Π is obtained :-

$$\frac{U_\infty}{u_\tau} = 1/\mathcal{S} = \frac{1}{k} \ln\left\{\frac{k R_{\delta^*}}{1+\Pi}\right\} + \frac{2\Pi}{k} \quad \text{——— A4.21}$$

Defining the shape factors :-

$$\mathcal{H} = \theta/\delta^* \quad \text{—— A4.22} \qquad J = \delta^{**}/\delta^* \quad \text{——— A4.23}$$

the momentum integral and energy integral equations are then written in the form :-

momentum

$$\frac{C_f}{2} = f^2 = \frac{d[\mathcal{H}\delta^*]}{dx} + \left(\frac{1}{\mathcal{H}} + 2\right)\frac{\mathcal{H}\delta^*}{U_\infty}\frac{dU_\infty}{dx} \qquad \text{——— A4.24}$$

energy

$$\frac{d}{dx}\left[U_\infty^3 J \delta^*\right] = 2D/\rho \qquad \text{——— A4.25}$$

where

$$D = \int_0^\infty \tau\left(\frac{\partial u}{\partial y}\right)dy$$

Equations A4.24 and A4.25 along with a differential form of the local friction law, A4.21, are then used to obtain the three differential equations needed to describe the development of δ^*, f and Π

Expanding and rearranging A4.24

$$\mathcal{H}\frac{d\delta^*}{dx} + \delta^*\left[\frac{d\mathcal{H}}{dx}\right] = f^2 - (2\mathcal{H}+1)\frac{\delta^*}{U_\infty}\frac{dU_\infty}{dx}$$

now $\mathcal{H} = g(\Pi, f) \quad \therefore \quad \dfrac{d\mathcal{H}}{dx} = \dfrac{\partial\mathcal{H}}{\partial\Pi}\dfrac{d\Pi}{dx} + \dfrac{\partial\mathcal{H}}{\partial f}\dfrac{df}{dx}$

The momentum equation can then be written in the form :-

$$\mathcal{H}\frac{d\delta^*}{dx} + \delta^*\left[\frac{\partial\mathcal{H}}{\partial\Pi}\right]\frac{d\Pi}{dx} + \delta^*\left[\frac{\partial\mathcal{H}}{\partial f}\right]\frac{df}{dx} = f^2 - (2\mathcal{H}+1)\frac{\delta^*}{U_\infty}\frac{dU_\infty}{dx} \qquad \text{——— A4.26}$$

Expanding and rearranging A4.25

$$J\frac{d\delta^*}{dx} + \delta^*\left[\frac{dJ}{dx}\right] = C_D - 3J\frac{\delta^*}{U_\infty}\frac{dU_\infty}{dx}$$

where $C_D = 2D/\rho U_\infty^3$ and is called the"Dissipation integral"

again $J = h(\Pi, f) \quad \therefore \quad \dfrac{dJ}{dx} = \dfrac{\partial J}{\partial\Pi}\dfrac{d\Pi}{dx} + \dfrac{\partial J}{\partial f}\dfrac{d\Pi}{dx}$

and therefore the energy equation can be written in the form :-

$$J\frac{d\delta^*}{dx} + \delta^*\left[\frac{\partial J}{\partial\Pi}\right]\frac{d\Pi}{dx} + \delta^*\left[\frac{\partial J}{\partial f}\right]\frac{df}{dx} = C_D - 3J\frac{\delta^*}{U_\infty}\frac{dU_\infty}{dx} \qquad \text{——— A4.27}$$

The final differential equation is obtained by differentiating the local friction law ie. equation A4.21, and results in :-

$$\frac{d\delta^*}{dx} + \delta^* \frac{(1+2\Pi)}{1+\Pi} \frac{d\Pi}{dx} + \frac{k\delta^*}{\xi^2} \frac{d\xi}{dx} = -\frac{\delta^*}{U_\infty} \frac{dU_\infty}{dx} \qquad \text{——— A4.28}$$

The only unknown in equations A4.26,A4.27 and A4.28 is now the dissipation integral, C_D.

For the case of turbulent equilibrium flows, ie. for the condition Π = constant and β_T = constant ,Alber derives an exact expression for C_D from equations A4.26— A4.28 resulting in:-

$$C_{D_{Equ.}} = \frac{\left[1+\beta_T(\mathcal{H}+1)\right]\left[\frac{kJ}{\xi^2} - \frac{\partial J}{\partial \xi}\right]\xi^2}{\left[\frac{k\mathcal{H}}{\xi^2} - \frac{\partial \mathcal{H}}{\partial \xi}\right]} - 2J\beta_T\xi^2 \qquad \text{——— A4.29}$$

where $\beta_T = \dfrac{\delta^* \frac{dp}{dx}}{\tau_0}$ or $\beta_T = \dfrac{-\delta^*}{\xi^2 U_\infty} \dfrac{dU_\infty}{dx}$

The dissipation integral is then'unhooked' from the pressure gradient parameter β_T by assuming that Π is uniquely related to β_T for nonequilibrium flows. A convenient curve fit given by White(1974) ie:-

$$\beta_T = (1.25\Pi)^{4/3} - 0.5 \qquad \text{——— A4.30}$$

is used in this case.

Using equation A4.30 in A4.29 allows equations A4.26 - A4.28 to be solved for the development of a general non-equilibrium turbulent boundary layer for a given set of initial conditions :-

C_{f_0}, δ^*_0, Π_0

Solution procedure :-

To recap,the equations to be solved are :-

momentum

$$\mathcal{H}\frac{d\delta^*}{dx} + \delta^* P\frac{d\Pi}{dx} + \delta^* Q\frac{df}{dx} = f^2 - (2\mathcal{H}+1)\frac{\delta^*}{U_\infty}\frac{dU_\infty}{dx} \qquad \text{— A4.31}$$

energy

$$J\frac{d\delta^*}{dx} + \delta^* R\frac{d\Pi}{dx} + \delta^* S\frac{df}{dx} = C_D - 3J\frac{\delta^*}{U_\infty}\frac{dU_\infty}{dx} \qquad \text{— A4.32}$$

friction law

$$\frac{d\delta^*}{dx} + \delta^* T\frac{d\Pi}{dx} + \frac{K\delta^*}{f^2}\frac{df}{dx} = -\frac{\delta^*}{U_\infty}\frac{dU_\infty}{dx} \qquad \text{— A4.33}$$

dissipation integral

$$C_D = \frac{\left[1+\beta(\mathcal{H}+1)\right]\left[\frac{kJ}{f^2} - S\right]f^2}{\left[\frac{k\mathcal{H}}{f^2} - Q\right]} - 2J\beta f^2 \qquad \text{— A4.34}$$

with $\beta = (1{\cdot}25\Pi)^{4/3} - 0{\cdot}5$

and $P = \frac{\partial\mathcal{H}}{\partial\Pi}$; $Q = \frac{\partial\mathcal{H}}{\partial f}$; $R = \frac{\partial J}{\partial\Pi}$; $S = \frac{\partial J}{\partial f}$

$$T = \frac{(1+2\Pi)}{(1+\Pi)}$$

The partial derivatives P, Q, R. and S which appear in the above equations are replaced by algebraic functions of Π and f derived from the wake integrations of A4.20 ie.

$$\frac{\delta^*}{\delta} = \frac{1+\Pi}{k\lambda} \qquad \text{— A4.35}$$

$$\frac{\theta}{\delta} = \frac{1+\Pi}{k\lambda} - \frac{(2+3{\cdot}18\Pi+1{\cdot}5\Pi^2)}{k^2\lambda^2} \qquad \text{— A4.36}$$

$$\frac{\delta^3}{\delta} = \frac{3\theta}{\delta} - \frac{\delta^*}{\delta} + \frac{(6+11{\cdot}14\Pi+8{\cdot}5\Pi^2+2{\cdot}56\Pi^3)}{k^3\lambda^3} \qquad \text{— A4.37}$$

and result in :-

$$\frac{\partial \mathcal{H}}{\partial \Pi} = P = \frac{1}{(1+\Pi)}\left[f\,\frac{3.18 + 3\Pi}{k} + (\mathcal{H} - 1)\right] \qquad \text{———— A4.38}$$

$$\frac{\partial \mathcal{H}}{\partial f} = Q = -\,\frac{2 + 3.18\Pi + 1.5\Pi^2}{k\,(1+\Pi)} = \frac{(\mathcal{H}-1)}{f} \qquad \text{———— A4.39}$$

$$\frac{\partial J}{\partial \Pi} = R = \frac{2-J}{(1+\Pi)} - \frac{f}{(1+\Pi)k}\left[3(3.18+3\Pi) + \frac{f}{k}\,(11.14 + 17\Pi + 7.68\Pi^2)\right]$$

$$\text{———— A4.40}$$

$$\frac{\partial J}{\partial f} = S = \left[\frac{J-2}{f}\right] + \frac{f}{k^2}\,\frac{(6 + 11.14\Pi + 8.5\Pi^2 + 2.56\Pi^3)}{(1+\Pi)} \qquad \text{— A4.41}$$

where

$$\mathcal{H} = \frac{\theta}{\delta^*} = 1 - \frac{f(2 + 3.18\Pi + 1.5\Pi^2)}{k\,(1+\Pi)}$$

and

$$J = \frac{\delta^{**}}{\delta} = 2 - \frac{3f(2 + 3.18\Pi + 1.5\Pi^2)}{k\,(1+\Pi)} + \frac{f^2}{k^2}\,\frac{(6 + 11.14\Pi + 8.5\Pi^2 + 2.56\Pi^3)}{(1+\Pi)}$$

Solving equations A4.31 - A4.33 for $\frac{d\Pi}{dx}$, $\frac{df}{dx}$ and $\frac{d\delta^*}{dx}$ results in, after some manipulation :-

$$\frac{d\Pi}{dx} = \frac{\left\{ f^2 - \dfrac{C_D\left(Q - \frac{k\mathcal{H}}{f^2}\right)}{\left(S - \frac{kJ}{f^2}\right)} - \left[(1+\mathcal{H}) - \dfrac{2J\left(Q\,\frac{k\mathcal{H}}{f^2}\right)}{\left(S - \frac{kJ}{f^2}\right)}\right]\dfrac{\delta^*}{U_\infty}\dfrac{dU_\infty}{dx}\right\}}{\delta^*\left[(P - \mathcal{H}T) - \dfrac{(R - JT)\left(Q - \frac{k\mathcal{H}}{f^2}\right)}{\left(S - kJ/f^2\right)}\right]} \qquad \text{——A4.42}$$

$$\frac{df}{dx} = \frac{\left\{ f^2 - \dfrac{C_D\,(P - \mathcal{H}T)}{(R - JT)} - \left[(1+\mathcal{H}) - \dfrac{2J(P - \mathcal{H}T)}{(R - JT)}\right]\dfrac{\delta^*}{U_\infty}\dfrac{dU_\infty}{dx}\right\}}{\delta^*\left[\left(Q - \frac{k\mathcal{H}}{f^2}\right) - \dfrac{\left(S - kJ/f^2\right)(P - \mathcal{H}T)}{(R - JT)}\right]} \qquad \text{—— A4.43}$$

$$\frac{d\delta^*}{dx} = -\left\{ \frac{\delta^*}{U_\infty}\frac{dU_\infty}{dx} + \frac{k\delta^*}{f^2}\frac{df}{dx} + \delta^* T\,\frac{d\Pi}{dx} \right\} \qquad \text{—— A4.44}$$

Using the wake integration results for P, Q, R and S ie. equations A4.38 - A4.41 and equations A4.30 and A4.34 then equations A4.42 - A4.44 can be solved for Π, C_f and δ^* using a Runge - Kutta technique.

APPENDIX 5

Software Listings

APPENDIX 5 Software Listings

Appendix 5 contains programme listings for both the Data Acquisition, Control and Data Reduction Package and the computational Boundary Layer Prediction Package. It also contains listings of the following programmes :-

1) TURBLEV -Page 250 - Described in section 3.9

2) IMPROF2 -Page 252 - Described in section 3.9

3) SIGCALC -Page 254 - Used for the calculation of σ from an experimental data file containing $\bar{\gamma}$, x data

On the following page a copy of the flow chart for the Data Acquisition, Control and Data Reduction Package, described in Chapter 5, is included. Next to the points where each new programme is 'called' or 'CHAINed' is the relevant page number on which the programme listing can be found within this Appendix.

The programme listings for the computational model (Tani/Alber), described in chapter 7, along with the listings for the graphics package start at page 258 and include

1) IGBLPR1 -Page 258 - Introductory programme to computational package

2) IGBLPR5 -Page 263 - Main programme

3) GRAFPC3 -Page 269 - Graphics programme used to display predictions

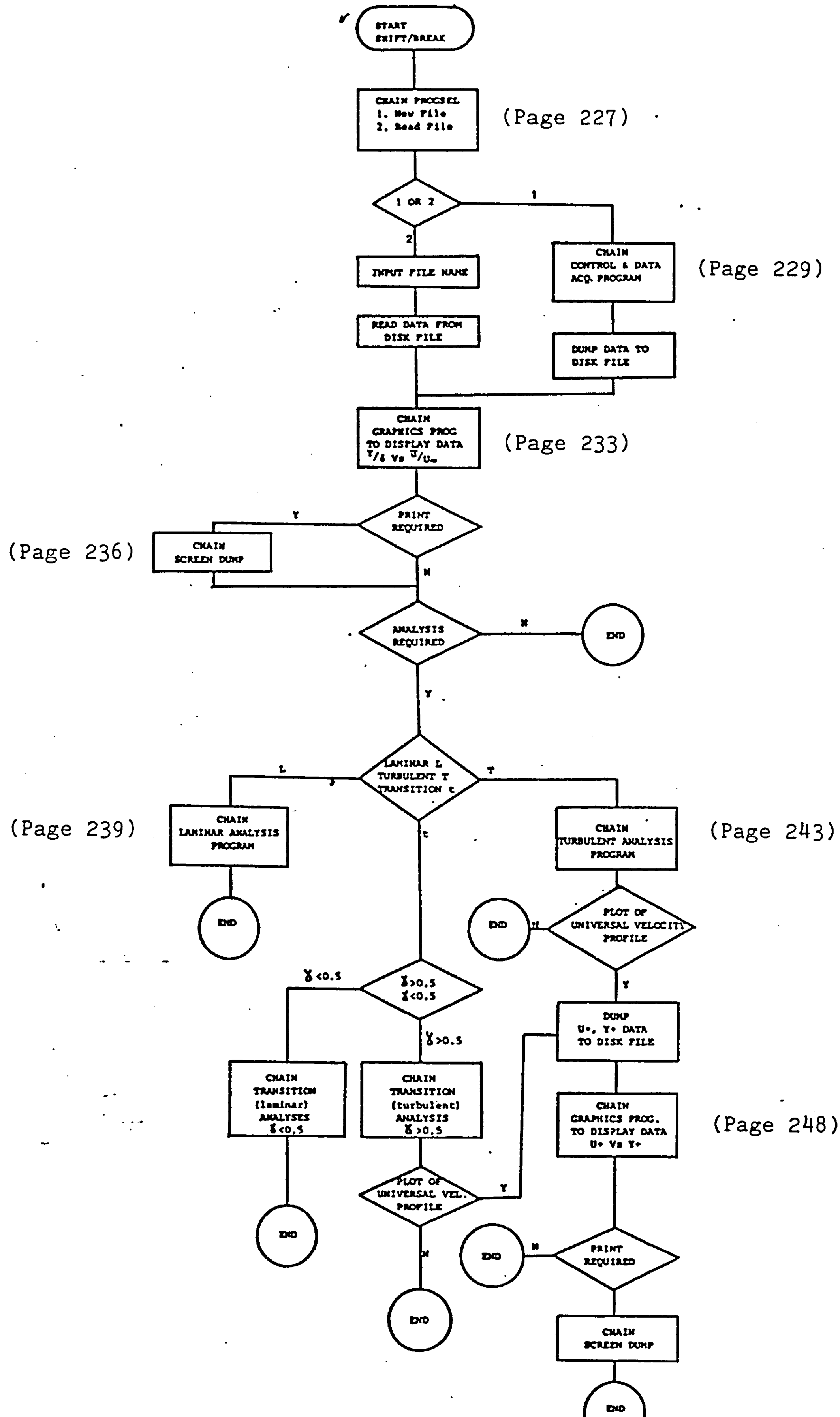
START SHIFT/BREAK
CHAIN PROGSEL 1. New File 2. Read File
(Page 227)
1 OR 2
1
2
INPUT FILE NAME
READ DATA FROM DISK FILE
CHAIN CONTROL & DATA ACQ. PROGRAM
(Page 229)
DUMP DATA TO DISK FILE
CHAIN GRAPHICS PROG TO DISPLAY DATA Y/δ Vs U/U∞
(Page 233)
PRINT REQUIRED
Y
N
CHAIN SCREEN DUMP
(Page 236)
ANALYSIS REQUIRED
END
LAMINAR L TURBULENT T TRANSITION t
L
T
t
CHAIN LAMINAR ANALYSIS PROGRAM
(Page 239)
CHAIN TURBULENT ANALYSIS PROGRAM
(Page 243)
PLOT OF UNIVERSAL VELOCITY PROFILE
γ>0.5 γ<0.5
γ<0.5
γ>0.5
DUMP U+, Y+ DATA TO DISK FILE
CHAIN TRANSITION (laminar) ANALYSES γ<0.5
CHAIN TRANSITION (turbulent) ANALYSIS γ>0.5
CHAIN GRAPHICS PROG. TO DISPLAY DATA U+ Vs Y+
(Page 248)
PLOT OF UNIVERSAL VEL. PROFILE
CHAIN SCREEN DUMP

Programme

<u>PROGSEL</u>

This programme is the introductory programme to the Data Acquisition, Control and Data Reduction Package

```
 10 CLOSE#0
 20 REM PROGSEL
 30 MODE7
 40 PRINTTAB(0,5);CHR$132"DO YOU WANT TO :"
 50 PRINTTAB(5,10);CHR$133"1.    READ AN EXISTING FILE"
 60 PRINTTAB(5,15);CHR$130"2.    CREATE A NEW FILE"
 70 VDU 31 0,24
 80 sel%=GET
 90 IF sel% = 49 GOTO 120
100 IF sel% = 50 CHAIN"5.4"
110 IF sel%<>49 OR sel%<>50 GOTO 40
120 CLS
130 PRINTTAB(0,10);CHR$132"DO YOU WANT TO SEE DISK CATALOG"
140 GOTO 160
150 PRINTTAB(0,10);CHR$132"DO YOU WANT TO SEE ANOTHER CATALOG"
160 IF GET$="N" GOTO 250
170 PRINTTAB(0,15);CHR$131;"WHICH DRIVE"
180 D%=GET
190 PROCdriverd(D%)
200 PRINTCHR$133;"PRESS SPACE TO CONTINUE"
210 space%=GET
220 IFspace%<>32GOTO200
230 CLS
240 GOTO150
250 CLS
260 PRINTTAB(5,12);CHR$134;"WHICH DRIVE IS FILE ON"
270 D% = GET
280 PROCdrive(D%)
290 CLS
300 PRINTTAB(5,12);CHR$134"INPUT NAME OF FILE TO BE READ"
310 INPUT TAB(16,14);E$
320 file%=OPENOUT("DATA")
330 PRINT#file%,E$
340 CLOSE# file%
350 *DR.0
360 CHAIN"6.3"
370 END
380 DEFPROCdriverd(D%)
390 IF D%=48THEN*.0
400 IF D%=49THEN*.1
410 IF D%=50THEN*.2
420 IF D%=51THEN*.3
430 ENDPROC
435 DEFPROCdrive(D%)
440 IF D%=48THEN*DR.0
450 IF D%=49THEN*DR.1
460 IF D%=50THEN*DR.2
470 IF D%=51THEN*DR.3
480 ENDPROC
```

Programme

5.4

Programme 5.4 is the main Data Acquisition and Control programme described in some detail in section 3.9

```
10  REM PROG 5.4 DATA ACQUSITION & CONTROL PROG
20  MODE3
30  VDU23,240,195,36,24,24,36,36,36,24
40  *IO
50  CLOSE# 0
60  ddr%=OPENUP"BUS &C002"
70  BPUT#ddr%,&FF
80  CLOSE# ddr%
90  pb%=OPENUP"BUS &C000"
100 BPUT#pb%,1
110 A%=OPENUP"CU-DAC8 &C000"
120 PRINTTAB(20,12) "SWITCH ON STEPPER MOTOR & H.W ANEMOMETER"
130 H=INKEY(400)
140 CLS
150 PRINT
160 PRINT
170 DIM Y3(40),B(40),u1(40),y1(40),u(40),y(40),RM3(40),IM3(40)
180 PROCcalcon
190 CLS
200 PRINTTAB(15,12)"INPUT TEMPERATURE IN Deg C"
210 INPUTTAB(40,14) t
220 PRINTTAB(15)"INPUT PRESSURE IN mm Hg"
230 INPUTTAB(40) z
240 CLS
250 PRINT
260 PRINT
270 PRINTTAB(15,6)"INPUT UPPER STEP INCREMENT"
280 INPUTTAB(40,8) STI1
290 PRINT
300 PRINTTAB(15)"INPUT LOWER STEP INCREMENT"
310 INPUTTAB(40) STI2
320 PRINT
330 PRINTTAB(15)"INPUT No OF Pts AT LOWER STEP INCREMENT"
340 INPUTTAB(40) P1%
350 PRINT
360 PRINTTAB(15)"INPUT Y DATUM IN mm"
370 INPUTTAB(40) Ydat
380 CLS
390 PRINT
400 PRINTTAB(15,12)"INPUT DIST. FROM L.E. IN mm"
410 INPUTTAB(40) X1
420 PRINT
430 PRINTTAB(15)"INPUT SPANWISE LOCATION IN mm"
440 INPUTTAB(40) Z
450 CLS
460 PRINTTAB(15,12)"NAME OF DATA FILE"
470 INPUTTAB(40) E$
480 CLS
490 K1 = STI1/YC2
500 K2 = STI2/YC2
510 PTR#A%=0
520 FOR I%=1TO100
530 YD%=BGET# A%
540 YD1%=YD1%+YD%
550 NEXT
560 YD2%=YD1%/100
570 VDU2
580 VDU 1,27,1,69
590 PRINT"                  Velocity       Y-Pos.       Intermittency     RMS-Vel."
600 PRINT"                    m/s           mm                "CHR$(240)"              m/s"
610 VDU 1,27,1,70
620 PRINT
630 FOR Q=1TO40
640 Y2%=0
650 FOR I%=1TO100
660 Y1%=BGET#A%
670 Y2%=Y2%+Y1%
680 NEXT
690 C2%=0
700 PTR#A%=2
710 FOR I%=1TO5000
720 C1%=BGET#A%
730 C2%=C2%+C1%
740 NEXT
750 C3%=C2%/5000
760 IM1%=0
770 PTR#A%=4
780 FOR I%=1TO1000
790 IM%=BGET#A%
800 IM1%=IM1%+IM%
810 NEXT
820 RM1%=0
```

```
830  PTR#A%=6
840  FOR I%=1TO1000
850  RM%=BGET#A%
860  RM1%=RM1%+RM%
870  NEXT
880  RM2%=RM1%/1000
890  IM2%=IM1%/1000
900  RM3(Q)=RM2%*RMC
910  IM3(Q)=(IM2%-1)*IMC
920  u1(Q) = (C2%/5000)*CC
930  Y3(Q)=Y2%/100
940  y1(Q)=Ydat+(Y3(1)-Y3(Q))*10.52*YC
950  n%=n%+1
960  o%=n%-P1%
970  u1(Q)=INT(u1(Q)*1000+0.5)/1000
980  y1(Q)=INT(y1(Q)*100+0.5)/100
990  IM3(Q)=INT(IM3(Q)*100+0.5)/100
1000 RM3(Q)=INT(RM3(Q)*100+0.5)/100
1010 SOUND 1,-15,145,3
1020 PRINT TAB(15);u1(Q);TAB(29);y1(Q);TAB(45);IM3(Q);TAB(59);RM3(Q)
1030 IFu1(Q)>=0.995*u1(Q-1) AND u1(Q)<=1.005*u1(Q-1) GOTO 1040 ELSE 1050
1040 IFu1(Q)>=0.995*u1(Q-2) AND u1(Q)<=1.005*u1(Q-2) GOTO 1180
1050 IFY3(Q)<10 GOTO1970
1060 PTR#A%=0
1070 IF n%>P1% GOTO 1130
1080 BPUT#pb%,0
1090 REPEAT UNTIL BGET#A%<(YD2%-n%*K2)
1100 BPUT#pb%,1
1110 X = n%*K2
1120 GOTO 1170
1130 BPUT#pb%,0
1140 REPEAT UNTIL BGET#A%<(YD2%-(X+o%*K1))
1150 BPUT#pb%,1
1160 BPUT#pb%,1
1170 NEXT Q
1180 uinf = (u1(Q)+u1(Q-1)+u1(Q-2))/3
1190 BPUT#pb%,1
1200 CLOSE#pb%:CLOSE#A%
1210 FOR i=1TOn%
1220 u(i)=u1(i)/uinf
1230 NEXT
1240 FOR i=1TOn%
1250 IF u(i) < 0.99 GOTO 1280
1260 d = y1(i)-((y1(i)-y1(i-1))*(u(i)-0.99)/(u(i)-u(i-1)))
1270 GOTO 1290
1280 NEXT
1290 PRINT
1300 PRINT
1310 PRINT
1320 PRINT
1330 PRINT
1340 PRINT"DIST.FROM L.E.=";X1;"mm","SPANWISE LOCATION =";Z;"mm"
1350 PRINT
1360 d = INT(d*100+0.5)/100
1370 PRINT"APPROX. EDGE OF BOUNDARY LAYER = ";d;"mm"
1380 PRINT
1390 uinf=INT(uinf*100+0.5)/100
1400 PRINT"FREE STREAM VELOCITY            = ";uinf"mm"
1410 PRINT
1420 PRINT
1430 PRINT
1440 VDU 1,27,1,69
1450 PRINT"      n      y (mm)   Vel. m/s    u/uinf     y/d       RMS       Gama"
1460 VDU 1,27,1,70
1470 PRINT
1480 FOR i=1TOn%
1490 y(i)=y1(i)/d
1500 u(i)=INT(u(i)*1000+0.5)/1000
1510 y(i)=INT(y(i)*1000+0.5)/1000
1520 IF y(i)>0.2 GOTO 1550
1530 AVIM2 = AVIM2+IM3(i)
1540 Ct%=Ct%+1
1550 PRINTTAB(6);i;TAB(13);y1(i);TAB(22);u1(i);TAB(34);u(i);TAB(43);y(i);TAB(51);RM3(i);TAB(60);IM3(i)
1560 NEXT
1570 VDU3 : CLS
1580 PRINTTAB(15,12)"DO YOU WANT TO INPUT EYEBALL VALUE OF"
1590 PRINTTAB(15)"INTERMITTENCY AT y/d=0.2 ?"
1600 IF GET$ = "N" THEN GOTO 1690
1610 ?&FE60=0
1620 PRINT
1630 PRINT
1640 PRINT
1650 PRINTTAB(15)"INPUT EYEBALL VOLTAGE FROM INTERM. VOLTMETER"
```

```
1660 INPUTTAB(40);EIM1
1670 EIM=EIM1/5
1680 GOTO1700
1690 EIM=0
1700 IFy(1)>0.2 GOTO1750
1710 AVIM3 = AVIM2/Ct%
1720 AVIM = INT(AVIM3*1000+0.5)/1000
1730 VDU 2
1740 GOTO1760
1750 AVIM=0
1760 PRINT
1770 PRINT
1780 PRINT
1790 PRINT"EYEBALL AVE OF INTERMITTENCY AT y/d=0.2  = ";EIM
1800 PRINT
1810 PRINT
1820 PRINT"AVE. OF INTERMITTENCY VALUES BELOW (y/d=0.2)= ";AVIM
1830 VDU 3
1840 *DISK
1850 PRINT
1860 PRINT"ON WHICH DRIVE IS DATA TO BE STORED"
1870 GOTO1910
1880 ON ERROR OFF
1890 CLOSE# 0
1900 PRINT"DISK FULL SELECT DRIVE OTHER THAN DRIVE ";D%-48
1910 D%=GET
1920 PROCdrive(D%)
1930 PROCfile(u,y,n%,uinf,X1,Z,d,E$,t,z,RM3,IM3,AVIM,EIM)
1940 CLS
1950 *DR.0
1960 CHAIN"6.3"
1970 PRINT"PROBE TRAVERSE OUT OF RANGE"
1980 END
1990 DEFPROCcalcon
2000 CC=7.920E-2
2010 YC=1.961E-2
2020 YC2=10.52*YC
2030 IMC=4.050E-3
2040 RMC=1.471E-2
2050 ENDPROC
2060 DEFPROCfile(u,y,n%,uinf,X1,Z,d,E$,t,z,RM3,IM3,AVIM,EIM)
2070 ON ERROR GOTO 1880
2080 X2%=OPENOUT("DATA")
2090 PRINT#X2%,E$
2100 CLOSE# X2%
2110 W%=OPENOUT (E$)
2120 PRINT#W%,n%,uinf,X1,Z,d,t,z,AVIM,EIM
2130 FOR I=1TOn%
2140 PRINT#W%,u(I),y(I)
2150 NEXT
2160 FOR I=1TOn%
2170 PRINT#W%,RM3(I),IM3(I)
2180 NEXT
2190 CLOSE# W%
2200 ENDPROC
2210 DEFPROCdrive(D%)
2220 IFD%=48THEN*DR.0
2230 IFD%=49THEN*DR.1
2240 IFD%=50THEN*DR.2
2250 IFD%=51THEN*DR.3
2260 ENDPROC
```

Programme

6.3

Programme 6.3 is a graphics programme used to display experimental data, from adata file, on axes of y/δ v's u/U_∞

```
10 CLOSE#0
20 REM PROG 6.3 LAMINAR/TURBULENT GRAPHICS PROGRAM
30 MODE 1
40 CLS
50 PROCdrive(D%)
60 DIM P1(102),Q1(102)
70 DIM u(40),y(40),RM3(40),IM3(40)
80 VDU 19,3,3,0,0,0
90 VDU 19,2,2,0,0,0
100 MOVE 125,825
110 DRAW 125,125
120 DRAW 1225,125
130 PRINTTAB(1,10);"Y"
140 PRINTTAB(1,11);"/"
150 PRINTTAB(1,12);"d"
160 PRINTTAB(25,30);"u/Uinf"
170 MOVE 1225,125
180 DRAW 1225,100
190 MOVE 675,125
200 DRAW 675,100
210 MOVE 125,825
220 DRAW 100,825
230 MOVE 125,475
240 DRAW 100,475
250 MOVE 125,125
260 PRINTTAB(0,6);"1.0"
270 PRINTTAB(0,17);"0.5"
280 PRINTTAB(19,29);"0.5"
290 PRINTTAB(37,29);"1.0"
300 PRINTTAB(4,4);"LAMINAR & TURBULENT B.L. PROFILES"
310 PROCRfile
320 *DR.0
330 VDU28,6,14,21,6,
340 COLOUR 130:COLOUR1
350 CLS
360 PRINT
370 PRINT" z = ";Z;" mm"
380 PRINT
390 PRINT" x = ";X1;" mm"
400 PRINT
410 PRINT" Uinf= ";uinf;" m/s"
420 PRINT
430 PRINT" d = ";d;" mm"
440 mu=(1.725+0.004375*t)/10^5
450 rho=(0.46535*z)/(t+273)
460 nu=mu/rho
470 dudx=-0.25
480 LAM=(d^2/(nu*1000000))*dudx
490 FOR Yphol=0 TO d STEP 0.05
500 Y=Yphol/d
510 X=(2*Y-2*Y^3+Y^4)+(LAM/6)*(Y-3*Y^2+3*Y^3-Y^4)
520 P=X*1100 +125
530 Q=Y*700 +125
540 DRAW P,Q
550 NEXT
560 DATA 0,0,.037,.066,.074,.133,.111,.199
570 DATA .185,.330,.259,.456,.333,.575
580 DATA .407,.681,.481,.772,.555,.846
590 DATA .630,.902,.703,.941,.740,.955
600 DATA .778,.967,.815,.976,.852,.983
610 DATA .889,.988,.926,.991,.963,.994
620 DATA 1.0,.997
630 MOVE 125,125
640 I = 0
650 FOR K = 1 TO 41
660 X1 = I
670 Y1 =X1^7
680 I=I+0.025
690 P1(K)=X1*1100+125
700 Q1(K)=Y1*700+125
710 DRAW P1(K),Q1(K)
720 NEXT K
730 GCOL 0,1
740 FOR I = 1 TO n
750 A =u(I)*1100+125
760 B =y(I)*700+125
770 MOVE A,B
780 PLOT 69,A,B
790 PLOT 69,A-8,B-8
800 PLOT 85,A+8,B-8
810 NEXT I
820 VDU26:VDU31 0,31
```

```
830 COLOUR 128
840PRINT"IS A PRINT OF GRAPH REQ'D"
850 IF GET$="N"GOTO 870
860 CHAIN"7.4"
870 PRINT"DO YOU WANT PROFILE ANALYSED"
880 IF GET$="N" GOTO 1020
890 PRINT "IS PROFILE LAMINAR(L),TURBULENT(T) OR TRANSITIONAL(t)"
900 A$ = GET$
910 IF A$ = "L"GOTO 950
920 IF A$ = "T"GOTO 960
930 IF A$ = "t"GOTO 970
940 GOTO890
950 CHAIN "8.3"
960 CHAIN "9.3"
970 PRINT" IS VALUE OF INTERMITTENCY @ y/d=0.2     GREATER THAN(G) OR LESS THAN(L) 0.5"
980 A$ = GET$
990 IF A$ = "L" THEN CHAIN"11.3L"
1000 IF A$ = "G" THEN CHAIN"11.3T"
1010 GOTO 970
1020 END
1030 DEFPROCRfile
1040 X2=OPENIN ("DATA")
1050 INPUT#X2,E$
1060 CLOSE# X2
1070 W=OPENIN (E$)
1080 INPUT#W,n,uinf,X1,Z,d,t,z,AVIM,EIM
1090 FOR I = 1 TO n
1100 INPUT#W,u(I),y(I)
1110 NEXT I
1120 FOR I = 1 TO n
1130 INPUT#W,RM3(I),IM3(I)
1140 NEXT I
1150 CLOSE# W
1160 ENDPROC
1170 DEFPROCdrive(D%)
1180 IFD%=48THEN*DR.0
1190 IFD%=49THEN*DR.1
1200 IFD%=50THEN*DR.2
1210 IFD%=51THEN*DR.3
1220 ENDPROC
```

Programme

10.3

Programme 10.3 is a screen dump programme which enables a hard copy of a graphics display, on the computer monitor, to be obtained from the Epson line printer

```
10 REM Hybrid program to dump all graphics MODEs
20 REM on the EPSON FT printer
30 DIM S% &FF
40 pass_number=S%
50 pattern0=S%+1
60 !pattern0=&0300
70 pattern4=S%+3
80 !pattern4=&3F00
90 pattern1=S%+5
100 !pattern1=&3F260400
110 pattern2=S%+9
120 !pattern2=&49844100
130 !(pattern2+4)=&FF6FB966
140 S%=S%+17
150 PROClimits
160 IF NOT graphics THEN PRINT"Not a graphics MODE. Can't dump.":VDU7:END
170 PROCassemble
180 REM enable printer, and set linefeed (send ESC A 8)
190 VDU2,1,27,1,65,1,8
200 REM clear paper
210 VDU1,10,1,10,1,10
220 FOR Y%=1023 TO 0 STEP-16
230 REM send bit code (ESC L 192 3 - 960 dots per line or 640 dots for MODE0)
240 VDU1,27,1,76,1,n1,1,n2
250 FOR X%=0 TO 1279 STEP step_size
260 !Xlo=X%+Y%*&10000
270 ?pass=0
280 CALL pixel
290 NEXT
300 VDU1,10
310 NEXT
320 REM reset linefeed and disable printer
330 VDU1,27,1,65,1,12,1,12,3
340 PRINT"DO YOU WANT TO ANALYSE PROFILE"
350 IF GET$ = "N" GOTO 510
360 PRINT"IS PROFILE LAMINAR(L),TURBULENT(T)"
370 PRINT"OR TRANSITIONAL(t)"
380 A$ = GET$
390 IF A$ = "L" GOTO 420
400 IF A$ = "T" GOTO 430
410 IF A$ = "t" GOTO 440
420 CHAIN "8.3"
430 CHAIN "9.3"
440 PRINT"IS VALUE OF INTERMITTENCY @ y/d=0.2 GREATER THAN(G) OR LESS THAN(L) 0.5"
450 A$ = GET$
460 IF A$ ="L" GOTO 490
470 IF A$ = "G" GOTO 500
480 GOTO 440
490 CHAIN"11.3L"
500 CHAIN"11.3T"
510 END
520 DEFPROClimits
530 DIM user 3
540 A%=&87
550 !user=USR(&FFF4)
560 mode=user?2
570 IF mode>5 OR mode=3 THEN graphics=FALSE ELSE graphics=TRUE
580 IF mode=0THEN n1=128:n2=2 ELSE n1=192:n2=3
590 IF mode=0 THEN step_size=2:?pass_number=1:?&80=pattern0 MOD 256:?&81=pattern0 DIV 256
600 IF mode=4 THEN step_size=4:?pass_number=3:?&80=pattern4 MOD 256:?&81=pattern4 DIV 256
610 IF mode=1 OR mode=5 THEN step_size=4:?pass_number=3:?&80=pattern1 MOD 256:?&81=pattern1 DIV 256
620 IF mode=2 THEN step_size=8:?pass_number=6:?&80=pattern2 MOD 256:?&81=pattern2 DIV 256
630 ENDPROC
640 DEFPROCassemble
650 osword=&FFF1
660 oswrch=&FFEE
670 Xlo=S%
680 Xhi=S%+1
690 Ylo=S%+2
700 Yhi=S%+3
710 value=S%+4
720 byte=S%+5
730 pass=S%+6
740 count_4=S%+7
750 S%=S%+8
760 FOR opt = 0 TO 2 STEP 2
770 P%=S%
780 [OPT opt
790 \SUBROUTINES
800 \to calculate POINT(X,Y)
810 .point        ldx #Xlo MOD 256
820               ldy #Xlo DIV 256
```

```
830              lda #9
840              jsr osword
850              rts
860 \subroutine to print a character
870 .printchar    lda #1
880              jsr oswrch
890              lda byte
900              jsr oswrch
910              rts
920 \decrement Y by 4
930 .dec_Y4       sec
940              lda Ylo
950              sbc #4
960              sta Ylo
970              bcc dec_Yhi
980              rts
990 .dec_Yhi      dec Yhi
1000             rts
1010 \increment Y by 16
1020 .inc_Y16     clc
1030             lda Ylo
1040             adc #16
1050             sta Ylo
1060             bcs inc_Yhi
1070             rts
1080 .inc_Yhi     inc Yhi
1090             rts
1100 \to rotate in two bits. Enter with X=pass, Y=colour
1110 .two_bits    lda (&80),Y        \select appropriate byte of pattern
1120             cpx #0             \if pass is 0 rotate
1130             beq rotate_in      \next two bits in
1140 .rotate_out  ror A              \otherwise dump two bytes
1150             ror A
1160             dex                \has X reached 0?
1170             bne rotate_out     \if not dump two more
1180 .rotate_in   ror A              \if so next two bits go into byte
1190             rol byte
1200             ror A
1210             rol byte
1220             rts
1230 \to calculate a whole byte
1240 .one_byte    jsr point
1250             ldy value
1260             lda pass
1270             and #3
1280             tax
1290             jsr two_bits
1300             jsr dec_Y4
1310             dec count_4
1320             bne one_byte       \if byte incomplete go back
1330             jsr printchar      \print the byte
1340             rts
1350 \MAIN PROGRAM
1360 \to calculate and print the pattern for one pixel
1370 .pixel       lda #4
1380             sta count_4        \reset counter
1390             jsr one_byte
1400             jsr inc_Y16
1410             inc pass
1420             lda pass
1430             cmp pass_number
1440             bne pixel
1450             rts
1460 ]
1470 NEXT
1480 ENDPROC
```

Programme

<u>8.3</u>

Programme 8.3 is used for the reduction of the mean laminar velocity profiles and is described in detail in section 4.2

```
10 MODE3
20 REM PROG B.3 LAMINAR BOUNDARY LAYER ANALYSIS PROG
30 DIM u1(50),u(50),y1(50),up(50),eta(50),y(50),e(50)
40 DIM RM3(50),IM3(50),uplus(50),yplus(50)
50 PROCdrive(D%)
60 PROCRfile
70 *DR.0
80 FOR i = 1 TO n
90 u1(i)=u(i)*uinf
100 y1(i)=y(i)*d
110 NEXT i
120 mu =(1.725 + 0.004375*t)/10^5
130 rho = (0.46535*z)/(t+273)
140 nu = mu/rho
150 REM CALCULATE SHEAR STRESS AND FRICTION COEFF.
160 FOR k = 1 TO n
170 IF u(1)>0.45 THEN 250
180 IF u(k) >= 0.45 THEN 210
190 sums = sums + u1(k)/y1(k)
200 L = L+1
210 NEXT k
220 t0 = mu*sums/L*1000
230 cf = 2 * t0/(rho*uinf^2)
240 GOTO 260
250 PRINT"FIRST U/Uinf POINT > 0.45 NO t0 VALUE CAN BE CALCULATED"
260 PROCplyint(u,y,n)
270 del1 = d*int2
280 theta = d*(int1 - int3)
290 del2 = d*(int1 - int4)
300 h12 = del1/theta
310 h32 = del2/theta
320 Rdis = uinf*del1/(nu*1000)
330 Rmom = uinf*theta/(nu*1000)
340 REM CALCULATE ERROR AND RMS ERROR OF FIT
350 FOR i =1 TO n
360 up(i) = a*y(i)+b*y(i)^2+c*y(i)^3
370 e(i) = up(i)-u(i)
380 acce = acce + e(i)^2
390 NEXT i
400 erms = SQR (acce/n)
410 VDU 1,27,1,14:PRINTTAB(12)"FILE",E$
420 PRINT
430 VDU 1,27,1,14:PRINT" DATA FOR LAMINAR B.L. VELOCITY PROFILE"
440 PRINT
450 PRINT
460 PRINT
470 PRINT"DISTANCE FROM LEADING EDGE = ";x;" mm"
480 PRINT
490 PRINT"SPANWISE LOCATION = ";Z;" mm"
500 PRINT
510 PRINT"AIR TEMPERATURE =";t;" Deg.C";"  ATMOSPHERIC PRESSURE =";z;" mmHg"
520 PRINT
530 PRINT
540 PRINT
550 PRINT
560 VDU 1,27,1,69
570 PRINT"          Y-MM     U-M/S      Y/D      U/UINF      ETA       ERROR"
580 PRINT
590 VDU 1,27,1,70
600 FOR i =1 TO n
610 eta(i) = (y1(i)/1000)*SQR(uinf*1000/(nu*x))
620 y(i) = y1(i)/d
630 y1(i)= INT(y1(i)*100+0.5)/100
640 u1(i) = INT(u1(i)*100+0.5)/100
650 y(i) = INT(y(i)*1000+0.5)/1000
660 u(i) = INT(u(i)*1000+0.5)/1000
670 eta(i) = INT(eta(i)*1000+0.5)/1000
680 e(i) = INT(e(i)*1000+0.5)/1000
690 PRINT TAB(10);y1(i);TAB(20);u1(i);TAB(30);y(i);TAB(39);u(i);TAB(51);eta(i);TAB(61);e(i)
700 NEXT
710 del1=INT(del1*100+0.5)/100
720 theta=INT(theta*100+0.5)/100
730 del2=INT(del2*100+0.5)/100
740 h12=INT(h12*100+0.5)/100
750 h32=INT(h32*100+0.5)/100
760 Rmom=INT(Rmom)
770 Rdis=INT(Rdis)
780 PRINT
790 PRINT "RMS ERROR OF FIT =",erms
800 PRINT
810 PRINT
820 PRINT
```

```
830 PRINT"LAMINAR BOUNDARY LAYER PARAMETERS"
840 PRINT
850 PRINT"APPROX EDGE OF BOUNDARY LAYER          = ";d " mm"
860 PRINT
870 PRINT " DISPLACEMENT THICKNESS               = ";del1" mm"
880 PRINT
890 PRINT "MOMENTUM THICKNESS                    = ";theta" mm"
900 PRINT
910 PRINT "ENERGY THICKNESS                      = ";del2" mm"
920 PRINT
930 PRINT "SHAPE FACTOR H12                      = ";h12
940 PRINT
950 PRINT "SHAPE FACTOR H32                      = ";h32
960 PRINT
970 PRINT "MOMENTUM TH. REYNOLDS NO.             = ";Rmom
980 PRINT
990 PRINT "DISPLACEMENT TH. REYNOLDS NO.         = ";Rdis
1000 PRINT
1010 IF u(1)>0.45 GOTO 1050
1020 PRINT "SKIN FRICTION COEFF.                 = ";cf
1030 PRINT
1040 PRINT "WALL SHEAR STRESS                    = ";t0"N/mm^2"
1050 VDU 3
1060 PRINT:PRINT:PRINT
1070 PRINT"DO YOU WANT THIS DATA PLOTTED ON"
1080 PRINT"THE UNIVERSAL VELOCITY PROFILE"
1090 IF GET$="Y" GOTO1100 ELSE 1120
1100 PROCPfile(u1,y1,t0,nu,n,E$)
1110 CHAIN"TUGRAF2"
1120 END
1130 DEF PROCplyint(u,y,n)
1140 LOCAL d
1150 d = y(n)
1160 FOR k = 1 TO n
1170 sy2 = sy2 + y(k)^2
1180 sy3 = sy3 + y(k)^3
1190 sy4 = sy4 + y(k)^4
1200 sy5 = sy5 + y(k)^5
1210 sy6 = sy6 + y(k)^6
1220 syu = syu + y(k)*u(k)
1230 sy2u = sy2u + y(k)^2*u(k)
1240 sy3u = sy3u + y(k)^3*u(k)
1250 NEXT k
1260 b1 = syu*((sy4*sy6)-(sy5*sy5))
1270 b2 = sy3*((sy2u*sy6)-(sy3u*sy5))
1280 b3 = sy4*((sy2u*sy5)-(sy3u*sy4))
1290 b0 =  b1 - b2 + b3
1300 c1 = sy2*((sy2u*sy6)-(sy3u*sy5))
1310 c2 = syu*((sy3*sy6)-(sy4*sy5))
1320 c3 = sy4*((sy3*sy3u)-(sy4*sy2u))
1330 c0 = c1 - c2 + c3
1340 d1 = sy2*((sy4*sy3u)-(sy5*sy2u))
1350 d2 = sy3*((sy3*sy3u)-(sy4*sy2u))
1360 d3 = syu*((sy3*sy5)-(sy4*sy4))
1370 d0 = d1 - d2 + d3
1380 e1 = sy2*((sy4*sy6)-(sy5*sy5))
1390 e2 = sy3*((sy3*sy6)-(sy4*sy5))
1400 e3 = sy4*((sy3*sy5)-(sy4*sy4))
1410 e = e1 - e2 + e3
1420 a = b0/e
1430 b = c0/e
1440 c = d0/e
1450 int1 = d^2*(a/2+(b/3)*d+(c/4)*d^2)
1460 int2 = d - int1
1470 pi31 = a^2/3+0.5*a*b*d
1480 pi32 = ((2*c*a+b^2)/5)*d^2
1490 pi33 = ((1/3)*b*c*d^3)+(c^2/7)*d^4
1500 int3 = d^3*(pi31 + pi32 + pi33)
1510 pi41 =(a^3/4)*d^4+((3*a^2*b)/5)*d^5
1520 pi42 =((3*c*a^2+3*a*b^2)/6)*d^6
1530 pi43 =((6*a*b*c+b^3)/7)*d^7
1540 pi44 =((3*c^2*a+3*b^2*c)/8)*d^8
1550 pi45 =((3*b*c^2)/9)*d^9
1560 pi46 =(c^3/10)*d^10
1570 int4 = pi41+pi42+pi43+pi44+pi45+pi46
1580 ENDPROC
1590 DEFPROCRfile
1600 X2=OPENIN"DATA"
1610 INPUT#X2, E$
1620 CLOSE# X2
1630 CLS
1640 VDU 2
1650 W = OPENIN E$
```

```
1660 INPUT#W,n,uinf,x,Z,d,t,z,AVIM,EIM
1670 FOR i = 1 TO n
1680 INPUT#W,u(i),y(i)
1690 NEXT i
1700 FOR i= 1 TO n
1710 INPUT#W,RM3(i),IM3(i)
1720 NEXT i
1730 CLOSE# W
1740 ENDPROC
1750 DEFPROCdrive(X%)
1760 IFD%=48THEN*DR.0
1770 IFD%=49THEN*DR.1
1780 IFD%=50THEN*DR.2
1790 IFD%=51THEN*DR.3
1800 ENDPROC
1810 DEFPROCPfile(u1,y1,t0,nu,n,E$)
1820 utau=SQR(t0/rho)
1830 FOR I = 1 TO n
1840 uplus(I)=u1(I)/utau
1850 yplus(I)=utau*y1(I)/(nu*1000)
1860 NEXT
1870 X3=OPENOUT"DATA1"
1880 PRINT#X3,n,E$
1890 FORI=1TOn
1900 PRINT#X3,uplus(I),yplus(I)
1910 NEXT I
1920 CLOSE# X3
1930 ENDPROC
```

Programme

<u>9.3</u>

Programme 9.3 is used for the reduction of the mean turbulent velocity profiles and is described in detail in section 4.3

```
10  REM PROG 9.3 TURBULENT BOUNDARY LAYER ANALYSIS PROG
20 REM THIS PROG WILL AUTOMATICALLY DELETE THE POINT NEAREST THE
30 REM WALL IF yt1 < 50
40 MODE 7
50 DIM y(40),u1(40),u(40),y1(40)
60 DIM utau(40),itut(40),e(40),yplus(40),uplus(40)
70 DIM resid(40),udef(40),RM3(40),IM3(40)
80 PROCdrive(D%)
90 PROCRfile
100 *DR.0
110 FOR i = 1 TO n
120 y1(i)=y(i)*d
130 u1(i)=u(i)*uinf
140 NEXT i
150 rho = (0.46535*z)/(t+273)
160 mu = (1.725 + 0.004375*t)/10^5
170 nu = mu/rho
180 Rx =INT(( uinf * x /(nu*1000))/1000)*1000
190 GOTO 360
200 FOR k = 2 TO n
210 y1(k-1) = y1(k)
220 u1(k-1) = u1(k)
230 u(k-1) = u(k)
240 y(k-1) = y(k)
250 RM3(k-1) = RM3(k)
260 IM3(k-1) = IM3(k)
270 NEXT k
280 y1(n) = 0
290 u1(n) = 0
300 u(n) = 0
310 y(n) = 0
320 RM3(n) = 0
330 IM3(n) = 0
340 n = n - 1
350 PRINT" Point Nearest Wall Has Been Deleted As yt1 < 50"
360 PROCloglaw(u1,y1,y,n,nu,uinf)
370 IF yt1 < 50 GOTO 200
380 PROCwalint(yt1,nu,utau1,uinf)
390 PROCparint(u,y,n,d)
400 sum1 = sum1 + s1
410 sum2 = sum2 + s2
420 sum3 = sum3 + s3
430 sum4 = sum4 + s4
440 del1 = sum2
450 theta = sum1 - sum3
460 del2 = sum1 - sum4
470 h12 = del1/theta
480 h32 =del2/theta
490 Rtheta = (uinf*theta)/(nu*1000)
500 Rdel1 = (uinf*del1)/(nu*1000)
510 pi = 0.205*uinf/utau1-0.5*LN(utau1*d/(nu*1000))-1.066
520 cf1 = 0.246/(EXP(1.561*h12)*Rtheta^0.268)
530 cf2 = 2.0*(utau1/uinf)^2
540 cf3 = 0.3/(EXP(1.33*h12)*(LOG(Rtheta))^(1.74+0.31*h12))
550 t0 = ((cf1+cf2+cf3)/3)*rho*uinf^2/2.0
560 VDU 2
570 VDU 1,27,1,14:PRINTTAB(12)"FILE",E$
580 PRINT
590 VDU 1,27,1,14:PRINT"DATA FOR TURBULENT B.L.VELOCITY PROFILE"
600 PRINT
610 PRINT
620 PRINT
630 PRINT
640 PRINT"AIR TEMPERATURE = ";t;" Deg.C";"   ATMOSPHERIC PRESSURE = ";z;" mmHg"
650 PRINT
660 PRINT"DISTANCE FROM L.E. = ";x;"  mm";"    SPANWISE LOCATION = ";Z;" mm"
670 PRINT
680 PRINT"FREESTREAM VELOCITY          = ";uinf" m/s"
690 PRINT
700 PRINT"PLATE REYNOLDS NUMBER        = ";Rx
710 PRINT
720 PRINT"APPROX. EDGE OF B.L.         = ";d" mm"
730 PRINT
740 PRINT
750 PRINT
760 PRINT
770 PRINT
780 VDU 1,27,1,69
790 PRINT"                   yplus       Uplus      Resid.       Udef."
800 PRINT
810 VDU 1,27,1,70
820 FOR i = 1 TO n
```

```
830 uplus(i) = INT(uplus(i)*10000+0.5)/10000
840 yplus(i) = INT(yplus(i)*10000+0.5)/10000
850 resid(i) = INT(resid(i)*10000+0.5)/10000
860 udef(i) = INT(udef(i)*10000+0.5)/10000
870 PRINT TAB(20);yplus(i);TAB(32);uplus(i);TAB(43)resid(i);TAB(56);udef(i)
880 y(i) = INT(y(i)*1000+0.5)/1000
890 u(i) = INT(u(i)*1000+0.5)/1000
900 NEXT i
910 PRINT
920 PRINT
930 PRINT
940 PRINT
950 PRINT
960 VDU 1,27,1,69
970 PRINT"                    Y-mm              Y/d          U/Uinf"
980 VDU 1,27,1,70
990 PRINT
1000 FOR i = 1 TO n
1010 PRINT TAB(20);y1(i);TAB(38);y(i);TAB(50);u(i)
1020 NEXT i
1030 PRINT
1040 del1=INT(del1*1000+0.5)/1000
1050 del2=INT(del2*1000+0.5)/1000
1060 theta=INT(theta*1000+0.5)/1000
1070 h12=INT(h12*1000+0.5)/1000
1080 h32=INT(h32*1000+0.5)/1000
1090 Rtheta=INT(Rtheta)
1100 Rdel1=INT(Rdel1)
1110 utau1=INT(utau1*1000+0.5)/1000
1120 pi=INT(pi*1000+0.5)/1000
1130 t0=INT(t0*1000+0.5)/1000
1140 PRINT
1150 PRINT
1160 PRINT
1170 PRINT
1180 PRINT"TURBULENT BOUNDARY LAYER PARAMETERS"
1190 PRINT
1200 PRINT
1210 PRINT"DISPLACEMENT THICKNESS     = ";del1" mm"
1220 PRINT
1230 PRINT"MOMENTUM THICKNESS         = ";theta" mm"
1240 PRINT
1250 PRINT"ENERGY THICKNESS           = ";del2" mm"
1260 PRINT
1270 PRINT"SHAPE FACTOR H12           = ";h12" mm"
1280 PRINT
1290 PRINT"SHAPE FACTOR H32           = ";h32
1300 PRINT
1310 PRINT"MOM. TH. REYNOLDS No.      = ";Rtheta
1320 PRINT
1330 PRINT"DISP. TH. REYNOLDS No.     = ";Rdel1
1340 PRINT
1350 PRINT"  cf (LUD/TILL)            = ";cf1
1360 PRINT"  cf (LOG-PLOT)            = ";cf2
1370 PRINT"  cf (COLES-FORM)          = ";cf3
1380 PRINT
1390 PRINT"WALL FRICTION VELOCITY     = ";utau1" m/s"
1400 PRINT
1410 PRINT"WALL SHEAR STRESS          = ";t0" N/m^2"
1420 PRINT
1430 PRINT"WAKE PARAMETER PI          = ";pi
1440 VDU 3
1450 PRINT
1460 PRINT
1470 PRINT
1480 PRINT"DO YO WANT A PLOT OF DATA ON UNIVERSAL"
1490 PRINT"TURBULENT B.L. VELOCITY PROFILE"
1500 A$ = GET$
1510 IF A$ = "Y" GOTO 1520 ELSE 1540
1520 PROCPfile(uplus,yplus,n,E$)
1530 CHAIN "TUGRAF2"
1540 END
1550 DEFPROCloglaw(u1,y1,y,n,nu,uinf)
1560 FOR k = 1 TO n
1570 utau(k) = 1
1580 GOTO 1600
1590 utau(k) = itut(k)
1600 yplus(k) = utau(k)*y1(k)/(nu*1000)
1610 itut(k) = u1(k)/(2.439*LN(yplus(k))+5.2)
1620 e(k) = utau(k) - itut(k)
1630 IF ABS(e(k))<=0.00001 THEN 1650
1640 GOTO 1590
1650 IF yplus(k) <= 30 OR y(k) >= 0.2 GOTO 1680
```

```
1660 l = l + 1
1670 sum = sum + utau(k)
1680 NEXT k
1690 utaul = sum/l
1700 FOR i = 1 TO n
1710 uplus(i) = ul(i)/utaul
1720 udef(i) =(uinf/utaul)-uplus(i)
1730 yplus(i) = utaul*yl(i)/(nu*1000)
1740 resid(i) = uplus(i) - (2.439*LN(yplus(i))+5.2)
1750 NEXT i
1760 ytl = yplus(3)
1770 ENDPROC
1780 DEFPROCwalint(ypl,nu,utaul,uinf)
1790 c1 = 540.6
1800 c2 = 6546.0
1810 c3 = 82770.0
1820 a = 2.439
1830 b = 5.2
1840 pi11 = a*(ypl*(LN(ypl)-1)-50*(LN(50)-1))
1850 pi12 = b*(ypl-50)
1860 int1w = pi11 + pi12
1870 pi21 = ypl*(LN(ypl))^2-50*(LN(50))^2
1880 pi22 = -2*(ypl*(LN(ypl)-1)-50*(LN(50)-1))
1890 pi23 = 2*b*a*(ypl*(LN(ypl)-1)-50*(LN(50)-1))
1900 pi24 = b^2*(ypl-50)
1910 int2w = a^2*(pi21 + pi22) + pi23 + pi24
1920 pi31 = ypl*(LN(ypl))^3-3*ypl*(LN(ypl))^2+6*ypl*(LN(ypl)-1)
1930 pi32 = -50*(LN(50))^3+3*50*(LN(50))^2-6*50*(LN(50)-1)
1940 pi33 = ypl*(LN(ypl))^2-50*(LN(50))^2
1950 pi34 = -2*(ypl*(LN(ypl)-1)-50*(LN(50)-1))
1960 pi35 = 3*a*b^2*(ypl*(LN(ypl)-1)-50*(LN(50)-1))
1970 pi36 = b^3*(ypl-50)
1980 int3w = a^3*(pi31 + pi32) + 3*b*a^2*(pi33 + pi34) + pi35 + pi36
1990 s1 = (c1 + int1w)*(nu/uinf)*1000
2000 s2 = (ypl*(nu/utaul)*1000) - s1
2010 s3 = (c2 + int2w)*(nu/uinf)*(utaul/uinf)*1000
2020 s4 = (c3 + int3w)*(nu/uinf)*(utaul/uinf)^2*1000
2030 ENDPROC
2040 DEFPROCparint(u,y,n,d)
2050 DIM a(30),b(30),c(30),det(30)
2060 DIM int1(30),int2(30),int3(30),int4(30)
2070 DIM int5(30),int6(30),int7(30),int8(30)
2080 n2 = n - 2
2090 FOR k = 3 TO n2
2100 det1 = 1*(y(k+1)*y(k+2)^2-y(k+2)*y(k+1)^2)
2110 det2 = y(k)*(y(k+2)^2-y(k+1)^2)
2120 det3 = y(k)^2*(y(k+2)-y(k+1))
2130 det(k) = det1 - det2 + det3
2140 a1 = u(k)*(y(k+1)*y(k+2)^2-y(k+2)*y(k+1)^2)
2150 a2 = y(k)*(u(k+1)*y(k+2)^2-u(k+2)*y(k+1)^2)
2160 a3 = y(k)^2*(u(k+1)*y(k+2)-u(k+2)*y(k+1))
2170 a(k) = (a1 - a2 + a3)/det(k)
2180 b1 = 1*(u(k+1)*y(k+2)^2-u(k+2)*y(k+1)^2)
2190 b2 = u(k)*(y(k+2)^2-y(k+1)^2)
2200 b3 = y(k)^2*(u(k+2)-u(k+1))
2210 b(k) = (b1 - b2 + b3)/det(k)
2220 c1 = 1*(y(k+1)*u(k+2)-y(k+2)*u(k+1))
2230 c2 = y(k)*(u(k+2)-u(k+1))
2240 c3 = u(k)*(y(k+2)-y(k+1))
2250 c(k) = (c1 - c2 + c3)/det(k)
2260 pi11 = a(k)*(y(k+1)-y(k))+b(k)*(y(k+1)^2-y(k)^2)/2
2270 pi12 = c(k)*(y(k+1)^3-y(k)^3)/3
2280 int1(k) = pi11 + pi12
2290 pi21 = a(k)*(y(k+2)-y(k+1))+b(k)*(y(k+2)^2-y(k+1)^2)/2
2300 pi22 = c(k)*(y(k+2)^3-y(k+1)^3)/3
2310 int2(k) = pi21 + pi22
2320 pi31 = (1.0-a(k))*(y(k+1)-y(k))-b(k)*(y(k+1)^2-y(k)^2)/2
2330 pi32 = -c(k)*(y(k+1)^3-y(k)^3)/3
2340 int3(k) = pi31 + pi32
2350 pi41 = (1.0-a(k))*(y(k+2)-y(k+1))-b(k)*(y(k+2)^2-y(k+1)^2)/2
2360 pi42 = -c(k)*(y(k+2)^3-y(k+1)^3)/3
2370 int4(k) = pi41 + pi42
2380 pi51 = a(k)*a(k)*(y(k+1)-y(k))
2390 pi52 = a(k)*b(k)*(y(k+1)^2-y(k)^2)
2400 pi53 = (2*a(k)*c(k)+b(k)*b(k))*(y(k+1)^3-y(k)^3)/3
2410 pi54 = b(k)*c(k)*(y(k+1)^4-y(k)^4)/2
2420 pi55 = c(k)*c(k)*(y(k+1)^5-y(k)^5)/5
2430 int5(k) = pi51+pi52+pi53+pi54+pi55
2440 pi61 = a(k)*a(k)*(y(k+2)-y(k+1))
2450 pi62 = a(k)*b(k)*(y(k+2)^2-y(k+1)^2)
2460 pi63 = (2*a(k)*c(k)+b(k)*b(k))*(y(k+2)^3-y(k+1)^3)/3
2470 pi64 = b(k)*c(k)*(y(k+2)^4-y(k+1)^4)/2
2480 pi65 = c(k)*c(k)*(y(k+2)^5-y(k+1)^5)/5
```

```
2490 int6(k) = pi61+pi62+pi63+pi64+pi65
2500 pi71 = a(k)*a(k)*a(k)*(y(k+1)-y(k))
2510 pi72 = 3*a(k)*a(k)*b(k)*(y(k+1)^2-y(k)^2)/2
2520 pi73 = a(k)*(a(k)*c(k)+b(k)*b(k))*(y(k+1)^3-y(k)^3)
2530 pi74 = b(k)*(6*a(k)*c(k)+b(k)*b(k))*(y(k+1)^4-y(k)^4)/4
2540 pi75 = 0.6*c(k)*(a(k)*c(k)+b(k)*b(k))*(y(k+1)^5-y(k)^5)
2550 pi76 = b(k)*c(k)*c(k)*(y(k+1)^6-y(k)^6)/2
2560 pi77 = c(k)*c(k)*c(k)*(y(k+1)^7-y(k)^7)/7
2570 int7(k) = pi71+pi72+pi73+pi74+pi75+pi76+pi77
2580 pi81 = a(k)*a(k)*a(k)*(y(k+2)-y(k+1))
2590 pi82 = 3*a(k)*a(k)*b(k)*(y(k+2)^2-y(k+1)^2)/2
2600 pi83 = a(k)*(a(k)*c(k)+b(k)*b(k))*(y(k+2)^3-y(k+1)^3)
2610 pi84 = b(k)*(6*a(k)*c(k)+b(k)*b(k))*(y(k+2)^4-y(k+1)^4)/4
2620 pi85 = 0.6*c(k)*(a(k)*c(k)+b(k)*b(k))*(y(k+2)^5-y(k+1)^5)
2630 pi86 = b(k)*c(k)*c(k)*(y(k+2)^6-y(k+1)^6)/2
2640 pi87 = c(k)*c(k)*c(k)*(y(k+2)^7-y(k+1)^7)/7
2650 int8(k) = pi81+pi82+pi83+pi84+pi85+pi86+pi87
2660 IF k = 3 GOTO 2680
2670 GOTO 2720
2680 sum1 = sum1 + int1(k)
2690 sum2 = sum2 + int3(k)
2700 sum3 = sum3 + int5(k)
2710 sum4 = sum4 + int7(k)
2720 IF k < n2 AND k > 3 GOTO 2740
2730 GOTO 2780
2740 sum1 = sum1 + 0.5*(int1(k) + int2(k-1))
2750 sum2 = sum2 + 0.5*(int3(k) + int4(k-1))
2760 sum3 = sum3 + 0.5*(int5(k) + int6(k-1))
2770 sum4 = sum4 + 0.5*(int7(k) + int8(k-1))
2780 IF k = n2 GOTO 2800
2790 GOTO 2840
2800 sum1 = sum1 + 0.5*(int1(k)+int2(k-1))+int2(k)
2810 sum2 = sum2 + 0.5*(int3(k)+int4(k-1))+int4(k)
2820 sum3 = sum3 + 0.5*(int5(k)+int6(k-1))+int6(k)
2830 sum4 = sum4 + 0.5*(int7(k)+int8(k-1))+int8(k)
2840 NEXT k
2850 sum1 = d*sum1
2860 sum2 = d*sum2
2870 sum3 = d*sum3
2880 sum4 = d*sum4
2890 ENDPROC
2900 DEFPROCRfile
2910 X2=OPENIN"DATA"
2920 INPUT#X2, E$
2930 W = OPENIN  E$
2940 INPUT#W,n,uinf,x,Z,d,t,z,AVIM,EIM
2950 FOR i = 1 TO n
2960 INPUT#W,u(i),y(i)
2970 NEXT i
2980 FOR i =1 TO n
2990 INPUT#W,RM3(i),IM3(i)
3000 NEXT i
3010 CLOSE# W
3020 ENDPROC
3030 DEFPROCPfile(uplus,yplus,n,E$)
3040 X3=OPENOUT"DATA1"
3050 PRINT#X3,n,E$
3060 FOR I=1 TO n
3070 PRINT#X3,uplus(I),yplus(I)
3080 NEXT I
3090 CLOSE# X3
3100 ENDPROC
3110 DEFPROCdrive(X%)
3120 IFD%=48THEN*DR.0
3130 IFD%=49THEN*DR.1
3140 IFD%=50THEN*DR.2
3150 IFD%=51THEN*DR.3
3160 ENDPROC
```

Programme

TUGRAF2

Programme TUGRAF2 is a graphics programme used for displaying experimental data on the Universal turbulent boundary layer velocity profile. ie on axes of $U+$ v's $y+$

```
10 REM GRAPHICS PROG."TUGRAF2" _ UNIVERSAL TURBULENT VELOCITY PROFILE PLOT"
20 DIM uplus(40),Lyplus(40)
30 DIM yplus(40)
40 MODE1
50 PROCRfile
60 VDU 19,3,3,0,0,0
70 VDU 19,2,4,0,0,0
80 MOVE 125,825
90 DRAW 125,125
100 DRAW 1225,125
110 PRINTTAB(8,2)"TURBULENT BOUNDARY LAYER"
120 PRINTTAB(7,4)"UNIVERSAL VELOCITY PROFILE"
130 PRINTTAB(15,7);"FILE ";E$
140 PRINTTAB(1,14) "U+"
150 PRINTTAB(29,30)"Ln Y+"
160 PRINT TAB(0,10)"20"
170 PRINTTAB(0,19)"10"
180 PRINTTAB(35,29)"6"
190 PRINTTAB(25,29)"4"
200 PRINTTAB(14,29)"2"
210 PRINTTAB(2,28)"0"
220 MOVE 125,125
230 FOR Uplus = 1 TO 12.5 STEP 0.5
240 LYplus=LN(Uplus)
250 U1 = Uplus*28+125
260 Y1 = LYplus*169+125
270 DRAW Y1,U1
280 NEXT
290 MOVE 471,405
300 FOR Uplus =10 TO 600 STEP 50
310 LYplus = (Uplus-5.0)/2.44
320 U1 = Uplus*28+125
330 Y1 = LYplus*169+125
340 DRAW Y1,U1
350 NEXT
360 MOVE1139,125:DRAW1139,100
370 MOVE801,125:DRAW801,100
380 MOVE463,125:DRAW463,100
390 MOVE125,685:DRAW100,685
400 MOVE125,405:DRAW100,405
410 GCOL 0,1
420 FOR I = 1 TO n
430 Lyplus(I)=LN(yplus(I))
440 B=uplus(I)*28+125
450 A=Lyplus(I)*169+125
460 MOVE A,B
470 PLOT 69,A,B
480 PLOT 69,A-8,B-8
490 PLOT 85,A+8,B-8
500 NEXT I
510 Print=INKEY(1500)
520 IF Print=32 GOTO530 ELSE 540
530 *RUN"MCEDUMP"
540 END
550 DEFPROCRfile
560 X3=OPENIN"DATA1"
570 INPUT#X3,n,E$
580 FOR I = 1 TO n
590 INPUT#X3,uplus(I),yplus(I)
600 NEXT I
610 CLOSE# X3
620 ENDPROC
```

Programme

TURBLEV

Programme TURBLEV is a data acquisition programme used to obtain the streamwise freestream turbulence distribution

```
>
 10 MODE7
 20 REM PROGRAM "TURBLEV" USED TO FIND FREESTREAM
 30 REM TURBULENCE LEVEL
 40 *ID
 50 CLOSE#0
 60 A%=OPENUP"CU-DAC8 &C000"
 70 CLS
 80 PRINTTAB(1,12)CHR$131"INPUT DIST. FROM L.E. IN mm"
 90 INPUTTAB(32,12) X
100 CLS
110 PROCcalcon
120 CLS
130 PRINTTAB(1,10)CHR$134"PLEASE WAIT VALUES ARE BEING"
140 PRINTTAB(1,12)CHR$134"        CALCULATED"
150 RMSS%=0
160 PTR#A%=6
170 FOR I=1TO10000
180 RMS%=BGET#A%
190 RMSS%=RMSS%+RMS%
200 NEXT
210 VELS%=0
220 PTR#A%=2
230 FOR I=1TO1000
240 VEL%=BGET#A%
250 VELS%=VELS%+VEL%
260 NEXT
270 FVEL=VELS%*VC/1000
280 RMSVEL=RMSS%*RMC/10000
290 FT=RMSVEL*100/FVEL
300 CLS
310 VDU2
320 PRINTTAB(1,6)CHR$129"DISTANCE FROM L.E.= ";X" mm"
330 PRINTTAB(1,8)CHR$129"FREESTREAMVELOCITY = ";INT(FVEL*100+0.5)/100;" m/s"
340 PRINTTAB(1,10)CHR$129"RMS VELOCITY = ";INT(RMSVEL*10000+0.5)/10000;" m/s"
350 PRINTTAB(1,12)CHR$129"FREESTREAM TURBULENCE LEVEL = ";INT(FT*100+0.5)/100"%"
360 VDU3
370 END
380 DEFPROCcalcon
390 PRINTTAB(0,6)CHR$132"WHICH RANGE IS RMS METER SET TO :-"
400 PRINT:PRINT:PRINT:PRINT
410 PRINTTAB(10)CHR$131"1.   0.01"
420 PRINT
430 PRINTTAB(10)CHR$131"2.   0.03"
440 PRINT
450 PRINTTAB(10)CHR$131"3.   0.1"
460 PRINT
470 PRINTTAB(10)CHR$131"4.   0.3"
480 B%=GET
490 req%=B%-48
500 ONreq%GOTO 510,530,550,570
510 RMC=4.902E-4
520  GOTO 580
530 RMC=1.471E-3
540  GOTO 580
550 RMC=4.902E-3
560  GOTO 580
570 RMC=1.471E-2
580 VC=7.95E-2
590 ENDPROC
```

Programme

IMPROF2

Programme IMPROF2 is a data acquisition Programme used to obtain the streamwise 'Near Wall' intermittency distribution. This data is stored in a data file in the form $\bar{\gamma}, x$

```
10  REM PROG "IMPROF2" FOR READING IN
20 REM INTERMITTENCY LEVELS
30 DIM EIM(70),AVIM(70),X(70),Z(70)
40 MODE7
50 *IO
60 CLOSE#0
70 A%=OPENUP"CU-DAC8 &C000"
80 I=1
90 GOTO 120
100  CLS:SUM%=0
110 I=I+1
120 PRINTTAB(1,10)CHR$130"INPUT DIST FROM L.E. IN mm"
130 INPUTTAB(30,10) X(I)
140 PRINTTAB(1,14)CHR$130"INPUT SPANWISE POS. IN mm"
150 INPUTTAB(30,14) Z(I)
160 CLS
170 PRINTTAB(1,10)CHR$129"WAIT WHILE INTERMITTENCY VALUES"
180 PRINT
190 PRINTTAB(8,12)CHR$129"ARE BEING READ IN"
200 PTR#A%=4
210 FOR K%=1 TO 10000
220 IM%=BGET#A%
230 SUM%=SUM%+IM%
240 NEXT K%
250 AVIM(I)=((SUM%/10000)-1)*3.984E-3
260 CLS
270 PRINTTAB(1,10)CHR$133"INPUT EYEBALL VALUE"
280 PRINTTAB(0,11)CHR$133
290 PRINTTAB(1,12)CHR$133"OF INTERMITTENCY Volts"
300 INPUTTAB(28,11) EVIM
310 EIM(I)=EVIM*2/10
320 CLS
330 PRINTTAB(0,10)CHR$129"MOVE PROBE TO NEXT POINT THEN"
340 PRINTTAB(0,12)CHR$129"PRESS RETURN"
350 PRINTTAB(0,14)CHR$130"IF RUN IS COMPLETE PRESS (C)"
360 B=GET
370 IF B<>67 GOTO 380 ELSE 390
380 IF B=13 GOTO 100 ELSE 330
390 CLS
400 VDU2
410 PRINTCHR$130"    X        GAMA         GAMA    Z "
420 PRINTCHR$130"    mm      ADC Val.     EYEBALL"
430 PRINT
440 FOR Q = 1 TO I
450 PRINTTAB(5);X(Q);TAB(15);INT(AVIM(Q)*100+0.5)/100;TAB(28)EIM(Q);TAB(34);Z(I)
460 NEXT
470 VDU3
480 *DR.0
490 END
```

Programme

SIGCALC

Programme SIGCALC is used to calculate the value of σ from experimental γ, x data obtained using programme IMPROF2

```
10  REM PROG SIGCALC
20 DIM X(30),AVIM(30),EIM(30),X1(30)
30 DIM G(30),eta1(60)
40 MODE7
50 CLS
60 IF H%=8GOTO120
70 PRINTTAB(1,8)CHR$134"INPUT NAME OF FILE TO BE READ"
80 PRINTTAB(0,12)CHR$134
90 INPUTTAB(11,12) NAME$
100 PRINTTAB(4,16)CHR$134"WHICH DRIVE IS FILE ON"
110 D%=GET
120 PROCdrive(D%)
130 PROCfilread(NAME$)
140 CLS
150 PRINTTAB(0,8)CHR$130"DO YOU WANT TO USE :-"
160 PRINTTAB(5,11)CHR$130"A. EYEBALL VALUES"
170 PRINTTAB(5,14)CHR$130"B. ADC VALUES "
180 PRINTTAB(5,17)CHR$130"C. BOTH EYE & ADC VALUES"
190 Qu%=GET
200 IF Qu%=65 GOTO230
210 IF Qu%=66 GOTO250
220 IF Qu%=67 GOTO270
230 PROCeyeball
240 GOTO280
250 PROCadc
260 GOTO280
270 PROCboth
280 PROCLeastsq(K)
290 MODE1
300 PROCplotGvX(Qu%)
310 VDU5
320 MOVE200,50:PRINT"PRESS SPACE TO CONTINUE"
330  W=GET
340 MODE7
350 PRINTTAB(5,10)CHR$132"WAIT WHILE SIGMA(mean)"
360 PRINTTAB(6,13)CHR$132"IS BEING CALCULATED"
370 PROCsigma(Qu%)
380 CLS
390 PRINTTAB(4,10)CHR$131"MEAN VALUE OF SIGMA = ";INT(AveSig)
400 PRINTTAB(6,14)CHR$132"PRESS SPACE TO CONTINUE"
410 B=GET
420 PROCfileput
430 *DR.0
440 CHAIN"PlotGvE"
450 DEFPROCdrive(D%)
460 *D.
470 IFD%=48THEN *DR.0
480 IFD%=49THEN *DR.1
490 IFD%=50THEN *DR.2
500 IFD%=51THEN *DR.3
510 ENDPROC
520 DEFPROCfilread(NAME$)
530 IFH%<>8GOTO570
540 file%=OPENIN"FLNAME"
550 INPUT#file%,NAME$
560 CLOSE# file%
570 ExpD%=OPENIN(NAME$)
580 INPUT#ExpD%,N,Tu,U0
590 FOR I=1 TO N
600 INPUT#ExpD%,X(I),EIM(I),AVIM(I)
610 NEXT
620 CLOSE# ExpD%
630 H%=0
640 ENDPROC
650 DEFPROCeyeball
660 K=0
670 FOR I=1TON
680 IF EIM(I)<=0.25 OR EIM(I)>=0.75 GOTO720
690 K=K+1
700 G(K)=EIM(I)
710 X1(K)=X(I)
720 NEXT
730 ENDPROC
740 DEFPROCadc
750 K=0
760 FOR I=1TON
770 IF AVIM(I)<=0.25 OR AVIM(I) >=0.75 GOTO810
780 K=K+1
790 G(K)=AVIM(I)
800 X1(K)=X(I)
810 NEXT
820 ENDPROC
```

```
830 DEFPROCboth
840 K=0
850 FOR I=1TON
860 IF EIM(I)<=0.25 OR EIM(I) >=0.75 GOTO900
870 K=K+1
880 G(K)=EIM(I)
890 X1(K)=X(I)
900 IF AVIM(I)<=0.25 OR AVIM(I)>=0.75 GOTO940
910 K=K+1
920 G(K)=AVIM(I)
930 X1(K)=X(I)
940 NEXT
950 ENDPROC
960 DEFPROCLeastsq(K)
970 FORJ=1TOK
980 SG=SG+G(J)
990 SX=SX+X1(J)
1000 SX2=SX2+X1(J)^2
1010 SGX=SGX+G(J)*X1(J)
1020 NEXT
1030 DEL=K*SX2-SX*SX
1040 M=(K*SGX-SG*SX)/DEL
1050 Const=(SX2*SG-SX*SGX)/DEL
1060 ENDPROC
1070 DEFPROCplotGvX(Qu%)
1080 Ct=0
1090 VDU19,3,3,0,0,0
1100 VDU19,2,2,0,0,0
1110 MOVE200,900:DRAW200,200:DRAW1200,200
1120 IFQu%=65GOTO1200
1130 FORI=1TON
1140 AVIMP=AVIM(I)*700+200
1150 XP=(X(I)-X(1))/1.5+200
1160 GCOL0,2
1170 PLOT69,XP,AVIMP
1180 NEXT
1190 IFQu%=67 GOTO1200 ELSE 1260
1200 FORI=1TON
1210 EIMP=EIM(I)*700+200
1220 XP=(X(I)-X(1))/1.5+200
1230 GCOL0,1
1240 PLOT69,XP,EIMP
1250 NEXT
1260 GCOL1,3
1270 FOR G=0.25 TO 0.75 STEP0.01
1280 XLS=(G-Const)/M
1290 GP=G*700+200
1300 XLSP=(XLS-X(1))/1.5+200
1310 IFCt>=1 GOTO1350
1320 MOVE XLSP,GP
1330 Ct=1
1340 NEXT
1350 DRAW XLSP,GP
1360 NEXT
1370 XBAR=(0.5-Const)/M
1380 XBARP=(XBAR-X(1))/1.5+200
1390 GCOL0,1
1400 MOVE XBARP,150:DRAW XBARP,900
1410 MOVE 150,550:DRAW 1200,550
1420 VDU5
1430 MOVEXBARP-130,100:PRINT"XBAR=";INT(XBAR)
1440 MOVE50,560:PRINT"0.5"
1450 GCOL0,3
1460 MOVE150,900:PRINT"G":MOVE150,860:PRINT"A"
1470 MOVE150,820:PRINT"M":MOVE150,780:PRINT"A"
1480 MOVE1100,150:PRINT"X mm"
1490 VDU4
1500 ENDPROC
1510 DEFPROCsigma(Qu%)
1520 K=0
1530 IFQu%=65GOTO1670
1540 FOR I=1TON
1550 Inc=1:etax1=-2.5:etax2=2.5
1560 GOTO 1590
1570 etax1=(eta-Inc):eta2x=eta:Inc=Inc/10
1580 IF ABS(Gcal-AVIM(I))<=0.01 GOTO1630
1590 FOR eta=etax1 TO etax2 STEP Inc
1600 PROCpolyeta(eta)
1610 IF Gcal>AVIM(I)GOTO1570
1620 NEXT eta
1630 eta1(I)=eta
1640 NEXTI
1650 IFQu%=67GOTO1660ELSE1790
```

```
1660 K=N
1670 FOR I=1TON
1680 K=K+1
1690 Inc=1:etax1=-2.5:etax2=2.5
1700 GOTO1730
1710 etax1=(eta-Inc):eta2x=eta:Inc=Inc/10
1720 IF ABS(Gcal-EIM(I))<=0.01 GOTO1770
1730 FOR eta=etax1 TO etax2 STEP Inc
1740 PROCpolyeta(eta)
1750 IF Gcal>EIM(I)GOTO1710
1760 NEXT eta
1770 eta1(K)=eta
1780 NEXTI
1790 IFQu%=67THEN L=2*N ELSE L=N
1800 SumSig=0:Ct2%=0
1810 FOR I = 1 TO L
1820 IF I>N THEN K=I-N ELSE K=I
1830 IFeta1(I)>-2.25 AND eta1(I)<-0.25GOTO1850ELSE1840
1840 IFeta1(I)>0.25 AND eta1(I)<2.25GOTO1850ELSE1880
1850 Sigma=(X(K)-XBAR)/eta1(I)
1860 SumSig=Sigma+SumSig
1870 Ct2%=Ct2%+1
1880 NEXT
1890 AveSig=SumSig/Ct2%
1900 ENDPROC
1910 DEFPROCpolyeta(eta)
1920 Meta=SQR(eta^2)
1930 IF eta=0 GOTO2000
1940 C1=0.8273*Meta
1950 C2=0.094*Meta^2
1960 C3=0.073*Meta^3
1970 C4=0.0165*Meta^4
1980 Gcal=0.5*(1+(eta/(Meta))*(C1-C2-C3+C4))
1990 GOTO2010
2000 Gcal=0.5
2010 ENDPROC
2020 DEFPROCfileput
2030 file%=OPENOUT"GvEData"
2040 PRINT#file%,N,XBAR,AveSig,Qu%
2050 FORI=1TON
2060 PRINT#file%,X(I),AVIM(I),EIM(I)
2070 NEXT
2080 CLOSE# file%
2090 ENDPROC
```

Programme

IGBLPR1

Programme IGBLPR1 is the introductory programme for the Tani/Alber computational model described in Chapter7. This programme is used to read in the initial input data and to estimate the $\left(\frac{U_\infty}{H_{32}} \frac{d H_{32}}{d U_\infty}\right)$ term required for the laminar boundary layer calculation by Tani's method

L.

```
10 REM PROG IGBLPR1 USED TO ESTIMATE DGDU TERM FOR TANI'S METHOD
20 MODE7
30 CLS
40 PRINT:PRINT:PRINT:PRINT
50 PRINTCHR$130"ATMOSPHERIC PRESSURE mmHg"
60 PRINT
70 INPUT TAB(15) z
80 PRINTCHR$130"AIR TEMPERATURE Deg C"
90 PRINT
100 INPUT TAB(15) t
110 PRINTCHR$130"FREESTREAM VELOCITY m/s"
120 PRINT
130 INPUT TAB(15) UO
140 PRINTCHR$130"LENGTH 0F PLATE mm"
150 PRINT
160 INPUT TAB(15) XMAX
170 PRINTCHR$130"FREESTREAM TURBULENCE"
180 INPUT TAB(15) Tu
190 PRINT
200 PRINTCHR$130"DO YOU WANT TO USE ABU-GHANNAM&SHAWS"
210 PRINTCHR$130"CORRELATION FOR THE ONSET OF TRANSITION"
220 INPUT TAB(15) Q$
230 IF Q$= "Y" GOTO290
240 PRINT
250 PRINTCHR$130"INPUT TRANSITION ONSET IN mm"
260 INPUT TAB(15) Xst
270 PRINT
280 GOTO300
290 Xst=0
300 PRINTCHR$130"DO YOU WANT A PRINTOUT OF"
310 PRINTCHR$130"TRANSITION VELOCITY PROFILES"
320 INPUT TAB(15) PRO$
330 CLS
340 PRINT
350 PRINT
360 PRINTCHR$131"THE FREESTREAM VELOCITY DISTRIBUTION IS"
370 PRINTCHR$131"DEFINED IN THE FORM :-"
380 PRINT
390 PRINTCHR$130;CHR$141;"U/UO = "CHR$141;"EX"CHR$140;"P";CHR$141;"+ A + BX + CX";CHR$140;"2";CHR$141;"+ DX"
CHR$140;"3"
400 PRINTCHR$130;CHR$141;"U/UO = ";CHR$141;"EX"CHR$140;" ";CHR$141;"+ A + BX + CX";CHR$140;" ";CHR$141;"+ DX
"CHR$140;" "
410 PRINT
420 PRINT
430 PRINTTAB(4)CHR$134"P = "
440 INPUTTAB(10,10); P
450 PRINT
460 PRINTTAB(4)CHR$134"E = "
470 INPUTTAB(10,12); E
480 PRINT
490 PRINTTAB(4)CHR$134"A = "
500 INPUTTAB(10,14); A
510 PRINT
520 PRINTTAB(4)CHR$134"B = "
530 INPUTTAB(10,16); B
540 PRINT
550 PRINTTAB(4)CHR$134"C = "
560 INPUTTAB(10,18); C
570 PRINT
580 PRINTTAB(4)CHR$134"D = "
590 INPUTTAB(10,20); D
600 PRINT
610 @%=&20309
620 MODE4
630 DGDU=0:A2DSTR2=0
640 DIM THETA(100),DSTR1(100),X(100),CfL(100),H(100),G(100),DSTR2(100)
650 DIM Z(12),UN5(12),U(100),a(100)
660 DIM A(10,20),AINV(10,10),C(10),B(10)
670 rho=(0.46535*z/(t+273))
680 mu=(1.725+0.004375*t)/10^5
690 nu=mu/rho
700 THETA(0)=0:DSTR1(0)=0:U(0)=UO:X(0)=0
710 CfL(0)=0:H(0)=0:G(0)=0:DSTR2(0)=0:a(0)=0
720 DX=10:SUM=0
730 I=1
740 DX=DX*10
750 GOTO780
760 IFX(I)>XMAX GOTO 850
770 I=I+1
780 X(I)=X(I-1)+DX
790 PROCQuadrature
800 IF LAM=0 GOTO 1020
```

```
810 IFLAM<-0.09GOTO820 ELSE 830
820 I=I-1:GOTO850
830 PROCTani
840 GOTO760
850 A1DSTR2=S1DSTR2/I
860 S1DSTR2=0
870 IF ABS(A1DSTR2-A2DSTR2)<0.0001GOTO990
880 A2DSTR2=A1DSTR2
890 PROCcurvefit
900 I=1:GOTO940
910 I=I+1
920 IF I<=N GOTO 940 ELSE 930
930 I=I-1:GOTO850
940 DGDU=C(2)+2*C(3)*U(I)+3*C(4)*U(I)^2
950 DUDX=(P*E*Q^(P-1)+B+2*C*Q+3*D*Q^2)*(UO*1000/XMAX)
960 LAM=DUDX*THETA(I)^2/(nu*1000000)
970 PROCTani
980 GOTO910
990 PROCPlotGvU
1000 IF LAM=0 GOTO1020
1010 IF GET=32 GOTO1020 ELSE 1010
1020 PROCfput
1030 CHAIN"IGBLPR5"
1040 END
1050 DEFPROCQuadrature
1060 LOCAL N,N1,N2
1070 Q=X(I)/XMAX
1080 UN=E*Q^P+A+B*Q+C*Q^2+D*Q^3
1090 DUDX=(P*E*Q^(P-1)+B+2*C*Q+3*D*Q^2)*(UO*1000/XMAX)
1100 N=11
1110 ST=DX/10
1120 XST=X(I)-(DX+ST)
1130 FOR K=1TON
1140 XST=XST+ST
1150 Z(K)=XST/XMAX
1160 UN5(K)=(E*Z(K)^P+A+B*Z(K)+C*Z(K)^2+D*Z(K)^3)^5
1170 NEXT
1180 SUM=SUM+UN5(1)+UN5(11)
1190 N1=N-1
1200 FOR K=2 TO N1 STEP2
1210 SUM=SUM+4*UN5(K)
1220 NEXT
1230 N2=N-2
1240 FOR K=3 TO N2 STEP2
1250 SUM=SUM+2*UN5(K)
1260 NEXT
1270 INUN5=ST*SUM/(3*1000)
1280 U(I)=UN*UO
1290 THETA(I)=SQR((0.45*nu*UO^5/U(I)^6)*INUN5)*1000
1300 LAM=DUDX*THETA(I)^2/(nu*1000000)
1310 IF LAM<-0.09GOTO1320 ELSE 1330
1320 I=I-1:GOTO850
1330 ENDPROC
1340 DEFPROCTani
1350 a=0
1360 TD=0.4-a/20
1370 TE=(4/35)+(a/105)-(a^2/252)
1380 TF=(876/5005)+(73/5005)*a-(23/5460)*a^2-(1/2860)*a^3
1390 TP=2*a*TE
1400  TQ=((4/35)*TF)*(48-4*a+3*a^2)
1410 H=TD/TE
1420 G=TF/TE
1430 ita=(LAM*(H-1)-LAM*U(I)*DGDU/G+TQ/(2*G^2)-(a^2/105)+(a^3/252))*(35/4)
1440 IF ABS(ita-a)<0.0001GOTO1470
1450 a=ita
1460 GOTO1360
1470 a(I)=ita
1480 TD=0.4-a(I)/20
1490 TE=(4/35)+(a(I)/105)-(a(I)^2/252)
1500 TF=(876/5005)+(73/5005)*a(I)-(23/5460)*a(I)^2-(1/2860)*a(I)^3
1510 H(I)=TD/TE
1520 G(I)=TF/TE
1530 DSTR1(I)=THETA(I)*H(I)
1540 DSTR2(I)=THETA(I)*G(I)
1550 CfL(I)=TP*nu*1000/(THETA(I)*U(I))
1560 S1DSTR2=S1DSTR2+DSTR2(I)
1570 ENDPROC
1580 DEFPROCcurvefit
1590 N=I
1600 LOCALI
1610 M=2
1620  MAX=2*M
1630
```

```
1640  REM INITIALISATION OF MATRICES
1650
1660  FOR I=1 TO M
1670  FOR J=1 TO MAX
1680  A(I,J)=0
1690  NEXT
1700  NEXT
1710  A(1,1)=N
1720  FOR I=2 TO M
1730  FOR K=1 TO N
1740  A(I,1)=A(I,1)+U(K)^(I-1)
1750  NEXT
1760  NEXT
1770  FOR J=2 TO M
1780  FOR K=1 TO N
1790  A(M,J)=A(M,J)+U(K)^(M+J-2)
1800  NEXT
1810  NEXT
1820  FOR J=2 TO M
1830  FOR I=1 TO (M-1)
1840  A(I,J)=A((I+1),(J-1))
1850  NEXT
1860  NEXT
1870  FOR I=1 TO M
1880  A(I,(M+I))=1
1890  B(I)=0
1900  C(I)=0
1910  NEXT
1920  FOR I=1 TO M
1930  FOR K=1 TO N
1940  B(I)=B(I)+G(K)*U(K)^(I-1)
1950  NEXT
1960  NEXT
1970
1980  REM MATRICES FULLY INITIALISED
1990
2000  L=1
2010  FOR J=1 TO (M-1)
2020  L=L+1
2030  FOR I=L TO M
2040  CONST=-(A(I,J)/A(J,J))
2050  FOR K=J TO MAX
2060  A(I,K)=A(I,K)+CONST*A(J,K)
2070  NEXT
2080  NEXT
2090  NEXT
2100
2110  L=0
2120  FOR J=M TO 2 STEP -1
2130  L=L+1
2140  FOR I=(M-L) TO 1 STEP -1
2150  CONST=-(A(I,J)/A(J,J))
2160  FOR K=MAX TO 2 STEP -1
2170  A(I,K)=A(I,K)+CONST*A(J,K)
2180  NEXT
2190  NEXT
2200  NEXT
2210
2220  FOR I=1 TO M
2230  ANOR=A(I,I)
2240  FOR J=1 TO MAX
2250  A(I,J)=A(I,J)/ANOR
2260  NEXT
2270  NEXT
2280
2290  K=0
2300  FOR J=(M+1) TO MAX
2310  K=K+1
2320  FOR I=1 TO M
2330  AINV(I,K)=A(I,J)
2340  NEXT
2350  NEXT
2360
2370  REM MATRIX INVERSION COMPLETE
2380
2390  FOR I=1 TO M
2400  FOR J=1 TO M
2410  C(I)=C(I)+AINV(I,J)*B(J)
2420  NEXT
2430  NEXT
2440 ENDPROC
2450 DEFPROCPlotGvU
2460 PROCcurvefit
```

```
2470 Ct=0
2480 VDU19,3,3,0,0,0
2490 MOVE 200,900:DRAW200,200:DRAW1200,200
2500 VDU5
2510 MOVE 100,800:PRINT"G"
2520 MOVE 1000,140:PRINT"U"
2530 VDU4
2540 Uscale=1000/ABS(U(1)-U(N))
2550 Gscale=700/0.1
2560 Ct1=0
2570 FOR K= 1 TO N
2580 IFU(N)<U(1)GOTO2610
2590 Uplot=(U(K)-U(1))*Uscale+200
2600 GOTO2620
2610 Uplot=(U(K)-U(N))*Uscale+200
2620 Gplot=(G(K)-1.5)*Gscale+200
2630 PLOT69,Uplot,Gplot
2640 NEXT
2650 FOR K=1TON
2660 G=C(1)+C(2)*U(K)+C(3)*U(K)^2+C(4)*U(K)^3+C(5)*U(K)^4+C(6)*U(K)^5+C(7)*U(K)^6
2670 IFU(N)<U(1)GOTO2700
2680 Uplot=(U(K)-U(1))*Uscale+200
2690 GOTO2710
2700 Uplot=(U(K)-U(N))*Uscale+200
2710 Gplot=(G-1.5)*Gscale+200
2720 IFCt>0.5GOTO2770
2730 Ct=1
2740 MOVE Uplot,Gplot
2750 PLOT69,Uplot,Gplot
2760 GOTO2780
2770 DRAWUplot,Gplot
2780 NEXT
2790 ENDPROC
2800 DEFPROCfput
2810 CH%=OPENOUT"TANDGDU"
2820 PRINT#CH%,C(1),C(2),C(3),C(4),z,t,XMAX,Tu,UO,P,E,A,B,C,D,Xst,PRO$,Q$
2830 CLOSE#CH%
2840 ENDPROC
```

Programme

IGBLPR5

Programme IGBLPR5 is the main boundary layer prediction computational programme.

```
 10 MODE7
 20 VDU15
 30 @%=&20309
 40 DIM THETA(350),DSTR1(350),X(350),Cf(350),H(350),G(350),DSTR2(350),U(350)
 50 DIM Z(12),UN5(12)
 60 DIM C(4),unL(21),unT(21),unt(21)
 70 DIM IN1(21),IN2(21),YD(21)
 80 PROCfread
 90 rho=(0.46535*z/(t+273))
100 mu=(1.725+0.004375*t)/10^5
110 nu=mu/rho
120 THETA(0)=0:DSTR1(0)=0:U(0)=U0:X(0)=0
130 Cf(0)=0:H(0)=0:G(0)=0:DSTR2(0)=0:a=1.857:Ka=0.41:LAM=0
140  PRINT"           X      Uinf      DSTR1      THETA      DSTR2      H12      H23      Cf"
150 PRINT
160 I=0
170 PROCPrint
180 DX=25:SUM=0
190 IF X(I)>XMAX OR I>349 GOTO 670
200 I=I+1
210 X(I)=X(I-1)+DX
220 PROCTani
230 PROCTrstart
240 U(I)=UL
250 DSTR1(I)=DSTR1L
260 THETA(I)=THETAL
270 DSTR2(I)=DSTR2L
280 H(I)=HL
290 G(I)=GL
300 Cf(I)=CfL
310 PROCPrint
320 IFQ$="Y" GOTO 350
330 IFX(I)>=Xst GOTO370
340 GOTO360
350 IF RTH > RTHS GOTO370
360 GOTO190
370 PROCInitcon
380 I=I+1
390 X(I)=X(I-1)+DX
400 IFX(I)>XMAX OR I>349 GOTO 670
410 VDU2
420 PROCTani
430 PROCAlber
440 PROCTran
450 U(I)=Ut
460 DSTR1(I)=DSTR1t
470 THETA(I)=THETAt
480 DSTR2(I)=DSTR2t
490 H(I)=Ht:G(I)=Gt
500 Cf(I)=Cft
510 LAMt=THETAt^2*dUdX/(nu*1000000)
520 PROCPrint
530 IF eta>2.25 GOTO 550
540 GOTO380
550 I=I+1
560 X(I)=X(I-1)+DX
570 IFX(I)>XMAX OR I>349 GOTO 670
580 PROCAlber
590 U(I)=UT
600 DSTR1(I)=DSTR1T
610 THETA(I)=THETAT
620 DSTR2(I)=DSTR2T
630 H(I)=HT:G(I)=GT
640 Cf(I)=CfT
650 PROCPrint
660 GOTO 550
670 CLS:PRINT:PRINT:PRINT
680 PRINTCHR$134"DO YOU WANT TO PUT THIS DATA ON FILE"
690 PRINT:PRINT
700 B$=GET$
710 IFB$="N"GOTO 730
720 PROCFput
730 END
740 DEFPROCPrint
750 XPR=(X(I)-X(0))/50
760 IF XPR<>INT(XPR)GOTO810
770 IF I>0 GOTO800
780 PRINTTAB(7);X(0);TAB(15);U(0);TAB(25);DSTR1(0);TAB(35);THETA(0);TAB(45);DSTR2(0);TAB(54);H(0);TAB(62);G(
0);TAB(71);"inf"
790 GOTO 810
800 PRINTTAB(7);X(I);TAB(15);U(I);TAB(25);DSTR1(I);TAB(35);THETA(I);TAB(45);DSTR2(I);TAB(54);H(I);TAB(62);G(
I);TAB(70);Cf(I)*1000
```

```
810 ENDPROC
820 DEFPROCQuadrature
830 LOCAL N,N1,N2
840 q=X(I)/XMAX
850 UNL=E*q^P+A+B*q+C*q^2+D*q^3
860 dUdX=(P*E*q^(P-1)+B+2*C*q+3*D*q^2)*(UO*1000/XMAX)
870 N=11
880 ST=DX/10
890 XST=X(I)-(DX+ST)
900 FOR K=1TON
910 XST=XST+ST
920 Z(K)=XST/XMAX
930 UN5(K)=(E*Z(K)^P+A+B*Z(K)+C*Z(K)^2+D*Z(K)^3)^5
940 NEXT
950 SUM=SUM+UN5(1)+UN5(11)
960 N1=N-1
970 FOR K=2 TO N1 STEP2
980 SUM=SUM+4*UN5(K)
990 NEXT
1000 N2=N-2
1010 FOR K=3 TO N2 STEP2
1020 SUM=SUM+2*UN5(K)
1030 NEXT
1040 INUN5=ST*SUM/(3*1000)
1050 UL=UNL*UO
1060 THETAL=SQR((0.45*nu*UO^5/UL^6)*INUN5)*1000
1070 LAM=dUdX*THETAL^2/(nu*1000000)
1080 ENDPROC
1090 DEFPROCTani
1100 PROCQuadrature
1110 IF LAM=0 GOTO 1260
1120 DGDU=C(2)+2*C(3)*UL+3*C(4)*UL^2
1130 a=0
1140 TD=0.4-a/20
1150 TE=(4/35)+(a/105)-(a^2/252)
1160 TF=(876/5005)+(73/5005)*a-(23/5460)*a^2-(1/2860)*a^3
1170 TP=2*a*TE
1180 TQ=((4/35)*TF)*(48-4*a+3*a^2)
1190 H=TD/TE
1200 G=TF/TE
1210 ita=(LAM*(H-1)-LAM*U(I)*DGDU/G+TQ/(2*G^2)-(a^2/105)+(a^3/252))*(35/4)
1220 IF ABS(ita-a)<0.0001GOTO1270
1230 a=ita
1240 GOTO1140
1250 GOTO 1270
1260 a=1.857
1270 TD=0.4-a/20
1280 TE=(4/35)+(a/105)-(a^2/252)
1290 TF=(876/5005)+(73/5005)*a-(23/5460)*a^2-(1/2860)*a^3
1300 TP=2*a*TE
1310 HL=TD/TE
1320 GL=TF/TE
1330 DSTR1L=THETAL*HL
1340 DSTR2L=THETAL*GL
1350 CfL=TP*nu*1000/(THETAL*UL)
1360 ENDPROC
1370 DEFPROCfread
1380 CH%=OPENIN"TANDGDU"
1390 INPUT#CH%,C(1),C(2),C(3),C(4),z,t,XMAX,Tu,UO,P,E,A,B,C,D,Xst,PRO$,Q$
1400 CLOSE#CH%
1410 ENDPROC
1420 DEFPROCTrstart
1430 IF Q$="N"GOTO 1530
1440 IF LAM>0 GOTO 1470
1450 FLAM=6.91+12.75*LAM+63.64*LAM^2
1460 GOTO1480
1470 FLAM=6.91+2.48*LAM-12.27*LAM^2
1480 RTHS=163+EXP(FLAM-(FLAM*Tu/6.91))
1490 GOTO 1510
1500 RTHS=(UL*Xst)/(nu*1000)
1510 RTH=THETAL*UL/(nu*1000)
1520 IFRTH<RTHS GOTO1700 ELSE 1570
1530 IFX(I)<Xst GOTO1700
1540 q=Xst/XMAX
1550 Ust=((E*q^P)+A+B*q+C*q^2+D*q^3)*UO
1560 RTHS=THETAL*Ust/(nu*1000)
1570 US=UL:LAMS=LAM:XS=X(I):THETAS=THETAL
1580 PRINT
1590 PRINTTAB(30)"START OF TRANSITION"
1600 PRINTTAB(31)"RTHETAs = ";RTHS
1610 IF LAM=0 GOTO 1660
1620 RS1=0.27-(0.25*Tu^3.5/(1+Tu^3.5))
1630 RS2=1/(1+1710*(-LAM^1.4)*EXP(-SQR(1+Tu^3.5)))
```

```
1640 RSig=RS1*RS2*1000000
1650 GOTO1670
1660 RSig=(0.27-(0.25*Tu^3.5/(1+Tu^3.5)))*1000000
1670 Sigma=RSig*nu*1000/US
1680 XBAR=2.25*Sigma+XS
1690 eta=-2.25
1700 ENDPROC
1710 DEFPROCTran
1720 LOCAL n
1730 BSUM=0:CSUM=0
1740 q=X(I)/XMAX
1750 UNt=E*q^P+A+B*q+C*q^2+D*q^3
1760 Ut=UNt*UO
1770 IF LAM<=0GOTO1800
1780 PLAM=70*LAM+310*LAM^2-5430*LAM^3+66000*LAM^4
1790 GOTO1810
1800 PLAM=73*LAM+109*LAM^2+709*LAM^3
1810 eta=(X(I)-XBAR)/Sigma
1820 Meta=SQR(eta^2)
1830 IF eta=0 GOTO 1880
1840 C1=0.8273*Meta:C2=0.094*Meta^2
1850 C3=0.073*Meta^3:C4=0.0165*Meta^4
1860 Gam=0.5*(1+(eta/Meta)*(C1-C2-C3+C4))
1870 GOTO1890
1880 Gam=0.5
1890 DL=63*THETAL/(7.4-(PLAM/15)-(PLAM^2/144))
1900 DT=DSTR1T*Ka/((1+Pi)*f)
1910 n=2/(HT-1)
1920 IF DL>DT GOTO 1950
1930 DEL=DT
1940 GOTO1960
1950 DEL=DL
1960 Utau=f*UT
1970 N=21
1980 DY=DEL/20
1990 Y=0
2000 FOR K=2TON
2010 Y=Y+DY
2020 IFY>=DL GOTO2070
2030 Lpr1=(2*Y/DL-2*(Y/DL)^3+(Y/DL)^4)
2040 Lpr2=PLAM*(Y/DL-3*(Y/DL)^2+3*(Y/DL)^3-(Y/DL)^4)/6
2050 unL(K)=Lpr1+Lpr2
2060 GOTO2080
2070 unL(K)=1.0
2080 IFY>=DT GOTO2110
2090 unT(K)=(Y/DT)^(1/n)
2100 GOTO2120
2110 unT(K)=1.0
2120 unt(K)=(1-Gam)*unL(K)+Gam*unT(K)
2130 IN1(K)=1-unL(K)*unT(K)
2140 IN2(K)=1-unL(K)*unT(K)*unt(K)
2150 YD(K)=Y/DEL
2160 NEXT
2170 BSUM=1.0+4*IN1(21)
2180 CSUM=1.0+4*IN2(21)
2190 N1=N-1
2200 FOR K=2 TO N1 STEP2
2210 BSUM=BSUM+4*IN1(K)
2220 CSUM=CSUM+4*IN2(K)
2230 NEXT
2240 N2=N-2
2250 FOR K=3 TO N2 STEP2
2260 BSUM=BSUM+2*IN1(K)
2270 CSUM=CSUM+2*IN2(K)
2280 NEXT
2290 Qt1=DY*BSUM/3
2300 Qt2=DY*CSUM/3
2310 DSTR1t=DSTR1L*(1-Gam)+DSTR1T*Gam
2320 THt1=(1-Gam)*((1-Gam)*THETAL-Gam*THETAL*HL)
2330 THt2=Gam*(Gam*THETAT-(1-Gam)*THETAT*HT)
2340 THt3=2*Gam*(1-Gam)*Qt1
2350 THETAt=THt1+THt2+THt3
2360 DS2t1=(1-Gam)*((1-Gam)^2*DSTR2L+Gam*(Gam-2)*DSTR1L)
2370 DS2t2=Gam*(Gam^2*DSTR2T+(Gam^2-1)*DSTR1T)
2380 DS2t3=3*Gam*(1-Gam)*Qt2
2390 DSTR2t=DS2t1+DS2t2+DS2t3
2400 Ht=DSTR1t/THETAt
2410 Gt=DSTR2t/THETAt
2420 Cft=(1-Gam)*CfL+Gam*CfT
2430 IF PRO$="Y"GOTO2440ELSE2530
2440 XPR=(X(I)-X(0))/50
2450 IF XPR<>INT(XPR) GOTO 2530
2460 PRINT"DELTA  = " DEL;" mm";"   Gamma = ";Gam:PRINT:PRINT
```

```
2470 PRINTTAB(10)"Velocity profile @ X= ";X(I);" mm"
2480 PRINT:PRINT
2490 PRINT"         Y/DELTA        U/Uinf"
2500 FOR K = 1 TO N
2510 PRINTTAB(10);YD(K);TAB(20);unt(K)
2520 NEXT
2530 ENDPROC
2540 DEFPROCAlber
2550 X=X(I)-DX
2560 PROCRunge
2570 DS=f*(1+Pi)/Ka
2580 TS=DS-f^2*(2+3.179*Pi+1.5*Pi^2)/(Ka^2)
2590 ST=3*TS-DS+f^3*(6+11.14*Pi+8.5*Pi^2+2.56*Pi^3)/(Ka^3)
2600 CfT=(2*f^2)*(1+0.035*Tu)
2610 HT1=DS/TS:GT=ST/TS
2620 HT=HT1*(1-0.02*Tu)
2630 DSTR1T1=Dstr
2640 THETAT1=DSTR1T1/HT1
2650 THETAT=THETAT1/(1+0.05*Tu)
2660 DSTR1T=HT*THETAT
2670 DSTR2T=THETAT*GT
2680 q=X(I)/XMAX
2690 dUdX=(UD*1000/XMAX)*((P*E*q^(P-1))+B+2*C*q+3*D*q^2)
2700 LAMT=THETAT^2*dUdX/(nu*1000000)
2710 ENDPROC
2720 DEFPROCRunge
2730 DSUM=0:PiR=Pi:FR=f:DstrR=Dstr
2740 q=X/XMAX
2750 UNT=(E*q^P)+A+B*q+C*q^2+D*q^3
2760 UT=UNT*UD
2770 dUdX=(UD*1000/XMAX)*((P*E*q^(P-1))+B+2*C*q+3*D*q^2)
2780 DSUM=DSUM+1
2790 D1=FR*(1+PiR)/Ka
2800 D2=D1-FR^2*(2+3.179*PiR+1.5*PiR^2)/(Ka^2)
2810 D3=3*D2-D1+FR^3*(6+11.14*PiR+8.5*PiR^2+2.56*PiR^3)/(Ka^3)
2820 J=D3/D1:GH=D2/D1
2830 AP=-(FR*(3.179+3*PiR)/Ka+(GH-1))/(1+PiR)
2840 AQ=(GH-1)/FR
2850 R1=FR*(11.14+17*PiR+7.68*PiR^2)/Ka+(9.537+9*PiR)
2860 AR=(2-J)/(1+PiR)-FR*R1/((1+PiR)*Ka)
2870 S1=FR*(6+11.14*PiR+8.5*PiR^2+2.56*PiR^3)/((1+PiR)*Ka^2)
2880 S=S1+(J-2)/FR
2890 Beta=(1.25*PiR)^(4/3)-0.5
2900 CD=((((1+Beta*(1+GH))*(Ka*J/(FR^2)-S)))/(Ka*GH/(FR^2)-AQ)-2*J*Beta)*FR^2
2910 T=(1+2*PiR)/(1+PiR)
2920 F1=DstrR*dUdX/(UT*1000)
2930 F2=F1*(1+GH-2*J*(AQ-Ka*GH/(FR^2))/(S-Ka*J/(FR^2)))
2940 F3=FR^2-CD*(AQ-Ka*GH/(FR^2))/(S-Ka*J/(FR^2))-F2
2950 F33=(AR-J*T)*(AQ-Ka*GH/(FR^2))/(S-Ka*J/(FR^2))
2960 F4=F3*1000/(DstrR*((AP-GH*T)-F33)):REM  ---------------------- dPi/dX
2970 F5=((1+GH)-(2*J*(AP-GH*T)/(AR-J*T)))*F1
2980 F6=FR^2-CD*(AP-GH*T)/(AR-J*T)-F5
2990 F7=(S-Ka*J/(FR^2))*(AP-GH*T)/(AR-J*T)
3000 F8=F6*1000/(DstrR*((AQ-Ka*GH/(FR^2))-F7)): REM  -------------- df/dX
3010 F9=-(F1+Ka*DstrR*F8/(1000*FR^2)+DstrR*T*F4/1000): REM  ------ dd*/dX
3020 IF DSUM=1GOTO3060
3030 IF DSUM=2GOTO3090
3040 IF DSUM=3GOTO3110
3050 IF DSUM=4GOTO3130
3060 K1=DX*F4/1000:L1=DX*F8/1000:M1=DX*F9
3070 X=X+DX/2
3080 PiR=Pi+K1/2:FR=f+L1/2:DstrR=Dstr+M1/2:GOTO2740
3090 K2=DX*F4/1000:L2=DX*F8/1000:M2=DX*F9
3100 PiR=Pi+K2/2:FR=f+L2/2:DstrR=Dstr+M2/2:GOTO2740
3110 K3=DX*F4/1000:L3=DX*F8/1000:M3=DX*F9:X=X+DX/2
3120 PiR=Pi+K3:FR=f+L3:DstrR=Dstr+M3:GOTO2740
3130 K4=DX*F4/1000:L4=DX*F8/1000:M4=DX*F9
3140 Pi=Pi+(K1+2*(K2+K3)+K4)/6
3150 f=f+(L1+2*(L2+L3)+L4)/6
3160 Dstr=Dstr+(M1+2*(M2+M3)+M4)/6
3170 ENDPROC
3180 DEFPROCInitcon
3190 q=X(I)/XMAX
3200 U(I)=UD*((E*q^P)+A+B*q+C*q^2+D*q^3)
3210 dUdX=(UD*1000/XMAX)*((P*E*q^(P-1))+B+2*C*q+3*D*q^2)
3220 IF dUdX=0 GOTO 3250
3230 H=1.5
3240 GOTO3260
3250  H=1.55
3260  CONST=3.0
3270 THETAT=THETA(I)/CONST
3280 RTHETA=THETAT*U(I)/(nu*1000)
3290 Dstr=THETAT*H
```

```
3300 CfT=0.3/(EXP(1.33*H)*(0.434294*LN(RTHETA))^(1.74+0.31*H))
3310 f=SQR(CfT/2)
3320 BETAT=-Dstr*dUdX/(f^2*U(I)*1000)
3330 Pi=0.8*(0.5+BETAT)^0.75
3340 ENDPROC
3350 DEFPROCFput
3360 N=I-1
3370 PRINTTAB(7,12)CHR$134"INPUT NAME OF FILE"
3380 INPUT TAB(15) PRED$
3390 PRINT:PRINT:
3400 PRINTTAB(1)CHR$134"ON WHICH DRIVE IS FILE TO BE STORED"
3410 B%=GET
3420 PROCDrive(B%)
3430 CH%=OPENOUT(PRED$)
3440 PRINT#CH%,N,XMAX
3450 FOR I= 1 TO N
3460 PRINT#CH%,DSTR1(I),THETA(I),DSTR2(I),Cf(I),X(I),U(I)
3470 NEXT
3480 CLOSE# CH%
3490 ENDPROC
3500 DEFPROCDrive(B%)
3510 IF B%=48 THEN *DR.0
3520 IF B%=49 THEN *DR.1
3530 IF B%=50 THEN *DR.2
3540 IF B%=51 THEN *DR.3
3550 ENDPROC
```

Programme

GRAFPC3

Programme GRAFPC3 is a graphics programme which can be used display the predicted development of the boundary layer parameters and to compare the predictions with experimental data held on a data file.

```
10 REM BOUNDARY LAYER PREDICTION GRAPHICS PACKAGE
20 Ct=0:Q2$="N"
30 DIM DSTR1(301),DSTR2(301),THETA(301)
40 DIM Cf(301),X(301),U(301)
50 DIM EDSTR1(30),ETHETA(30),EDSTR2(30)
60 DIM ECf(30),EH12(30),EH32(30),EX(30)
70 MODE7
80 PROCIntro
90 MODE4
100 PROCAxes
110 IF Q3$="N" GOTO 130
120 PROCFPread
130 IF Q$="N" GOTO160
140 PROCFEread
150 IF Q3$="N" GOTO 170
160 PROCDSTR1
170 IFQ$="N"GOTO190
180 PROCEXDSTR1
190 IFQ2$="Y"GOTO310
200 IF Ct=1 GOTO 280
210 VDU4:PRINTTAB(9,1)"PRESS SPACE TO CONTINUE"
220 PRINTTAB(10,3)"NEXT GRAPH THETA vs X"
230 B=GET
240 CLS
250 IF B<>32 GOTO 210
260 Ct=1
270 GCOL 0,0: GOTO150
280 Ct=0
290 GCOL0,1
300 IF Q3$="N" GOTO 320
310 PROCTHETA
320 IFQ$="N"GOTO 340
330 PROCEXTHETA
340 IFQ2$="Y"GOTO450
350 IF Ct=1 GOTO 430
360 VDU4:PRINTTAB(9,1)"PRESS SPACE TO CONTINUE"
370 PRINTTAB(10,3)"NEXT GRAPH DSTR2 vs X"
380  B=GET
390 CLS
400 IF B<>32 GOTO 360
410 Ct=1
420 GCOL0,0:GOTO300
430 Ct=0:GCOL0,1
440 IF Q3$="N" GOTO 460
450 PROCDSTR2
460 IFQ$="N"GOTO 480
470 PROCEXDSTR2
480 IFQ2$="Y"GOTO590
490 IF Ct=1 GOTO 570
500 VDU4:PRINTTAB(9,1)"PRESS SPACE TO CONTINUE"
510 PRINTTAB(10,3)"NEXT GRAPH Cf vs X"
520 B=GET
530 CLS
540 IF B<>32 GOTO 500
550 Ct=1
560 GCOL0,0:GOTO440
570 Ct=0:GCOL0,1
580 IF Q3$="N" GOTO 600
590 PROCCf
600 IFQ$="N"GOTO 620
610 PROCEXCf
620 IFQ2$="Y"GOTO730
630 IF Ct=1 GOTO 710
640 VDU4:PRINTTAB(9,1)"PRESS SPACE TO CONTINUE"
650 PRINTTAB(10,3)"NEXT GRAPH H12 vs X"
660 B=GET
670 CLS
680 IF B<>32 GOTO 640
690 Ct=1
700 GCOL0,0:GOTO580
710 Ct=0:GCOL0,1
720 IF Q3$="N" GOTO 740
730 PROCH12
740 IFQ$="N"GOTO 760
750 PROCEXH12
760 IFQ2$="Y"GOTO870
770 IF Ct=1 GOTO 850
780 VDU4:PRINTTAB(9,1)"PRESS SPACE TO CONTINUE"
790 PRINTTAB(10,3)"NEXT GRAPH H32 vs X"
800 B=GET
810 CLS
820 IF B<>32 GOTO 780
```

```
830 Ct=1
840 GCOL0,0:GOTO720
850 Ct=0:GCOL0,1
860 IF Q3$="N" GOTO 880
870 PROCH32
880 IFQ$="N"GOTO 900
890 PROCEXH32
900 IFQ2$="Y"GOTO 970
910 CLS
920 IF Q3$="N" GOTO 980
930 PRINTTAB(10,1)"DO YOU WANT PRINTOUT "
940 PRINTTAB(6,3)"OF ALL GRAPHS COMBINED  Y/N"
950 INPUT TAB(20) Q2$
960 IFQ2$="Y"GOTO160
970 VDU26
980 END
990 DEFPROCAxes
1000 VDU28,0,5,39,0
1010 VDU19,3,3,0,0,0
1020 MOVE 225,750:DRAW 225,150
1030 DRAW 1125,150
1040 MOVE 1150,150:DRAW 1150,750
1050 VDU5
1060 MOVE200,250:DRAW225,250
1070 MOVE170,260:PRINT"1"
1080 MOVE200,350:DRAW225,350
1090 MOVE170,360:PRINT"2"
1100 MOVE200,450:DRAW225,450
1110 MOVE170,460:PRINT"3"
1120 MOVE200,550:DRAW225,550
1130 MOVE170,560:PRINT"4"
1140 MOVE200,650:DRAW225,650
1150 MOVE170,660:PRINT"5"
1160 MOVE200,750:DRAW225,750
1170 MOVE170,760:PRINT"6"
1180 MOVE0,700:PRINT"DSTR1"
1190 MOVE0,625:PRINT"THETA"
1200 MOVE0,550:PRINT"DSTR2"
1210 MOVE0,475:PRINT"  Cf"
1220 MOVE1175,350:DRAW1150,350
1230 MOVE1175,360:PRINT"1"
1240 MOVE1175,550:DRAW1150,550
1250 MOVE1175,560:PRINT"2"
1260 MOVE1175,750:DRAW1150,750
1270 MOVE1175,760:PRINT"3"
1280 MOVE1190,675:PRINT"H12"
1290 MOVE1190,600:PRINT"H32"
1300 ENDPROC
1310 DEFPROCIntro
1320 PRINTTAB(6,4)CHR$134"DO YOU HAVE A PREDICTED"
1330 PRINTTAB(12)CHR$134"DATA FILE  Y/N"
1340 INPUT TAB(20) Q3$
1350 PRINT:PRINT:PRINT
1360 IF Q3$="N"GOTO1390
1370 PRINTTAB(2)CHR$134"INPUT NAME OF PREDICTED DATA FILE"
1380 INPUT TAB(16) PRED$
1390 PRINT:PRINT:PRINT:
1400 PRINTTAB(6)CHR$134"DO YOU HAVE AN EXPERIMENTAL"
1410 PRINTTAB(12)CHR$134"DATA FILE   Y/N"
1420 INPUT TAB(20) Q$
1430 IF Q$="N" GOTO 1470
1440 PRINT
1450 PRINTTAB(4)CHR$134"NAME OF EXPERIMENTAL DATA FILE"
1460 INPUT TAB(16) EXDAT$
1470 PRINT
1480 IF Q3$ ="Y" GOTO 1520
1490 PRINTTAB(16)CHR$134"INPUT XMAX"
1500 INPUT TAB(20) XMAX
1510 PRINT
1520 PRINTTAB(7)CHR$134"WHICH DRIVE ARE FILES ON"
1530 B%=GET
1540 PROCDrive(B%)
1550 ENDPROC
1560 DEFPROCFPread
1570 CH%=OPENIN(PRED$)
1580 INPUT#CH%,N,XMAX
1590 FOR I=1TON
1600 INPUT#CH%,DSTR1(I),THETA(I),DSTR2(I),Cf(I),X(I),U(I)
1610 NEXT
1620 CLOSE#CH%
1630 ENDPROC
1640 DEFPROCDSTR1
1650 IFQ2$="Y"GOTO1670
```

```
1660 VDU5:MOVE 400,800:PRINT"DSTR1 vs X/XMAX":VDU4
1670 DS1P=DSTR1(1)*100+150
1680 XP=(X(1)/XMAX)*900+225
1690 MOVE XP,DS1P
1700 FOR I = 1 TO N
1710 DS1P=DSTR1(I)*100+150
1720 XP=(X(I)/XMAX)*900+225
1730 DRAW XP,DS1P
1740 NEXT
1750 ENDPROC
1760 DEFPROCTHETA
1770 IFQ2$="Y"GOTO1790
1780 VDU5:MOVE 400,800:PRINT"THETA vs X/XMAX":VDU4
1790 THP=THETA(1)*100+150
1800 XP=(X(1)/XMAX)*900+225
1810 MOVE XP,THP
1820 FOR I = 1 TO N
1830 THP=THETA(I)*100+150
1840 XP=(X(I)/XMAX)*900+225
1850 DRAW XP,THP
1860 NEXT
1870 ENDPROC
1880 DEFPROCDSTR2
1890 IFQ2$="Y"GOTO1910
1900 VDU5:MOVE 400,800:PRINT"DSTR2 vs X/XMAX":VDU4
1910 DS2P=DSTR2(1)*100+150
1920 XP=(X(1)/XMAX)*900+225
1930 MOVE XP,DS2P
1940 FOR I=1 TO N
1950 DS2P=DSTR2(I)*100+150
1960 XP=(X(I)/XMAX)*900+225
1970 DRAW XP,DS2P
1980 NEXT
1990 ENDPROC
2000 DEFPROCCf
2010 IFQ2$="Y"GOTO2030
2020 VDU5:MOVE 450,800:PRINT"Cf vs X/XMAX":VDU4
2030 CfP=Cf(2)*100*1000+150
2040 XP=(X(2)/XMAX)*900+225
2050 MOVE XP,CfP
2060 FOR I=2 TO N
2070 CfP=Cf(I)*100*1000+150
2080 XP=(X(I)/XMAX)*900+225
2090 DRAW XP,CfP
2100 NEXT
2110 ENDPROC
2120 DEFPROCH12
2130 IFQ2$="Y"GOTO2150
2140 VDU5:MOVE 450,800:PRINT"H12 vs X/XMAX":VDU4
2150 HP=DSTR1(1)/THETA(1)*200+150
2160 XP=(X(1)/XMAX)*900+225
2170 MOVE XP,HP
2180 FOR I=1 TO N
2190 HP=DSTR1(I)/THETA(I)*200+150
2200 XP=(X(I)/XMAX)*900+225
2210 DRAW XP,HP
2220 NEXT
2230 ENDPROC
2240 DEFPROCH32
2250 IFQ2$="Y"GOTO2270
2260 VDU5:MOVE 450,800:PRINT"H32 vs X/XMAX":VDU4
2270 GP=DSTR2(1)/THETA(1)*200+150
2280 XP=(X(1)/XMAX)*900+225
2290 MOVE XP,GP
2300 FOR I=1 TO N
2310 GP=DSTR2(I)/THETA(I)*200+150
2320 XP=(X(I)/XMAX)*900+225
2330 DRAW XP,GP
2340 NEXT
2350 ENDPROC
2360 DEFPROCEXDSTR1
2370 FOR I= 1 TO N1
2380 DS1P=EDSTR1(I)*100+150
2390 XP=EX(I)/XMAX*900+225
2400 PLOT69,XP,DS1P
2410 NEXT
2420 ENDPROC
2430 DEFPROCEXTHETA
2440 FOR I= 1 TO N1
2450 THP=ETHETA(I)*100+150
2460 XP=EX(I)/XMAX*900+225
2470 PLOT69,XP,THP
2480 NEXT
```

```
2490 ENDPROC
2500 DEFPROCEXDSTR2
2510 FOR I= 1 TO N1
2520 DS2P=EDSTR2(I)*100+150
2530 XP=EX(I)/XMAX*900+225
2540 PLOT69,XP,DS2P
2550 NEXT
2560 ENDPROC
2570 DEFPROCEXCf
2580 FOR I= 1 TO N1
2590 CfP=ECf(I)*100+150
2600 XP=EX(I)/XMAX*900+225
2610 PLOT69,XP,CfP
2620 NEXT
2630 ENDPROC
2640 DEFPROCEXH12
2650 FOR I= 1 TO N1
2660 HP=EDSTR1(I)/ETHETA(I)*200+150
2670 XP=EX(I)/XMAX*900+225
2680 PLOT69,XP,HP
2690 NEXT
2700 ENDPROC
2710 DEFPROCEXH32
2720 FOR I= 1 TO N1
2730 GP=EDSTR2(I)/ETHETA(I)*200+150
2740 XP=EX(I)/XMAX*900+225
2750 PLOT69,XP,GP
2760 NEXT
2770 ENDPROC
2780 DEFPROCFEread
2790 ch%=OPENIN(EXDAT$)
2800 INPUT#ch%,N1,Tu,U0
2810 FORI=1TON1
2820 INPUT#ch%,EX(I),EDSTR1(I),ETHETA(I),EDSTR2(I),ECf(I)
2830 NEXT
2840 CLOSE#ch%
2850 ENDPROC
2860 DEFPROCDrive(B%)
2870 IF B%=48 THEN *DR.0
2880 IF B%=49 THEN *DR.1
2890 IF B%=50 THEN *DR.2
2900 IF B%=51 THEN *DR.3
2910 ENDPROC
```